Chapter 1

Introduction

1.1 DNA

Deoxyribonucleic acid (DNA) is a nucleic acid which contains the genetic information used in the development and functioning of all known living organisms. All the information needed to synthesise other components of a cell such as proteins, enzymes and RNA molecules is derived from DNA. Chemically, DNA is a biopolymer built from monomers called nucleotides. Each nucleotide contains a pentose-2-deoxyribose sugar, a phosphate group and one of the purine (fused five- and six membered heterocyclic compounds) or pyrimidine (six membered rings) bases (Figure 1). There are four bases which are present in deoxyribonucleotides: adenine (A), guanine (G) (purine bases), cytosine (C) and thymine (T) (pyrimidine bases) (Figure 2). In the structure of a nucleotide the phosphate group is joined by a phosphodiester bond with the C5 position of deoxyribose, and the purine or pyrimidine base is connected from a ring nitrogen to the C1 position of the pentose ring. A moiety which lacks the phosphate is called a nucleoside (Figure 1) [1-4].

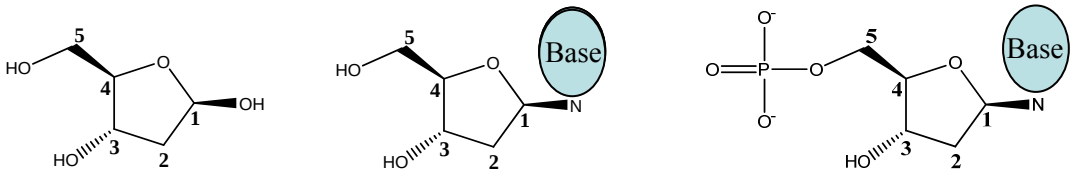

Figure 1: Structure of deoxyribose (A), nucleoside (B), nucleotide (C). Base- one of the purine or pyrimidine bases.

The backbone of DNA is made from 2-deoxyribose molecules joined together by phosphodiester bonds between 5' phosphate group of one nucleotide and 3' hydroxyl group of a second nucleotide. Each of the DNA strands has two asymmetric ends: 3' end with free hydroxyl group and 5' end with terminal phosphate group (Figure 3). The numbers refer to carbon atoms present in the 5 member deoxyribose ring.

Inside living organisms, DNA is usually present as a pair of two antiparallel, complementary strands which form a double helix structure stabilised by hydrogen bonds between the purine and pyrimidine bases and by π- π stacking interactions between adjoining bases. Watson and Crick found that each type of base in one strand can form hydrogen bonds only with one type of base in the second strand: adenine

only bonds with thymine by two hydrogen bonds, while cytosine only bonds with guanine by forming three hydrogen bonds (Watson-Crick base pairing, Figure 4) [1-4].

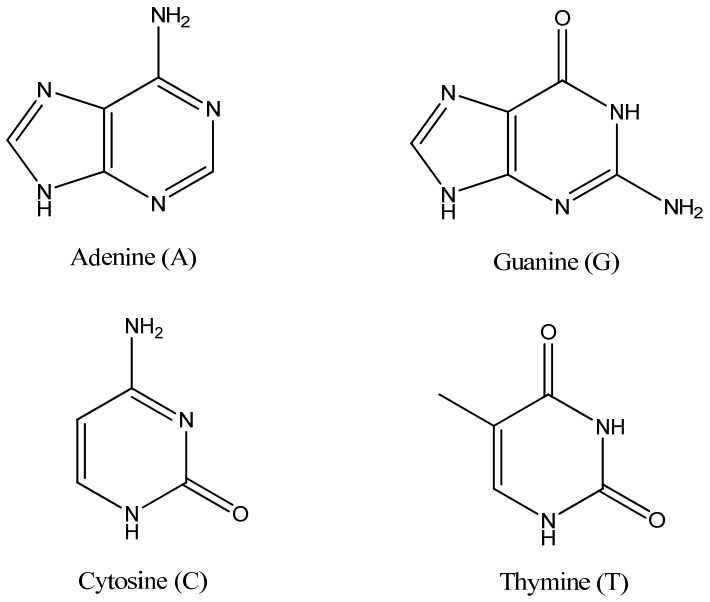

Figure 2: Purine and pyrimidine bases present in DNA strands.

The hydrogen bonds between bases in complementary DNA strands can easily break down and reform. This reversible and specific interaction between base pairs is crucial for DNA replication and translation [1-3]. The two complementary strands that form the DNA double helix are called the coding strand and the template strand.

During DNA replication the two strands of the double helix separate and two new strands, complementary to the original coding and template strands, are formed in a complicated process involving enzymes: helicases (which allow separation of the strands), polymerases (which can add free deoxyribonucleotides to 3' ends of newly forming strands) and primases (which are responsible for formation of primers, short oligonucleotides which can start formation of a new strand). Both strands are synthesised in the 5' to 3' direction which means that the strand complementary to the original 3'-5' strand is formed continuously, while the strand complementary to the original 5'-3' strand is formed in small fragments which are then joined together by DNA ligases. In the replication process two identical copies of original double helix are formed [1-3]. The replication process is used in the lab through polymerase chain reaction (PCR), a technique which allows amplification of DNA across several orders of magnitude. During the PCR process, a mixture containing the DNA to be

amplified, the four types of deoxyribonucleotides, the enzyme-Taq polymerase, primers complementary to the DNA to be amplified and buffers containing Mg^{2+} ions is heated to 95°C which causes the denaturation of the DNA strand. The temperature is then lowered to 37-50°C which allows attachment of primers to the separated DNA strands. In the next step the reaction mixture is heated to 72°C, and strands complementary to the original DNA strand are formed in the presence of Taq polymerase. Identical copies of DNA to be amplified are formed. The process can be repeated several times with a large number of copies of the original DNA sample to be obtained [1].

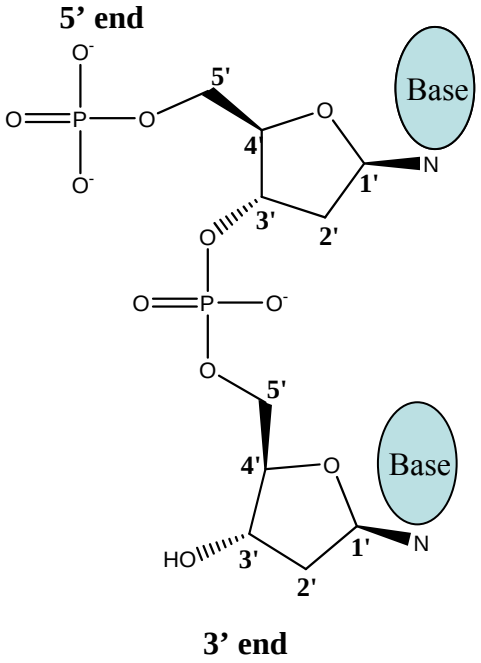

Figure 3: Structure of a single stranded DNA backbone; Base-one of the purine or pyrimidine bases.

Transcription is a process of formation of an RNA copy of the DNA coding strand. RNA (ribose nucleic acid) is almost identical to DNA but has a 2' hydroxyl group on the ribose sugar. In the DNA transcription process the two strands of DNA double helix separate, but only the strand complementary to the template and identical to the coding strand is formed. This copy of the coding strand is called messenger RNA (mRNA). The function of mRNA is to carry genetic information from DNA to the ribosomes (complexes of RNA and proteins), where proteins are synthesised through a process called translation. The sequence of nucleotides in mRNA determines the

sequence of amino acids in the proteins. Every three base sequence in mRNA is called a codon and is specific for a particular amino acid. There are also three 'stop' codons which signal that the synthesis of the protein is finished. In the translation process transfer RNA (tRNA), which carries amino acids, reads the genetic information from mRNA. tRNA contains an anticodon, formed by three nucleotides, with sequence complementary to a specific codon found in mRNA. tRNA carries amino acids in the order dictated by the mRNA to the ribosomes where the protein chains are produced.

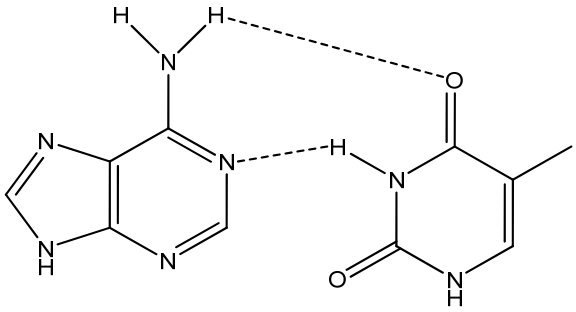

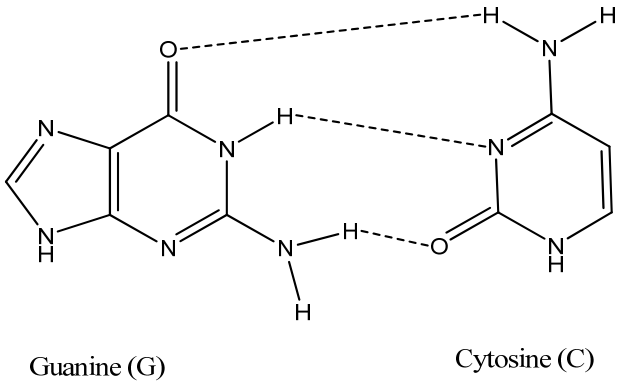

Figure 4: The two types of Watson-Crick base pairing possible. Top: The formation of two hydrogen bonds between adenine and thymine. Bottom: The formation of three hydrogen bonds between guanine and cytosine.

1.2 Traditional DNA detection methods

Sequence specific DNA detection is a vital area of life science research due to its application in the diagnosis of pathogenic and genetic diseases [5-12]. Hybridisation of two single stranded oligonucleotides to form a double stranded DNA and its dissociation into two single strands is essential to DNA detection assays. Many detection techniques rely upon hybridisation of labelled (radioactive, fluorescent,

chemiluminescent) oligonucleotide probes to a complementary target [5, 7, 8-12]. The sensitivity of the techniques depend mainly upon the specific activity of the labels attached to the oligonucleotide probes. There are also detection techniques which rely upon enzymes to generate colorimetric, fluorescent or chemiluminescent signals, although the colorimetric methods are restricted due to their poor sensitivity [12].

Radioactive labels offer high sensitivity, however their use has also numerous disadvantages, such as: disposal problems, health risks, low stability of radioactively labelled probes and requirements of specially trained personnel [6, 9, 12].

Chemiluminescent labels offer an increase in the sensitivity and a decrease in the time required for DNA detection when compared with radioactive labels [10, 12]. The other advantage is that the technique requires little instrumentation [10]. The biggest disadvantage of using chemiluminescent labels are the complicated procedures involving numerous reagents that are needed to generate the luminescent intermediates [11].

Fluorescent labels are the most commonly used labels in DNA detection assays. These labels are relatively inexpensive and easy to use. Their biggest disadvantage is that fluorescence spectra produced tend to have broad overlapping outputs thus limiting multiplexing capacity of the technique. Quantitative measurements are challenging because of low fluorescence intensities and susceptibility to photobleaching [12].

The biggest overall disadvantage of traditional DNA detection assays is that they all require amplification of the genetic material present in the original sample by PCR.

1.3 Nanoparticle based methods for DNA detection

Nanoparticle based DNA detection methods offers numerous advantages over traditional DNA detection assays, such as: rapid detection, good selectivity, a colorimetric response and little or no instrumentation [5, 7, 13-15]. These methods are based upon hybridisation of two sets of oligonucleotide functionalised metallic nanoparticles, containing different DNA strands, to a target which is complementary to both probes. The target crosslinks nanoparticles by hybridisation which can be monitored with the naked eye (solution will change colour if hybridisation occurs), by UV-Vis spectroscopy or by surface enhanced (resonance) Raman scattering (SE(R)RS). Due to their unique optical properties (surface plasma resonance

absorption, resonance light scattering) and the possibility of easy modification of their surface, gold and silver nanoparticles are commonly used in nanoparticle based DNA detection assays [15, 16].

1.3.1 Gold nanoparticle probes

Due to their unique optical properties, a variety of surface coatings possible and their biocompability, gold nanoparticles are commonly used in nanoparticle based methods for detection of DNA, proteins or enzyme activities [16]. The optical properties of metallic nanoparticles depend upon the collective oscillation of electrons across the nanoparticle surface, which are in resonance with the incident electromagnetic radiation (surface plasmon resonance). For gold nanoparticles the resonance frequency of this oscillation lies in the visible region of the electromagnetic spectrum. Due to their high surface area to volume ratio nanoparticles are very sensitive to any changes occurring in their environment, such as: surface modification, aggregation or change of dielectric properties of the surrounding medium [16, 17]. Changes in the nanoparticle's environment lead to colorimetric changes of their colloidal solution [16].

After the synthesis of gold colloid, the nanoparticles are surrounded by a weakly bound layer of charged ligand (e. g. citrate), which provides the repulsive forces between nanoparticles necessary to prevent uncontrolled aggregation of the nanoparticle solution [8, 18, 19]. In order to use gold nanoparticles in biomolecule detection assays, the nanoparticle surface has to be modified. Many ways to achieve this exist, such as: electrostatic interaction, specific recognition (antibody-antigen, biotin-avidin) or covalent coupling [13, 16, 21-25, 28, 29, 39]. Electrostatic adsorption is a very simple process however the binding is usually not strong enough to use prepared probes in biological studies that require several washing steps, use of solutions with high salt concentration and a long incubation. The other disadvantage of this method is non-specific interaction of analytes with the nanoparticle surface which decreases the detection sensitivity [16]. Covalent binding offers numerous advantages when compared with other surface modification methods, such as high stability of prepared probes and good selectivity [16]. Colloidal gold can be stabilised with numerous molecules containing thiol, disulfide or thioester, such as: thiolated or disulfide modified oligonucleotides, alkanethiols, thiolated ethylene glycol [13, 16,

21-25, 28, 29, 39]. Gold nanoparticles functionalized with thiolated oligonucleotides and aggregation of these conjugates induced by hybridization of the probes to the complementary target DNA strand has been well characterized. These type of probes are commonly used in colorimetric DNA detection systems.

1.3.1.1 Unmodified nanoparticle based DNA detection

The use of unmodified gold nanoparticles in DNA detection assays has been reported in the literature [8, 27]. This method is based on the fact that single- and double- stranded DNA (ssDNA and dsDNA) have different electrostatic properties. Single stranded DNA can uncoil and expose its bases, which promote the adsorption on to the nanoparticle's surface. With the negative phosphate backbone sufficiently distant, attractive Van der Waals forces between the bases and metal surface make DNA adsorption possible [8, 27]. Double stranded DNA has a stable double helix geometry, so the uncoiling needed to expose the bases is not possible. Repulsion between the negatively charged phosphate backbone and the layer of negatively charged stabilising ligands (e. g. citrate) on the nanoparticle surface prevents the adsorption of dsDNA on to the gold surface [8]. In the DNA detection system described by Li *et al.* [8] 0.2 M NaCl in 10 mM phosphate buffer (0.2 M PBS) and gold nanoparticles were added to a solution containing ssDNA with or without complementary target. If there was only ssDNA present in the sample the oligonucleotides adsorb to the nanoparticles stabilising them, resulting in the nanoparticle suspension remaining red in colour after addition of the salt/buffer solution. If there was a double stranded DNA present in the sample, fast aggregation of nanoparticles, and a red to blue colour change was observed. This is due to the dsDNA not adsorbing to the nanoparticle and the addition of the salt screens the repulsive interactions between nanoparticles and causes aggregation. The presence of dsDNA in this system can also be detected by fluorescence spectroscopy. When a fluorescent label is added to the ssDNA the addition of nanoparticles causes adsorption of the oligonucleotide to the gold surface and fluorescence quenching is observed (due to the fluorescence quenching ability of the metal surface). If dsDNA is present in the solution the adsorption of DNA on the metal surface does not occur and the fluorescence persists [8]. Single base mismatches can be detected by allowing the dsDNA from solutions containing perfectly complementary and mismatched target to

dehybridize in water, without salt, for 2 mins before addition of gold colloid and salt/buffer solution. An obvious colour difference was observed between perfectly matched and imperfect samples due to the lower binding strength for mismatched than for perfectly matched dsDNA [8].

1.3.1.2 Thiolated oligonucleotide functionalized gold nanoparticles probes

In order to functionalize gold nanoparticles with oligonucleotides, a thiol modified single stranded DNA (ssDNA) is added to the nanoparticle solution, then left for approximately 6 hrs [6, 21]. Then, concentrated phosphate buffer is added to obtain a final buffer concentration in the sample of 10 mM [6]. Due to the electrostatic repulsions between negatively charged phosphate backbones of the thiolated ssDNA, the number of oligonucleotides which will attach to the nanoparticle surface depends strongly on the ionic strength of the immobilization solution [23, 24]. To achieve high DNA surface coverages, high NaCl concentration should be used due to its screening effect. However, addition of a large amount of salt may destabilise the nanoparticles and cause their irreversible aggregation. Therefore, during preparation of nanoparticles functionalized with thiolated oligonucleotides, time consuming, slow, salt-aging steps are employed [6, 23]. The other problem which has to be overcome during preparation of oligonucleotide functionalised nanoparticles is that of non-specific adsorption of ssDNA on to the metal surface. Thiolated oligonucleotides can interact with the metal surface not only through the gold-sulphur bond, but also via the amine groups present in the DNA bases. To prevent this non-specific oligonucleotide adsorption, mercaptohexanol can be added to ssDNA modified gold nanoparticles. Mercaptohexanol can displace some of the non-specifically adsorbed oligonucleotides and make the thiolated ssDNA bind to the gold surface only via a metal-sulphur bond. The amount of the mercaptohexanol added and the reaction time need to be precisely controlled, because excessive displacement of thiolated oligonucleotides may result in destabilised nanoparticles [23]. The amount of thiolated oligonucleotides which will attach to gold nanoparticles depends strongly upon salt concentration, type of DNA spacer (region between recognition sequence and thiol modifier), the length of DNA strand, base sequence and the nanoparticle size [23, 24].

After surface modification the gold surface absorbance band is usually slightly red shifted and a decrease in the band intensity is also observed. The observed signal lowering is due to a decrease in the concentration of nanoparticles during the workup of the oligonucleotide functionalized nanoparticles. The red shift is caused by the surface modification, however it might also be caused by the change in dielectric constant around the nanoparticles (the conjugates are usually resuspended in PBS, the bare nanoparticles in water), or by centrifugation steps which may affect size distribution (Figure 5) [7, 22].

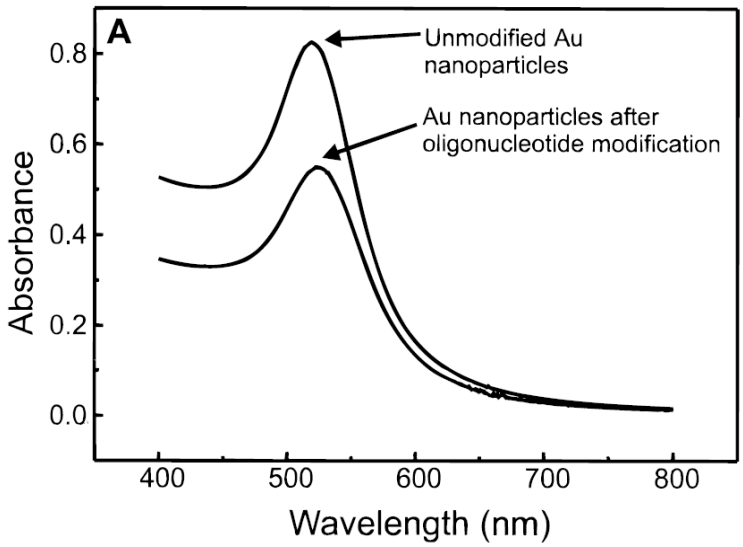

Figure 5: **UV-Vis spectra of gold nanoparticles and gold nanoparticle functionalized with thiolated 12-base oligonucleotides in 0.3 M PBS [7].**

1.3.1.2.1 Cross-linking DNA detection system

In a typical nanoparticle-DNA detection system two sets of oligonucleotide functionalized nanoparticles are synthesised. The two sets of nanoparticles are functionalised with a DNA sequence that is half complementary to a target oligonucleotide. The nanoparticle probes are mixed in a 1:1 molar ratio followed by the addition of the complementary target. The target cross-links the nanoparticles by hybridisation, which results in nanoparticle aggregation and thus a red-to-purple colour change is observed (Figure 6) [5, 6, 7, 20, 13, 21, 22]. Due to the steric reasons and the high negative charge of the DNA backbone on the nanoparticle surface the

hybridisation process can be slow at room temperature, however it can be affected rapidly by warming it at 50°C for 5 mins [6], or 70°C for 5-10 mins [21].

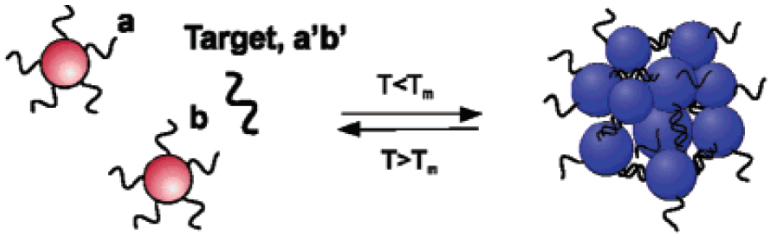

Figure 6: **Hybridization of two gold nanoparticles probes in the presence of complementary target DNA [21].**

The hybridisation process can be visualised not only with the naked eye (red to purple colour change), it can also be monitored by the UV-Vis spectroscopy. A mixture of gold nanoparticles with oligonucleotides immobilised on the surface appears red in colour and has a strong absorbance at about 520 nm. When a complementary target is added to the solution containing two types of oligonucleotide functionalised nanoparticle probes, reversible aggregation of nanoparticles is observed-the solution appears purple in colour. Formation of the aggregates leads to a red shift of the gold surface plasmon band from 520 nm to 574 nm (Figure 7) [7, 13, 21].

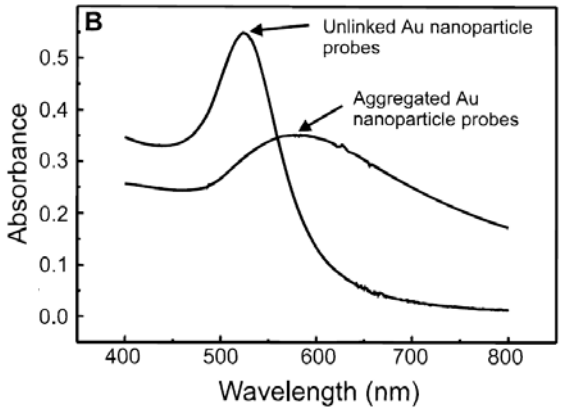

Figure 7: **UV-Vis spectra of a solution of DNA functionalized (12 bases) nanoparticle probes and of a solution containing two oligonucleotide functionalised nanoparticle probes in the presence of a 24 base complementary target [7].**

The optical properties of gold nanoparticles are strongly dependent upon the distance between nanoparticles and can be controlled by controlling the length of the target DNA molecule used to cross-link the nanoparticles by hybridisation. Mirkin *et al.* [22] prepared two batches of 15.4 nm gold nanoparticles functionalised with

thiolated 12 base long ssDNA. One of three different target sequences was then added to the solution containing both probes. Each of the targets had 12 base sticky ends and a spacer containing 0, 24 or 48 bases. The formation of aggregates was followed by monitoring the surface plasmon band in the UV-Vis as a function of time. It was found that the rate of hybridisation was dependent on the length of the complementary target used. Addition of the shortest target, without spacer bases exhibited the largest changes on the UV-Vis spectrum at the fastest rate (Figure 8).

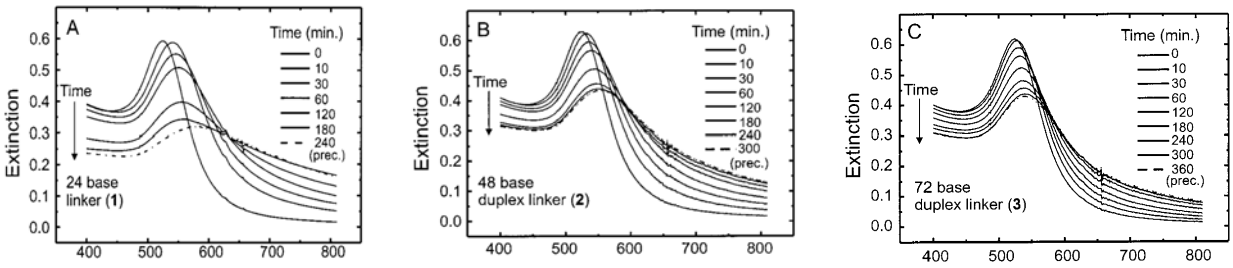

24 base linker **48 base linker** **72 base linker**

Figure 8: Changes in the UV-Vis spectra as a function of time for samples containing two types of oligonucleotide functionalised gold nanoparticles probes and a complementary target containing 24, 48 or 72 bases [22].

1.3.1.2.1.1 Melting properties of DNA linked Au nanoparticles aggregates

The DNA linked gold nanoparticle aggregates can be dispersed by heating them above the duplex melting temperature (Tm) [6, 7, 13, 21, 25]. The hybridisation/denaturation process can be observed by monitoring the absorbance at 260, 520 or 650-700 nm as a function of time [7, 21]. The melting profiles of duplex DNA strands supporting the polymeric network of gold nanoparticles exhibit extraordinary sharp transitions when compared to unlabelled or conventional fluorophore labelled DNA. The observed sharp transitions are due to the dense loading of oligonucleotides, which increases binding sites between nanoparticles, and a subsequent cooperative mechanism of dehybridisation due to the presence of multiple DNA target strands [13, 25]. The melting properties of DNA linked nanoparticle aggregates depends on: density of oligonucleotides on the nanoparticles surface, nanoparticle size, salt concentration and interparticle distance [21, 25].

The high DNA surface coverage offers many advantages, such as high stability of formed conjugates, especially at elevated salt concentrations and increased

hybridisation efficiency. In terms of melting profiles Tm value decreases and the melting transition broadens when the probe density decreases [21, 25].

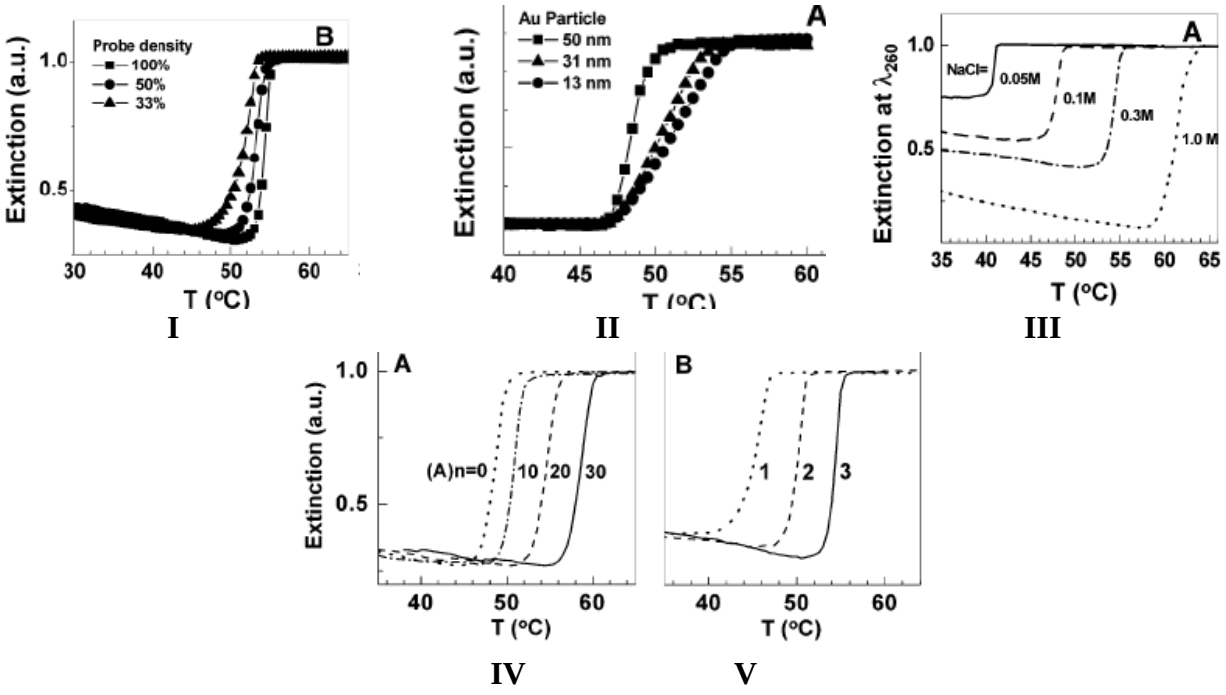

Figure 9: The effect of: I- probe oligonucleotide density, II-nanoparticle size, III-salt concentration, IV- nanoparticle distance (different length of target DNA); V-probes orientation (1- head to head, 2-head to tail, 3-tail to tail) on melting properties of nanoparticle aggregates [21].

The size of nanoparticles used for probe preparation also has influence on the melting profiles of formed duplexes. Jin *et al.* [21] found in their study that melting transitions were sharper for larger nanoparticles, which is caused by higher oligonucleotides surface density (Figure 9). Hurst and co-workers [25] observed that in the case of large gold nanoparticles (150 nm), at high salt concentration (1M), formation of one base pair connection (G-C) between nanoparticles exhibited melting transition typical for duplexes formed by longer sequences (>10 bases) between two types of small nanoparticles probes. This is caused by the ability of larger nanoparticles to form more DNA linkages due to their lesser curvature. Numerous weaker interactions can lead to a cumulative interaction strong enough to induce aggregation of nanoparticles. Free DNA strands (not attached to metallic nanoparticles) which contain only one base pair complementary region won't hybridise under the same conditions [25]. It was found that 4-8, 6-19, 8-33 additional bases has to be added to free DNA duplex to reach the Tm values similar to the one of

aggregates formed from 15, 60 or 150 nm gold nanoparticles functionalised with only 3 base pairs. This is caused by the possibility of three dimensional hybridisation on the nanoparticles surface, which is not possible for free DNA in solution (in this case only a single DNA duplex can form) [25].

Increase in the salt concentration of the solution containing two types of oligonucleotide functionalised nanoparticles probes and a complementary target causes an increase in hybridisation rate. It also influences the melting profiles of the gold nanoparticle probes. When the salt concentration increases it stabilizes the duplexes on the nanoparticle surface, which causes an increase in the Tm value (Figure 9). The screening effect of the salt minimizes electrostatic repulsions between oligonucleotide functionalized nanoparticles which allows more hybridisation events to take place [21].

The interparticle distance is also an important factor which may cause changes in the melting profiles of oligonucleotide functionalised nanoparticle probes. In the experiment designed by Jin *et al.* [21], four different complementary target sequences containing 0, 10, 20, 30 base length spacers between recognition sequence and thiol functionality were added to a solution containing two types of oligonucleotide functionalised gold nanoparticles probes. It was found that the Tm increased when the length of the spacer increased, and also there was a linear relation between Tm value and the spacer length (Figure 9). In another experiment designed by the same group the interparticle distance was changed, not by changing the length of target DNA, but by placing the nanoparticles at a different position on the oligonucleotide (3' or 5'), so when hybridisation occured the nanoparticles were in different orientation to each other: head to head, head to tail or tail to tail (Figure 10).

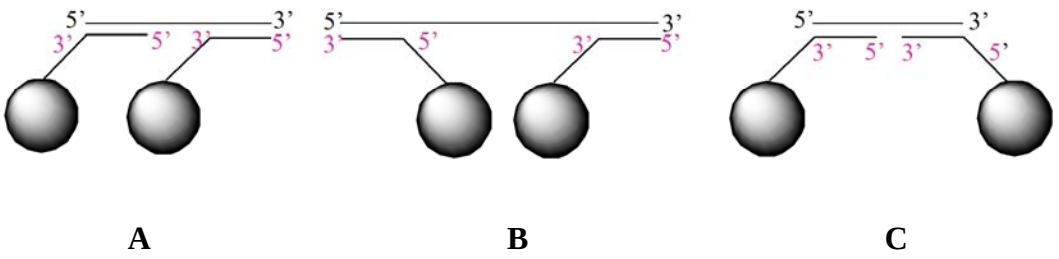

Figure 10: Different orientations of gold nanoparticles probes hybridised to complementary target: A-head to tail, B-head to head, C-tail to tail.

This experiment confirmed that Tm increases when interparticle distance increases (Figure 9). It was concluded that electrostatic interactions which are sensitive to interparticle distance are the dominant factor which has an influence on Tm value when the distance between nanoparticles changes [21].

Detection of a single base mismatch, a one base deletion or a one base insertion is possible in the previously described nanoparticle based DNA detection system. When an imperfect target is used in this DNA detection assay both precipitation and changes in surface plasmon resonance are observed upon hybridisation. Formed aggregates also exhibit sharp melting profiles, however, observed Tm values are lower for duplexes formed in the presence of imperfect targets (Figure 11) [7].

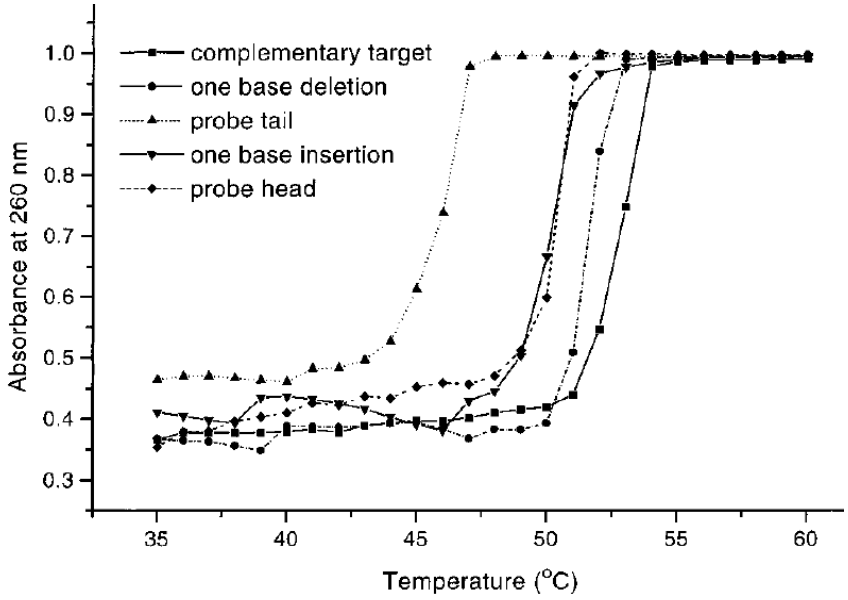

Figure 11: Thermal dissociation curves for Au nanoparticles probes with fully complementary and imperfect targets [7].

1.3.1.2.1.2 Northwestern Spot Test

The hybridisation process in a cross-linking nanoparticle based DNA detection system can also be monitored by spotting aliquots of a mixture containing gold nanoparticle-DNA aggregates onto a reverse phase silica gel plate (Northwestern Spot Test). In the presence of complementary target a blue spot appears after drying on the silica plate. After heating the solution above the duplex dissociation temperature and spotting the aliquot on a reverse phase silica plate, the spot is red (the rehybridization process is not occurring on the solid support even in the temperatures below Tm of a

duplex). The Northwestern spot test can also be used to distinguish between fully complementary and imperfect targets containing one base-pair mismatches, one base insertion or one base deletion when the probes are orientated in a tail-to-tail arrangement. If they are aligned in head to tail fashion the discrimination between fully complementary and imperfect targets is not possible [7]. In the presence of non-complementary target the spot remains red [6, 7].

1.3.1.2.2 Non cross-linking DNA detection system

Despite aggregation of oligonucleotide functionalised nanoparticles in the cross-linking system described above, hybridisation of nanoparticle probes to complementary target without a cross-linking mechanism has also been reported in the literature [26, 41, 43-45]. Sato and co-workers [26] indicated that addition of target complementary in sequence and length to poly (*N*- isopropylacrylamide) particles or 15 nm Au nanoparticles functionalised with one type of oligonucleotide caused rapid aggregation of particles at high salt concentration. In the absence of the complementary target or presence of imperfect target no colour change was observed. The opposite behaviour was observed by Baptista and co-workers [41, 43-45]. This group reported that after addition of target complementary in sequence and the length to gold nanoparticles functionalised with thiolated oligonucleotides no colour change was observed, however the aggregates were formed in the presence of imperfect target. The differences observed were explained by different nature of the targets used in the experiments (complementary target [26], clinical DNA sample containing complementary target [41, 43-45]).

1.3.1.3 Multiple thiol modified oligonucleotide - gold nanoparticles probes

Although thiol modified oligonucleotide functionalised gold nanoparticles are commonly used as probes in DNA detection assays, there are some disadvantages of those probes under conditions such as: high NaCl concentrations (0.3 – 1 M); treatment with biological buffer additives such as dithiothreitol (DTT), a stabiliser for polymerase enzyme in the PCR process, and prolonged or cycled temperatures [15, 28, 30]. A study with fluorophore labelled oligonucleotides indicated that DTT and mercaptoethanol displace alkylthiol capped oligonucleotides from the nanoparticle

surface [28]. It was also found that gold nanoparticles larger than 30 nm in diameter, when functionalised with mono-thiolated oligonucleotides slowly decompose at elevated temperatures (40-90°C) and in high salt concentration buffers (0.3 - 1 M) [28].

Stakenborg and co-workers [29] proposed the use of mercaptohexanol or 1-mercapto-6-hexyl tri (ethylene) glycol as backfilling molecules, which should be added to oligonucleotide functionalised nanoparticles to increase their stability. It was found that addition of these molecules reduced non-specific adsorption of DNA on the nanoparticles and also led to more radial configuration of the attached DNA. Prepared probes were more stable at higher salt concentrations, however their thermal stability was lower (when compared to thiolated oligonucleotide functionalised nanoparticles), which might be caused by lower numbers of DNA strands attached per nanoparticle, and by the fact that some of the oligonucleotides might be removed from the metal surface after heating [29]. The use of other molecules to increase the stability of oligonucleotide functionalised nanoparticles has also been reported. For example Zhao *et al.* [31] proposed the use of deoxynucleotides for that purpose and Claridge and co-workers [32] covered the nanoparticles with a polymeric layer before addition of oligonucleotides. The use of deoxynucleotides increased the stability towards higher salt concentration, but this stability was weakened or destroyed at higher temperatures [31]. The biggest disadvantage of the technique suggested by Claridge was irreversible formation of the polymer coating on the nanoparticles surface which might hinder the attachment of oligonucleotides to the gold nanoparticles [32].

Dougan *et al.*[15] found that oligonucleotide modified with the inexpensive, commercially available, simple disulphide - thioctic acid enhanced the stability of metallic nanoparticles when compared with mono-thiol oligonucleotide functionalised nanoparticles. In their approach, the *N*-hydroxysuccinimidyl ester of thioctic acid was reacted with the 3' or 5' functionalised terminal amine group of ssDNA. Thioctic acid modified oligonucleotides were attached to the surface of gold nanoparticles using a standard protocol similar to the attachment of thiol modified ssDNA, however the salt aging process was much faster (2 days, 5 days for thiol modified oligonucleotides) and the process much less time consuming. To compare the stability of thiol- and thioctic acid modified oligonucleotide functionalised gold nanoparticles the probes were treated with DTT at 40°C.

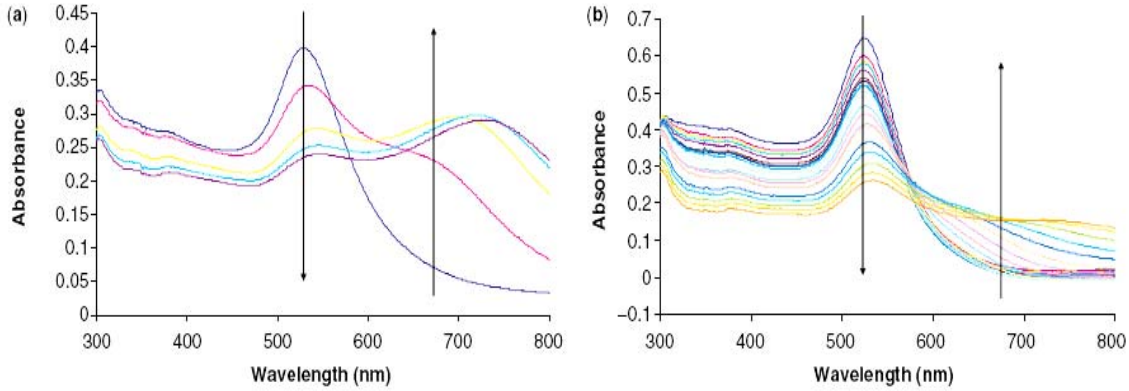

Figure 12: UV-Vis spectra showing degradation of Au-(a) thiolated DNA (1 min intervals) and (b) thioctic acid modified oligonucleotide (10 mins intervals) conjugates upon treatment with DTT [15].

It was found that the probes prepared with thioctic acid modified oligonucleotides were far more stable towards precipitation than the nanoparticles functionalised with thiolated oligonucleotides (Figure 12). This enhancement in the stability of the formed conjugates is caused by the fact that the reduced thioctic acid-dihydrothioctic acid binds to the gold surface through both sulphur atoms and forms a stable monolayer on the nanoparticle surface [15]. In other experiments performed by the same group [15] the oligonucleotide surface coverage was compared for the probes prepared with thiolated and thioctic acid modified oligonucleotides. It was found that less DNA strands attach to gold nanoparticles when disulphide modified ssDNA was used for probe preparation. So when the conjugate stability is not an issue the yield of the conjugation process can be improved by the use of alkyl-thiolated oligonucleotides [15]. Letsinger *et al.* [30] described the use of a steroic cyclic disulphide (epiandrosterone) to modify oligonucleotides before their attachment to the gold nanoparticle surface. The stability of the prepared probes was compared to the stability of probes prepared with oligonucleotides functionalised with mercaptohexyl or acyclic disulphide. It was found that probes prepared in the presence of cyclic disulphide were much more resistant to attack by DTT than standard probes prepared with thiol or acyclic disulphide modified ssDNA. The reaction of acyclic disulphide with gold probably involves the cleavage of the S-S bond. Oligonucleotides containing this kind of modification will be linked to gold nanoparticles surface through a single S-Au bond, and they will exhibit similar stability as the probes prepared with thiolated oligonucleotides [30].

Further enhancement in the conjugate stability was observed when a trithiol was used as a terminal modification of oligonucleotides [28]. The use of trithiol modified oligonucleotides to functionalise large (>30 nm) gold nanoparticles make it possible to form conjugates which are stable enough for use in hybridisation based DNA detection assays. It was not possible when thiolated oligonucleotides were used for that purpose [28]. Although there is a big difference in the stability of the gold nanoparticle probes prepared in the presence of thiol, cyclic disulphide and trithiol modified oligonucleotides, all of them can be used in nanoparticle based DNA detection systems. The melting properties of nanoparticle aggregates formed from all kinds of probes are qualitatively the same [28]. It can be concluded that the type of molecule used to modify oligonucleotides before their addition to gold colloid has a big influence on the probe's stability but has very little effect on the hybridisation and melting properties of the formed conjugates [28].

1.3.1.4 Oligonucleotide conformation on gold nanoparticles surface

It is well known that oligonucleotides modified with thiolated moieties can bind strongly to the gold nanoparticle surface by forming a covalent bond between sulphur and the metal surface, however non-specific secondary interactions between oligonucleotides and nanoparticles also occur. All nucleosides have free functional groups, such as amine or carbonyl groups, that could act as a ligands for the gold nanoparticle surface. The phosphate groups along the phosphate backbones can electrostatically bind to nanoparticles as well (Figure 13) [33-35]. Non-specific oligonucleotide absorption causes a decrease in surface coverage, which may lower the stability of the formed conjugates.

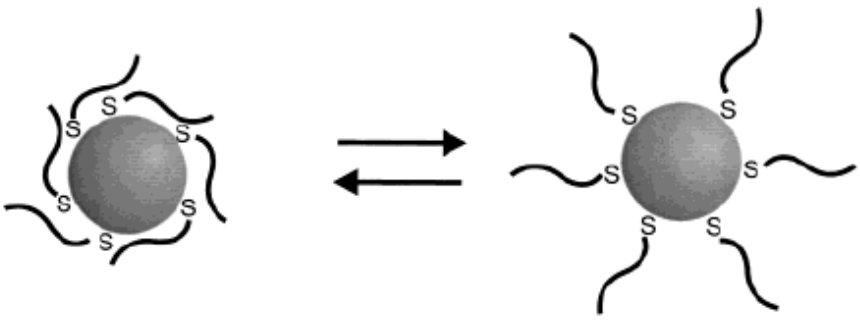

Figure 13: Non-specific absorption of oligonucleotides on nanoparticles surface (left), nanoparticle functionalised with thiolated oligonucleotides specifically, via S-Au bond (right) [33].

One of the ways to prevent non-specific adsorption of oligonucleotides onto the nanoparticle surface is to add mercaptohexanol to ssDNA-Au nanoparticle conjugates. It destabilises the DNA adsorption via bases and changes the conformation of DNA on the nanoparticle surface to be more suitable for hybridisation. Mercaptohexanol concentration and reaction time need to be controlled to achieve the desired effect; too long reaction times and too high mercaptohexanol concentrations may cause significant displacement of oligonucleotides from the nanoparticles surface [35].

It was found that the coverage of gold nanoparticles with oligonucleotides is strongly dependent upon the sequence of ssDNA used. Oligonucleotides rich in thymidine exhibit higher surface coverages and also higher stability, when compared with conjugates prepared with oligonucleotides rich in other types of bases [33]. Numerous experiments indicate that the affinity of a single nucleoside for Au nanoparticles surface is biggest for cytosine and guanine, smaller for adenine, and the smallest for thymine. Oligonucleotides with high G and C content have a tendency to wrap around nanoparticles. In case of oligonucleotides rich in A and T this tendency is significantly reduced. The surface coverages observed for the conjugates prepared with oligonucleotides rich in A and T are much higher that those observed for gold nanoparticles prepared with ssDNA containing more G and C. Higher surface coverages increases the stability of the formed conjugates at higher salt concentrations [33-35]. Storhoff *et al.* [33] compared the stability of gold nanoparticles functionalised with oligonucleotides containing only one type of nucleobases (A, C, T, G). The surface coverage and stability of the probes prepared with ssDNA containing only T was much higher than for any other conjugates. Increase in the number of bases present in the oligonucleotides from 5 to 15 caused a further increase in the stability of the conjugates. The stability of Au nanoparticles functionalised with oligonucleotides containing other types of nucleobases were insensitive to length of ssDNA used for probe preparation [33].

To increase the surface coverage of Au nanoparticles probes a spacer containing a few T or A bases can be added to oligonucleotides between the thiol functionality and recognition sequence [15, 36]. The increase in surface coverage is not the only benefit of using spacers. The spacer distances the recognition sequence from the nanoparticles surface which increases the hybridisation efficiency due to a decrease in the steric hinderance caused by competing oligonucleotides [36]. Dougan *et al.* [15] reported that the surface coverage of Au nanoparticles functionalised with thioctic

acid modified oligonucleotides is smaller than for standard Au-thiolated DNA conjugates. When the oligonucleotides containing a poly T spacer were used a significant increase in the surface coverage for conjugates containing thioctic acid modified oligonucleotides was observed. The surface coverage of those conjugates was higher than the one observed for standard thiolated probes. The increase in surface coverage caused the increase in the stability of the conjugates towards high salt concentration. When a poly A spacer was used, the surface coverages of the probes prepared with thiolated or thioctic acid modified oligonucleotides were similar, however thioctic acid modified probes were more stable towards precipitation. It can be concluded that the presence of spacer bases and their type has a big influence on surface coverage of the conjugates produced [15].

1.3.2 Silver nanoparticle probes

The application of gold nanoparticles functionalised with oligonucleotides in DNA detection has been widely characterised [5-38]. Silver nanoparticles exhibit 100 times greater extinction coefficient than gold nanoparticles, which offers a significant increase in sensitivity, when absorption spectroscopy is used to detect them [15, 36-38]. Unfortunately, the same synthesis procedure cannot be used for the preparation of oligonucleotide functionalised silver nanoparticles as it can for gold. Addition of salt to a silver nanoparticle suspension in the same increments as used during gold nanoparticle probe preparation causes irreversible aggregation of nanoparticles. One of the ways to overcome the stability issues is to cover the silver surface with a thin layer of gold; Ag/Au core-shell nanoparticles exhibit the chemical stability of gold and the optical properties of silver nanoparticles [5, 37-40]. Thompson *et al.* [36] reported that preparation of stable oligonucleotide functionalised silver nanoparticles is possible when the following protocol is used: alkylthiol modified oligonucleotides were added to silver nanoparticles solution. After 24 hrs of equilibration 60mM phosphate buffer was added to obtain a final buffer concentration of 10 mM and the sample was allow to equilibrate for further 24 hrs. Small portions of salt were then added every 24 hrs to obtain a final salt concentration of 0.3 M. In the protocol proposed by Vidal [37] thiolated oligonucleotides were added to silver nanoparticles, then the pH was adjusted from 6 to 5 by addition of NaH_2PO_4 (pH=4.1). After 24 hrs, salt was added in 3 steps (every 8 hrs). It was found that the pH is a very important

factor during the functionalisation process. The charge of the oligonucleotide depends on the pH. Lowering the pH during probe preparation allows more ssDNA to adsorb onto the silver surface, thus increasing the stability of the conjugates. At lower pH, oligonucleotides have a less stretched conformation which allows them to pack more closely on the metal surface due to lower electrostatic repulsion between neighbouring strands [37].

Modification of silver nanoparticles with oligonucleotides causes a red shift and a slight broadening of the surface plasmon band (Figure 14). The similar effect was observed for Au nanoparticles after surface modification [36]. Silver nanoparticle probes can be used for sequence specific DNA detection in the same format of a sandwich assay as their gold counterparts. When two sets of silver nanoparticle probes containing different DNA strands were mixed together in a 1:1 molar ratio, and target complementary to both probes was added, the probes hybridised to the target, which caused aggregation of the nanoparticles [36, 38].

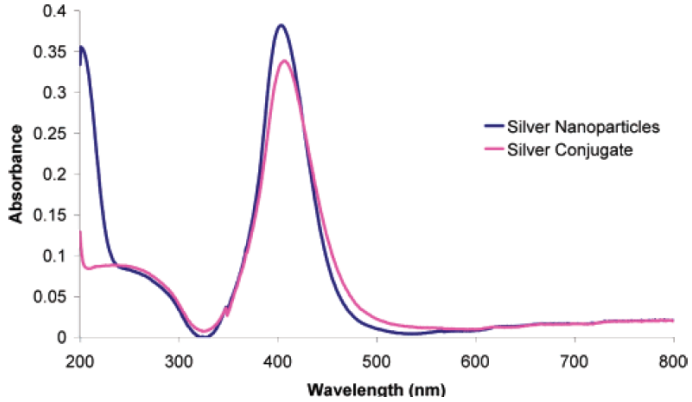

Figure 14: UV-Vis spectra of silver nanoparticles and silver nanoparticles modified with 5'-thiol modified oligonucleotide (22 bases) [36].

The hybridisation process can be monitored by the naked eye, (the colloid will change colour when aggregation occurs) or by UV-Vis spectroscopy (the silver surface plasmon band broadens and decreases) (Figure 15) [36, 37, 38].

Silver nanoparticle probes exhibit sharp melting transitions similar to the ones observed for gold nanoparticle conjugates. It had been attributed to increased cooperativity of the melting process, due to the presence of multiple linkages in the nanoparticle aggregates network [37, 38]. Lee *et al.* [38] investigated the influence of salt concentration on the melting properties of oligonucleotide functionalised silver nanoparticles. The same effect was observed as for gold nanoparticles probes,

addition of salt causes an increase of Tm value due to enhanced screening which decreases the electrostatic repulsions between the oligonucleotides [38].

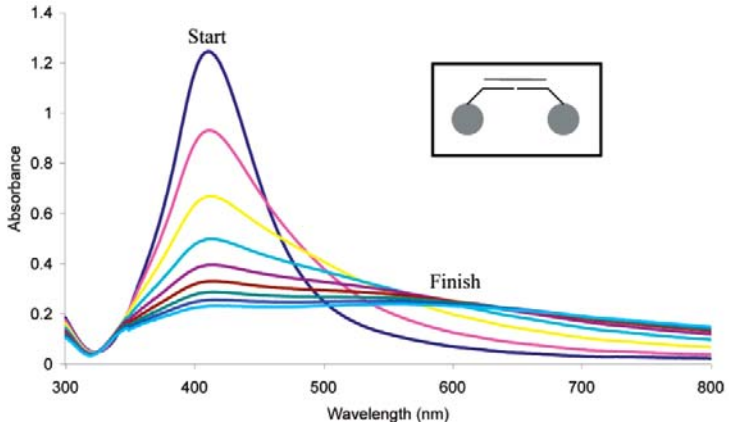

Figure 15: Changes on the UV-Vis spectrum of the sample containing two silver nanoparticle probes in the presence of fully complementary target, the probes are in a tail to tail orientation [36].

Detection of single base mismatches is possible in a silver nanoparticle based DNA detection system by comparing the melting profiles of the conjugates formed in the presence of fully complementary and imperfect target. When the duplex is formed in the presence of a mismatched target, a decrease in Tm value is observed (Figure 16) [36].

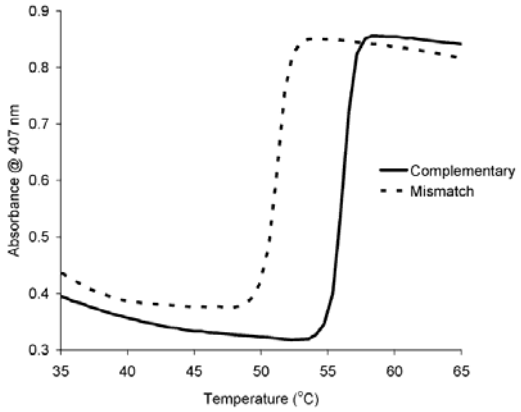

Figure 16: Melting profiles of silver nanoparticle probes in the presence of a fully complementary target and a target containing 1 base mismatch [36].

When thioctic acid modified oligonucleotides were used to prepare silver nanoparticle probes, an increase in the stability of the conjugates was observed. Addition of DTT solution to the silver nanoparticle probes prepared with thiolated

oligonucleotides caused very fast precipitation of nanoparticles. When thioctic acid modified oligonucleotides were used with silver nanoparticles the addition of DTT caused aggregation of the nanoparticles at a much slower rate (Figure 17) [15]. Although the stability of nanoparticles functionalised with thioctic acid modified oligonucleotides is higher, the surface coverages observed for those kind of conjugates are lower than those observed for thiolated DNA-Ag probes. The use of spacer bases has a big influence on gold nanoparticle surface coverages. Similar behaviour was observed for silver nanoparticle probes. The incorporation of a poly T spacer to thioctic acid modified oligonucleotides caused the increase in surface coverage from 21.1 to 331 pmol/cm^2 [15]. When a poly A spacer was used for the same purpose a much smaller increase in the surface coverage value was observed (21.1-105.7 pmol/cm^2) [15].

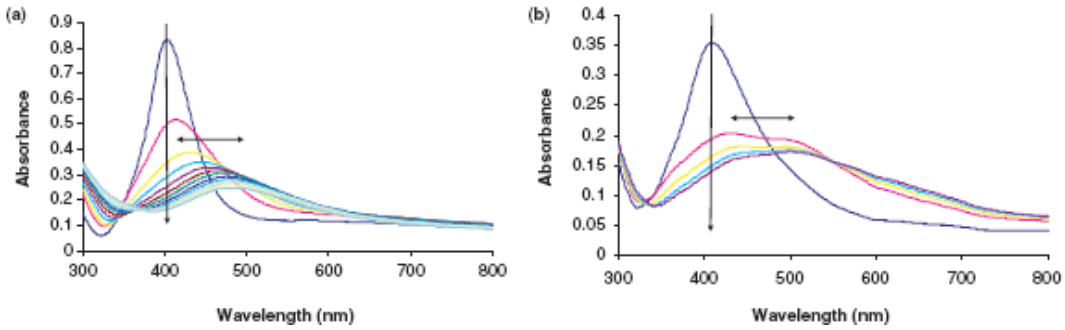

Figure 17: UV-Vis spectra showing degradation of Ag-(a) thiolated DNA (1 mins intervals) and (b) thioctic acid modified oligonucleotide (10 mins intervals) conjugates upon treatment with DTT [15].

1.3.3 Mixed metal nanoparticle probes

Due to their unique optical properties gold and silver nanoparticles have been widely used for the development of new biomolecule detection techniques and biomedical applications [5-8, 13-25, 27-33, 36-40, 42-45]. Gold nanoparticles can be easily functionalised with thiolated oligonucleotides, however their optical properties are weaker than the one observed for silver nanoparticles. On the other hand silver nanoparticles exhibit very strong optical properties but their low stability make it difficult to functionalise them with oligonucleotides [36-45]. Preparation of mixed metal nanoparticles gives the opportunity to combine the most beneficial properties of

gold and silver nanoparticles and prepare the metallic nanoparticles which exhibit optical properties of silver but chemical stability of gold nanoparticles [5, 39-45]. Synthesis and use of mixed metal nanoparticles for the detection of DNA in a sandwich assay format had been reported by many authors [5, 37-45].

Ag/Au core-shell nanoparticles exhibit chemical stability of gold nanoparticles and optical properties of silver nanoparticles. They can be prepared by passivation of silver nanoparticles with *bis*-(*p*-sulfonatophenyl)-phenylphosphine (BSPP). The gold shells are then grown on the Ag surface by treating them with $HAuCl_4$ and sodium borohydride at 0°C. The diffusion of gold atoms to silver nanoparticles is possible in a thermally activated process, lowering the temperature at which the shell is growing allows to avoid alloying [5, 39]. The extinction spectrum of Au/Ag core shell nanoparticles is very similar to the one of silver nanoparticles. The only difference is slight dampening of the silver plasmon band (10%) and the presence of a small gold plasmon band at 500 nm, when there is one layer of Au on the Ag surface. If there are two monolayers of gold formed on silver nanoparticles the silver surface plasmon band is dampened by about 50% and the gold surface plasmon band exhibits a more intense peak at the same wavelength. If the Au/Ag alloys are formed then the surface plasmon band of the obtained nanoparticles is red shifted, and broadened (Figure 18) [5, 39].

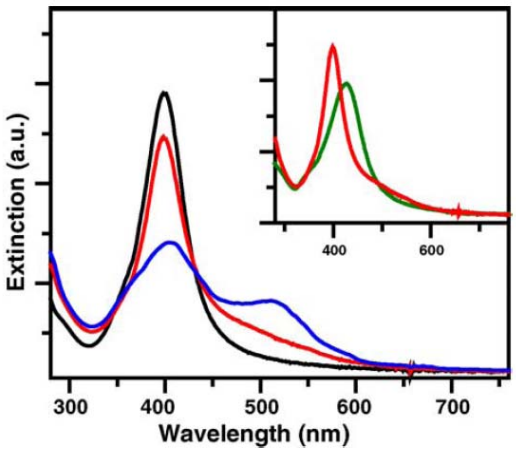

Figure 18: **Extinction spectra of Ag core (black), and Ag/Au core-shell nanoparticles with a shell thickness of one monolayer (red) and two monolayers (blue). The inset shows Ag/Au core shell nanoparticles with a shell thickness of monolayer and Ag/Au alloy nanoparticles [5].**

Au/Ag core-shell nanoparticles can be functionalised with thiolated oligonucleotides in the same way as their gold counterparts. Oligonucleotide functionalised Au/Ag core shell nanoparticles exhibit stability of ssDNA modified pure gold nanoparticles and can be resuspended in buffers containing up to 1 M NaCl concentration. Au/Ag alloy nanoparticles do not exhibit such stability and irreversibly aggregate under comparable conditions [5, 39]. Au/Ag core-shell nanoparticles after functionalisation with oligonucleotides can be used for the detection of specific DNA sequences. Unfortunately no distinct colour change is observed in this system. Formation of aggregates causes only darkening of the nanoparticle solution. The hybridisation process can be monitored by spotting the aliquot of the mixture containing both probes and the target on a C_{18} reverse-phase TLC plate. In the presence of complementary target a yellow-to-brown colour change is observed. In the case of the Au/Ag core-shell nanoparticles similar changes are observed in the UV-Vis spectrum upon hybridisation as in the pure gold system-the plasmon resonance band is dampened and red shifted (Figure 19) [5, 39].

Aggregates formed from Au/Ag core shell nanoparticles can be dispersed by heating them above the Tm of the formed duplexes. These type of probes exhibit similar sharp melting profiles as their pure gold counterparts (Figure 19) [5, 39].

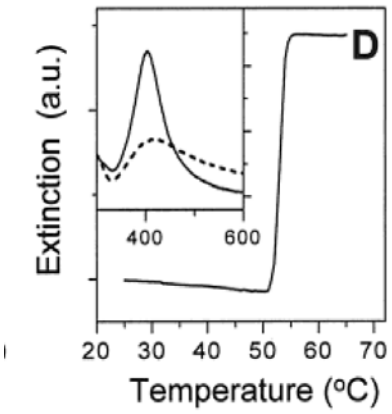

Figure 19: Melting curve of aggregates formed from hybridized oligonucleotides modified Ag/Au core shell nanoparticles in 0.3 M PBS; the insert shows the changes in the UV-Vis spectrum in the same system [39].

In the experiment performed by Cao *et al.* the effect of salt concentration on melting behaviour of aggregates formed from oligonucleotide functionalised gold and Au/Ag core-shell nanoparticles was compared. It was found that both investigated systems

have very similar melting behaviour. This is probably due to the fact that nanoparticles used in this study have similar diameters, and similar surface coverages. The increase of salt concentration causes in both cases the increase of Tm value (Figure 20) [5, 39].

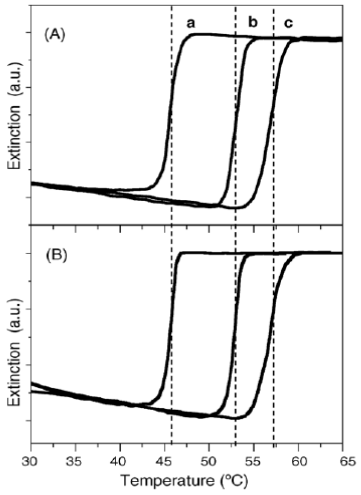

Figure 20: Thermal denaturation curves of aggregates formed from hybridized oligonucleotide modified (A)-Ag/Au core-shell, (B)-Au nanoparticles (a-0.1 M NaCl, b-0.3 M NaCl, c-0.5 M NaCl) [5].

The use of Au/Ag core-shell nanoparticles for the detection of specific DNA sequences had also been reported in the literature. Lim and co-workers [40] synthesised Au/Ag core-shell nanoparticles which are very stable at high temperatures and at high salt concentration. In their protocol gold nanoparticles were functionalised with thiolated oligonucleotides at first, then the silver shell was grown on the gold nanoparticle surface in the presence of hydroquinone and $AgNO_3$. Spacers need to be incorporated within the thiolated oligonucleotides used for Au nanoparticles functionalisation to give enough space for the silver shell to grow on the gold surface without covering the recognition sequence. The concentrations of oligonucleotide functionalised Au nanoparticles and $AgNO_3$ during the silver shell growth process has to be strictly controlled. If it is not, large, anisotropic microparticles without biorecognition properties might be formed. This is due to covering the recognition sequence in the silver shell. High stability of the nanoparticles synthesised using this method is probably due to the fact that the DNA strands are in this case embedded in the silver shell, not just attached to Au surface [40]. Formation of a silver shell on the gold surface causes a red to orange colour change.

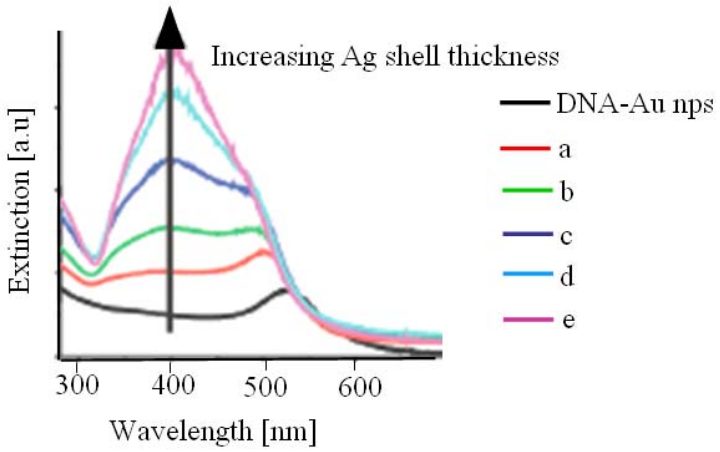

Figure 21: **UV-Vis spectrum of Au/Ag core shell nanoparticles with different silver shell thickness (a-the thinnest silver shell, e-the thickest silver shell) [40].**

The UV-Vis spectrum of Au/Ag core shell nanoparticles is strongly dependent upon the thickness of the silver shell. The thicker the shell the more the plasmon band is shifted to a shorter wavelength and the silver plasmon band becomes dominant (Figure 21) [40].

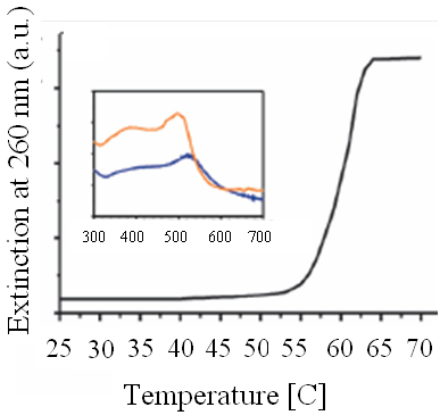

Figure 22: **Sharp melting transitions observed from aggregates formed from Au/Ag core-shell nanoparticles probes in the presence of a complementary target. The insert shows UV-Vis spectra of the same probes with (blue line) and without (red line) target [40].**

DNA embedded Au/Ag core-shell nanoparticles can be used as probes in a cross-linking DNA detection system. This process can be monitored by the naked eye (orange to dark blue colour change is observed), on a reverse phase TLC plate (spotting the aliquot of the solution containing both probes and a complementary target affords a grey spot) and by UV-Vis spectroscopy (red shift and dampening of the surface plasmon band is observed) (Figure 22). Sharp melting transitions were

also observed from the aggregates. The aggregation of the nanoparticles was not observed in the presence of non-complementary or mismatched targets [40].

Doria [41] and Link [42] reported the use of alloy nanoparticles, which can be easily synthesised in a one step citrate co-reduction process, for the detection of specific DNA sequences. Alloy nanoparticles exhibit an intense, single, surface plasmon resonance band as silver nanoparticles (Figure 18) [5, 41] and they can be modified with thiolated oligonucleotides as gold nanoparticles [41]. Cao *et al.* [5] reported difficulties during preparation of oligonucleotide functionalised Au/Ag alloy nanoparticles. The alloy nanoparticles used in his study contained only 16% of Au. Doria and co-workers [41] suggested that increasing the proportion of Au during the citrate co-reduction process may help overcome the observed difficulties. Alloy nanoparticles prepared using the method described by this group contained more Au (47%), thus the gold availability on the nanoparticles surface increased and the nanoparticles could be easily functionalised with thiolated oligonucleotides using the same protocol as for gold nanoparticles [41]. The modification of the surface of alloy nanoparticles with oligonucleotides causes a red shift of the surface plasmon resonance peak, analogous to what has been observed for their pure gold counterparts after functionalisation with thiolated ssDNA [41].

Au/Ag alloy nanoparticles functionalised with thiolated oligonucleotides have been used as probes in a non-cross-linking DNA detection assay. In the presence of complementary target the probe solution remained yellow and no changes in the position of the surface plasmon band was observed in the UV-Vis spectrum. In the absence of target or in the presence of non complementary target, a yellow-to-blue colour change and a red shift of the surface plasmon band was observed [41-43].

1.4 DNA detection by SERRS

1.4.1 Raman Spectroscopy

Raman spectroscopy, similar to infrared spectroscopy, is a spectroscopic technique which detects vibrations in molecules and allows the identification of substances from characteristic fingerprint spectra obtained [46]. There are several possible ways for light to interact with matter: the light can be absorbed, scattered or pass through the material. The photon is absorbed only when its energy corresponds to the energy gap

between the ground and excited states of a molecule. Light absorption is used in numerous spectroscopic techniques such as: X-ray absorption, infrared absorption, electronic absorption, fluorescence emission or vacuum ultraviolet spectroscopy. In order to be scattered from a molecule, the incident photon does not need to have energy which matches the difference between energy levels in a molecule. When the light is scattered from a molecule most scattered photons have the same energy as the incident photons. This commonly occurring process is known as the elastic light scattering or Rayleigh scattering. Rayleigh scattering does not involve any energy change. A small fraction of light can be inelastically scattered from a molecule. In this process energy is transferred from the incident photon to the molecule or from the molecule to the scattered photon. As a result the scattered photons have different energy than the incident photons. The process of inelastic light scattering is known as the Raman effect. When the laser interacts with electrons of a molecule it causes polarization of the electron cloud and virtual states with energy dependent upon the frequency of light source used are created. At room temperature most molecules are present at the lowest energy vibrational levels. The type of Raman scattering in which the absorption of energy from incident photon to molecule causes promotion of the molecule to a higher energy vibrational state is called the Stokes scattering. Some molecules can be present in excited vibrational states. When the light is scattered from a molecule in an excited state, energy transfer from the molecule to the scattered photon occurs. This process is known as the anti-Stokes scattering (Figure 23). The anti-Stokes scattering is a much weaker process than the Stokes scattering, although both spectra contain the same frequency information [46-47].

Raman scattering causes changes in vibrational, rotational or electronic energy of a molecule. The energy difference between the incident and scattered photon is equal to the energy of a vibration of the scattering molecule. Vibration needs to cause a change in the polarizability of the electron cloud of the molecule in order to be a source of intense Raman scattering, thus symmetric vibrations give the greatest scattering. In contrast, in infrared spectroscopy which is a vibrational technique as well, the most intense absorption is observed from the vibrations which cause changes in the dipole moment of the molecule, so asymmetric vibrations give the most intense response. Due to that selection rule Raman scattering and infrared spectroscopy are often used as a complementary techniques which, when used together, allow for better vibrational characterization of a molecule. The only exception from the above

selection rules are centrosymmetric molecules, which do not have bands active in both Raman scattering and infrared spectroscopy (mutual exclusion rule) [46, 47].

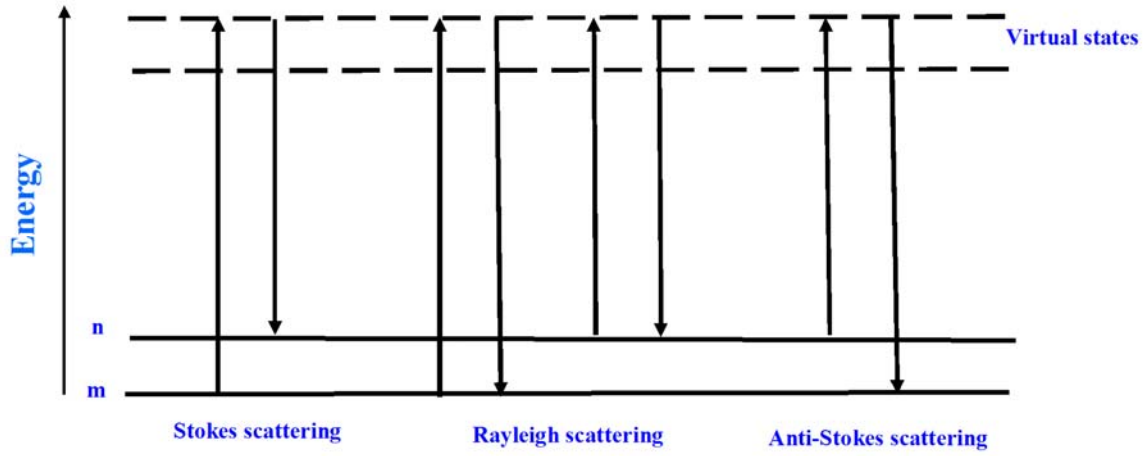

Figure 23: Diagram of Rayleigh and Raman scattering [46].

A plot of the intensity of scattered light versus energy difference is a Raman spectrum. Raman spectroscopy is commonly used in chemistry, since vibrational information is very specific to the chemical bonds present in the molecule. It therefore provides a fingerprint by which specific molecules can be identified [46-47].

1.4.2 Surface Enhanced Raman Scattering (SERS)

Although Raman spectroscopy is a very powerful tool for characterizing the physical and chemical properties of materials, this method suffers from a number of limitations, such as very weak signals and fluorescent interference which is usually much more intense and can swamp the weak Raman signal. Surface enhanced Raman scattering (SERS) is a more sensitive form of Raman spectroscopy in which the Raman active molecule of interest is in close contact with a suitable, roughened metal surface [46, 49, 50-52]. Large signal enhancement is attributed to high electromagnetic fields associated with surface plasmon resonances at the interstices between nanoparticles (hot spots) [48].

This technique was reported for the first time by Martin Fleischman and co-workers in 1974, when strong Raman signals from pyridine adsorbed on a silver electrode were observed [46, 49]. SERS gives an enhancement factor of 10^6 in

scattering efficiency when compared with normal Raman scattering [46, 49]. Many different metals can be used for enhancement, however gold and silver are the most commonly used [51].

SERS offers numerous advantages when compared with normal Raman Scattering: higher sensitivity; fingerprint spectra obtained in this technique make it possible to identify components of a mixture without extensive separation procedures. The other advantage of using of metal surfaces for enhancement is the fluorescence quenching ability of the metals used [51].

1.4.3 Surface Enhanced Resonance Raman Scattering (SERRS)

Surface enhanced resonance Raman scattering (SERRS) is an extremely sensitive form of Raman spectroscopy in which a coloured molecule is adsorbed onto a suitable roughened metal surface. The combination of surface enhancement provided by adsorption of the analyte on a metal surface, and a molecular resonance from the chromophore which is present in the molecule of interest gives a vibrational spectrum with very high sensitivity (Figures 24 and 25).

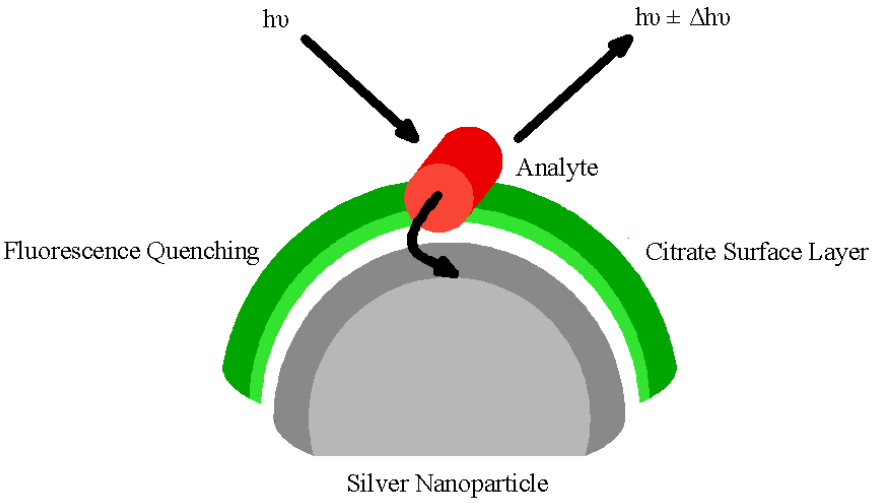

Figure 24: The SERRS process involving adsorption of a coloured analyte on to the silver nanoparticle covered in a citrate surface layer [53].

In order to observe enhancement, the molecule needs to be adsorbed on to the metal surface and the excitation frequency of the light source has to be close to the absorption maximum of the dye and the plasmon of metal surface [46, 49, 53]. Many metals can be used to provide the surface, such as gold, silver, copper, aluminium,

however it was observed that silver, especially silver nanoparticles are a source of the largest enhancement [46, 49, 53]. Further development indicated that after aggregation of nanoparticles the observed SERRS signal is even more intense [50, 58, 67]. The experiments performed by Faulds *et al.* [58] indicated that during the aggregation process a wide range of differently sized aggregates is formed, however only clusters which have a plasmon resonance close to the excitation frequency will cause the signal enhancement. SERRS gives an enhancement factor of 10^{10} over normal Raman scattering and gives the possibility of detection on a single molecule level [46, 49, 53].

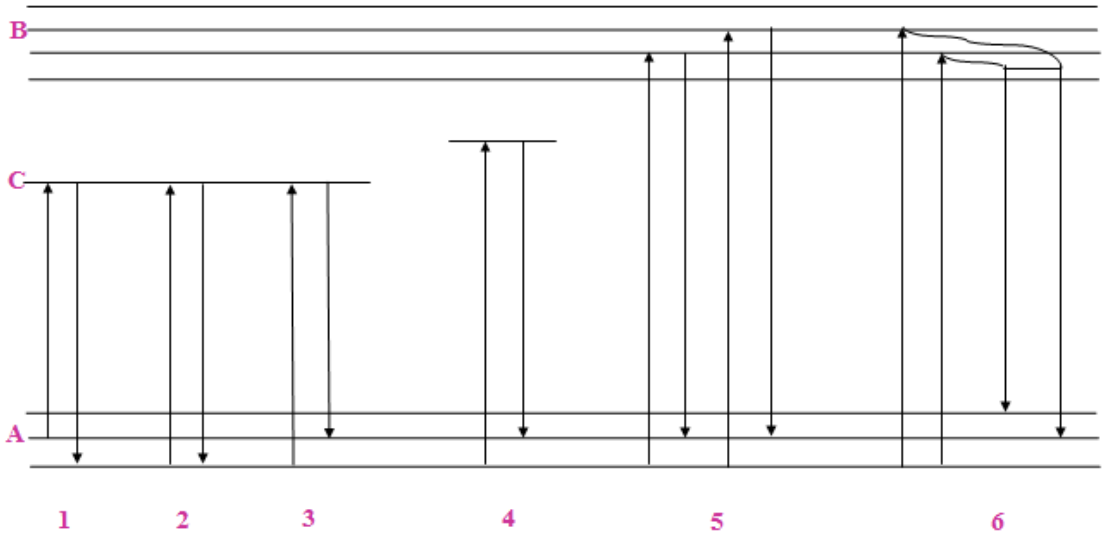

Figure 25: Jablonsky diagram of: Raman scattering (1-anti-Stokes, 3-Stokes), Rayleigh scattering (2), pre-resonance Raman scattering (4), resonance Raman scattering (5) and fluorescence (6). A-ground electronic state, B-excited electronic state, C-virtual energy levels.

The enhancement provided by the surface is explained by resonance between the optical fields and the surface plasmon resonance of the metal nanoparticles which enhances the electromagnetic field. The biggest enhancement was observed for electromagnetic 'hot spots' which are defined as interstices in a SERS substrate e. g nanoparticles (electromagnetic enhancement) [54-55]. Further enhancement observed in the presence of a molecule which is in resonance with the excitation frequency of the light source is explain by a chemical enhancement mechanism attributed to a charge-transfer interaction of molecules adsorbed on the metal surface [54-55].

Due to the sharp fingerprint spectra produced SERRS allows identification of the components of a mixture without separation. This techniques offers numerous advantages over other commonly used analytical tools, such as fluorescence: the power required to obtain scattering is low, the sensitivity is at a single molecule level and there is the possibility of analysing aqueous samples as water is a weak Raman scatterer. An additional advantage of SERRS is the ability of metal surfaces to quench any fluorescence produced so a wide range of fluorophores including fluorescent dyes can be used to prepare SERRS active analytes [46, 53]. One of the most important limitations of SERRS is the need to adsorb the analyte on the metal surface and the fact that not all molecules give a good SERRS signal. One of the ways to overcome this is to add a strong SERRS label to the analyte. A wide range of different chromophores can be used for that purpose due to the fluorescence quenching ability of the metal surfaces [46, 53].

Nowadays most DNA detection methods are based upon hybridisation of fluorescently labelled oligonucleotides to complementary targets and the detection of the product by fluorescence spectroscopy [5, 7-12, 51, 56]. This commonly used technique has numerous disadvantages such as the fact that the spectra produced tend to have broad overlapping outputs which make it impossible to identify components of a mixture without separation. The other drawback of this technique is requirement to amplify the number of DNA copies present in the original sample by PCR, which increases the risk of contamination and false-positive results [50, 51, 56, 63]. SERRS offers numerous advantages over fluorescence spectroscopy, such as sensitivity at a single molecule level and also, due to the fingerprint spectra obtained, the identification of the components of a mixture is possible without separation [56, 57, 63, 70]. Faulds *et al.* compared detection limits of fluorescence spectroscopy and SERRS and found that the SERRS detection limits were at least three orders of magnitude lower than the one observed for fluorescence spectroscopy [56]. Therefore this indicates that SERRS can be a more sensitive technique and can be a very powerful tool for biomolecular diagnostics [51, 56, 63].

1.4.4 Detection of specific DNA sequences by SERRS

In order to obtain a SERRS a coloured molecule of interest has to be immobilised on a suitable, roughened metal surface. DNA does not meet the requirements for

SERRS due to the lack of a visible chromophore in its structure and also the presence of the highly negatively charged phosphate backbone which prevents electrostatic interaction with the metal surface [49, 53, 54, 59, 63, 64, 66, 67, 70, 79, 80, 85]. Barhoumi *et al.* [52] reported that the SERS signal might be obtained from Au nanoshells functionalised with thiolated oligonucleotides after heating the probes to 95°C to ensure extended conformation of DNA on the nanoparticles surface, however regardless of the oligonucleotides composition and sequence the spectra obtained were dominated by adenine signals even for strands with low adenine content.

1.4.4.1 Preparation of SERRS active DNA

To obtain a SERRS signal from a DNA sequence a coloured molecule has to be attached to a DNA strand and also some form of positive charge needs to be present in solution to screen the electrostatic repulsions between the negatively charged phosphate backbone and the metal surface, to allow electrostatic adsorption of DNA. The other way to attach DNA to nanoparticles is to modify the DNA strand with a label containing group which will bind strongly to the nanoparticles surface, e. g thioctic acid for gold nanoparticles or benzotriazole for silver nanoparticles [49, 53, 59, 63, 64]. Either a non-sequence specific intercalator or a specific label covalently attached to a unique probe can be used as a coloured label [49, 53, 54, 59, 63, 64, 66, 67, 70, 79, 80, 85].

1.4.4.1.1 Intercalating dyes

In the case of the DNA intercalation, a ligand of appropriate size and chemical nature fits itself between the DNA base pairs or in the minor groove of double stranded DNA. When double stranded DNA is present in the solution containing intercalator, the dye will intercalate between base pairs. When oligonucleotide functionalised nanoparticles are used as probes, the dye, when intercalating, will adsorb on the metal surface which will be a source of a strong SERRS signal. The disadvantage of using intercalating dyes is that sequence specific information is not generated and also there is no discrimination between DNA bound intercalator, and the intercalator adsorbed on the metal surface but not complexed to the DNA [49, 70].

1.4.4.1.2 Electrostatic adsorption of dye labelled DNA on to the metal surface

Covalent attachment of a dye to a DNA strand offers numerous advantages over the use of intercalating dyes, such as a large number of commercially available fluorophores and dyes which can be used for this purpose (the metal surface will quench any fluorescence produced) and generation of sequence specific information [49, 59]. If the fluorophore used is negatively charged then the overall charge of the oligonucleotide is negative and the electrostatic adsorption of DNA on to the nanoparticle surface is not possible. Some kind of charge neutralising agent, e. g. spermine or poly-*L*-lysine has to be added to the solution to reduce the DNA charge. The use of spermine, which is also an aggregating agent has an additional advantage. It will cause aggregate formation, thus providing maximum enhancement in SERRS. The neutralisation of the DNA backbone is not sufficient enough to electrostatically adsorb oligonucleotides modified with a negatively charged label on the nanoparticles surface and modified DNA bases such as propargylamine modified 2'-deoxyuridine need to be incorporated into the DNA as well. These modified bases contain primary aliphatic amine groups which are protonated at physiological pH [59, 63, 66, 70, 79, 80]. Previously it was recommended to use 6 modified bases in order to obtain a SERRS signal from the oligonucleotide functionalised with a negatively charged label [59, 63, 66, 70]. McKenzie *et al.* [59] compared the SERRS signal obtained from silver nanoparticles functionalised with oligonucleotides modified with a negatively charged dye and containing zero, one, two, four or six 5-aminopropargylamine-2'-deoxyuridine bases. Spermine was used as a charge neutralising agent. It was found that the intensity of the SERRS signal increases when the number of modified bases present in DNA backbone increases, however for low probe concentrations, the oligonucleotides containing 4 or 6 modified bases gave the same analytical response as the probe which contained only two propargylamine modified bases. It was concluded that incorporation of two modified bases to oligonucleotides is the preferred modification in order to obtain an intense SERRS signal from the probe containing a negatively charged dye (Figure 26 A) [59, 63].

These two actions (the use of charge neutralising agent and the incorporation of propargylamine modified bases into DNA backbone) will change the overall DNA charge to positive and allow the electrostatic adsorption of modified DNA on to the nanoparticle surface [49, 79, 80].

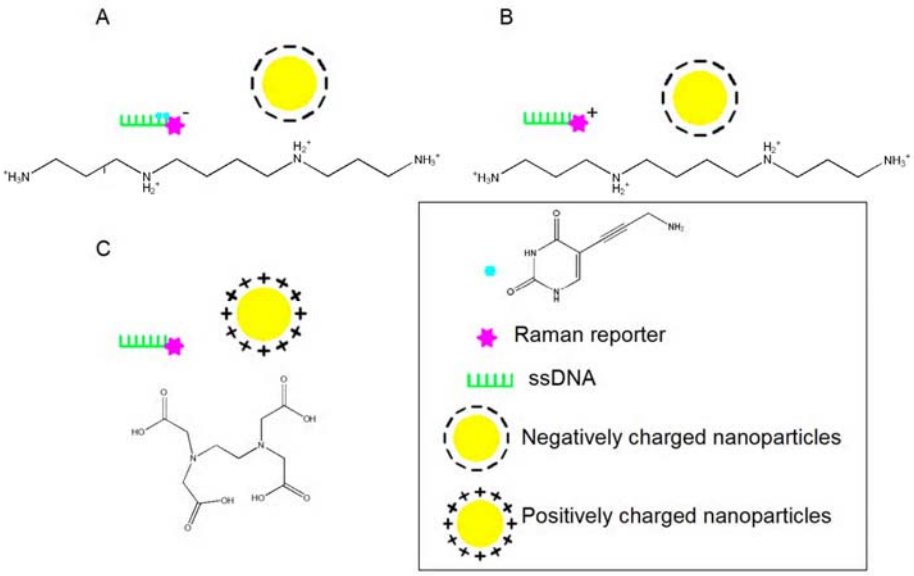

Figure 26: **Preparation of SERRS active DNA by electrostatic adsorption of dye labelled oligonucleotides to nanoparticle surface, A- when negatively charged dye is used, B-when positively charged dye is used, C-when positively charged nanoparticles are used.**

If a positively charged dye is used to modify oligonucleotides, the incorporation of modified bases into the DNA backbone is not necessary, however a charge neutralising agent should be used to make adsorption of oligonucleotides on to the nanoparticles surface possible. If spermine is used as a charge neutralising agent it will cause nanoparticle aggregation thus increasing the SERRS signal intensity (Figure 26 B) [49, 59].

A different approach of obtaining a SERRS signal from dye labelled DNA was reported by Gill and co-workers [71]. Positively charged cetyl trimethyl ammonium bromide (CTAB) coated silver nanoparticles were mixed with Rhodamine 6G labelled single stranded DNA in Tris-Tween buffer. The addition of the negatively charged oligonucleotide to the solution containing positively charged nanoparticles caused slow aggregate formation due to the reduced electrostatic repulsions between the nanoparticles and the development of a SERRS signal with time. In order to reduce electrostatic repulsions between the positively charged nanoparticles, molecules containing multiply carboxyl groups [citrate-(3 carboxyl groups), EDTA-(4 carboxyl groups)] were used in a similar manner as spermine. It was found that addition of a charge neutralising agent increased the aggregate formation rate. It was noticed that

the efficiency of EDTA, which contained more carboxyl units was better. The use of positively charged silver nanoparticles offers several advantages over the assays based on negatively charged nanoparticle probes. A wide range of positively and negatively charged dyes can be used to functionalised oligonucleotides without the need of incorporation of modified bases into the DNA backbone which lowers the cost of probe preparation. Also, polycarboxyls used as a charge neutralising agents do not interact with oligonucleotides (polyamines such as spermine adsorb onto DNA molecules) (Figure 26 C) [71].

1.4.4.1.3 Covalent attachment of dye-labelled DNA on to the metal surface

SERRS active oligonucleotide functionalised nanoparticles can also be prepared by adsorption of thiolated or disulphide modified dye labelled oligonucleotides on metallic nanoparticle surfaces using the well known sulphur-Au (or Ag) surface chemistry [63, 54, 67, 78]. When this approach is used there is no need for incorporation of modified bases into the DNA backbone, or the use of an aggregating agent as the addition and hybridisation of the functionalised nanoparticles to a target oligonucleotide causes aggregation [67, 78]. This approach is commonly used in SERRS based DNA detection assays [60, 64, 68, 73, 74].

In order to prepare SERRS active oligonucleotide functionalised nanoparticles a custom made label containing a Raman active tag and a surface complexing group which will replace the weakly bound layer of charged ligands initially used to stabilise nanoparticles may be used [49, 50, 53]. The use of such a label causes the formation of a protective layer on the nanoparticle surface, thus increasing the stability [61]. For example benzotriazole, which binds strongly to silver nanoparticles can be made into an azo-dye form in such a way that it will still have additional chemical functionality (phosphoramidite, maleimide or COOH group) which will allow attachment of an oligonucleotide to the label [53, 56, 63]. The synthesised label contains a Raman active fluorophore-azo dye, a surface complexing group-benzotriazole, and a chemical functionality for biomolecule attachment [53]. Similar approach was presented by Mackenzie and co-workers [65]. Trifunctional linkers containing thioctic acid to allow adsorption of the label on the metal surface, a Raman active tag and a free carboxyl group which can be reacted with biomolecules of interest were synthesised (Figure 27) [65].

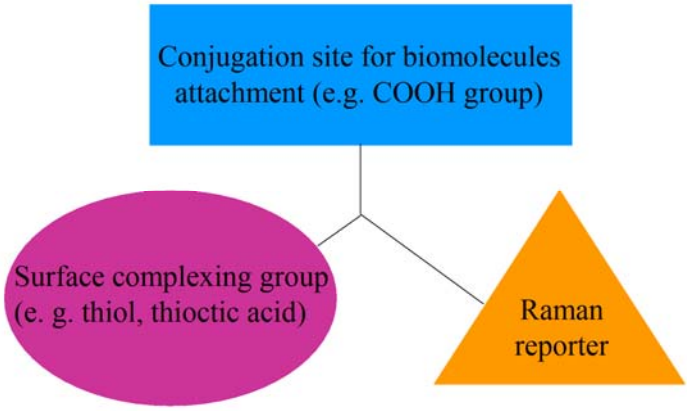

Figure 27: Label allowing preparation of SERRS active nanoparticles for biomolecules detection.

The formed conjugates exhibit very high stability, offer the possibility of conjugation with different types of biomolecules and can be used in a wide range of biological and bioanalytical applications [65].

Doering and co-workers [72] proposed a slightly different approach allowing the preparation of SERRS active, stable gold nanoparticles. Core-shell nanoparticles containing a gold core for optical enhancement, reporter molecule (organic dyes containing an isothiocyanate group or multiple sulphur atoms to allow adsorption on gold surface) for spectroscopic signature and a silica shell for protection and conjugation purposes were synthesised. The nanoparticles were stable in aqueous electrolytes and organic solvents and gave a strong SERRS response however the use of such probes for biomolecule detection has not been reported [72].

A different approach in order to obtain SERRS active silver nanoparticles with possibility of functionalising them with biomolecules was presented by Cormack *et al.* [61]. A Raman active label was synthesised by reacting the anhydride unit of a commercially available copolymer of styrene and maleic anhydride with a SERRS active benzotriazole based azo dye. The chromophore contained an ethylamine fragment with a free carboxyl group which was used for biomolecule attachment. The presence of the benzotriazole unit within the label allowed the attachment of macromolecules to the silver nanoparticles surface. The label was synthesised in such a way that the more hydrophobic part of the polymer containing the azo dye and the benzotriazole was located in close proximity to the silver surface. The more hydrophilic part containing the carboxylate groups pointed outwards allows multiple attachment points for biomolecules. The nanoparticles exhibited very high stability at

high NaCl concentrations and gave permanent, intense SERRS signal even after storing them for one month [61].

Wang and co-workers [62] prepared a mixed monolayer of a Raman label, containing an aromatic thiol or disulphide, and antibody on gold nanoparticles. However they noticed that exchange of the weakly adsorbed antibodies was occurring between the nanoparticles labelled with different Raman tags which gave false results. To overcome this problem they synthesised a bifunctional Raman label containing a source of strong Raman scattering, a disulphide group which allows the adsorption of the label on gold nanoparticles surface and a succinimidyl group which could be reacted with a biomolecule of interest, in this case an antibody. In an alternative approach, in order to eliminate the time consuming label synthesis process a mixed monolayer of two commercially available thiolates was prepared on a gold nanoparticle surface. One of the thiolates contained succinimidyl functionality to allow biomolecule (antibody) attachment, the other one contained a strong Raman scatterer. Covalent attachment of the antibody significantly minimizes the possibility of antibody exchange between nanoparticles. Probes prepared in the described method gave a strong SERRS response and offered the possibility of detection of components of a mixture without extensive separation procedures [62].

1.4.4.2 Homogenous DNA detection assay

A homogenous assay which allows detection of multiple targets in a short time was proposed by MacAskill *et al.* [81]. The method is based upon the much stronger affinity ssDNA has to a metallic nanoparticle surface compared to the one observed for dsDNA. When fluorescently labelled single stranded DNA is present in the silver nanoparticle suspension oligonucleotides will adsorb on to the silver nanoparticles surface which will be a source of Raman scattering. However when a target complementary to the labelled sequence is added to the system, dsDNA, which will not adsorb strongly on the silver surface, is formed, thus a decrease in the intensity of SERRS signal is observed. The method was used to detect methicilin-resistant *Staphylococcus aureous* (MRSA). The identification of the absence or presence of the MRSA was possible within 3 hours; the conventional culturing methods used for that purpose required 48 hrs [81].

1.4.4.3 Indirect DNA detection

The vast majority of SERRS based DNA detection assays rely upon the observed enhancement of SERRS signal when Raman active dye functionalised nanoparticle probes hybridise to a complementary target (Figure 28).

Vo-Dinh *et al.* [73, 74] reported detection of the HIV Gag Gene [73] and breast cancer susceptibility gene BRCA 1 [74, 77] by SERRS. In order to detect the HIV gene, the capture DNA strand was bound to a polystyrene substrate, then PCR amplified target modified with cresyl fast violet (CFV) was added. The polystyrene substrate was then covered with a thin layer of silver. When the CFV labelled probes hybridised to the capture strand bound to the polystyrene support, strong SERRS signals were observed [73]. A similar method was used within the same group to detect the breast cancer BRCA 1 gene. In this case the capture strand was covalently attached to a glass plate covered with a thin layer of silver. After addition of Rhodamine 6G, Rhodamine B or Rhodamine 110 labelled oligonucleotides, strong SERRS signals were observed if the hybridisation of the dye labelled strand to the strand attached to silver coated glass plate occurred [74, 77].

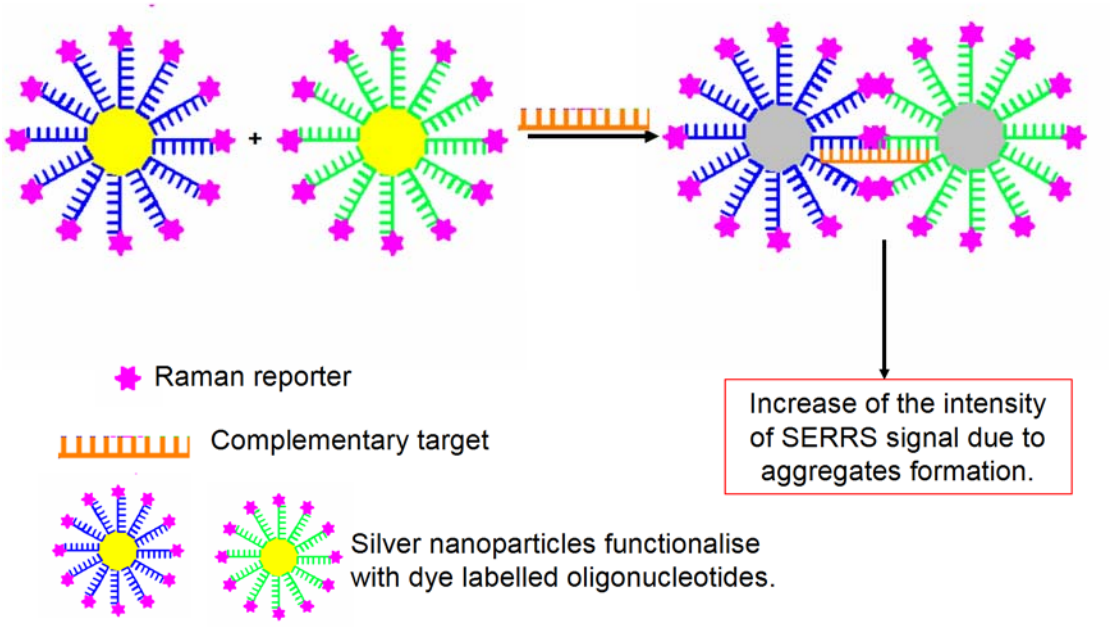

Figure 28: Typical SERRS based DNA detection assay.

Cao and co-workers reported that for 13 nm Au nanoparticles functionalised with thiolated, dye modified oligonucleotides no SERRS signals were obtained,

however coating of those probes with a layer of silver (Ag^+, hydroquinone) resulted in a strong SERRS response from several dyes used in this study (Cy 3, Cy 3.5, TAMRA, Texas Red, Rhodamine 6G) [64]. Six different DNA sequences and two RNA targets with a single nucleotide polymorphism were successfully detected using this method. Stokes *et al.* [67] indicated that careful selection of chromophore used for oligonucleotide modification make it possible to obtain strong SERRS signals from thiolated oligonucleotide functionalised Au nanoparticles without covering them with a layer of silver. In that experiment the detection limits of gold and silver nanoparticles with oligonucleotides modified with commercially available dyes (Cy 3.5, Cy 5.5, Bodipy, TR-X, Rox, Cy 5) were compared. It was found that when the light source excitation frequency is in resonance with the molecular chromophore present within the probe, the signal intensity observed from Au nanoparticles is greater than the one observed from silver nanoparticles. The use of non-toxic gold nanoparticles in the place of silver in SERRS based DNA detection assays gives the possibility of using this technique in a wide range of molecular biodiagnostics applications [67]. Creation of stable, non-toxic probes allowing the detection of the biomolecules inside living organisms is currently one of the biggest challenges of the molecular diagnostics. Biocompatible, stable, SERRS active gold nanoparticle probes open up the possibility of in vivo, real-time detection of the biomolecules of interest.

A similar DNA detection assay was presented by Mahajan *et al.* [83]. FAM labelled, thiolated oligonucleotides were immobilised on a gold surface. When Cy 3 modified complementary target was added the intensity of FAM signals on the observed SERRS spectrum decreased, however new bands assigned to Cy 3 appeared. When the target was removed during denaturation only FAM signals were observed. The hybridisation/denaturation process was repeated several times and the same spectroscopic changes were observed in each case. Detection of mutations and single nucleotide polymorphisms using the same assay were presented by the same group. In the experiment, adsorption of thiolated oligonucleotides on the gold surface was followed by treatment with mercaptohexanol to ensure an upright DNA conformation and prevent non-specific binding. Fluorescently labelled, complementary or mismatched targets were then added and strong SERRS signals were observed upon hybridisation. In order to detect mismatches the temperature was slowly increased while SERRS spectra were recorded. By plotting the intensity of a SERRS band versus temperature, Tm of the duplexes can be found. The Tm of duplexes formed in

the presence of imperfect targets is lower than the one observed for dsDNA formed in the presence of fully complementary target, thus the mutations and single nucleotide polymorphisms can be easily detected in the SERRS melting system [83].

A mixed metal SERRS DNA detection system, where two different sequences are immobilised on different type of metallic nanoparticles was reported by the Graham group [84]. 13 nm Au nanoparticles were functionalised with thiolated oligonucleotides and the Raman reporter-malachite green isothiocyanate. A second probe was prepared by functionalisation of 13 nm Au or 35 nm Ag nanoparticles with thiolated oligonucleotides only. Addition of a complementary target to the solution containing the dye coded Au probe and the oligonucleotide functionalised silver nanoparticles caused a significant increase in the intensity of the SERRS signal. In a similar experiment, where two sets of gold nanoparticle probes were used, addition of a complementary target caused only small changes in the SERRS spectrum. It was concluded that gold-gold plasmon resonance coupling is not as effective as gold-silver or silver-silver plasmon resonance coupling. The mixed metal system offers numerous advantages over previously used single metal assays. It was confirmed that only one of the probes has to be modified with reporter molecule and due to higher stability and better known surface chemistry it is more advantageous to use gold nanoparticles for that purpose. Silver nanoparticles provide much better enhancement effects than their gold counterparts [84].

Thuy and co-workers [82] reported an easy to use, rapid and robust SERS based DNA detection assay, where gold nanoparticles functionalised with thiolated oligonucleotides were used, but the presence of a fluorescent label or precise temperature control was not necessary. Two sets of gold nanoparticles functionalised with different, thiolated sequences were prepared. One of the oligonucleotides used contained a photolinking group (5-carboxylvinyl-2'-deoxyuridine) which reacts with the cytosine present in the second strand after UV radiation exposure. When two probes were mixed together in cacodylate buffer, which acted as hybridisation buffer and Raman reporter molecule, and the complementary target added, the target cross-linked the nanoparticles by hybridisation. After exposure of the sample to UV radiation covalent bonds between the oligonucleotides attached to the gold nanoparticles were formed by photoligation. The SERS signal from cacodylate ions present in interspaces between nanoparticles was successfully detected. When one probe, target DNA or UV exposure was absent SERS signal was not produced [82].

In other approach presented by Graham *et al.* [50, 60] silver nanoparticles were modified with a benzotriazole based azo-dye first, then thiolated oligonucleotides were added to form the conjugates. Two sets of dye coded oligonucleotide functionalised nanoparticles containing different probe sequences but the same chromophore were prepared. When a target complementary to both probes was added to the solution, controlled aggregation of the nanoparticles caused by hybridisation of the probes to target occurred and an enhancement of the intensity of SERRS signal was observed [60]. The use of different dye-coded nanoparticles functionalised with different probe sequences allowed the identification of multiple targets within the same sample [60]. The biggest disadvantage of the presented method is the possibility of irreversible aggregation of the nanoparticles after addition of hydrophobic, often positively charged dyes to the silver nanoparticles. A method which overcomes this problem was reported from the same group. McKenzie *et al.* [68] functionalised silver nanoparticles with thiolated, poly-ethylene glycol (PEG) modified oligonucleotides at first. These stable conjugates were then incubated in aqueous solution of SERRS active dye. The use of the PEG spacer increased the surface coverage and stability of the probes and prevented their non-specific aggregation in the presence of the dye [68, 69]. Such probes were successfully used in a SERRS based DNA detection system [68]. A similar approach was used in the Irudayaraj group for the simultaneous detection of eight DNA sequences in a mixture. The only difference is that non-fluorescent Raman tags, such as 4-mercaptopyridine were used for probe preparation [76]. Aggregation of metallic nanoparticles after addition of Raman active dyes to their suspension might be beneficial in order to obtain SERRS active probes for biomolecules detection.

1.4.4.4 Overall summary

SERRS is a very powerful technique, which can be used for the detection of biomolecules. It offers numerous advantages over the methods commonly used for that purpose, such as higher sensitivity (detection of single molecules was reported by many authors [49-53, 55-57, 67, 70, 78, 81]) and the possibility of the detection of components of a mixture without extensive separation procedures. The biggest problem which has to be overcome in order to use this technique for DNA detection is to prepare SERRS active DNA. This can be achieved by adsorption of DNA on a

suitable metal surface, and addition to DNA strand a Raman active molecule. Many ways to prepare such probes exist, e. g. electrostatic adsorption of dye labelled oligonucleotides on nanoparticles surface in the presence of charge neutralising agent [49, 59, 63, 66, 70, 79, 80], covalent attachment of thiolated, dye modified oligonucleotides to Au or Ag nanoparticles surface [54, 64, 67, 73, 74, 78, 83, 84], the use of multifunctional labels, which contain a Raman active tag, a surface complexing group and a conjugation site allowing biomolecules attachment [65] or formation of mixed monolayers of thiolated oligonucleotides and molecules containing Raman reporters [50, 53, 56, 60, 63, 68, 69, 76] on nanoparticles surface. The number of techniques allowing preparation of SERRS active probes for biomolecules detection and the advantages of this technique over other, traditional detection assays make it a very powerful tool in molecular biodiagnostics.

1.5 SERS as a tool for pH sensing.

Development of a nanosized, optical probe capable of providing information about the changes in the chemical environment inside living cells is a very important area of cell biology and biochemistry research [88, 89, 94]. The pH values inside different compartments of a cell varies due to their specific functions. Also the pH value inside some organelles, such as endosomes can also change over time. It was reported that acidification of endosomal pH plays a central role in numerous pathologies such as cystic fibrosis, kidney diseases and certain types of cancer. The possibility to measure the chemical changes inside living cells would allow improved understanding of the biochemistry of diseases [87, 88, 94, 95].

The use of SER(R)S measurements inside cells is of growing interest. This kind of measurement enables spatial resolution allowing the chemical probing of intracellular structures. The collection times are suitable for studying cellular processes and many stable probes and labels can be used which increases the multiplexing ability of the technique [87, 97]. Many authors reported that gold and silver nanoparticles can be used as nanosensors after their introduction inside living cells [55, 87-93, 95, 99]. Biocompatible gold nanoparticles introduced into cells deliver enhanced Raman signals of the biological molecules present in the cell. This can allow information to be obtained about structures present within the cell. Both gold and silver nanoparticles, after labelling them with a Raman active tag, can be used to analyse

intracellular structures by observing the SERS spectra of the reporter molecules used as probes [87-93, 95]. Metallic nanoparticles functionalised with reporter molecules exhibiting pH dependent SERS signals can be used as an intracellular pH meter [55, 87, 88, 89, 95, 98, 99]. Numerous Raman active molecules have been used to prepare such probes. The use of 4-mercaptobenzoic acid, whose carboxyl group will dissociate at higher pH values, as a pH sensing molecule has been reported in the literature (Figure 31) [55, 87, 95, 98, 99]. Kneipp *et al.* [55, 87, 95] functionalised gold nanoparticles with 4-mercaptobenzoic acid. Plotting the ratio of intensity of COO^- stretching mode at 1423 cm^{-1} (which can be used to indicate the dissociation of carboxyl group) against the intensity of aromatic ring vibrations at 1076 cm^{-1} versus pH value of the surrounding solution allowed the generation of a calibration curve, which was used to detect the pH value inside living cells [55, 87, 95, 98]. The use of the intensities of two peaks within the same SERRS spectrum allows quantitative measurement without any corrections regarding cellular background [55, 87]. The sensor allowed detection of a pH range between 5.8 and 7.6.

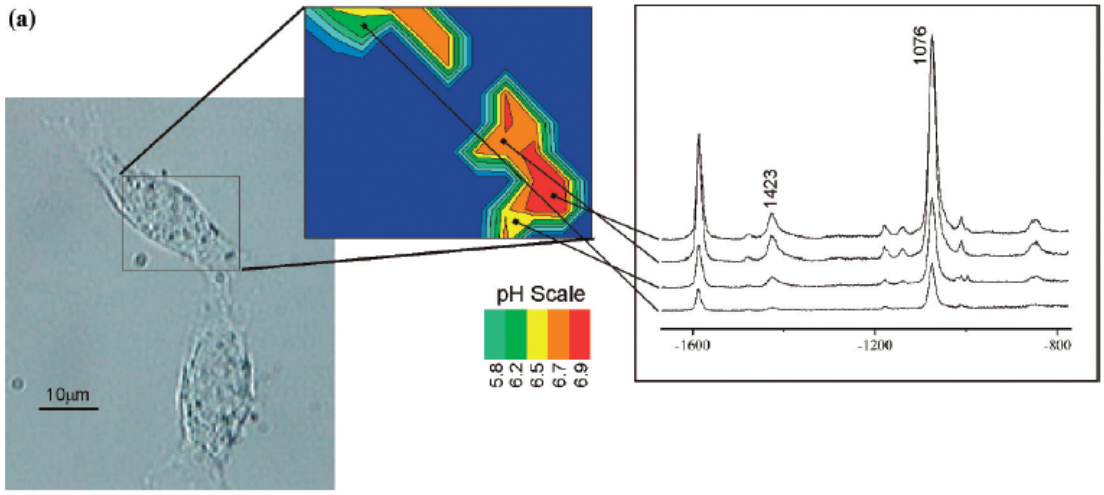

Figure 29: **Photomicrograph of NIH/3T3 cell after incubation with nanoparticle probes (left); pH map of the same cell (middle), SERS spectra collected in different parts of the cell (right) [87, 95].**

4-mercaptobenzoic acid functionalised gold nanoparticles were introduced into the cell line NIH/3T3 by fluid-phase uptake. It was reported that nanoparticle probes after incubation with the cell usually accumulate in endosomes and lysosomes [87, 93, 95, 140]. The SERRS spectra were then collected from the cell area, which allows creation of a pH map of a cell (Figure 29) [87, 95]. It was reported that the pH value

inside endosomes decreases with incubation time with the SERS active probe, which was explained by endosome maturation after probe uptake. Creating the pH map of the same cell after different incubation times with nanoparticle based probes allows better understanding of physiological and metabolic processes within the cell. For example this method make it possible to follow the pathway of all endocytosed materials.

The use of 4-mercaptopyridine as a pH sensing Raman reporter has been reported in the literature as well (Figure 30) [85, 88, 90]. Jensen *et al.* [88] attached 4-mercaptopyridine to silica-gold core-shell nanoparticles, then recorded the SERRS spectra of such probes in buffers with pH values between 1.5-9. The biggest changes in the intensity at different pH values were observed for the Raman peaks at 1000 cm^{-1} (increases when pH decreases due to greater aromaticity of protonated form of 4-mercaptopyridine), 1100 cm^{-1} (increases when pH increases due to increased double bond character of the C-S bond), 1610 cm^{-1} (decreases when pH increases, due to protonation of 4-mercaptopyridine) and 1575 cm^{-1} (increases when pH increases, the peak is derived from non-aromatic C=C vibrational modes in non-protonated molecule) [88, 90]. In order to obtain pH curves the ratios of the intensities of the peaks at 1000 cm^{-1} and 1100 cm^{-1} or 1610 cm^{-1} and 1575 cm^{-1} were plotted against the pH value of the buffer. The use of silica-Au core-shell nanoparticles functionalised with 4-mercaptopyridine allowed the analysis of pH between 3-7 [88].

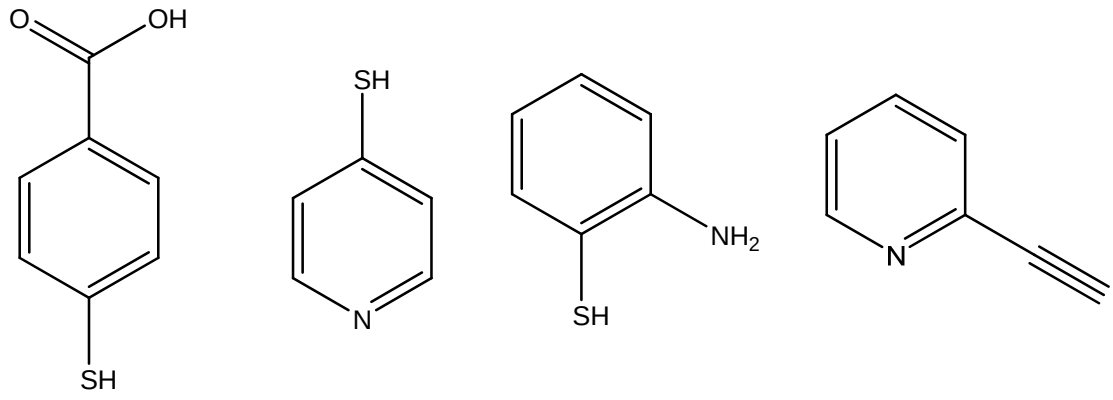

Figure 30: pH sensing molecules; (1) 4-mercaptobenzoic acid, (2) 4-mercaptopyridine, (3) 2-aminothiophenol, (4) 2-ethynylpyridine

Nowak-Lavato and co-workers reported the use of 4-mercaptopyridine as a pH sensing molecule for the detection of intracellular pH in RBL-2H3 cell [90]. A mixed layer of 4-mercaptopyridine (pH sensing molecule) and 2, 4-□-dinitrophenol-*L*-Lysine (targeting molecule, DNP) was created on Au-Ag core-shell nanoparticles. SERRS signals obtained from DNP were very weak, even after its adsorption on the enhancing surface, so its contribution to the nanoprobe SERRS spectrum was very mild. The described sensor allowed detection of pH values between 4.5-7.5 [90].

2-aminothiophenol is another Raman active molecule which, after its adsorption on metallic nanoparticles surface has been used for pH sensing [89]. The use of silver borohydride nanoparticles functionalised with 2-aminothiophenol for detection of intracellular pH in pancreas carcinoma cells was reported by Wang and co-workers [89]. SERS spectra of the nanoprobes were taken at 20 different buffers with pH values between 3-8. Taking the intensity of the 1505 cm^{-1} band (benzene ring vibrations) with respect to the 1390 cm^{-1} band (NH_2 rocking mode, intensity increases when pH of the surrounding medium increases) at different pH values allowed preparation of a pH calibration curve, which was then used to find the pH value inside the cell [89]. The nanosensor made it possible to analyse pH values between 3 and 8 [89].

The described nanosensor allows detection of pH values between 3 and 8, however the detection of more acidic or alkaline pH values was also reported in the literature [86, 91]. Lim *et al.* [86] reported the use of 15 nm gold nanoparticles functionalised with 2-ethynylpyridine to detect the pH between 12-14. The use of those probes inside living cells has not been reported. Lee and co-workers used yeast *iso*-1-cytochrome *c* attached to silver nanoparticles to detect pH dependent structural changes.

1.6 Aims of the work

The aim of this work is to prepare novel, SERRS active nanoparticle probes which can be used to detect specific DNA sequences in a sandwich assay format. This involves the design and the synthesis of multifunctional linker molecules containing a surface seeking group (thioctic acid) allowing attachment to the nanoparticle surface; a conjugation site-free functionality (carboxyl group), which could be reacted with biomolecules of interest; a PEG unit, which reduces non-specific interactions and increases the stability of formed conjugates and a Raman reporter (Figure 31).

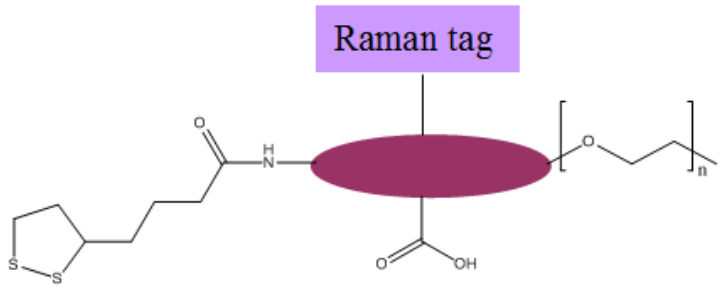

Figure 31: The structure of the linker.

Four different linkers containing fluorescent (aminofluorescein, fluorescein, TAMRA) or non-fluorescent (BHQ) Raman tag; a PEG unit of different length; thioctic acid as a surface complexing group and a free carboxyl group allowing conjugation of the linkers to biomolecules, were designed. Addition of such a linker to nanoparticles should increase nanoparticle stability and will also give the opportunity to attach DNA strands to prepared conjugates and therefore make it possible to obtain SERRS signals from oligonucleotide functionalised nanoparticles, which are usually not SERRS active (in case of metallic nanoparticles functionalised with thiolated oligonucleotides).

Two different coupling chemistries, commonly used for bioconjugates preparation involving the use of *N*-(3-dimethylaminopropyl)-*N*'-ethyl carbodiimide hydrochloride (EDC·HCl) with *N*-hydroxysulfosuccinimide (sulfo NHS) and a novel method which uses 4-(4,6-dimethoxy-1,3,5-triazin-2-yl)-4-methylmorpholinium chloride (DMT MM) for amide bond formation, will be assessed.

Prepared SERRS active oligonucleotide functionalised nanoparticles will then be used as probes in a hybridisation based DNA detection assay.

An additional aim of this work is to design nanoparticle based, pH sensitive, SERS active probe allowing intracellular pH detection by SERS. As it was found that nanoparticles are taken up by the cells, then trapped in endosomes, formation of such a probe would allow the monitoring of the acidification of endosomal pH, which is thought to play a central role in a number of pathologies including cystic fibrosis, kidney diseases and certain types of cancer. pH sensitive, SERS active probes offering the opportunity of conjugation of such a probe to biomolecules will also be prepared, as it was found that attachment of nuclear localization sequences or cell penetrating peptides to the metal surface make it possible to deliver nanoparticles inside other than endosomes components of a cell.

Chapter 2

Synthesis of SERRS active metallic nanoparticles

This chapter describes the synthesis of four different multifunctional linkers (aminofluorescein linker, fluorescein linker, TAMRA linker and BHQ linker), which can be used to functionalize metallic nanoparticles (gold and silver) in order to make them SERRS active. The preparation and full characterisation of the linker-nanoparticle conjugates is also presented within this chapter.

2.1 Introduction

Development of simple, sequence specific DNA detection methods is a vital area of life science research due to its application in the diagnosis of pathogenic and genetic diseases [5-15]. The majority of traditional DNA detection methods are based upon detection of PCR amplified genetic material by fluorescence spectroscopy. The biggest disadvantages of this technique are the need for amplification of the number of DNA copies present in the original sample and the fluorescence spectra produced tend to have broad overlapping outputs thus limiting the multiplexing capacity of the technique [12]. An alternative to traditional DNA detection assays is based on hybridisation of silver or gold nanoparticles functionalized with oligonucleotides complementary to the target. These probes offer numerous advantages such as: rapid detection, colorimetric response, good selectivity and little or no instrumentation required [5, 7, 13-15]. The hybridisation of the probes to a complementary target can be monitored by UV-Vis spectroscopy or by surface enhanced resonance Raman scattering (SERRS) [49, 53, 70]. In this method primary enhancement is provided by a suitable, roughened metal surface. An additional enhancement comes from the chromophore within the analyte, which results in a very high sensitivity of the detection method, which allows detection of components in a mixture without the need for extensive separation procedures [46, 49, 53, 56, 60, 70, 80].

Due to the fluorescence quenching ability of metal surfaces, a wide range of dyes and fluorescent labels can be used as Raman tags [49, 53, 56, 78]. Due to different combinations of properties (absorption and emission maxima, different functional groups present within molecules, polarity, micro-environmental dependence of fluorescence) fluoresceins and rhodamines are the most commonly used fluorescent markers [100-102]. Rhodamines exhibit great photostability and pH insensitivity from low to neutral pH [100]. The biggest advantages of the fluoresceins are their high chemical and physical stability and commercial availability, however their

fluorescence is pH dependant and they exhibit relatively high photobleaching [102-108]. The broad fluorescence emission spectrum is another general drawback of fluorescent dyes[101]. The use of non-fluorescent Raman active labels, such as Black Hole Quencher (BHQ), offers numerous advantages, such as: lower background fluorescence, an increase in signal to noise ratio and higher sensitivity [109].

In order to covalently attach oligonucleotides to the surface of metallic nanoparticles, sequences can be modified with either a surface complexing group [54, 64, 67, 73, 74, 78, 83, 84] or a label which contains a surface complexing group, a Raman active tag and a conjugation site for biomolecule attachment can be added to nanoparticles at first, then it can be reacted with biomolecule of interest [65]. Surface seeking groups are specific chemical functionalities, which can bind strongly to the metal nanoparticles surface and replace the weakly bound layer of charged ligands present from nanoparticle synthesis, which stabilize the colloidal nanoparticles. In the case of gold and silver nanoparticles, oligonucleotides are most commonly functionalized with alkylthiols before their addition to nanoparticles [13, 16, 21-25, 28, 29, 38, 39, 110]. Further studies indicated that the use of a cyclic disulphide [15, 30] or trithiol [28] in place of an alkylthiol increases the stability of the formed conjugates[15, 28, 30]. However the hybridisation properties of the oligonucleotide functionalized nanoparticle conjugates prepared with monothiol, cyclic disulphide or trithiol modified oligonucleotides are comparable [28, 38].

Many different methods to obtain SERRS active oligonucleotide functionalized metallic nanoparticles have been reported in the literature e.g. electrostatic adsorption of dye labeled oligonucleotides on to the nanoparticles surface [49, 59, 63, 66, 70, 79, 80]; covalent attachment of oligonucleotides modified with mono- or multithiols and Raman active dyes [54, 64, 67, 73, 74, 78, 83, 84]; the use of multifunctional labels containing a Raman reporter molecule, a surface complexing group and free functional groups which allow the attachment of biomolecules [65] or formation of mixed monolayers of thiolated oligonucleotides and Raman reporters or molecules containing Raman active units [50, 53, 56, 60, 63, 68, 69, 76].

In order to use the stability of the cyclic disulphide linker within a SERRS approach, a specific resonant chromophore needs to be incorporated within the linker. This has to be done in such a way as to ensure that the label is close enough to the surface to experience enhancement whilst still allowing attach of a specific

oligonucleotide probe to the nanoparticles. This would produce a nanoparticle with a permanent SERRS signal and DNA hybridisation capabilities.

In this work four different linkers containing a cyclic disulphide (thioctic acid), a resonant chromophore (i.e. either a fluorescent dye such as 6-aminofluorescein, fluorescein, tetramethyl rhodamine-TAMRA or a non-fluorescent label such as Black Hole Quencher-BHQ), a conjugation site (free carboxyl group) and polyethylene glycol (PEG) unit (3 mer or 41mer) were synthesized and then used to pre-functionalize gold and silver nanoparticles ready for future bioconjugation. The conjugates had a permanent SERRS signal and exhibited very high stability and could be stored for several weeks at room temperature. The linkers molecules could be stored in a dry form for several months without any observable decomposition. The presence of the free carboxyl group within the linker offers the possibility to react the conjugates with biomolecules, such as amino modified DNA, to form nanoparticles with a permanent SERRS signal and DNA hybridisation capabilities. A significant increase in the SERRS signal would be observed following target DNA hybridisation. This new class of linkers offers improved preparation of dye tagged nanoparticles and simplifies the often lengthy procedures commonly used.

2.2 Synthesis of linkers which can be used to pre-functionalise metallic nanoparticles

SERRS active oligonucleotide functionalised metallic nanoparticles can be prepared by covalent attachment of a label containing a Raman reporter molecule and a chemical functionality, suitable for reaction with the sequence of interest. Four different linkers allowing preparation of such probes have been synthesised. Each of the linkers contain thioctic acid which allows covalent attachment to gold and silver nanoparticles via two metal-sulphur bonds, one of the available fluorescent or non-fluorescent Raman reporters and a free carboxyl group which can be reacted with amino modified DNA or other biomolecules. A PEG unit (3 mer or 41 mer) is also included which prevents non-specific adsorption of oligonucleotides on the metal surface, increases aqueous solubility and the stability of the conjugates [65, 69].

2.2.1 Synthesis of linkers containing a fluorescent dye as a Raman reporter

Three different linkers containing fluorescent dyes as the Raman reporter were successfully synthesised: fluorescein linker (F), aminofluorescein linker (Af) and TAMRA linker (T). Fluorescein and TAMRA linkers were synthesised around a lysine core which was chosen due to the presence of three functional groups within the molecule which could be easily functionalised by the use of well known peptide coupling chemistry. The use of the lysine during synthesis of the aminofluorescein linker was not necessary because 6-aminofluorescein itself contains two functional groups: an aromatic amine which can be reacted with thioctic acid and a phenol group, which after simple modification can be reacted with polyethylene glycol. All fluorescent linkers contained 3 PEG units within the structure which was proven to increase the stability of the gold and silver nanoparticles conjugates formed with the use of such a linker [65, 69].

2.2.1.1 Synthesis of the 6-aminofluorescein linker (Af)

The synthesis of the aminofluorescein linker is outlined in the Figure 32. In the first stage of the synthesis 6-aminofluorescein was locked into its fluorescent form. It is well known that fluoresceins can exist in a fluorescent quinoid form, and a non-fluorescent lactoid form. The equilibrium between these two forms is reflected in fluoresceins pH dependent fluorescence. To overcome the tautomerization problem the fluorophore can be locked into its quinoid form by conjugation of its 2' carboxylic group with a nucleophile (secondary amine [102, 107, 110] or alcohol [102, 107, 108, 111]). Because it was reported that the esterification of the 2'carboxyl group of fluorescein gives an excellent yield [107, 111] this method was chosen to lock 6-aminofluorescein into its fluorescent form. In the first step of synthesis of Af, esterification of 6-aminofluorescein in refluxing acidic ethanol afforded an ester (**1**). The aim of the next step was to introduce a carboxylic functionality to the molecule. This can be achieved by alkylation of the 3' phenol group using *tert*-butyl bromoacetate in the presence of *N, N'*-diisopropylethylamine (DIPEA) or potassium carbonate [108, 111]; coupling of 3'O-(hydroxyalkyl) fluorescein methyl esters with dimethoxytrityl protected hydroxyalkyl chlorides under basic conditions [111] or

alkylation of the 3' phenol group of fluoresceins methyl ester under Mitsunobu conditions [111].

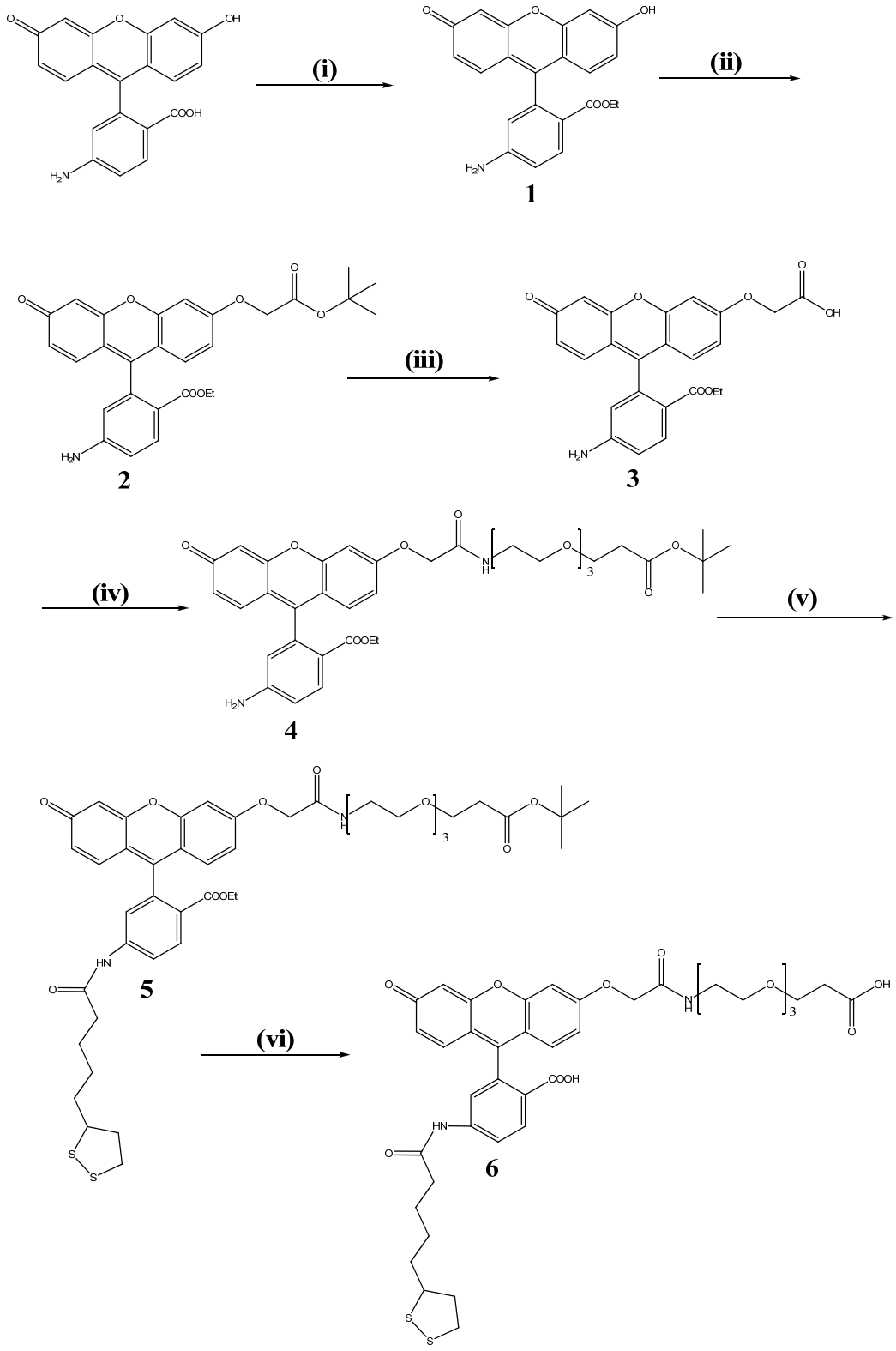

Figure 32: Synthesis of the 6-aminofluorescein linker (6); (i) EtOH, H_2SO_4, 99%; (ii) $BrCH_2COOtBu$, K_2CO_3, DMF, 56%; (iii) TFA, DCM, 52%; (iv) *tert*-butyl-12-amino-4, 7, 10-trioxadodecanoate, HATU, DIPEA, DMF, 25%; (v) thioctic acid, DIC, DCM, 97%; (vi) TFA, DCM, 98%.

The reaction described by Burchak *et al.* [107] has been shown not to involve an aromatic amine group and proceeds selectively on the 3' phenol group of aminofluorescein and also gives an excellent yield [107]. This method was used to introduce the carboxyl group into ester (**1)**. Alkylation of molecule (**1**) with *tert*-butyl bromoacetate in the presence of potassium carbonate in DMF followed by the cleavage of the *tert*-butyl ester using TFA in DCM afforded compound (**3**). The free carboxyl group of the new moiety was then coupled with *tert*-butyl-12-amino-4, 7, 10-trioxadodecanoate in the presence of O-(7-azabenzotriazol-1-yl)-*N, N, N', N'*-tetramethyluronium (HATU) and DIPEA to form molecule (**4**), which was then acylated with thioctic acid in the presence of *N, N'*-diisopropylcarbodiimide (DIC) to form, after cleavage of *tert*-butyl ester group, the desired aminofluorescein linker (**6**) in 7% overall yield (Figure 32). The details of the synthesis of the aminofluorescein linker are described in section 6.1.1.

2.2.1.2 Synthesis of the fluorescein linker (F)

Two linkers with different geometries but containing very similar chromophores (aminofluorescein and fluorescein), the same surface complexing group and PEG (3 mer), but different geometry were synthesised to check the influence of the linker geometry on the obtained SERRS signal. Fluorescein and 6-aminofluorescein have very similar chemical structures, however fluorescein contains only one functional group (phenol), therefore the linker has to be synthesised around the lysine core. The aminofluorescein linker has a linear structure with the chromophore placed between the surface complexing group and PEG, thus after attachment of the linker onto the nanoparticles the label will be closer to the metal surface. Where as the use of multifunctional molecules during synthesis of the fluorescein linker changes the geometry of the obtained linker to a T-shaped with the chromophore placed further away from the surface seeking group.

The fluorescein linker was synthesised around the lysine core. In the first stage of the synthesis fluorescein was locked into its fluorescent, quinoid form using the same chemistry as during the aminofluorescein linker synthesis – its 2' carboxyl group was esterified with ethanol to form ester (**7**). Alkylation of the 3' phenol group of the ester with *tert*-butyl bromoacetate in the presence of potassium carbonate, followed by cleavage of the *tert*-butyl ester group by TFA afforded the fluorescein derivative (**9**)

(Figure 33). In the next step of the synthesis Fmoc-Lys(Boc)-OH was reacted with *tert*-butyl-12-amino-4, 7, 10-trioxadodecanoate in the presence of DIC to form molecule (**10**) (Figure 34).

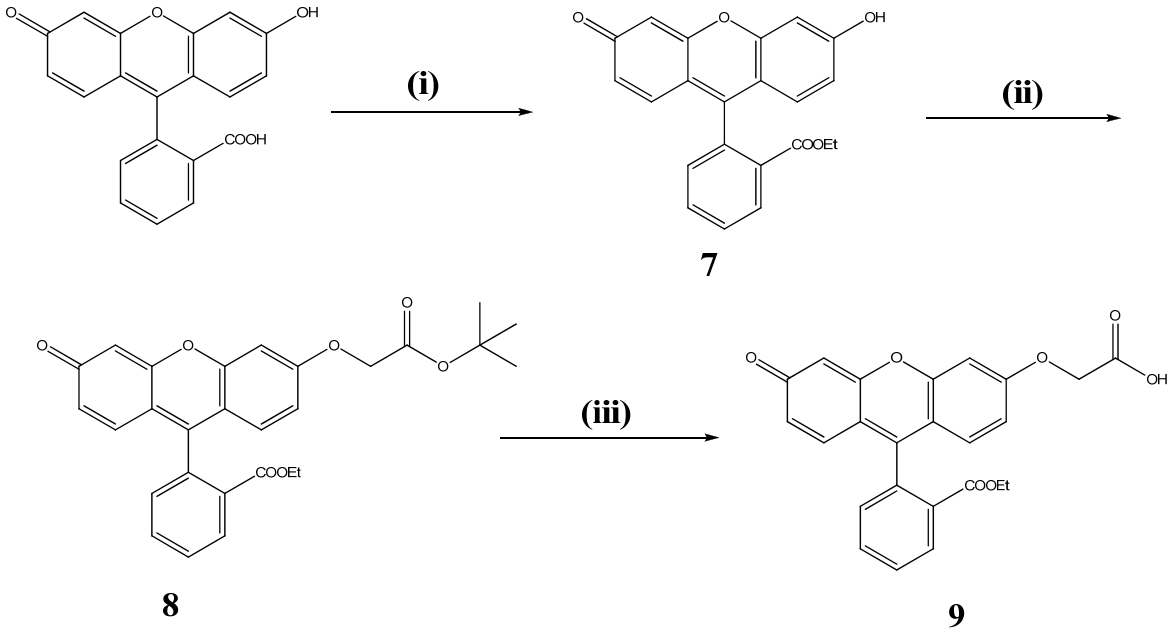

Figure 33: Synthesis of the 2-{9-[2-(ethoxycarbonyl)phenyl]-3-oxo-3*H*-xanthen-6-yloxy}acetic acid (9); (i) EtOH, H_2SO_4, 75%; (ii) $BrCH_2COOtBu$, K_2CO_3, DMF, 62%; (iii) TFA, DCM, 57%.

Chemoselective deprotection of the *N*-Boc group is a very important transformation in chemical synthesis. There are a large number of available reagents which allows this transformation. These include strong acids (TFA, HCl, HBr, H_2SO_4, HNO_3) or Lewis acids ($ZnBr_3$, $BF_3{\cdot}Et_2O$) [112, 113]. The deprotection can also be achieved under thermal [112] or neutral conditions (In, Zn) [113]. The biggest disadvantage of the above procedures is the lack of selectivity- these methods will remove both the *N*-Boc and *tert*-butyl ester groups from the protected molecules. Other disadvantages include: high acidity, strong oxidizing conditions, long reaction times and low yields [112, 113]. The selectivity problems can be overcome by the use of bismuth (III) chloride in a mixture of acetonitrile and water (50:1, v/v) at 55°C [113]. Under these conditions $BiCl_3$ selectively removes *N*-Boc groups in the presence of *tert*-butyl esters. This method was used in the next step where the *N*-Boc group was selectively cleaved from molecule (**10**) in the presence of $BiCl_3$. The primary amine group was then reacted with thioctic acid in the presence of DIC to form molecule

(**12**). The Fmoc group was then removed from molecule (**12)** by the use of 20% of piperidine in acetonitrile (molecule **13**, Figure 34).

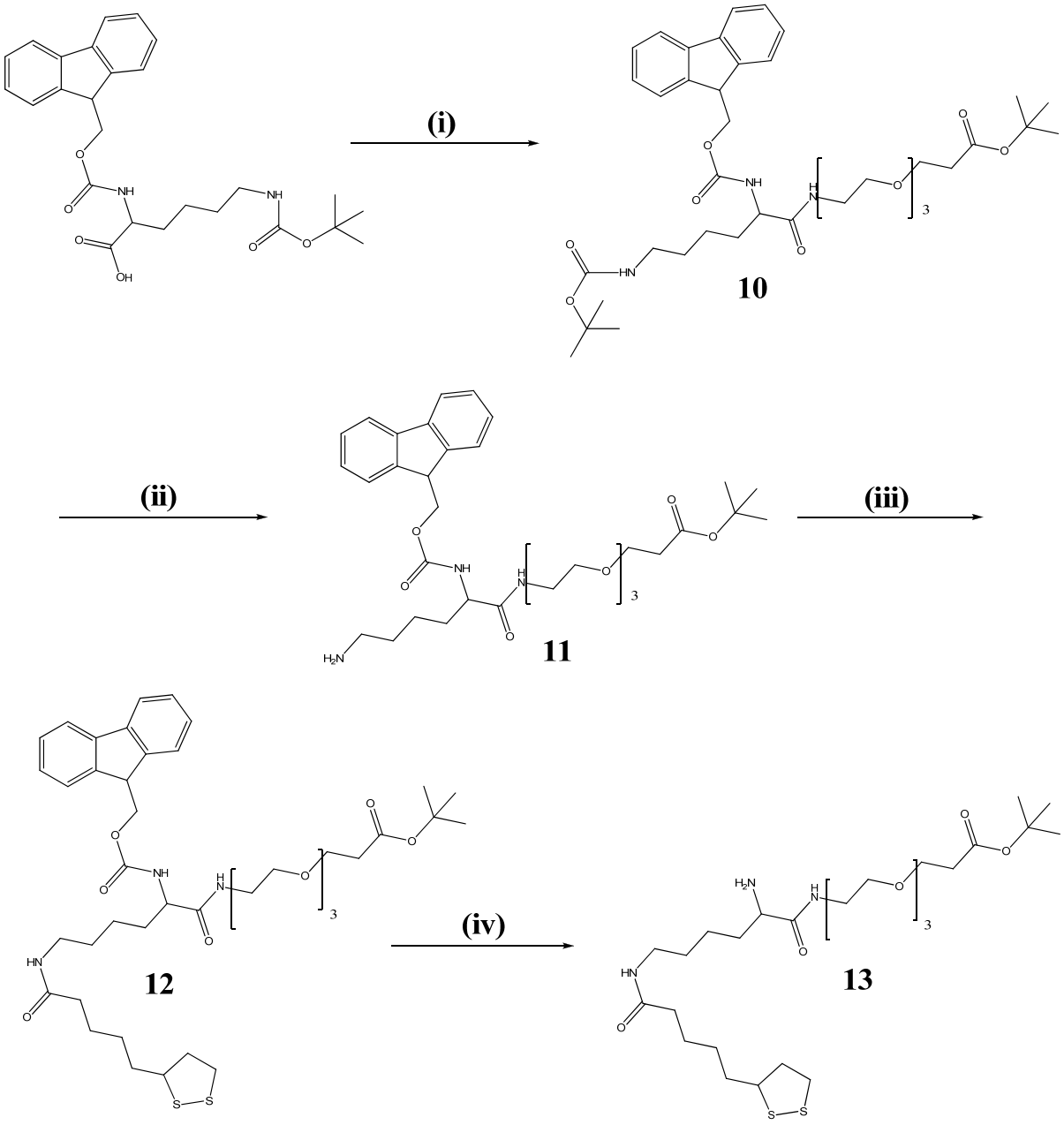

Figure 34: Synthesis of the *tert*-butyl 15-amino-25-(1, 2-dithiolan-3-yl)-14, 21-dioxo-4, 7, 10-trioxa-13, 20-diazapentacosan-1-oate (13); (i) *tert*-butyl-12-amino-4, 7, 10-trioxadodecanoate, DIC, DCM, 92%; (ii) $BiCl_3$, CH_3CN/H_2O, 31%; (iii) thioctic acid, DIC, DCM, 29%; (iv) 20% piperidine, CH_3CN, 92%.

Coupling of the fluorescein derivative (**9**) with *tert*-butyl 15-amino-25-(1, 2-dithiolan-3-yl)-14, 21-dioxo-4, 7, 10-trioxa-13, 20-diazapentacosan-1-oate (**13**) in the

presence of HATU and DIPEA followed by the cleavage of the *tert*-butyl ester afforded the fluorescein linker (**15)** with an overall yield of 3% (Figure 35). The details of the synthesis of the fluorescein linker are described in sections 6.1.1 and 6.1.2.

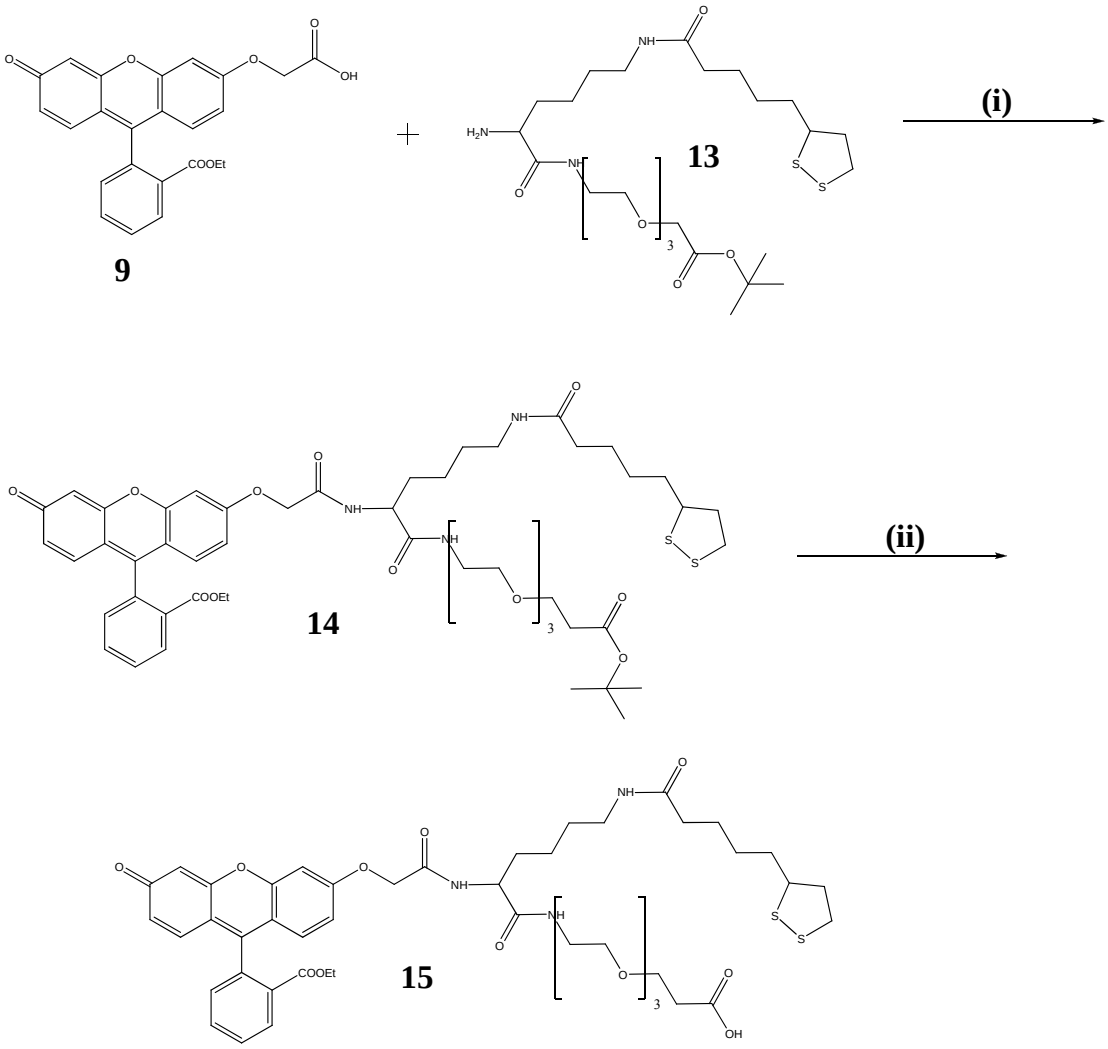

Figure 35: **Synthesis of the fluorescein linker (15); (i) HATU, DIPEA, DMF, 60%; (ii) TFA, DCM, 57%.**

2.2.1.3 Synthesis of the TAMRA linker

TAMRA contains only one reactive group (COOH) available for further conjugation, thus the TAMRA linker, similarly to the fluorescein linker, was synthesised around the lysine core. The synthesis of the TAMRA linker is presented in Figure 36. In the first step of the synthesis of the TAMRA linker Fmoc-Lys(Boc)-OH was coupled with *tert*-butyl-12-amino-4,7,10 trioxadodecanoate in the presence

of DIC to produce the amide (**10**) (Figure 34). After cleavage of the Fmoc group in the presence of piperidine in acetonitrile, (**16**) was coupled with thioctic acid in the presence of DIC. Both the *N*-Boc and *tert*-butyl groups were removed from (**17**) using TFA in DCM (1:1) giving (**18**).

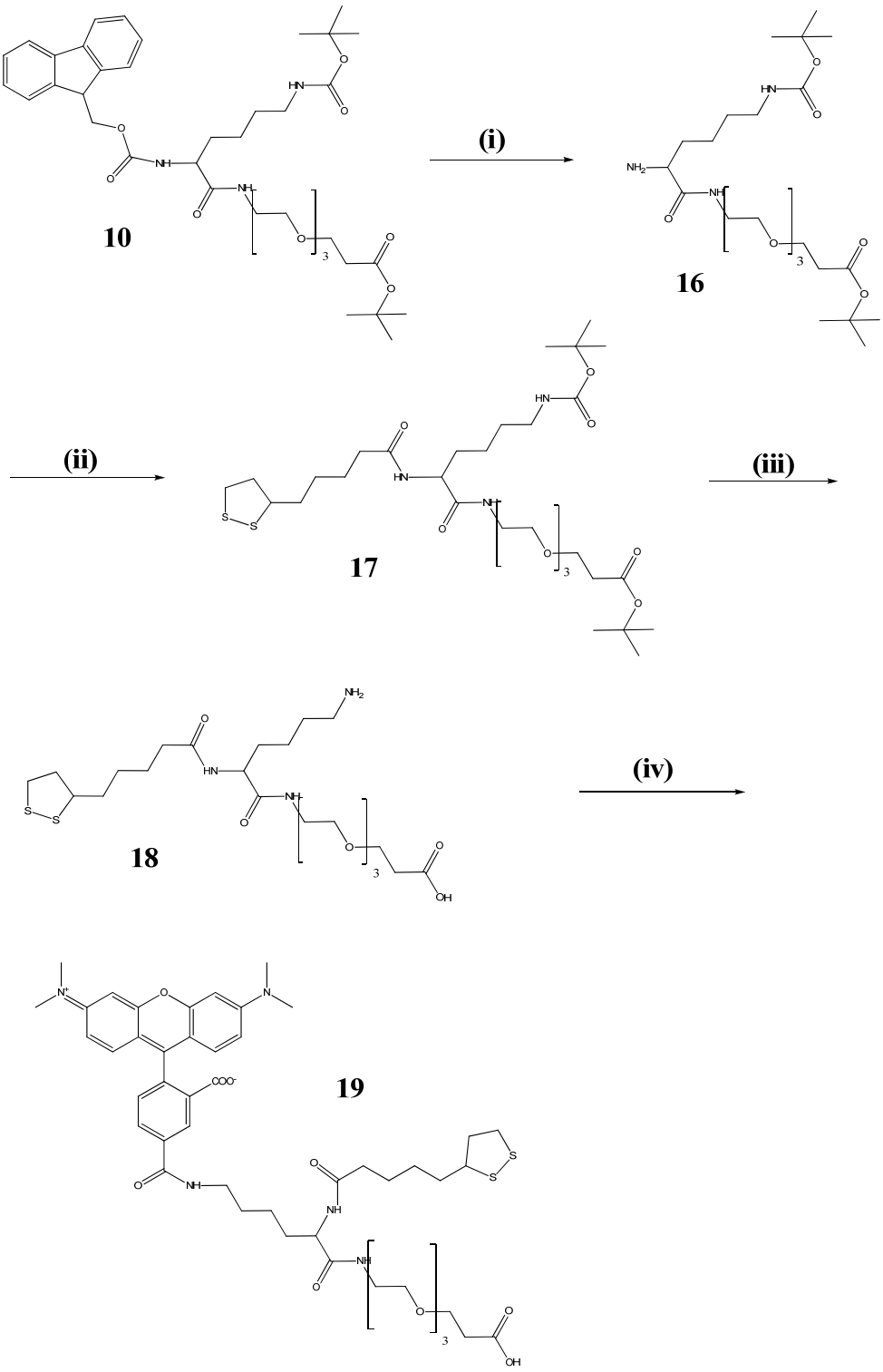

Figure 36: Synthesis of the TAMRA linker (19); (i) 20% piperidine, CH3CN, 92%; (ii) thioctic acid, DIC, DCM, 85%; (iii) TFA, DCM, 89%; (iv) TAMRA SE, 37%.

In contrast to fluoresceins, which exist in a non-fluorescent lactoid form at acidic pH, rhodamines can exist in a fluorescent quinoid form at neutral and acidic pH. The non-fluorescent lactoid form exists only at basic pH [100]. A large number of rhodamine conjugates are synthesized from 4' or 5' activated rhodamine derivatives (active ester, acid chloride) [101, 102]. In the synthesis of this TAMRA linker the succinimidyl ester of 5-tetramethyl rhodamine (TAMRA SE) was used. This molecule was coupled with (**18**) to give the desired TAMRA linker (**19**) with 27% overall yield (Figure 36). The details of the synthesis of the TAMRA linker are described in section 6.1.3.

2.2.2 Synthesis of a linker containing a non fluorescent Raman tag (BHQ) and a highly stabilizing PEG unit

Due to the fluorescence quenching ability of metallic nanoparticles a wide range of commercially available fluorescent dyes can be used as Raman active reporters during preparation of SERRS active, oligonucleotide functionalised gold and silver nanoparticles. However the use of a non-fluorescent Raman reporter for that purpose offers higher sensitivity due to the lower fluorescence background and hence an increased signal to noise ratio [109]. Therefore Black Hole Quencher (BHQ), was chosen as a non-fluorescent reporter molecule to synthesise a linker which could be used for pre-functionalisation of gold and silver nanoparticles.

The BHQ linker was synthesised around a lysine core in a similar way as the fluorescein and TAMRA linkers. In the first step of the synthesis the Fmoc group was selectively cleaved from 2-(*N*-Boc), 6-(*N*-Fmoc)-diamino caproic acid, by the use of 20% piperidine in acetonitrile. The primary amine group of molecule (**20**) was then reacted with 1-{[(5-dithiolane-3-yl)pantanoyl]oxy}-2, 5-pyrrolidinedione to form, after deprotection of the Boc group using TFA in DCM, molecule (**22**). In the next step compound (**22**) was reacted with BHQ succinimidyl ester (BHQ SE) giving the dye linked cyclic disulphide (**23**) (Figure 37).

To ensure the high stability of the formed conjugates, highly stabilising PEG (41 mer) was chosen to be incorporated within the linker structure. The use of such a big molecule in chemical synthesis makes the purification of obtained products difficult and very time consuming. One of the ways to overcome this is to perform the synthesis on a solid support. Solid phase synthesis offers the possibility of very simple purification of formed products by filtration. This technique was used to

perform the synthesis of the BHQ linker.

Wang resin, which can be easily reacted with succinic anhydride to form free carboxyl groups available for further conjugation, was used as a solid support in the synthesis of the BHQ linker. The ester linkage formed in this process has a good stability to various reaction conditions, but it can be easily removed with trifluoroacetic acid. Additionally, a carboxyl group is formed at the end of the synthesised molecule when it is cleaved from the solid support. In the case of the BHQ linker, this process delivered reactive functionality, allowing for the subsequent attachment of biomolecules.

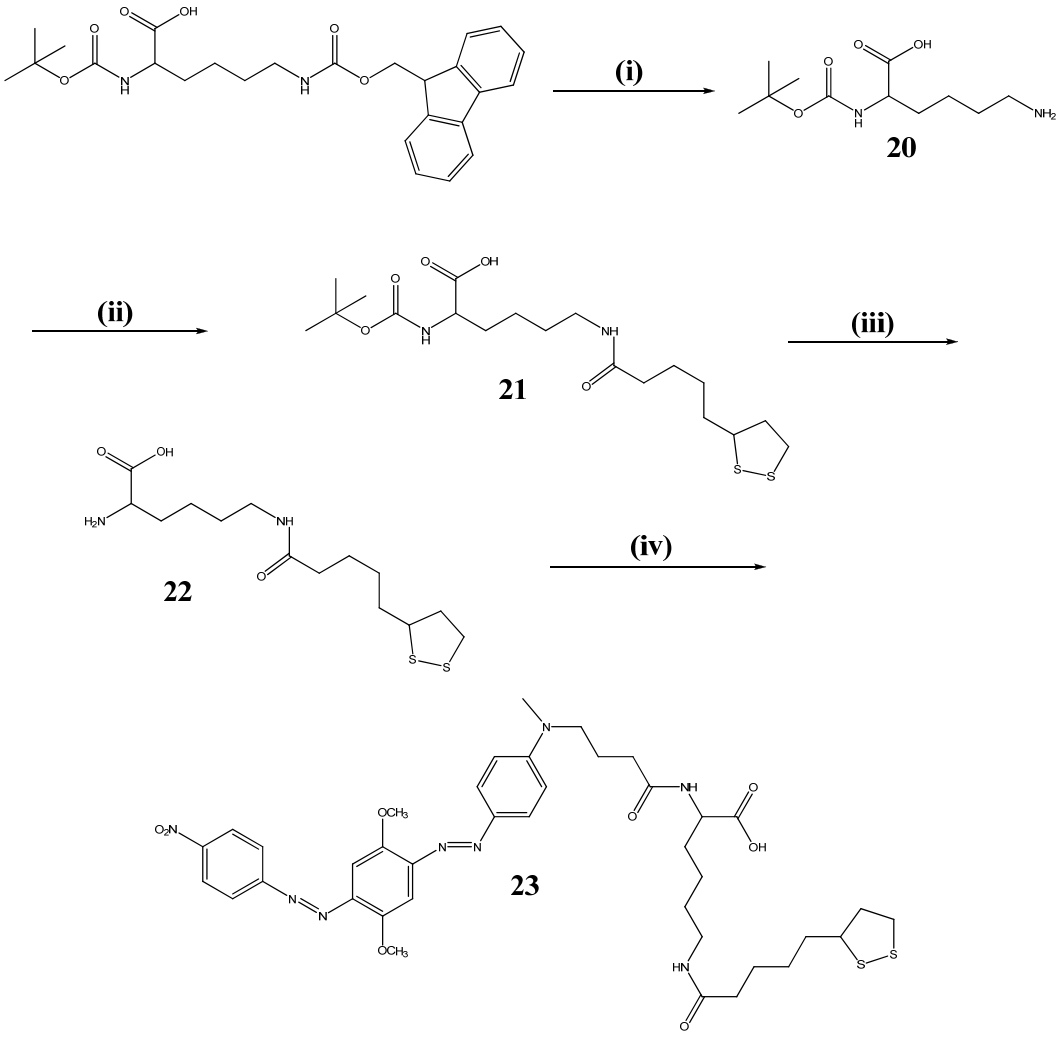

Figure 37: Synthesis of the 6-[5-(1, 2-dithiolan-3-yl)pentanamido]-2-(4-{[4-(1E)-(2, 5-dimethoxy-4-{[4-nitrophenyl]diazenyl}phenyl)methyl]amino}hexanoic acid (23); (i) 20% piperidine, CH_3CN, 99%; (ii) 1-{[(5-dithiolane-3-yl)pantanoyl]oxy}-2, 5-pyrrolidinedione, DCM, 46%; (iii) TFA/DCM, 99%; (iv) BHQ SE, DCM, Et_3N, 76%.

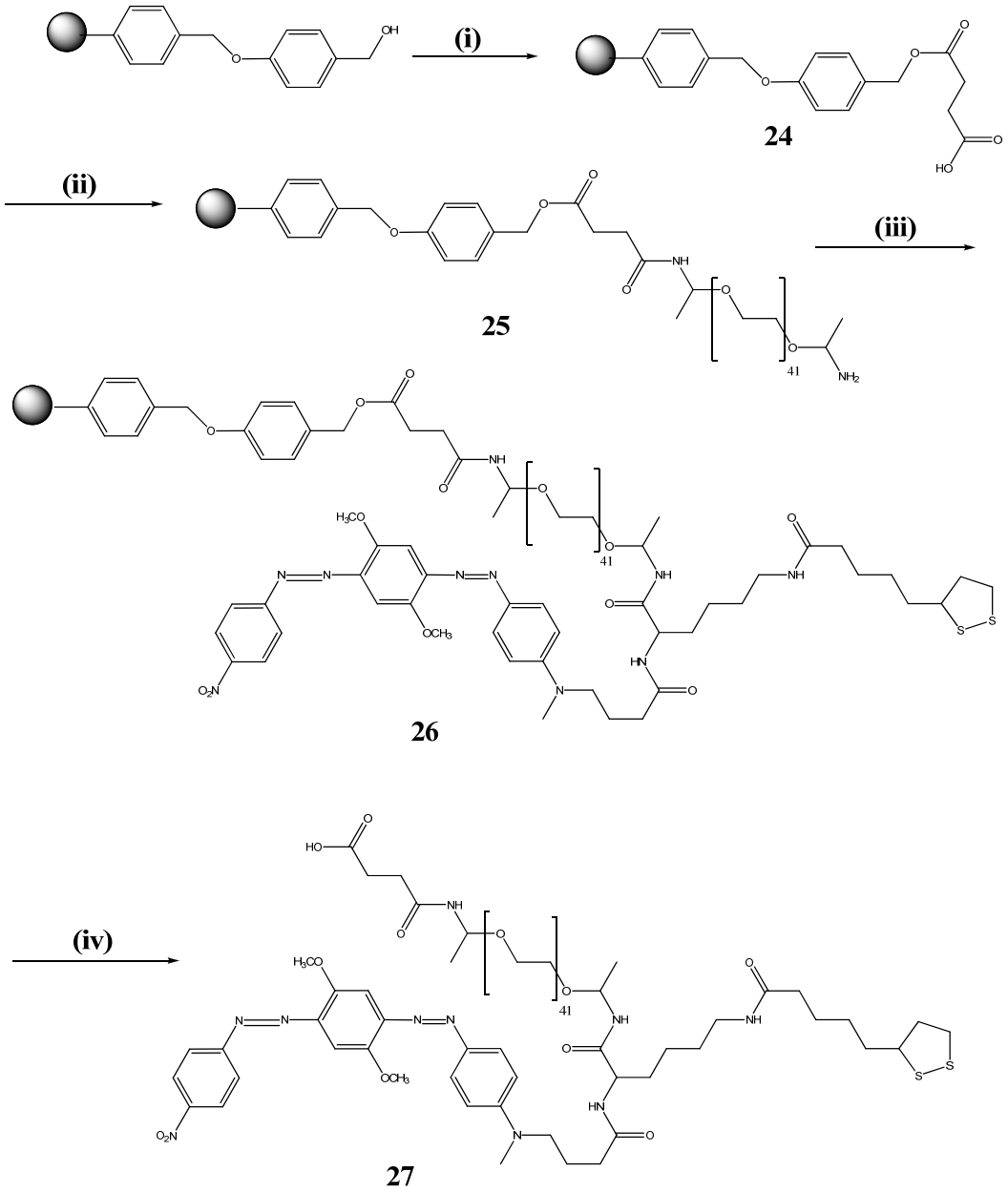

Figure 38: Synthesis of the BHQ linker (27); (i) succinic anhydride, DMAP, DCM; (ii) O, O'-Bis-(2-aminopropyl) polypropylene glycol-block-polyethylene glycol-block polypropylene glycol 1900 (PEG 41) DIC, DCM; (iii) 6-[5-(1, 2-dithiolan-3-yl)pentanamido]-2-(4-{[4-(1E)-(2, 5-dimethoxy-4-{[4-nitrophenyl]diazenyl}phenyl)methyl]amino}hexanoic acid (23), DIC, DCM; (iv) 10% TFA/DCM.

In the first step of the solid phase synthesis, Wang resin was reacted with succinic anhydride in the presence of 4-dimethylaminopyridine (DMAP) to form solid support (**24**) containing a free carboxyl group. This group was then reacted with O, O'-Bis-(2-aminopropyl) polypropylene glycol-block-polyethylene glycol-block polypropylene glycol 1900 (PEG 41) to form (**25**). In the next step of the synthesis the primary

amine groups on the surface of the modified resin (**25**) were coupled with 6-[5-(1, 2-dithiolan-3-yl)pentanamido]-2-(4-{[4-(1E)-(2, 5-dimethoxy-4-{[4-nitrophenyl]diazenyl}phenyl)methyl]amino}butanamido)hexanoic acid (**23)** in the presence of *N, N*'-diisopropylcarbodiimide (DIC). The newly formed BHQ linker (**27**) was cleaved from the solid support by the use of 10% TFA in DCM (Figure 38). The details of the synthesis of the BHQ linker are described in section 6.1.4.

2.3 Preparation of linker functionalised nanoparticles

All the synthesized linkers were used to functionalize the following types of nanoparticles: citrate stabilized Au (18, 50 nm), citrate stabilized Ag (40 nm) and EDTA stabilized Ag (40 nm). Experimental details regarding preparation of linker-nanoparticle conjugates are given in section 6.3.1. The plasmon band of all the nanoparticles was red shifted (usually 2-4 nm) after addition of the linkers, which confirmed the modification of the nanoparticle surface (Figure 39). The attachment of the linker onto the nanoparticles causes an increase of their size, thus a red shift of the plasmon band is observed. The lowering of the 50 nm Au surface band upon modification with the BHQ linker is due to the workup of the functionalized nanoparticles which required a few washing and centrifugation steps resulting in the loss of some material.

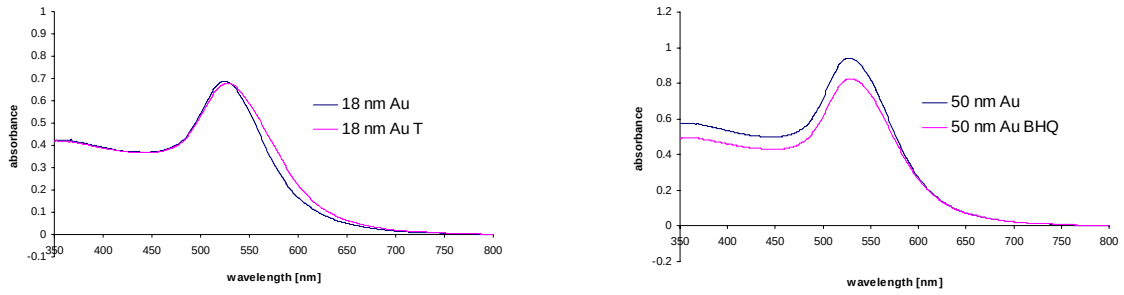

Figure 39: Red shift of 18 nm Au gold surface band observed after addition of the TAMRA linker (left, 4 nm); 50 nm gold surface plasmon band observed after addition of the BHQ linker (right, 2 nm).

Number of linkers molecules attached to each type of nanoparticles was calculated using the method described by Demers *et al.* [110] (Table 1). A solution of dithiothreitol (DTT) in alkaline phosphate buffer was used to displace the linker molecules from the nanoparticle surface. Then the fluorescence spectra of the supernatants obtained after nanoparticles centrifugation were obtained. The amount of

linker molecules which were attached per nanoparticle was calculated by dividing the linker concentration (obtained from the calibration curve created by taking the fluorescence spectra of linker solutions with know concentrations) by the nanoparticle concentration (calculated from the Beer-Lambert equation for the samples prior to DTT addition). The experimental details are described in section 6.4.1.

The number of 6-aminofluorescein linkers attached to 50 nm gold nanoparticles and BHQ linkers attached to each type of nanoparticles used could not be calculated using the described method. In the case of the BHQ linker the reporter molecule used for linker synthesis is not fluorescent and could not be quantified in the same way as for fluoresceins. Addition of DTT to the solution containing 50 nm Au nanoparticles functionalized with the aminofluorescein linker did not cause aggregation of the nanoparticles, so DTT did not displace the linker from the nanoparticle surface, even at a concentration four times higher than the one used to displace the other linkers from nanoparticles surface (Figure 40). This indicates the stability of this particular linker.

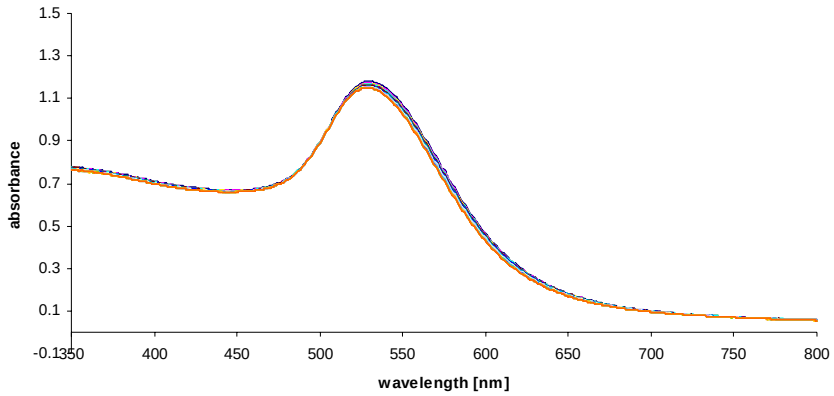

Figure 40: UV-Vis spectrum of 50 nm gold nanoparticles functionalized with 6-aminofluorescein linker after addition of DTT (0.4M concentration in the sample). Spectra were taken every 60 mins for 48 hrs.

The highest surface coverage was obtained for all types of nanoparticles functionalized with the TAMRA linker. This might be due to the presence of the positively charged dye in the structure. Positively charged molecules will be attracted by the negatively charged nanoparticle surface, so more linker molecules can be adsorbed on to the metal surface. In the case of neutral fluorescein and aminofluorescein linkers this additional, electrostatic force is not present, thus less linker molecules are attached to the metal surface. The observed differences in the

surface coverage observed for different linkers might also be caused by different packing geometries on the metal surface.

Both types of silver nanoparticles used in this study after functionalisation with all types of linkers were not stable in buffers, e. g. 10 mM phosphate buffer or 0.1M PBS. 50 nm Au nanoparticles functionalized with TAMRA or fluorescein linkers were not stable under these conditions as well. 18 nm gold nanoparticles functionalized with either of the four linkers, and also 50 nm Au nanoparticles functionalized with 6-aminofluorescein and BHQ linkers were stable in 0.1M PBS for several weeks and could be easily reacted with amino-modified DNA under commonly used conditions.

Table 1: Number of linker molecules attached to each type of nanoparticle used.

Linker	Type of nanoparticles	No of linker molecules attached per one nanoparticle	Surface coverage [pmol/cm^2]
6-aminofluorescein	18 nm Au	298±29	93±9
	Ag citrate	4202±282	139±21
	AgEDTA	1653±158	54±5
fluorescein	18 nm Au	90±33	28±10
	50 nm Au	3248±220	107±7
	Ag citrate	2145±388	70±12
	AgEDTA	578±62	15±4
TAMRA	18 nm Au	8100±324	2547±102
	50 nm Au	2927±787	890±26
	Ag citrate	114000±2080	3780±69
	AgEDTA	5613±940	185±31

2.3.1 SERRS of formed conjugates

SERRS spectra of all the linker-nanoparticle conjugates were taken at three different laser excitation frequencies: 514, 633 and 785 nm. Experimental details are described in section 6.4.5.

2.3.1.1 Excitation at 514 nm

Good SERRS spectra at 514 nm were obtained for the aminofluorescein linker conjugates, however very weak SERRS signals were obtained from the nanoparticles functionalized with the fluorescein linker under the same excitation frequency (Figure 41). Fluorescein and 6-aminofluorescein have very similar chemical structures, however their respective linker geometry is different which causes variations in the SERRS response. In the case of the 6-aminofluorescein linker, the fluorescent label is closer to the metal surface so it experiences a larger enhancement and gives a better SERRS signal. In both cases stronger signals were obtained from silver nanoparticles.

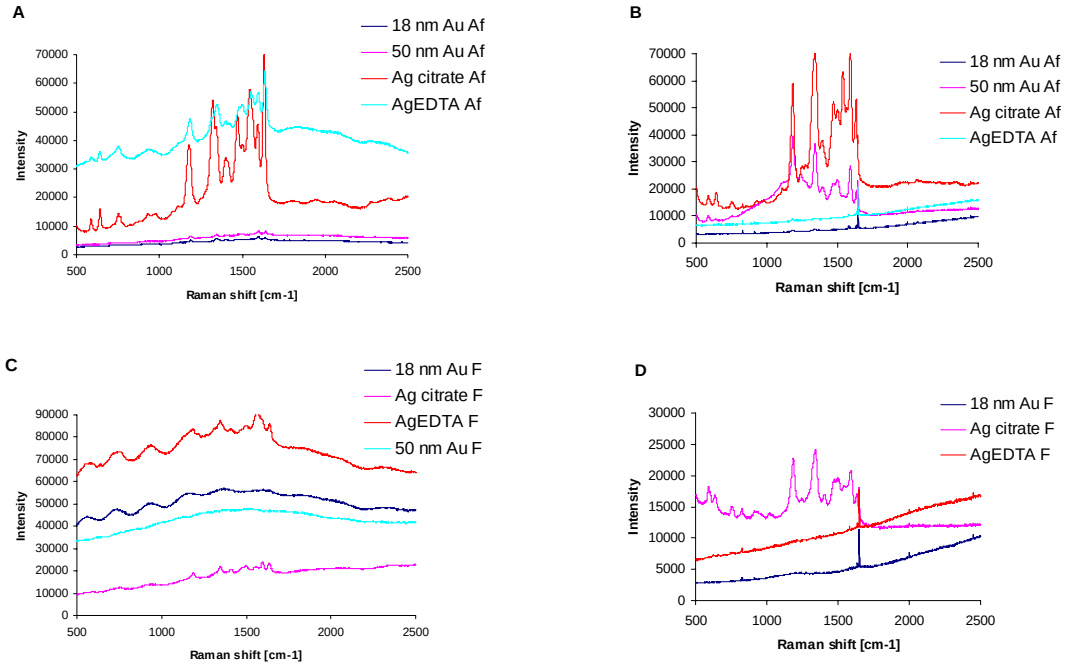

Figure 41: **SERRS spectra of all types of nanoparticles investigated functionalised with the fluorescein (F) and 6-aminofluorescein (Af) linkers at laser excitation frequencies of 514 and 633 nm (A- Af at 514 nm, B- Af at 633 nm, C- F at 514 nm, D- F at 633 nm). In the case of the fluorescein linker conjugates spectra were taken from aggregated samples (sat. NaCl was used as an aggregating agent). SERRS spectra of aminofluorescein conjugates were taken from non-aggregated samples.**

No SERRS signals from the TAMRA linker conjugates were obtained at 514 nm, while only very weak SERRS signals from all the BHQ linker conjugates (Figure 42, 44 and 45) were obtained. The excitation frequency of the light source used was not close enough to the absorption maximum of the chromophores present within these

linker structures (557 nm for TAMRA, 579 nm for BHQ), thus only a poor SERRS response was obtained

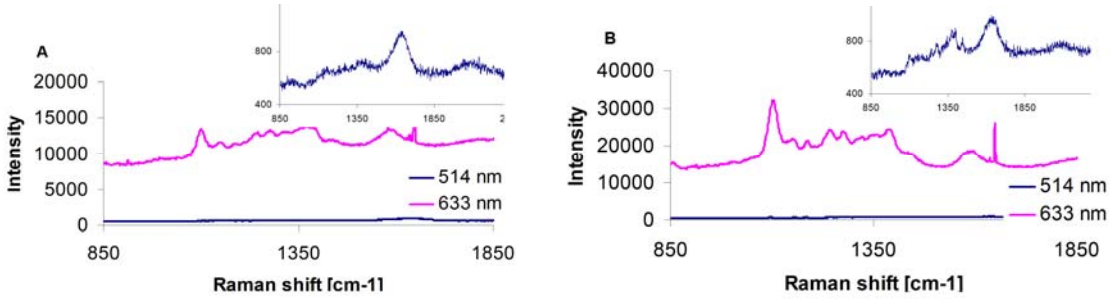

Figure 42: **SERRS spectra of 18 (A) and 50 (B) nm Au nanoparticles functionalised with the BHQ linker at 514 and 633 laser excitation frequencies. Spectra were taken from aggregated nanoparticles. Sat NaCl was used as an aggregating agent.**

2.3.1.2 Excitation at 633 nm

All types of nanoparticles functionalized with the TAMRA linker gave the strongest SERRS response at a laser excitation frequency of 633 nm (Figure 43).

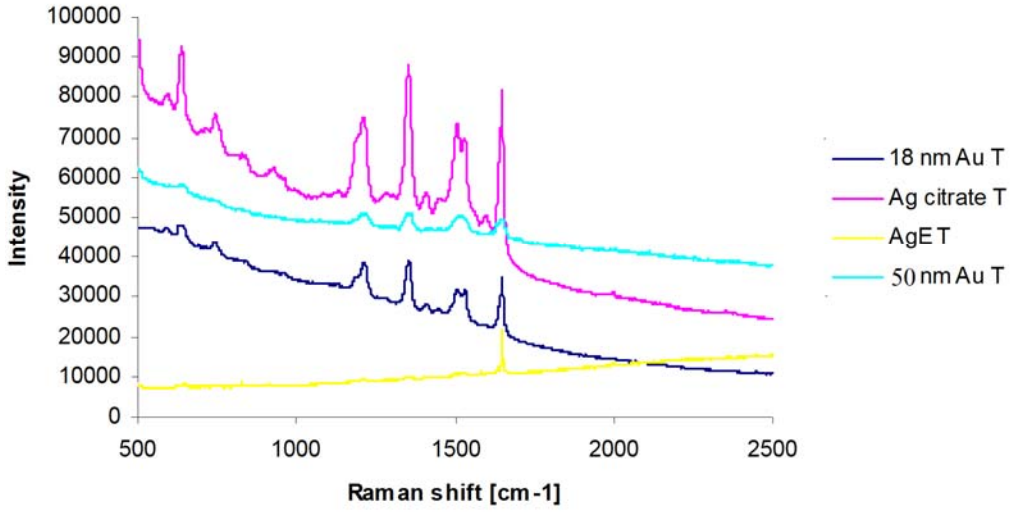

Figure 43: **SERRS spectra of the TAMRA linker (T) functionalised nanoparticles at 633 nm. All spectra except Ag EDTA T and 50 nm Au T were taken from not aggregated NPs, sat. NaCl was used as an aggregating agent.**

SERRS signals using an excitation of 633 nm were also obtained for the nanoparticles functionalized with aminofluorescein and fluorescein linkers, however the signal was much weaker for the fluorescein linker conjugates (Figure 41). The observed difference in the signal intensities obtained from these linkers, containing very similar

chromophores, is again due to the different geometries of these linkers. A similar trend was observed at 514 nm. SERRS signals were obtained from all types of nanoparticles functionalized with the BHQ linkers at 633 nm (Figures 42, 44, 45).

2.3.1.3 Excitation at 785 nm

None of the conjugates formed with the fluorescent TAMRA, fluorescein or aminofluorescein linkers gave SERRS signals with a laser excitation frequency of 785 nm. This was due to the fact that the excitation frequency of the light source used was far removed from the absorption maximum of the chromophores present within the linkers (557 nm for TAMRA, 495 nm for aminofluorescein and fluorescein) and the plasmon of the metal colloids (400 nm for Ag, 520 nm for Au). Both types of silver nanoparticles, when functionalized with the BHQ linker gave a SERRS response at 785 nm, however the addition of an aggregating agent (sat. NaCl) was necessary to obtain the signal (Figure 44 and 45). It has been reported that formation of nanoparticle aggregates causes significant increase in the intensity of SERRS signals [50, 58, 67].

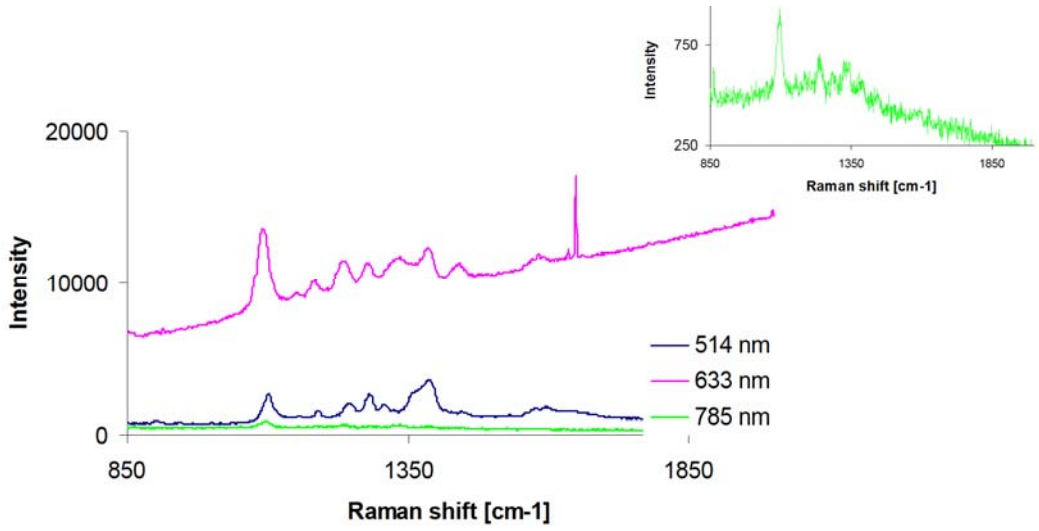

Figure 44: **SERRS spectra of Ag EDTA stabilised nanoparticles functionalized with the BHQ linker at different laser excitation frequencies. All spectra were taken from aggregated nanoparticles-sat NaCl was used as an aggregating agent.**

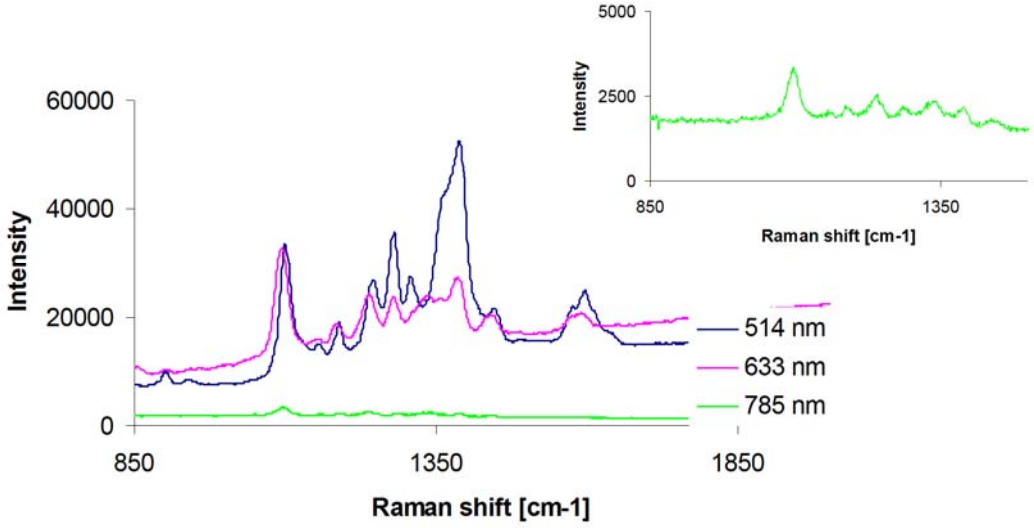

Figure 45: **SERRS spectra of Ag citrate stabilised nanoparticles functionalized with the BHQ linker at different laser excitation frequencies. All spectra were taken from aggregated nanoparticles-sat NaCl was used as an aggregating agent.**

2.3.2 Zeta size and zeta potential of the linker-nanoparticle conjugates

The sizes of the nanoparticles were measured using the technique of the Dynamic Light Scattering (DLS). Experimental details are described in section 6.4.3. This technique measures the Brownian motion of the nanoparticles and relates them to their size. The nanoparticles are illuminated with laser light, and the fluctuations of the scattered light analysed. The nanoparticle diameter obtained by this technique is called the hydrodynamic diameter and is the diameter of the sphere which has the same translational diffusion coefficient as the particle being measured. The value for this coefficient depends on the size of the particle core, surface structure and the type and concentration of the ions present in the sample. The sizes obtained by DLS are often bigger than those measured by electron microscopy which only visualises the conductive particle core [117-119].

The extinction coefficient values of bare gold and silver nanoparticles, indicated in the synthetic method used for their preparation, were used in all calculations. The DLS technique was used to compare the sizes of different types of linker conjugates**.** As expected the hydrodynamic diameter of both types of Au nanoparticles slightly increased after attachment of a linker. Interestingly the size of linker modified silver

nanoparticles (citrate and EDTA stabilized) was smaller than the size of the bare silver nanoparticles. This is probably due to the fact that the electrostatic and steric repulsion potential of the modified nanoparticles is higher than the one for bare nanoparticles. Therefore the repulsion force between linker-nanoparticle conjugates is larger than the same force between citrate or EDTA capped nanoparticles. Linker functionalized silver nanoparticles are better separated from each other than unmodified silver nanoparticles, thus the decrease of the hydrodynamic diameter is observed after surface modification. No change in the zeta size of the conjugates was observed for 18 nm Au and Ag EDTA nanoparticles after functionalisation with the fluorescein linker and also 18 nm Au nanoparticles functionalized with the TAMRA linker (blue color in the Table 2).

Table 2: **Zeta average size of formed conjugates.**

Linker	Type of nanoparticles	Zeta average size of colloid [nm]	Zeta average size of linker functionalized nanoparticles [nm]
6-aminofluorescein	18 nm Au	46.70±0.94	50.90±0.70
	50 nm Au	51.63±0.25	54.13±1.25
	Ag citrate	87.00±1.87	78.40±1.97
	AgEDTA	58.46±1.00	55.93±1.56
fluorescein	18 nm Au	46.70±0.94	46.1±0.61
	50 nm Au	50.10±0.36	53.33±0.60
	Ag citrate	87.00±1.87	83.30±1.70
	AgEDTA	58.46±1.00	59.33±1.14
TAMRA	18 nm Au	53.43±0.55	52.93±1.95
	50 nm Au	50.10±0.36	70.40±1.83
	Ag citrate	87.00±1.87	77.80±2.02
	AgEDTA	58.46±1.00	56.40±0.20
BHQ	18 nm Au	46.70±0.94	50.13±2.25
	50 nm Au	51.63±0.25	54.13±1.25
	Ag citrate	87.00±1.87	84.56±4.76
	AgEDTA	58.46±1.00	58.30±1.74

The concentrations of the samples were as follows: 18 nm Au conjugates: $7.95 \cdot 10^{-10}$ M, 50 nm Au conjugates $2.52 \cdot 10^{-11}$ M, silver nanoparticles conjugates $3 \cdot 10^{-11}$ M. The samples were resuspended in water.

To confirm that linker molecules were attached to silver nanoparticles, the size of Ag citrate colloid and Ag citrate-BHQ conjugates were measured by differential centrifugal sedimentation (DCS). DCS is a powerful technique allowing measurement of nanoparticles in the range of 2 nm-80 microns. The advantages of this method are: high resolution capability, high sensitivity and accurate, reproducible results. This method is based on the fact that particles, which have a different density than the fluid in which they are suspended, sediment at rates which depend on the gravitational field strength, density difference, fluid viscosity, particle size and shape. Inside the DCS instrument the particles are centrifuged at constant speed and temperature. All the parameters are thus constant, except the time required for the particles to settle a known distance in a fluid of known viscosity and density. This time is measured and the particle size can then be calculated [131].

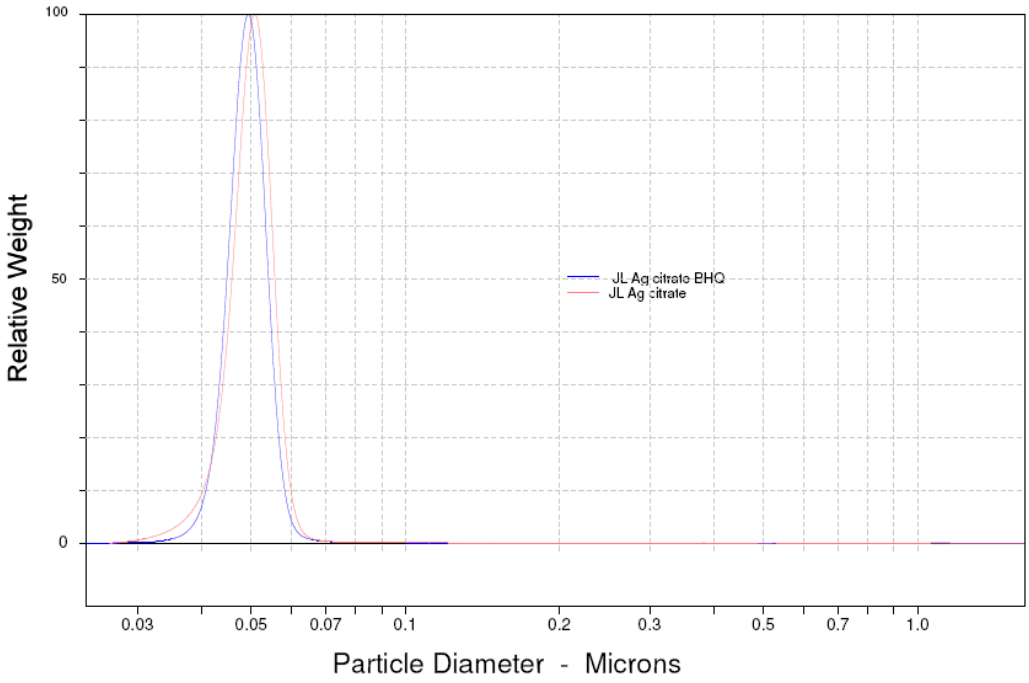

Figure 46: DCS graph of Ag citrate nanoparticles and Ag citrate-BHQ conjugates.

A DSC graph of Ag citrate colloid and Ag citrate-BHQ conjugates is shown in Figure 46. A silver density of 10.5 g/cm^3 was used to calculate the nanoparticle sizes. It can be concluded that the size of the modified silver nanoparticles is smaller than the size of bare Ag citrate nanoparticles, however the same density value was used to calculate this value. In reality the density of the BHQ linker layer on the nanoparticles surface is much lower than the density of silver. Thus if the correct density value for

the coating could be known, the real size of the nanoparticles could be calculated. Based on the fact that the density of Ag citrate-BHQ conjugates is significantly lower than the density of Ag it can be concluded that the conjugates are actually larger than the bare Ag nanoparticles.

Table 3: Zeta potential of linker-nanoparticle conjugates.

Linker	Type of nanoparticles	Zeta potential of colloid [mV]	Zeta potential of linker functionalized nanoparticles [mV]
6-aminofluorescein	18 nm Au	-37.7±9.0	-44.7±8.1
	50 nm Au	-34.3±4.0	-47.9±2.9
	Ag citrate	-33.4±3.6	-35.6±5.5
	AgEDTA	-37.0±4.7	-40.3±5.4
fluorescein	18 nm Au	-34.5±9.0	-29.4±3.4
	50 nm Au	-29.5±6.0	-26.7±2.2
	Ag citrate	-33.4±3.6	-35.1±3.8
	AgEDTA	-37.0±4.7	-42.4±3.0
TAMRA	18 nm Au	-56.3±6.5	-24.8±5.6
	50 nm Au	-34.3±4.0	-27.0±3.5
	Ag citrate	-33.4±3.6	-22.2±2.9
	AgEDTA	-37.0±4.7	-22.0±3.5
BHQ	18 nm Au	-34.5±9.0	-31.2±6.5
	50 nm Au	-29.5±6.0	-41.5±
	Ag citrate	-33.4±3.6	-38.9±4.3
	AgEDTA	-42.4±3.0	-29.4±4.2

The concentrations of the analyzed samples were as follows: 18 nm Au conjugates: $2.65 \cdot 10^{-10}$ M, 50 nm Au conjugates: $8.4 \cdot 10^{-12}$ M, silver nanoparticles conjugates $1 \cdot 10^{-11}$ M. The samples were resuspended in water.

Zeta potential is used to asses the charge stability of disperse colloidal systems. Metallic nanoparticles have a layer of weakly bound charged ligands on their surface present from their synthesis. This surface charge has a big influence on the distribution of ions present in the sample. Their presence results in the formation of a layer around the nanoparticles which is different than the bulk solution. When the nanoparticles move, this hydration sphere is moving as a part of the particle. The zeta potential is a measure of the potential at this layer when the nanoparticle is moving in

the bulk solution. Nanoparticles with high zeta-potentials of the same charge sign will repel each other and confer stability to the dispersion [120]. If the zeta potential value approaches zero the nanoparticles will be unstable and will tend to aggregate.
Experimental details regarding the measurements of zeta potential of prepared conjugates are described in section 6.4.3. High zeta-potential values obtained for most of the linker-nanoparticle conjugates prepared indicate that the modified nanoparticles exhibit high stability. For 18 nm Au nanoparticles functionalized with the TAMRA linker the zeta potential changes from -56.3 to –24.8 mV after surface modification, which is caused by addition of the positively charged reporter moiety. The same behavior was observed for other types of conjugates prepared with the TAMRA linker.

2.4 Conclusions

Four different linkers (aminofluorescein, fluorescein, TAMRA and BHQ), which can be used to functionalize gold and silver nanoparticles to: increase their stability, make them SERRS active and also give the opportunity for attachment of biomolecules, were successfully synthesized with good yields. All the synthesized linkers were used to functionalize the following types of nanoparticles: 18 nm citrate stabilised Au, 50 nm citrate stabilised Au, 40 nm citrate stabilised Ag and 40 nm EDTA stabilised Ag. All the conjugates were successfully prepared however differences in conjugates stability were observed. Both types of silver nanoparticles used in this study, functionalized with any of the linkers were not stable in the buffers usually used for conjugation of linker modified nanoparticles with DNA. Similar behavior was observed for 50 nm gold nanoparticles functionalized with TAMRA and fluorescein linkers. All other prepared conjugates were stable in 0.1 M PBS for several weeks and could be easily reacted with amino-modified DNA under commonly used conditions.

Aminofluorescein and fluorescein linkers contain within their structures very similar fluorescent dyes, however the geometry of these compounds is different. It was observed that the linker geometry has influence on the intensity of the SERRS signal obtained from the system and also on the number of linker molecules attached to metallic nanoparticles surface. Both fluorescein and aminofluorescein linker conjugates gave SERRS signals at 514 nm and 633 nm, however the intensity of the

signals was higher for aminofluorescein linker conjugates. Despite the very similar chemical structures of the fluorescent dyes used for the synthesis of these linkers, the geometry of the compounds was different. In the case of the aminofluorescein linker, adsorption onto the nanoparticle surface results in the label being closer to the metal surface. Therefore it experiences a larger enhancement and thus more intense SERRS signals are obtained. The number of linker molecules which attached to nanoparticles surface was significantly higher for the aminofluorescein linker when compared with the fluorescein linker. Observed difference can be explained by different geometry of synthesized linkers. The aminofluorescein linker is significantly smaller so more molecules can be packed on to the metal surface.

The highest surface coverage values were obtained for the TAMRA linker conjugates. This can be explained by the presence of positively charged dye within TAMRA linker, which is attracted by the negatively charged surface of the nanoparticles. TAMRA linker conjugates gave good SERRS response at 633 nm.

All types of conjugates formed with the BHQ linker gave a good SERRS response at a laser excitation frequency of 633 nm. Additionally, both types of silver nanoparticles used, after functionalisation with this linker gave intense SERRS signals at laser excitation frequencies of 514 and 785 nm.

The DLS measurements of the hydrodynamic diameter of bare nanoparticles and after linker attachment confirmed the surface modification. The zeta potential values measured for all types of conjugates indicate that they exhibit high stability. Less negative zeta potential values observed for all types of nanoparticles after TAMRA containing linker attachment is a direct result of the linker containing a positive charge.

The presence of a free carboxyl group within the synthesized linkers makes it possible to conjugate linker functionalized nanoparticles to amino-modified oligonucleotides or other biomolecules of interest. Oligonucleotide functionalized nanoparticles can then be used as probes for the detection of specific DNA sequences in a sandwich assay format.

Chapter 3

Preparation of SERRS active, oligonucleotide functionalized nanoparticles

---

This chapter describes the preparation of nanoparticle-linker-oligonucleotide conjugates by coupling linker terminal COOH group with amino-modified oligonucleotides. The following DNA sequence was used in all experiments described within this chapter: 5' AAA AGC TAA GTC T 3'(strand 1, Appendix A). The strand was modified with C6 amino-modifier on the 5' end. The properties of the prepared conjugates are also described within this chapter.

3.1 Introduction

In order to prepare SERRS active, oligonucleotide functionalized nanoparticles the terminal COOH groups of the linker-nanoparticle conjugates was reacted with amino-modified oligonucleotides. Many different coupling reagents can be used to form an amide linkage between the carboxyl group of one molecule and the primary amine group of a second molecule. Carbodiimides, such as *N, N'*-dicyclohexylocarbodiimide (DCC); *N, N'*-diisopropylcarbodiimide (DIC); *N*-(3-dimethylaminopropyl)-*N'*-ethyl carbodiimide hydrochloride (EDC·HCl); 1-cyclohexyl-3-(2-morpholinoethyl) carbodiimide (CMC) are the most commonly used [2, 121].

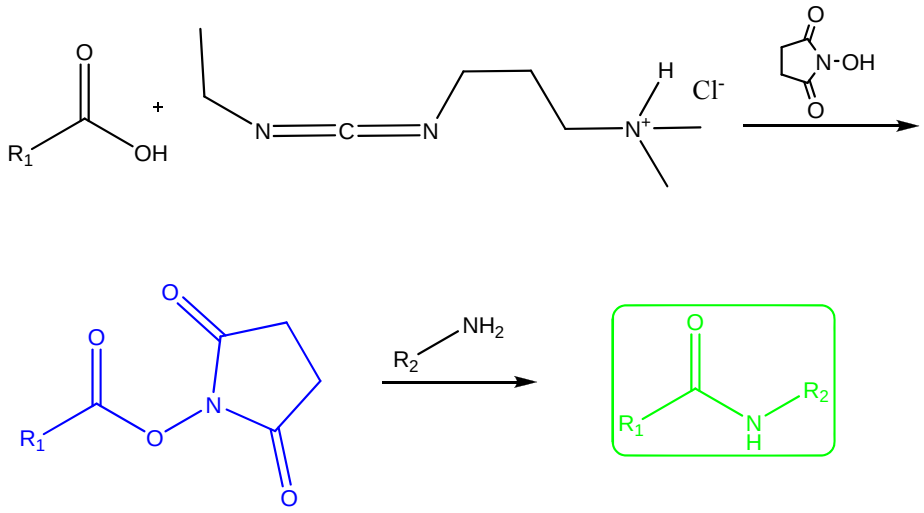

Figure 47: Two step formation of an amide bond in the presence of EDC·HCl and NHS.

Due to the fact that DIC and DCC are insoluble in water they can not be used during bioconjugate preparation which usually requires the use of aqueous buffer solutions. EDC·HCl is a water soluble carbodiimide commonly used to form an amide linkage between biomolecules and the surface of a nanoparticle. Additionally the isourea side product formed during this reaction is also water soluble, which

simplifies purification. The biggest disadvantage of this reaction is the very fast hydrolysis (a few seconds) of the active ester (o-acylisourea) leaving group formed in the reaction of EDC·HCl with the carboxyl group, while the reaction of this active group with primary amines is very slow [121]. One of the ways to overcome these problems is to use EDC·HCl with *N*-hydroxysulfosuccinimide (sulfo NHS) [65, 121]. In the first stage of this coupling reaction a sulfo-NHS ester of a moiety containing a carboxyl group is formed. This hydrophilic, reactive group is water soluble, is slowly hydrolyzed in an aqueous environment and rapidly leaves in the presence of primary amines allowing the creation of stable amide linkages between the activated carboxyl group and attacking nucleophile (NH_2) (Figure 47). The coupling reaction has to be performed in a suitable buffer system to ensure its maximum efficiency [121], however the use of the buffers might be problematic when the coupling reaction is performed on the surface of metallic nanoparticles. If the nanoparticles to be conjugated to DNA are not stable enough the addition of the buffer may cause their irreversible aggregation.

1-cyclohexyl-3-(2-morpholinoethyl) carbodiimide (CMC) is also a water soluble carbodiimide, however the possibility of side reactions with sulfhydryl groups, phenols, alcohols and other nucleophiles which lead to the formation of unreactive covalent complexes and fast hydrolysis of the active ester group formed during its reaction with the COOH group make it difficult to use during bioconjugate preparation. The use of CMC with sulfo-NHS has not been reported in the literature [121].

N, N'-carbonyldiimidazole (CDI) is another zero-length crosslinker allowing formation of amide linkages between carboxylic acids and primary amines. The formation of the activated carboxylic acid must take place in dry organic solvents, the presence of more than 0.1% of water in the reaction mixture causes fast hydrolysis and inactivation of the active intermediate. The conjugation reaction might be performed in an aqueous environment, however the use of organic solvents for that purpose provide greater yields [121].

Kunishima and co-workers described the use of another amide bond forming reagent - 4-(4,6-dimethoxy-1,3,5-triazin-2-yl)-4-methylmorpholinium chloride (DMT MM) [122, 123]. DMT MM allows simple, one-step condensation of carboxylic acids and amines in water and alcohols (Figure 48) with yields much higher than those

observed for the same coupling reaction performed in the presence of EDC·HCl or DCC [122, 123].

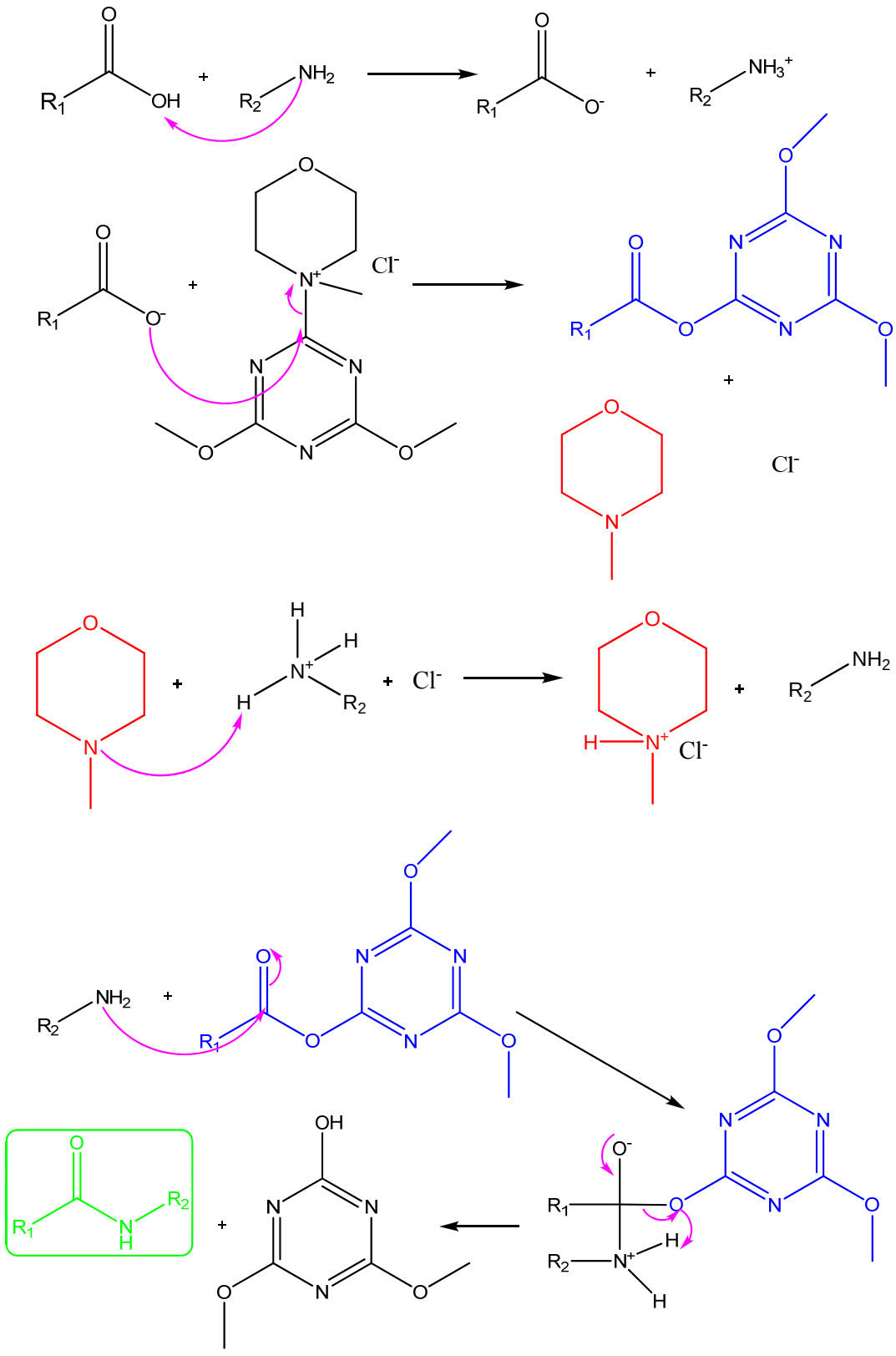

Figure 48: Mechanism of DMT MM activated amidation of carboxylic acids.

Another advantage of using this reagent is the possibility of performing the coupling reaction in water, therefore DMT MM could be used to prepare biomolecule functionalized metallic nanoparticles when stability problems occur.

Two different chemistries allowing conjugation of amino-modified oligonucleotides to the terminal carboxyl groups of linker molecules attached to the nanoparticle surface were investigated. The first requires the use of EDC·HCl and sulfo NHS and is most commonly used for conjugation of biomolecules to free functional groups attached to the nanoparticle surface [121]. The other, novel method uses the less costly, more efficient DMT MM approach in a simple, one-step condensation of the free carboxyl group of the linker attached to the nanoparticle surface with amino-modified DNA. This reaction was performed in different solvent systems in order to optimize its conditions. DMT MM has not previously been used for the preparation of bioconjugates. This new method offers an improved ease of synthesis of dye tagged nanoparticles and simplifies the often lengthy procedures commonly used.

3.2 Synthesis of oligonucleotide functionalized nanoparticles

In order to react the linker functionalized nanoparticles with amino-modified oligonucleotides, the linker modified nanoparticles prepared as described in section 2.3 were resuspended in 0.1 M PBS, pH = 7.6. Then EDC·HCl and sulfo NHS were added to the reaction mixture. After 30 mins of activation, amino-modified oligonucleotides were added to the reaction mixture and the sample allowed to react for 16 hrs at room temperature. The sample was then centrifuged, the supernatant removed and the pellet resuspended with 0.1 or 0.3 M PBS. The experimental details are described in section 6.3.3.

All silver nanoparticles functionalized with the different available linkers were not stable under the conditions used for the EDC·HCl and sulfo NHS coupling reaction. The same behavior was observed for 50 nm Au nanoparticles functionalized with fluorescein and TAMRA linkers. 18 nm Au nanoparticles functionalized with all types of prepared linkers and 50 nm Au nanoparticles functionalized with aminofluorescein and BHQ linkers were stable under these conditions and could be conjugated to amino-modified ssDNA in the presence of EDC·HCl and sulfo NHS.

The number of DNA strands attached to each type of conjugate was calculated using the DNAse I method described by McKenzie *et al.* (Table 4) [124]. Fluorescently labeled oligonucleotides (Strand 1, Appendix A was used in all experiments) were used during probe preparation. The sequence used contained C6 amino-modifier on the 3' end and TAMRA or FAM on the 5' end. Sequence modified with TAMRA was used for quantification of number of DNA strands attached to nanoparticles functionalized with fluorescein and aminofluorescein linkers, whereas strand modified with FAM was used for quantification of number of oligonucleotides attached to nanoparticles functionalized with TAMRA and BHQ linkers. DNAse I, which catalyses the hydrolysis of phosphodiester linkages in the DNA backbone, was added to the samples. Hydrolysis of any bond along the oligonucleotide attached to a nanoparticle will cause the release of the fluorescent dye into the bulk solution. Dividing the concentration of the fluorescent dye in the bulk solution (which is the same as the concentration of oligonucleotides attached to the surface of the nanoparticles) by the nanoparticles concentration within the same sample, allows the number of DNA strands attached to one nanoparticle to be quantified. This assumes 100% efficiency of the DNAse I [124]. The experimental details are described in section 6.4.2.

It was found that the highest surface coverage was obtained for TAMRA linker functionalized 18 nm gold nanoparticles. For the same type of gold nanoparticles functionalized with fluorescein, aminofluorescein and BHQ linkers the number of DNA strands attached to the conjugates was found to be much lower. In the case of fluorescein and aminofluorescein linkers the results suggest that some nanoparticles are not functionalized with oligonucleotides at all. The higher surface coverage observed for the TAMRA linker conjugates is probably due to the larger number of terminal COOH groups, available for conjugation. It was previously shown that significantly more TAMRA linkers were attached to the nanoparticles, compared with fluorescein and aminofluorescein linkers (Chapter 2.3). For larger gold nanoparticle conjugates more DNA strands were attached to the nanoparticles functionalized with BHQ linker than the same type of nanoparticles functionalized with the aminofluorescein linker.

Table 4: No of DNA strands attached to formed conjugates in the presence of EDC·HCl, sulfo NHS and DMT MM.

Type of conjugate	Coupling agent	No of DNA strands attached to one nanoparticle	Surface coverage [pmol/cm^2]
18 nm Au Af	EDC·HCl, sulfo NHS	0.31±0.01	0.097±0.004
	DMT MM	0.51±0.03	0.16±0.009
50 nm Au Af	EDC·HCl, sulfo NHS	9.36±1.53	0.23±0.04
	DMT MM	11.33±3.75	0.28±0.09
Ag citrate Af	EDC·HCl, sulfo NHS	-	-
	DMT MM	-	-
Ag EDTA Af	EDC·HCl, sulfo NHS	-	-
	DMT MM*	63.04±0.17	2.09±0.007
18 nm Au F	EDC·HCl, sulfo NHS	0.16±0.036	0.026±0.006
	DMT MM	0.18±0.028	0.029±0.005
50 nm Au F	EDC·HCl, sulfo NHS	-	-
	DMT MM	-	-
Ag citrate F	EDC·HCl, sulfo NHS	-	-
	DMT MM	-	-
Ag EDTA F	EDC·HCl, sulfo NHS	-	-
	DMT MM*	144.42±11.55	4.78±0.38
18 nm Au T	EDC·HCl, sulfo NHS	9.48±0.29	1.54±0.05
	DMT MM	9.23±0.53	1.50±0.008
50 nm Au T	EDC·HCl, sulfo NHS	-	-
	DMT MM	-	-
Ag citrate T	EDC·HCl, sulfo NHS	-	-
	DMT MM	-	-
Ag EDTA T	EDC·HCl, sulfo NHS	-	-
	DMT MM*	1646±174	54.42±5.75
18 nm Au BHQ	EDC·HCl, sulfo NHS	1.25±0.19	0.21±0.03
	DMT MM	0.69±0.07	0.11±0.013
50 nm Au BHQ	EDC·HCl, sulfo NHS	32.2±1.41	0.81±0.04
	DMT MM	73.36±20.31	1.87±0.55
Ag citrate BHQ	EDC·HCl, sulfo NHS	-	-
	DMT MM*	18.71±3.64	0.62±0.13
Ag EDTA BHQ	EDC·HCl, sulfo NHS	-	-
	DMT MM*	9.05±1.92	0.30±0.06

Af-Aminofluorescein linker, F-Fluorescein linker, T-TAMRA linker, BHQ-BHQ linker; *-coupling reaction was performed in water.

In the next experiment the same oligonucleotide functionalized conjugates were prepared in the presence of DMT MM. DMT MM was synthesized following the protocol described by Kunishima *et al.* [122, 123]. 2-chloro-4, 6-dimethoxy-1, 3, 5-triazine (CDMT) was reacted with *N*-methylmorpholine (NMM) in THF at room temperature. The product (DMT MM) was then filtered off and used without further purification (Figure 49). The experimental details are described in section 6.1.6.

The conditions used for the DMT MM coupling reaction were similar to those used for amide linkage formation in the presence of EDC·HCl, sulfo NHS. Linker functionalized nanoparticles prepared as previously described (Chapter 2.3) were resuspended in 0.1 M PBS pH = 7.6. Amino-modified oligonucleotides and DMT

MM dissolved in water were then added. The reaction mixture was allowed to react for 16 hrs, then the samples were centrifuged, supernatants were discarded and the pellets resuspended in 0.1 M or 0.3 M PBS. It has been reported that DMT MM is also effective when the amide bond formation reaction is performed in water [122, 123]. Therefore conjugation of linker functionalized nanoparticles, not stable in phosphate buffer, with amino-modified DNA was performed in water. The experimental details are described in section 6.3.4. In the case of Ag citrate nanoparticles functionalized with aminofluorescein, fluorescein and TAMRA linkers and also 50 nm Au nanoparticles functionalized with TAMRA and fluorescein linkers, addition of ssDNA to the conjugates resuspended in water caused irreversible aggregation of the nanoparticles. The oligonucleotide functionalized nanoparticles could not be prepared.

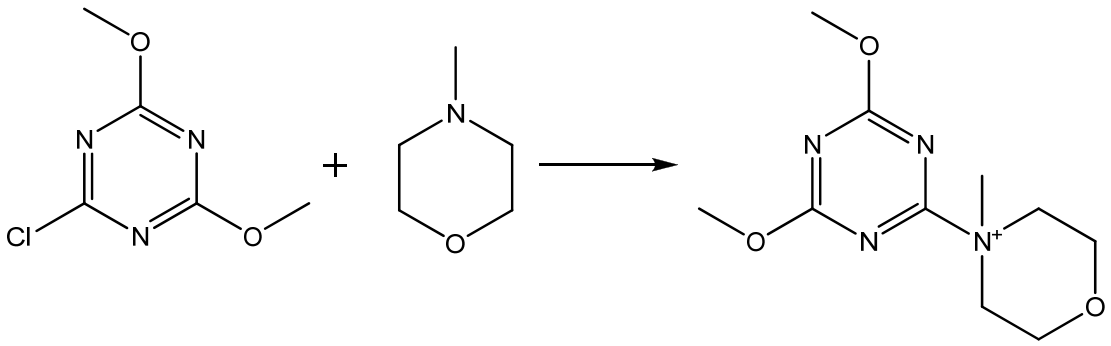

Figure 49: Synthesis of the DMT MM.

The number of DNA strands attached to each type of conjugate was quantified using the DNAse I method [124]. Experimental details are given in section 6.4.2. It was observed that for smaller gold nanoparticles both amide bond forming reagents exhibit similar effectiveness. In the case of 50 nm Au nanoparticles more DNA strands attached to the particles when DMT MM was used. In the case of the BHQ linker, the surface coverage obtained for probes prepared in the presence of DMT MM was more than twice that observed for conjugates prepared with EDC·HCl, sulfo NHS. The opportunity of performing the coupling reaction in water makes it possible to conjugate Ag EDTA nanoparticles functionalized with all linker types and also Ag citrate nanoparticles functionalized with BHQ linker, with oligonucleotides. Unfortunately the oligonucleotide functionalized nanoparticles were not stable in the

buffers which are usually used for DNA hybridisation, thus they can not be used as probes for detection of specific DNA sequences. In the case of silver nanoparticles functionalized with the linkers containing fluorescent Raman labels within their structure the short PEG unit (3 mer) was found not to be stabilizing the nanoparticles enough. The use of longer PEG was required to stabilize these bigger nanoparticles. Low numbers of DNA strands attached to the BHQ-silver conjugates indicate that there was a low number of the BHQ linker moieties immobilized on the metal surface, thus low numbers of COOH groups, available for conjugation, were present on the surface. This causes the low stability of the BHQ-silver conjugates in the hybridisation buffer.

It was reported that DMT MM is more effective as an amide bond forming reagent if the reaction is performed in alcohols, such as methanol, ethanol or isopropanol. Methanol can not be used as a solvent during functionalisation of nanoparticles with oligonucleotides because DNA is not soluble in MeOH and would precipitate from the reaction mixture. To compare the effectiveness of DMT MM in different solvent systems, BHQ functionalized 50 nm gold nanoparticles were reacted with amino-modified oligonucleotides in the following solvent systems: 10% MeOH in water, water and 0.1 M PBS pH=7.6. The pH of the solvent may influence the effectiveness of the amide linkage formation by DMT MM, therefore the coupling reaction was also performed in 0.1 M PBS pH=7.0. Experimental details are given in section 6.3.4. The number of DNA strands attached to each type of conjugate was calculated using the DNAse I method (Table 5) [124]. It was found that the highest surface coverage was obtained when the coupling reaction was performed under neutral conditions and in water.

In order to check if a similar effect would be observed for nanoparticles functionalized with a linker containing a fluorescent dye and a shorter PEG unit 18 nm Au nanoparticles functionalized with the TAMRA linker were reacted with oligonucleotides in the presence of DMT MM in water. The number of DNA strands attached to one nanoparticle was calculated using the DNAse I method [124]. It was found that the surface coverage obtained for the conjugates prepared under these conditions was more than twice (3.71±0.57) that observed for conjugates prepared in the presence of DMT MM in phosphate buffer (1.50±0.008).

Table 5: Number of DNA strands attached to 50 nm Au nanoparticles functionalized with the BHQ linker in different solvent systems.

Solvent used for amide bond formation reaction	No of DNA strands attached to one Au nanoparticle	Surface coverage [pmol/cm^2]
0.1M NaCl in 10mM phosphate buffer pH=7.0	57.6±20.24	1.106±0.50
0.1M NaCl in 10mM phosphate buffer pH=7.6	73.36±20.31	1.866±0.55
10% MeOH in water	50.92±9.55	1.27±0.24
water	139.9±11.17	3.495±0.27

In most of the cases the number of DNA strands which attached to one nanoparticle in the presence of DMT MM, when the coupling reaction was performed in water, was about two times higher than the number of oligonucleotides attached in the presence of the same coupling agent in phosphate buffer. The lower yield of the conjugation reaction performed in the phosphate buffer might be caused by the screening effect of the salt ions present in the reaction mixture. DMT MM was found to be a more efficient, less costly amide bond formation reagent which offers the opportunity for the preparation of oligonucleotide functionalized nanoparticles in a simple one-step process performed in water.

Due to the very low DNA surface coverages obtained for 18 nm Au-aminofluorescein and 18 nm Au-fluorescein, these linkers were reacted with amino-modified DNA before their attachment to nanoparticles. A similar experiment was performed for TAMRA and BHQ linkers. The reactions were performed in the presence of EDC·HCl / sulfo NHS and DMT MM under the same conditions as those used for the conjugation of amino-modified oligonucleotides to linker functionalized nanoparticles. The products were purified by HPLC. In all cases a new peak, corresponding to a moiety which absorbs at 260 nm and also at the absorbance maximum of the dye incorporated within the linker structure, appeared on the analytical chromatogram, however the MALDI of the purified products did not indicate their presence at the expected molecular masses. The experimental details are described in section 6.3.6. It was concluded that the conjugation reaction worked, however its efficiency was very low, thus the presence of the expected products was not confirmed by MALDI. This is probably caused by the formation of hydrogen bonds within the linker structure, which results in the terminal COOH groups not

being available for the conjugation reaction. This method was not used to prepare oligonucleotide functionalized nanoparticles.

3.3 Properties of oligonucleotide functionalized nanoparticles

3.3.1 Gel electrophoresis

One of the ways which allows confirmation of DNA attachment to nanoparticle based probes is gel electrophoresis. Gel electrophoresis is a powerful technique widely used in the separation of DNA of different sizes. In this method, charged particles migrate in a porous matrix (for example agarose gel) under an electric field. Particle mobility depends on their charge and size. If the change in charge dominates the change in size then the mobility of Au nanoparticles increases (addition of negative charge) or drastically decreases (addition of positive charge). In the case of negatively charged Au particles the attachment of negatively charged DNA molecules causes an increase of size which is seen as a retardation of the nanoparticle band on the gel [125-130].

1.5% agarose gels were prepared, then loaded with all prepared conjugates (linker-nanoparticle, DNA-linker-nanoparticle) as well as bare gold and silver nanoparticles in order to compare their mobility. All gels were run in 0.5xTBE (Tris/Borate/EDTA buffer) for 60 mins at 120 mV. Experimental details are described in section 6.4.4.

3.3.1.1 The BHQ linker conjugates

Figure 50 shows the agarose gel of all the BHQ linker conjugates. As expected non-functionalised gold nanoparticles aggregated in the loading wells and did not move in the gel. This is caused by the low stability of colloidal nanoparticles in buffers or the solutions containing high salt concentrations. The mobility of both types of gold nanoparticles functionalised with the BHQ linker was slightly lower than the mobility of the same conjugates after DNA attachment. The addition of negative charge (in this case DNA) has in this case greater influence on nanoparticle mobility than the increase of the size of the conjugates, thus bands 3 and 6 moved slightly further in the gel than bands 2 and 5 (Figure 50).

Surprisingly both types of silver nanoparticles used in this study did not aggregate after loading them onto the agarose gels. Silver citrate nanoparticles were seen to aggregate slowly while moving through the gel (Figure 50, band 7) forming a long,

green band. The change of colour from yellow to green indicates that aggregation of nanoparticles had occurred. Bare Ag EDTA nanoparticles did not aggregate under the gel electrophoresis conditions used.

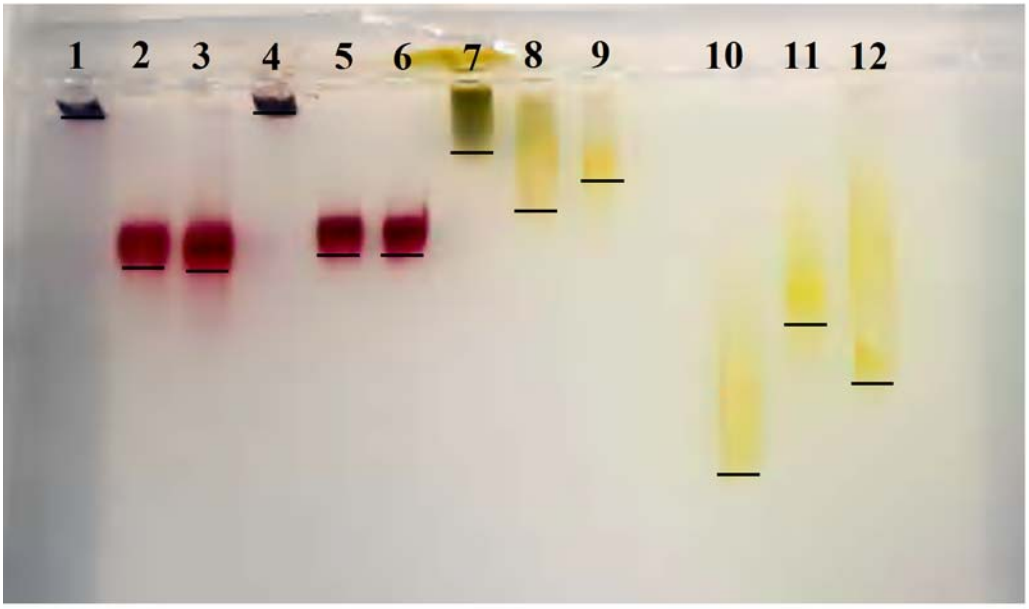

Figure 50: **Agarose gel of all the BHQ conjugates: 1- 18 nm Au colloid, 2- 18 nm Au-BHQ, 3- 18 nm Au-BHQ-DNA, 4- 50 nm Au, 5- 50 nm Au-BHQ, 6- 50 nm Au-BHQ-DNA, 7- Ag citrate, 8- Ag citrate-BHQ, 9- Ag citrate-BHQ-DNA, 10- Ag EDTA, 11- AgEDTA-BHQ, 12- AgEDTA-BHQ-DNA.**

Silver citrate-BHQ conjugates have a higher mobility in the gel compared to the same nanoparticles after oligonucleotide conjugation, which would indicate that the increase of size is the more dominant factor influencing the particle mobility, than the addition of negative charge (DNA) to the modified nanoparticles.

Functionalisation of Ag EDTA nanoparticles, with the BHQ linker, led to a decrease in the mobility of the conjugates in the agarose gel, which was seen as a retardation of the band 11 (Figure 50). This is due to an increase in the physical size of the conjugates. The addition of negatively charged DNA to Ag EDTA-BHQ conjugates increases the mobility of the prepared probes in the agarose gel.

3.3.1.2 The aminofluorescein linker conjugates

Figure 51 shows the agarose gel of all the aminofluorescein linker conjugates. In the case of 18 nm Au-Af-DNA two bands were observed on the gel. One of them corresponds to 18 nm Au nanoparticles functionalized with the aminofluorescein

linker, the second corresponds to the same conjugates after oligonucleotides attachment. The results obtained are with close agreement to the data presented in Table 4, indicating that after conjugation of 18 nm Au functionalised with the aminofluorescein linker to oligonucleotides, the oligonucleotides are attached only to some part of the nanoparticles. Nanoparticles functionalized with the linker were also present in the sample. For larger Au nanoparticles functionalized with the aminofluorescein linker only small change in the mobility of the conjugates was observed after conjugation to oligonucleotides. This is due to the fact that there is a very small amount of DNA attached to the probes (Table 4, Chapter 3). Addition of the aminofluorescein linker to Ag EDTA nanoparticles decreased the mobility of these nanoparticles, due to an increase in size of the conjugates, however attachment of the oligonucleotides (negative charge) caused it to increase.

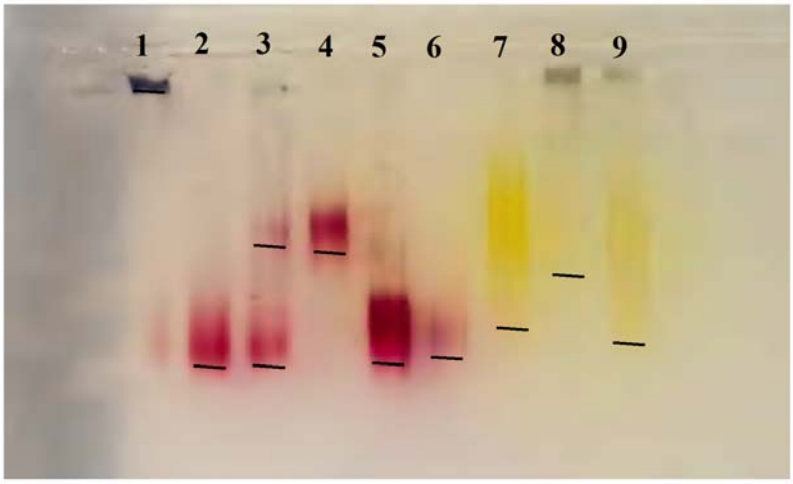

Figure 51: **Agarose gel of all the aminofluorescein conjugates: 1- 18 nm Au colloid, 2- 18 nm Au-Af, 3- 18 nm Au-Af-DNA, 4- 50 nm Au colloid, 5- 50 nm Au-Af, 6- 50 nm Au-Af-DNA, 7- AgEDTA colloid, 8- AgEDTA-Af, 9- AgEDTA-Af-DNA.**

3.3.1.3 The fluorescein linker conjugates

The fluorescein linker Au nanoparticle conjugates were similar to the case of the aminofluorescein linker conjugates, due to the very low number of DNA strands attached to the nanoparticles, no mobility difference prior to and after oligonucleotide attachment was observed (Figure 52). The mobility of the fluorescein linker-Ag EDTA conjugates was lower than the mobility of bare silver nanoparticles, which is caused by the increase of the size of the nanoparticles after linker attachment.

Addition of oligonucleotides (negative charge) to the conjugates increased their mobility.

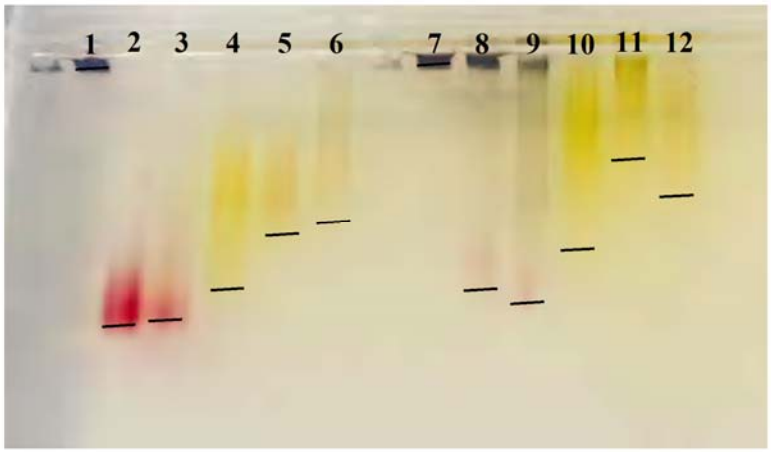

Figure 52: **Agarose gel of formed fluorescein and TAMRA linker conjugates: 1, 7- 18 nm Au colloid, 2- 18 nm Au-F, 3- 18 nm Au-F-DNA, 4, 10- AgEDTA colloid, 5- AgEDTA-F, 6- AgEDTA-F-DNA, 8- 18 nm Au-TAMRA linker, 9- 18 nm Au-TAMRA linker-DNA, 11- AgEDTA-TAMRA linker, 12-AgEDTA-TAMRA linker-DNA.**

3.3.1.4 The TAMRA linker conjugates

In the case of 18 nm Au TAMRA conjugates, aggregation of most of the nanoparticles loaded into the wells occurred, which was probably caused by the low stability of the conjugates under the gel electrophoresis conditions. The mobility of the TAMRA functionalised nanoparticles was lower than the mobility of the same size of Au nanoparticles functionalised with the fluorescein linker. This difference is caused by the addition of positive charge (TAMRA linker), which usually leads to the retardation of the band on the gel [127, 128]. Due to the small amount of DNA attached to Au-TAMRA conjugates, no big difference in the mobility of gold nanoparticles functionalized with the TAMRA linker, before and after addition of oligonucleotides, was observed.

The mobility of the Ag EDTA nanoparticles after surface modification with the TAMRA linker was lower than the mobility of the same type of nanoparticles functionalised with the fluorescein linker (bands 5 and 11, Figure 52) which is caused by the presence of positive charge within the TAMRA linker structure. Similarly as for other Ag EDTA conjugates, addition of the TAMRA linker to silver nanoparticles caused a decrease in the nanoparticle mobility while the addition of oligonucleotides caused its increase.

3.3.2 Zeta particle size and zeta potential

The hydrodynamic diameter of oligonucleotide functionalized nanoparticles was measured using DLS (Table 6). The experimental details are described in section 6.4.3. For most of the conjugates a small increase in the hydrodynamic diameter was observed after DNA attachment. For Ag EDTA-Af-DNA, Ag EDTA-BHQ-DNA and Ag citrate-BHQ-DNA conjugates a large increase in the hydrodynamic size was observed after conjugation of oligonucleotides. In the case of 18 nm Au-F-DNA, Ag EDTA-F-DNA and 18 nm Au-BHQ-DNA no difference in the hydrodynamic diameter was observed after oligonucleotides attachment (blue color in Table 6).

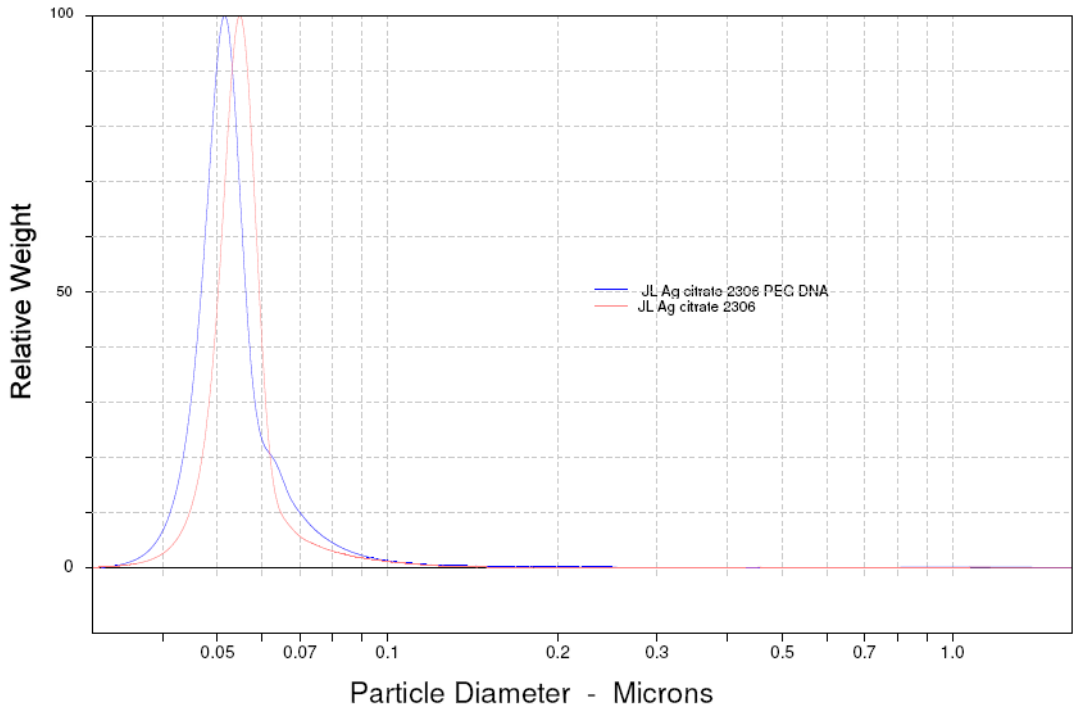

Figure 53: DSC graph of Ag citrate nanoparticles and Ag citrate-BHQ-DNA conjugates.

The results indicate that small aggregates (dimers, trimers) were formed during conjugation of Ag EDTA-Af, Ag EDTA-BHQ and Ag citrate-BHQ to oligonucleotides. The size of the Ag citrate-BHQ-DNA conjugates was measured by DSC (Figure 53). A silver density of 10.5 g/ml was used to calculate both samples sizes. Based on the fact that the density of the oligonucleotide functionalized nanoparticles is significantly lower than the density of Ag nanoparticles it can be concluded that the DNA functionalized nanoparticles are larger than bare Ag citrate nanoparticles.

Table 6: **Zeta average size of the conjugates.**

Linker	Type of nanoparticles	Zeta average size of colloid [nm]	Zeta average size of linker functionalized nanoparticles [nm]	Zeta average size of oligonucleotide-linker-nanoparticle conjugates [nm]
6-aminofluorescein	18 nm Au	46.70±0.94	50.90±0.70	55.7±0.90
	50 nm Au	51.63±0.25	54.13±1.25	56.40±0.26
	Ag citrate	87.00±1.87	78.40±1.97	-
	AgEDTA	58.46±1.00	55.93±1.56	94.65±8.98
fluorescein	18 nm Au	46.70±0.94	46.1±0.61	47.37±0.83
	50 nm Au	50.10±0.36	53.33±0.60	-
	Ag citrate	87.00±1.87	83.30±1.70	-
	AgEDTA	58.46±1.00	59.33±1.14	59.73±3.44
TAMRA	18 nm Au	53.43±0.55	52.93±1.95	57.17±5.08
	50 nm Au	50.10±0.36	70.40±1.83	-
	Ag citrate	87.00±1.87	77.80±2.02	-
	AgEDTA	58.46±1.00	56.40±0.20	67.67±0.81
BHQ	18 nm Au	46.70±0.94	50.13±2.25	50.73±1.81
	50 nm Au	51.63±0.25	54.13±1.25	57.87±0.40
	Ag citrate	87.00±1.87	84.56±4.76	144.33±10.7
	AgEDTA	58.46±1.00	58.30±1.74	93.70±5.51

The concentrations of the samples were as follows: 18 nm Au conjugates: $7.95 \cdot 10^{-10}$ M, 50 nm Au conjugates $2.52 \cdot 10^{-11}$ M, silver nanoparticles conjugates $3 \cdot 10^{-11}$ M. The samples were resuspended in water.

The zeta potential values were measured for all types of DNA-linker-nanoparticle probes (Table 7). Experimental details are described in section 6.4.3. Most of the oligonucleotide functionalized nanoparticles have a high negative zeta potential, which indicates that the probes are stable, however in the case of all the Ag EDTA-linker conjugates, a large decrease in zeta potential after oligonucleotide attachment was observed. This indicates that the stability of oligonucleotide functionalized Ag EDTA nanoparticles is very low. Addition of 10 mM phosphate buffer to the probes caused their irreversible aggregation. Closer to zero zeta potential values indicate the reduction of colloid stability.

Table 7: Zeta potential of linker-nanoparticle conjugates.

Linker	Type of nanoparticles	Zeta potential of colloid [mV]	Zeta potential of linker functionalized nanoparticles [mV]	Zeta potential of oligonucleotide-linker-nanoparticle conjugates [mV]
6-aminofluorescein	18 nm Au	-37.7±9.0	-44.7±8.1	-46.0±8.5
	50 nm Au	-34.3±4.0	-47.9±2.9	-21.8±6.3
	Ag citrate	-33.4±3.6	-35.6±5.5	-
	AgEDTA	-37.0±4.7	-40.3±5.4	-13.2±5.1
fluorescein	18 nm Au	-34.5±9.0	-29.4±3.4	-32.1±1.7
	50 nm Au	-29.5±6.0	-26.7±2.2	-
	Ag citrate	-33.4±3.6	-35.1±3.8	-
	AgEDTA	-37.0±4.7	-42.4±3.0	-13.1±5.3
TAMRA	18 nm Au	-56.3±6.5	-24.8±5.6	-30.5±3.6
	50 nm Au	-34.3±4.0	-27.0±3.5	-
	Ag citrate	-33.4±3.6	-22.2±2.9	-
	AgEDTA	-37.0±4.7	-22.0±3.5	-8.7±3.3
BHQ	18 nm Au	-34.5±9.0	-31.2±6.5	-32.0±3.2
	50 nm Au	-29.5±6.0	-41.5±	-32.7±2.3
	Ag citrate	-33.4±3.6	-38.9±4.3	-28.0±2.0
	AgEDTA	-42.4±3.0	-29.4±4.2	-8.1±5.4

The concentrations of the analyzed samples were as follows: 18 nm Au conjugates: $2.65 \cdot 10^{-10}$ M, 50 nm Au conjugates: $8.4 \cdot 10^{-12}$ M, silver nanoparticles conjugates $1 \cdot 10^{-11}$ M. The samples were resuspended in water.

3.3.3 SERRS

In order to compare the intensity of SERRS signals obtained from linker-nanoparticle conjugates, with the intensity of the signal obtained from the same conjugates after oligonucleotide attachment, SERRS spectra were taken using excitation at 633 nm, which was proven to be the most suitable for all linkers investigated (Chapter 2). The concentration of the probes were as follows: 7.56×10^{-11} M for 50 nm Au and both types of silver nanoparticles used and 3.25×10^{-9}M for 18 nm Au. All experimental details are given in section 6.4.5.

The intensity of SERRS signals obtained from 18 nm Au-Af-DNA conjugates is higher than the intensity of the signals obtained from the same conjugates prior to oligonucleotide attachment (Figure 54).

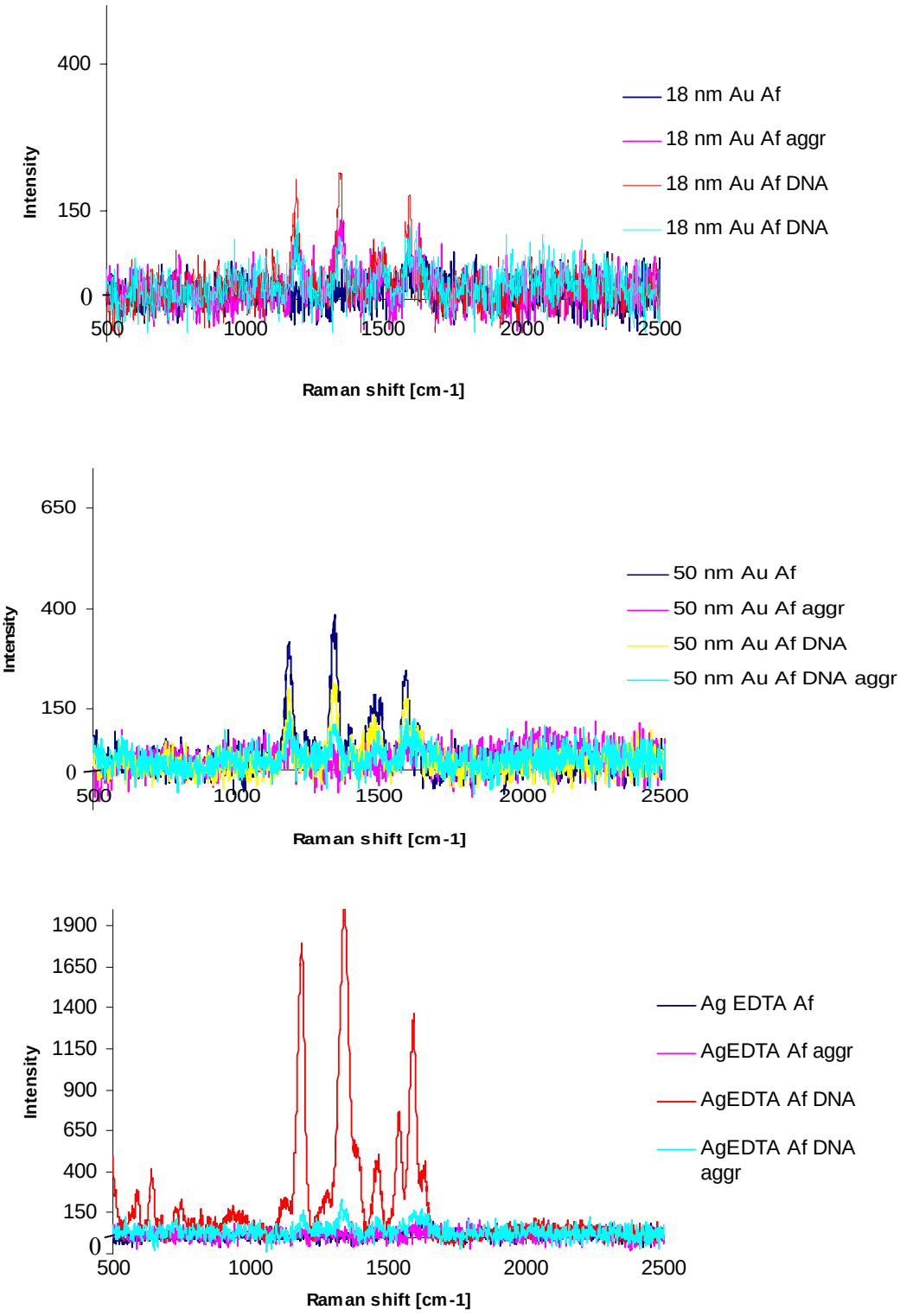

Figure 54: **SERRS spectra of the aminofluorescein linker (Af) conjugates using excitation at 633 nm; Au/Ag Af- nanoparticles functionalized with the aminofluorescein linker; Au/Ag Af DNA- nanoparticles functionalized with the aminofluorescein linker conjugated to oligonucleotides; aggr.-aggregating agent (sat. NaCl) was added to the sample in order to obtain max. enhancement.**

The change in the intensity of SERRS signal after oligonucleotide attachment might be explained either by formation of aggregates during conjugation of the oligonucleotides, or by a change in the orientation of the linker on the nanoparticle surface after addition of ssDNA in such a way that vibrational modes within the Raman reporter molecule will experience stronger or weaker surface enhancements.

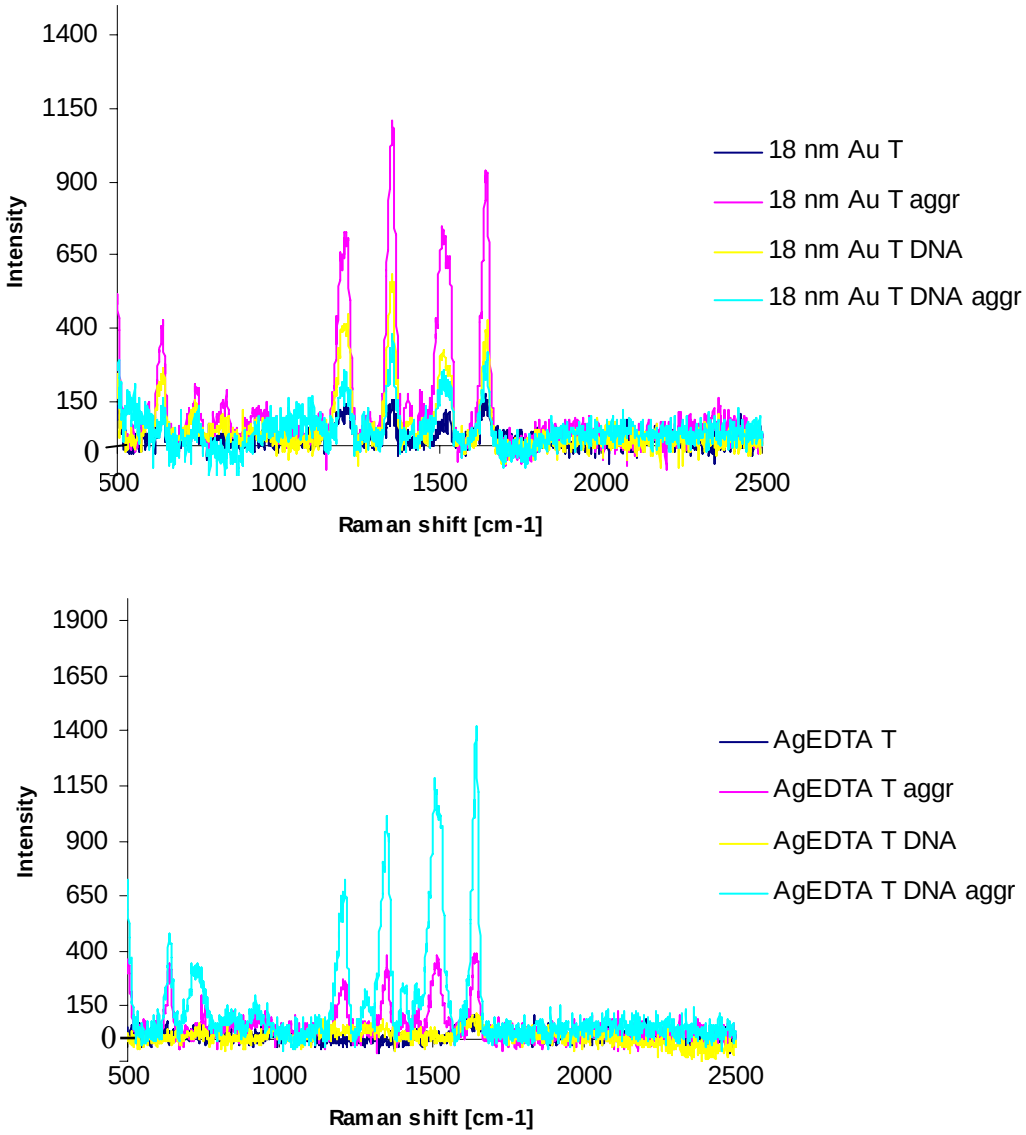

Figure 55: **SERRS spectra of the TAMRA linker (T) conjugates at 633 nm; Au/Ag T-nanoparticles functionalized with the TAMRA linker; Au/Ag T DNA-nanoparticles functionalized with the TAMRA linker, conjugated to oligonucleotides; aggr.- aggregating agent (sat. NaCl) was added to the sample in order to obtain max. enhancement.**

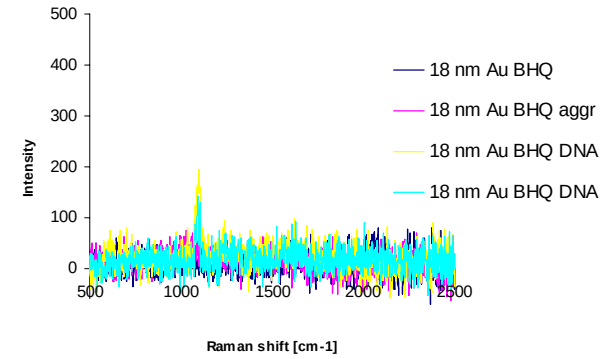

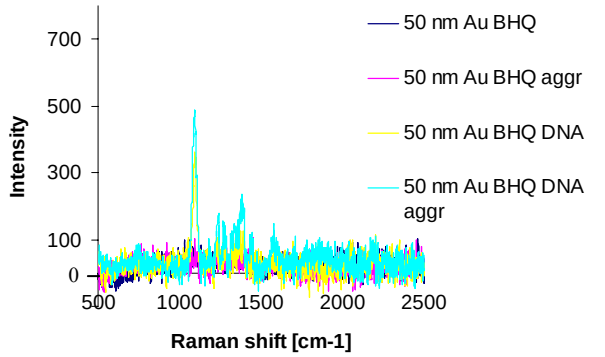

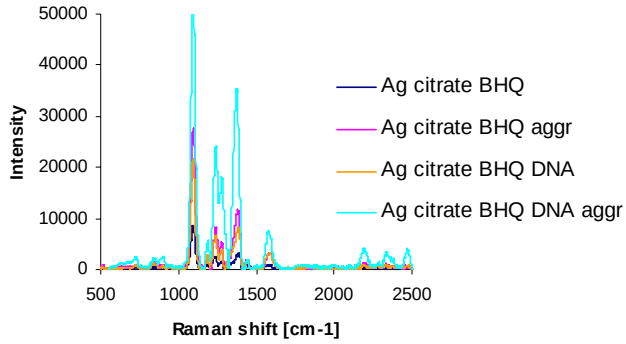

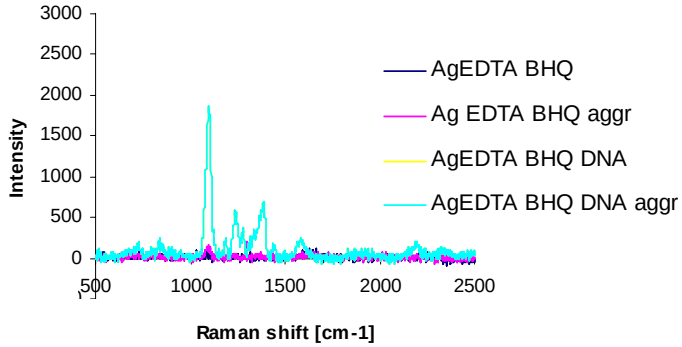

Figure 56: **SERRS spectra of the BHQ linker conjugates using excitation at 633 nm; Au/Ag BHQ- nanoparticles functionalized with the BHQ linker; Au/Ag BHQ DNA-nanoparticles functionalized with the BHQ linker, conjugated to oligonucleotides; aggr.- aggregating agent (sat. NaCl) was added to the sample in order to obtain max. enhancement.**

The surface selection rule of SERRS states that the component of the dipole moment perpendicular to the surface will be excited more strongly than the parallel component [134]. The increase of the intensity of the CH stretching modes of the para substituted aminofluorescein aromatic ring between 1100 and 1600 cm^{-1} [135] indicate that attachment of DNA to aminofluorescein linker functionalized gold nanoparticles changes the orientation of the linker on the surface from tangential to normal, thus increasing the observed SERRS signal. The DLS measurements (Table 2, Chapter 2) did not indicate the formation of aggregates during the preparation of 18 nm Au-Af-DNA. Thus it can be concluded that the observed signal enhancement was probably caused by the change of orientation of the linker on the nanoparticle surface after oligonucleotide attachment, so that the Raman reporter molecule present within the linker experiences a stronger surface enhancement.

Similar results were obtained from 18 nm Au-T (Figure 55) and 50 nm Au-BHQ conjugates (Figure 56), and also Ag EDTA-T conjugates after addition of aggregating agent (Figure 55).

For larger Au-Af conjugates, stronger SERRS signals were obtained from the conjugates prior to oligonucleotide attachment (Figure 54). Addition of oligonucleotides to 50 nm Au-Af conjugates may alter the orientation of the Raman reporter molecule on the surface in such a way that it experiences weaker surface enhancement, which lowers the intensity of the observed SERRS signal.

DLS measurements (Table 2, Chapter 2) indicated that small aggregates were formed during conjugation of Ag EDTA-Af to oligonucleotides, which resulted in a very strong SERRS signals observed for Ag EDTA-Af-DNA (Figure 54). Similar results were obtained for Ag citrate-BHQ-DNA conjugates (Figure 56). A small difference in the intensity of SERRS signal was observed for 18 nm Au-Af, 18 nm Au-T, 18 nm Au-BHQ, 50 nm Au-BHQ and Ag EDTA-T conjugates after conjugation to oligonucleotides which is another indication that this change is occurring due to surface orientation effects, not due to aggregate formation. When the aggregates are formed much stronger signal enhancement is observed.

SERRS signals obtained from all types of oligonucleotide functionalized fluorescein linker conjugates (Figure 57) were very weak. Therefore, SERRS is not the best method to monitor hybridisation of fluorescein linker probes to a complementary target. Very weak SERRS signals were also observed for 18 nm Au-BHQ conjugates (Figure 56).

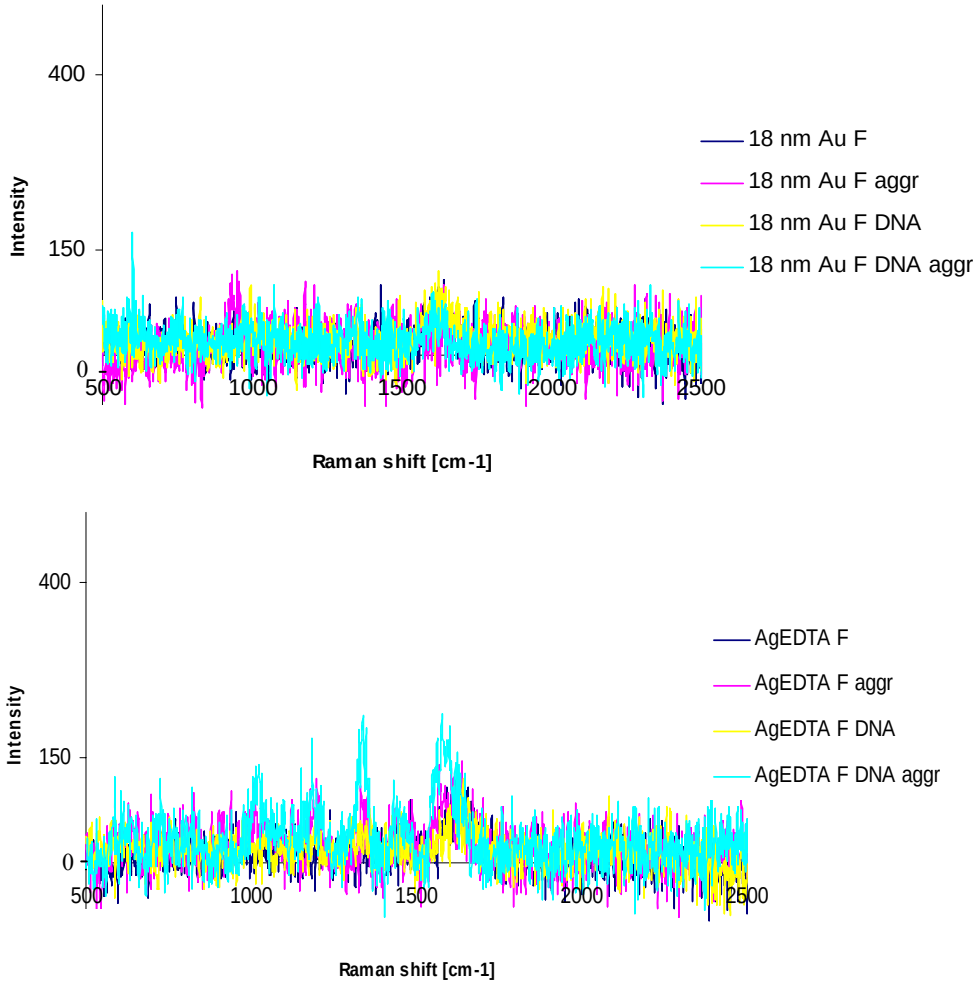

Figure 57: **SERRS spectra of the fluorescein linker (F) conjugates at 633 nm; Au/Ag F-nanoparticles functionalized with the fluorescein linker; Au/Ag F DNA-nanoparticles functionalized with the fluorescein linker, conjugated to oligonucleotides; aggr.- aggregating agent (sat. NaCl) was added to the sample in order to obtain max. enhancement.**

3.4 Conclusions

Two different methods allowing conjugation of linker-functionalized nanoparticles to amino-modified oligonucleotides were investigated: traditional, requiring the use of the commonly used EDC·HCl, sulfo NHS reagents; and a novel one, which uses DMT MM as an amide bond forming reagent. It was found that for smaller gold nanoparticles functionalized with all linkers both coupling chemistries used (under the same conditions) exhibit similar effectiveness. For 50 nm Au-linker conjugates DMT MM, used under the same conditions as EDC·HCl, was much more effective. The

DMT MM coupling reaction can be performed not only in buffers, but also in water or alcohols. In order to find optimal conditions for amide formation the reaction was performed in water, phosphate buffer (pH=7.0 and pH=7.6) and in 10% MeOH in water. It was found that the greatest yield was obtained when the coupling reaction was performed in water.

Due to the low stability of the silver nanoparticle-linker conjugates in the buffers usually used for amide linkage formation it was not possible to form the conjugate in the presence of EDC·HCl, sulfo NHS. When DMT MM was used as a coupling agent, the oligonucleotide conjugation reaction could be performed in water, thus this method allows preparation of oligonucleotide functionalized silver nanoparticles.

DMT MM, a less costly, more efficient amide bond forming reagent, allows reaction of the terminal COOH of the linkers attached to the metallic nanoparticles with amino-modified DNA in a simple, one step process, which is most effective when water is used as the reaction solvent. The use of this method allows the stability problems that occur during attachment of oligonucleotides to silver nanoparticles in the presence of EDC·HCl to be overcome. This new method offers improved ease of production of dye tagged nanoparticles and simplifies the often lengthy procedures commonly used.

Both, gel electrophoresis and DLS confirmed that there was DNA attached to all the oligonucleotide-linker-nanoparticle conjugates. Gel electrophoresis also confirmed covalent attachment of linkers on to the metal surface. It has been reported in the literature that only covalent attachment of a molecule to nanoparticle surface causes changes in the nanoparticle mobility in agarose gel [127]. If molecules, for example oligonucleotides, are electrostatically bound to nanoparticles surface the mobility of bare nanoparticles is the same as the mobility of nanoparticles with oligonucleotides electrostatically attached to their surface.

Most of the conjugates had a high, negative zeta potential indicating their high stability. The only exceptions were oligonucleotide functionalized AgEDTA nanoparticles which had low, negative zeta potential values. These probes were not stable and addition of 10 mM phosphate buffer caused their irreversible aggregation.

For most of the oligonucleotide functionalized nanoparticles, a small increase in the intensity of the SERRS signal after oligonucleotide attachment was observed. This was caused by a change in orientation of the Raman reporter molecule (built within the linker structure) with respect to the nanoparticle surface, after oligonucleotide

attachment, in such a way that the label experienced stronger surface enhancement. DLS measurements indicated that a large increase in the intensity of SERRS signal observed for Ag EDTA-Af and Ag citrate-BHQ conjugates after oligonucleotide attachment was caused by the formation of small aggregates during the conjugation process.

All types of fluorescein linker conjugates and 18 nm Au-BHQ-DNA conjugates gave no SERRS signal using an excitation of 633 nm. It was concluded that SERRS is not a suitable technique to monitor hybridisation of such probes with their complementary target.

Due to the low stability of all synthesized Ag-linker-DNA conjugates, and also 50 nm Au nanoparticles functionalized with the TAMRA or the fluorescein linkers and conjugated to oligonucleotides, these probes were not carried forward to further work.

Chapter 4

Hybridisation assay

This chapter describes the use of the following conjugates: 18 nm Au-aminofluorescein linker-DNA; 50 nm Au-aminofluorescein linker-DNA; 18 nm Au-fluorescein linker-DNA; 18 nm Au-TAMRA linker-DNA; 18 nm Au-BHQ linker-DNA and 50 nm Au-BHQ linker-DNA, as a probes in the detection of specific DNA sequences in a sandwich assay format.

4.1 Introduction

In a nanoparticle aggregation based DNA detection assay involving SERS gold or silver nanoparticles are functionalized with specific DNA sequences. When two probes containing different DNA strands are mixed together in a 1:1 molar ratio and target complementary to both probes is added, the target cross-links the nanoparticles by hybridisation. This process can be monitored by the naked eye (a colloid will change color upon aggregation), by extinction spectroscopy (usually broadening and a red shift of the metal surface plasmon band is observed) or by SERRS (aggregation of nanoparticles causes an increase in the intensity of the SERRS signal) [5-7, 13, 15, 20-22, 28, 30]. Gold and silver nanoparticles functionalized with thiolated [5, 7, 13, 20-22, 35] or multithiol modified [15, 28, 30] oligonucleotides are most commonly used as probes in the detection assay described above. Due to the lack of Raman reporter in this kind of conjugate, the hybridisation process can not be monitored by SERRS. In order to make this kind of detection possible, Raman active nanoparticles conjugated to oligonucleotides need to be used as probes. Many ways that allow their preparation are described in the literature [53, 54, 56, 60, 61, 63, 64, 67, 72, 74, 77, 78, 81, 82]. The use of a linker containing thioctic acid as a surface complexing group, a Raman tag and a free carboxyl group for amino-modified DNA attachment was chosen for that purpose within this work.

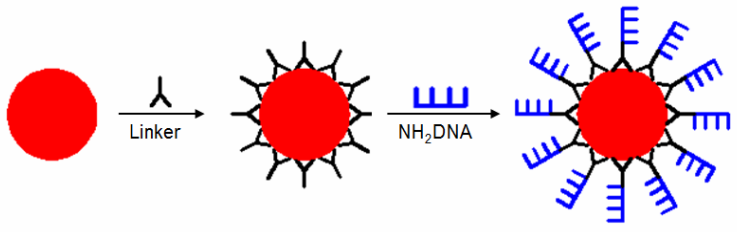

Figure 58: Preparation of oligonucleotide functionalized nanoparticles.

The oligonucleotide functionalized nanoparticles were prepared by addition of one of the synthesized linkers (aminofluorescein, fluorescein, TAMRA, BHQ) to colloidal

nanoparticles (Au or Ag), then the terminal COOH group of the linker was conjugated to amino-modified DNA in the presence of the amide linkage forming reagent-DMT MM, which was found to be much more efficient than commonly used for that purpose EDC·HCl / sulfo NHS (Figure 58). All experimental details are described in sections 6.3.1, 6.3.3 and 6.3.4.

In a typical hybridisation assay two sets of prepared nanoparticle probes were mixed in a 1:1 molar ratio. Then complementary or non-complementary target was added. In the presence of complementary target aggregation of the nanoparticles occurs, which causes the increase of the intensity of the SERRS signal observed from the system, and also a decrease and a red shift of the metal surface plasmon band. If non-complementary target is used the changes in the SERRS or extinction spectrum obtained from the system are not observed (Figure 59).

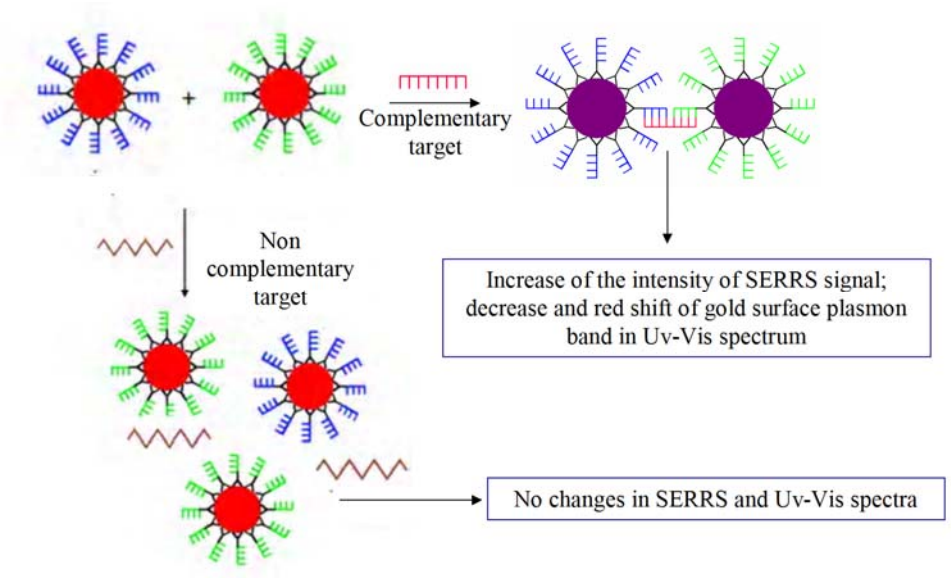

Figure 59: Schematic representation of the hybridisation assay.

Oligonucleotide functionalized nanoparticles, prepared in this work, were used as probes in the hybridisation assay outlined in Figure 59. The hybridisation of the probes to complementary target was investigated for three different probe orientations: head to tail, head to head and tail to tail (Figures 60 and 61). If not otherwise stated the same DNA sequences, as presented on Figures 60 and 61, were used to functionalize linker-nanoparticle conjugates in all experiments. Each of used sequences contained 3 adenine spacer between the C6 amino modifier and the

recognition sequence. Amine modification was incorporated either on the 5' or on the 3' end of oligonucleotides, dependent upon the orientation of the probes to each other during their hybridisation to the complementary target. In order to check if used sequences hybridize to complementary target, melting analysis (at 260 nm) of the samples containing two probes and complementary target in hybridisation buffer (0.1 M PBS), were performed. It was found that for all sequences used melting curves characteristic for oligonucleotides in solution were obtained. The concentration of the probes was kept constant for each type of nanoparticle conjugate in all experiments: for 18 nm Au nanoparticles probes 1.62 nM, for 50 nm Au nanoparticles probes 3.78×10^{-11} M.

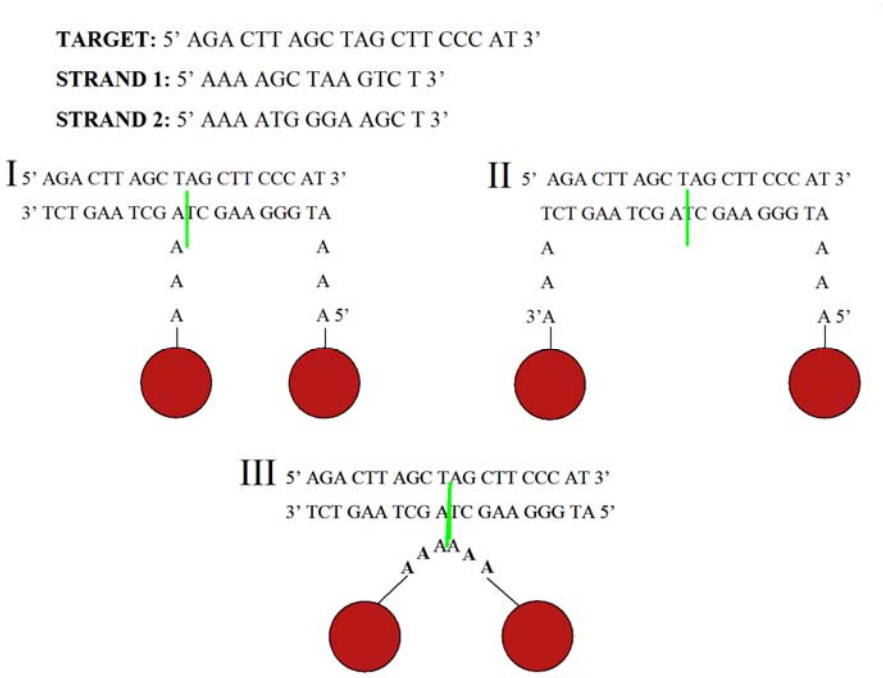

Figure 60: **DNA sequences used in the hybridisation experiments. I-probes orientated in a head-to-tail fashion, II-probes orientated in a tail-to-tail fashion, III-probes orientated in a head-to-head fashion.**

The concentration of complementary or non-complementary targets used was the same as the concentration of oligonucleotides attached to the nanoparticle surface, e. g. if it was calculated that 10 DNA strands attached to one nanoparticle the target concentration was ten times higher than the nanoparticle concentration. The experiments were also performed for target concentrations the same as the nanoparticle concentration, and also 10, 50, 100, 500 and 1000 times higher in

concentration, however it was found that the best results in all cases were obtained when the amount of target used was equal to the amount of DNA strands attached to the nanoparticle probes.

The following DNA sequences were used as non-complementary targets in all experiments: 5' AGG GGA GAT TCA GTG TGG TG 3' for probes prepared with sequences 1 and 2 (Figure 60) and 5' TTC TTT ACA TCT GGG AGC GG 3' for probes prepared with sequences 3 and 4 (Figure 61). All hybridisation experiments were performed in 0.1 M PBS pH=7.2. All experimental details regarding hybridisation assay, are described in section 6.5.

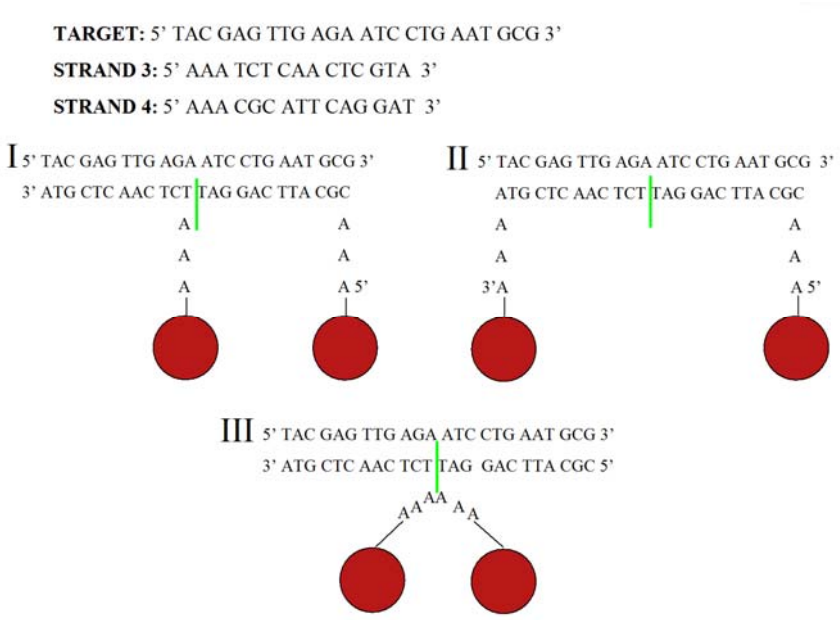

Figure 61: **DNA sequences used in the hybridisation experiments. I-probes orientated in a head-to-tail fashion, II-probes orientated in a tail-to-tail fashion, III-probes orientated in a head-to-head fashion.**

4.2 Hybridisation assay

The following oligonucleotide functionalized nanoparticles were used as probes in the nanoparticle aggregation based DNA detection assay: 18 nm Au-aminofluorescein linker-DNA; 50 nm Au-aminofluorescein linker-DNA; 18 nm Au-fluorescein linker-DNA; 18 nm Au-TAMRA linker-DNA; 18 nm Au-BHQ linker-DNA and 50 nm Au-BHQ linker-DNA. Ag EDTA nanoparticles functionalized with all types of linkers synthesised and also Ag citrate nanoparticles functionalized with the BHQ linker, could be conjugated to amino-modified DNA, when DMT MM in water was used as a coupling agent. However, the oligonucleotide functionalized silver nanoparticles were

not stable in buffers usually used for DNA hybridisation, thus they were not used as probes in the DNA detection assay. The gold nanoparticle probes were prepared by addition of the linker to gold nanoparticle suspension followed by the conjugation of the linker terminal COOH group with amino-modified DNA, in the presence of DMT MM, in water. The conjugates were used as probes in DNA detection assay outlined in Figure 59. All the experimental details regarding probes preparation and hybridisation assay are described in sections 6.3.1, 6.3.4 and 6.5.

4.2.1 The TAMRA linker probes

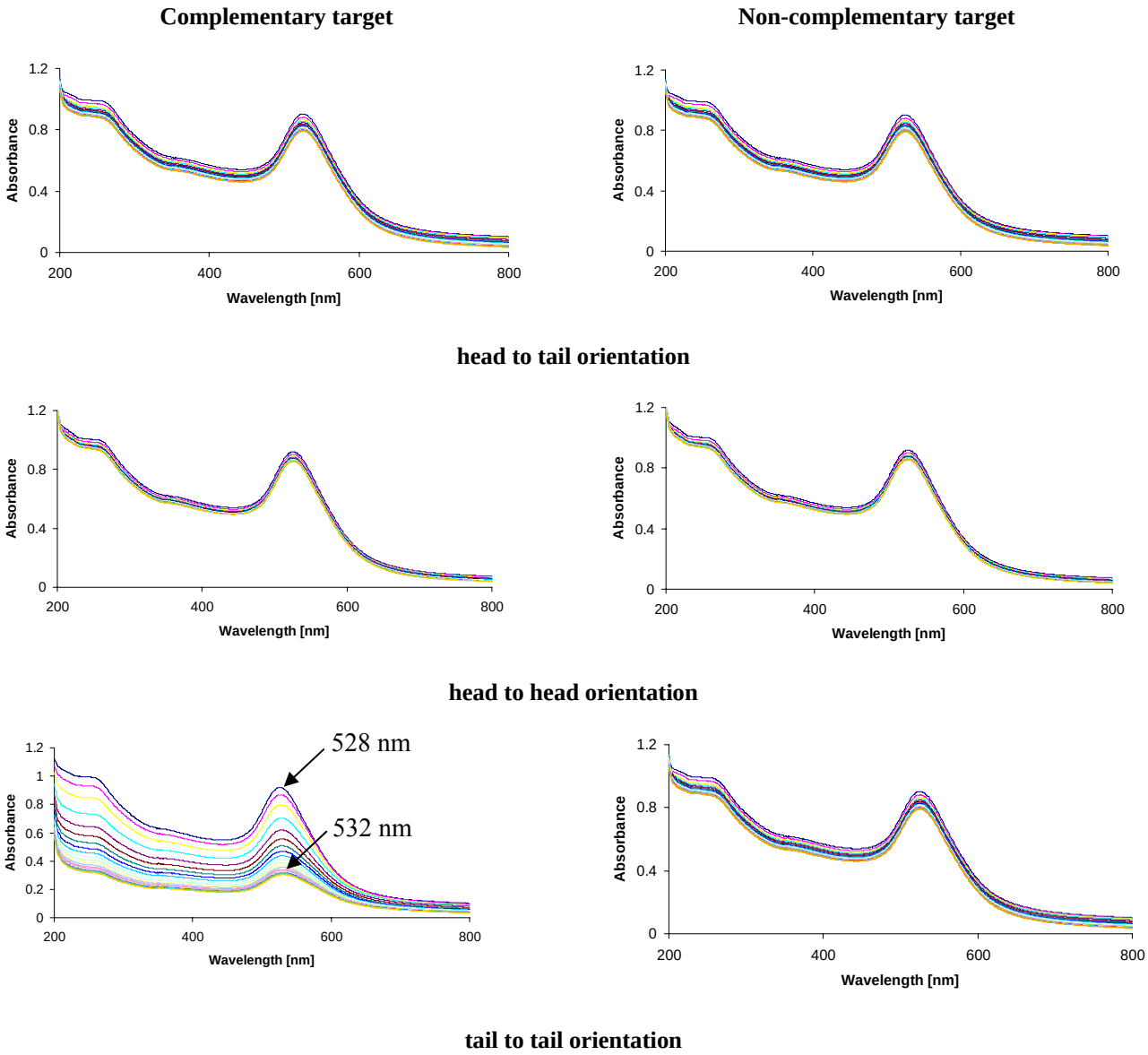

Figure 62: **Changes on the UV-Vis spectra observed with time for the samples containing two 18 nm Au-T-DNA (sequences 1 and 2) probes (1.62 nM) and complementary or non-complementary target ($4.05 \cdot 10^{-8}$ M) for different probes orientations.**

The changes observed in the extinction spectra after addition of complementary or non-complementary target to the solution containing two 18 nm Au-T probes conjugated to the sequences 1 and 2 (Figure 60) are shown on Figure 62.

When the probes were situated in a head to tail or a head to head fashion no changes in the extinction spectra after addition of complementary target were observed. The control samples did not differ from the samples containing both probes and perfect target. When the samples were orientated to each other in a tail-to-tail fashion, addition of the complementary target caused a decrease, broadening and small red shift (4 nm) of the gold surface plasmon band. The colour of the sample changed slightly after 20 hrs after addition of the fully complementary sequence, however no purple colour indicating aggregates formation was observed. No changes in the gold surface plasmon band and in the colour were observed for the sample containing non-complementary target. The melting analysis of the tail-to-tail sample were performed by monitoring the absorbance at 260 and 520 nm as a function of time (Figure 63). The expected Tm value for the sequence used is 62^0C. No sharp melting profile typical for aggregates formed during hybridisation of nanoparticle probes to complementary target was observed.

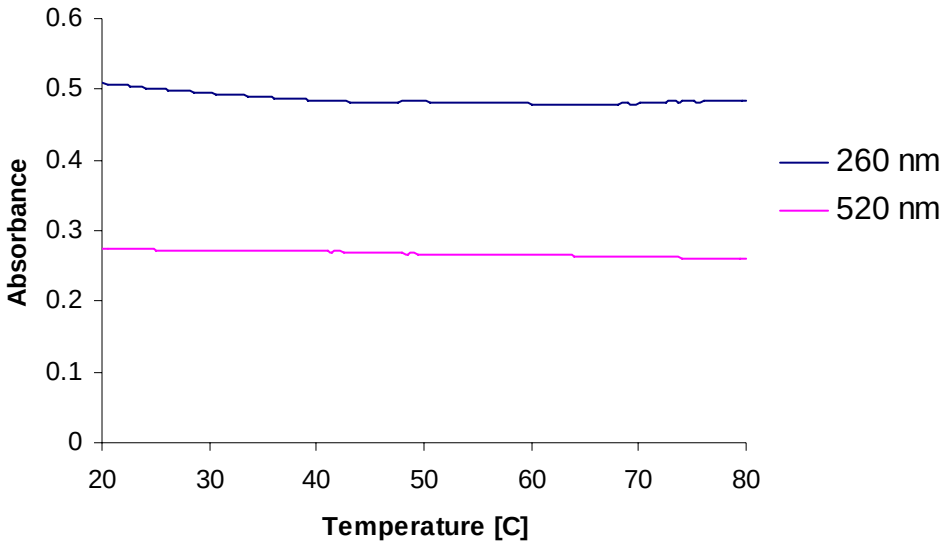

Figure 63: **Melting profiles of aggregates formed from 18 nm Au-T-DNA (sequences 1 and 2) probes in tail to tail orientation at 260 nm and 520 nm. 3 cycles of heating were performed for each sample.**

The changes in the intensity of the SERRS signal obtained from tail-to-tail sample after addition of complementary and non-complementary target are presented on

Figure 64. No increase of the signal intensity after addition of complementary target was detected. The changes in the signal intensity for the sample containing the fully complementary sequence are similar to the changes observed for the control sample. Similar results were obtained for other probe orientations investigated.

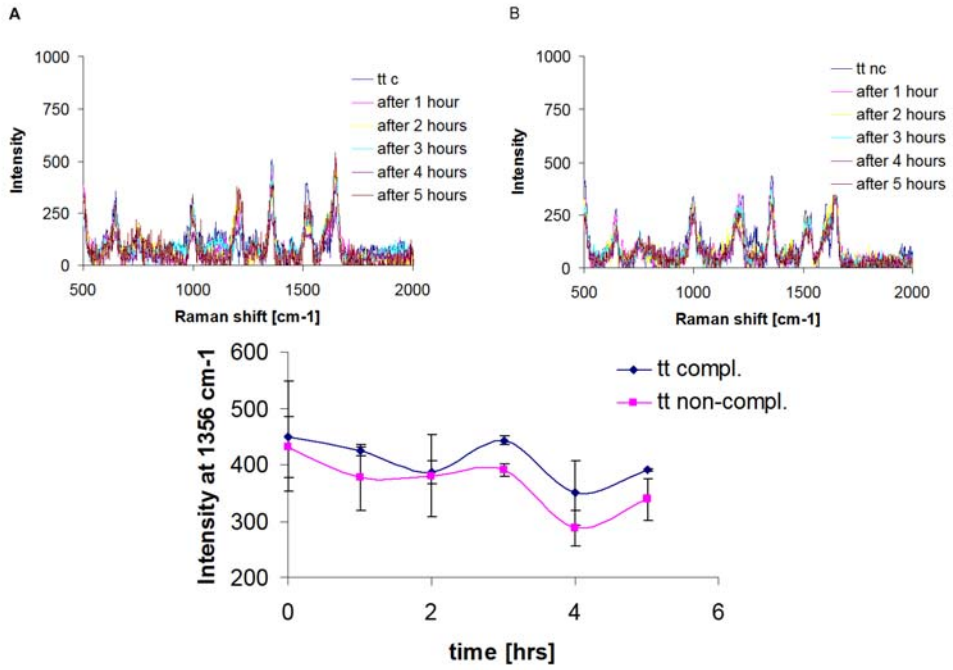

Figure 64: **Changes in the intensity of the SERRS signal (at 633 nm) observed after addition of target (complementary (A) or non-complementary (B)) to the solution containing two 18 nm Au-T-DNA (sequences 1 and 2) probes hybridizing to the target in a tail to tail fashion. The bottom graph shows changes in the intensity of the peak at 1356 cm^{-1} with time, after addition of complementary and non-complementary target.**

18 nm Au-T conjugated to sequences 3 and 4 (Figure 61) were used as probes in experiments similar to those described above (probes and targets concentrations and all hybridisation conditions were the same as in hybridisation assay performed with the use of 18 nm Au-T functionalized with sequences 1 and 2). The changes observed in extinction and SERRS spectra after addition of complementary or non-complementary target are shown in Appendix B and summarised in Table 8.

No big difference in the position and intensity of gold plasmon band for samples containing complementary target and control samples were noted (Figure B1, Appendix B). No significant difference in the intensities of the SERRS signals obtained from samples containing fully complementary and imperfect sequence were observed (Figure B2, Appendix B). Additionally, melting profiles obtained by monitoring the absorbance at 260 and 520 nm as a function of temperature did not confirm formation of nanoparticle aggregates in the sample containing both probes

and complementary target (Figure B3, Appendix B), thus it can be concluded that detection of specific DNA sequence by the use of 18 nm Au-T-DNA probes was not successful. Similar observations were noted for all probes orientations investigated.

Table 8: **Changes observed in the extinction and SERRS spectra after addition of complementary or imperfect target to the solution containing 18 nm Au-T-DNA (sequences 3 and 4) .**

Probes orientation	Target	Changes observed in the UV-Vis spectrum	Changes observed in the SERRS spectrum	Melting analysis	
				260 nm	520 nm
head to head	compl.	Decrease of the gold plasmon band, no red shift observed.	No significant changes observed.	Sharp melting curves not observed.	Sharp melting curves not observed.
head to head	non-compl.	Decrease of the gold plasmon band, no red shift observed.	No significant changes observed.	Sharp melting curves not observed.	Sharp melting curves not observed.
head to tail	compl.	Decrease of the gold plasmon band, no red shift observed.	No significant changes observed.	Sharp melting curves not observed.	Sharp melting curves not observed.
head to tail	non-compl.	Decrease of the gold plasmon band, no red shift observed.	No significant changes observed.	Sharp melting curves not observed.	Sharp melting curves not observed.
tail to tail	compl.	Decrease of the gold plasmon band, no red shift observed.	No significant changes observed.	Sharp melting curves not observed.	Sharp melting curves not observed.
tail to tail	non-compl.	Decrease of the gold plasmon band, no red shift observed.	No significant changes observed.	Sharp melting curves not observed.	Sharp melting curves not observed.

Probes concentration: 1.62 nM, target concentration: 4.05×10^{-8}M; SERRS experiments were performed using excitation at 633 nm. Spectra presented in Apendix B.

4.2.2 The aminofluorescein linker probes.

The changes observed in the extinction and SERRS spectra, after addition of complementary or non-complementary target to the solution containing aminofluorescein linker probes, are shown in Appendix C and summarized in the Table C1, Appendix C.

In the case of the gold nanoparticles functionalized with the aminofluorescein linker and conjugated to sequences 1 and 2 no red shift, decrease or broadening of gold surface plasmon band and no red to purple colour change, indicating aggregate formation, were observed after target addition (figures C1 and C3, Appendix C). Similar was observed for smaller gold nanoparticles conjugated to sequences 3 and 4 (Figure C5, Appendix C). Addition of complementary target to the samples

containing two 50 nm Au-Af-DNA (functionalized with sequences 3 and 4) caused a small decrease of gold plasmon band, however no red shift was observed. Similar changes were noted when an imperfect target was used in place of fully complementary sequence (Figure C7, Appendix C). Similar behavior was noted for all probes orientations investigated.

It can be concluded that no significant differences in the extinction spectra, allowing discrimination between samples containing fully complementary and non-complementary target were noted.

As observed previously (Chapter 3), SERRS signals can be obtained from 18 nm Au-Af-DNA and 50nm Au-Af-DNA, thus the changes in the samples containing two sets of gold nanoparticles probes after addition of complementary or non-complementary target were monitored by this technique. The lack of SERRS signal from the system indicates that no aggregates were formed and the hybridisation of the probes to the fully complementary target did not occur. The same observations were noted for both sizes of gold probes used and for all probe orientations investigated (head to tail, head to head and tail to tail) (Figures C2, C4, C6 and C8, Appendix C).

It was found that no aggregates were formed after addition of complementary target to the solution containing two types of the aminofluorescein linker functionalised gold nanoparticles (18 and 50 nm) conjugated to DNA (sequences 1 and 2; 3 and 4), thus no melting analysis of those samples were performed.

For both types of Au-Af-DNA probes investigated no red to purple colour change, no significant changes on UV-Vis spectra and no SERRS signals were observed when target complementary in sequence and length was added to the sample containing two sets of gold probes. It can be concluded that Au-Af-DNA conjugates can not be used as a probes in this DNA detection assay.

4.2.3 The fluorescein linker probes

The changes observed in the extinction spectra, after addition of complementary or non-complementary target to the solution containing fluorescein linker probes, are shown on Figures D1 and D3 and summarized in Table D1, Appendix D. It was found that no SERRS signals were obtained from fluorescein linker functionalized gold nanoparticles conjugated to oligonucleotides, thus SERRS was not used to monitor

the changes in the sample containing the fluorescein linker probes and the complementary or imperfect target.

For the samples containing probes (Au-F-DNA-sequences 1 and 2), which, after hybridisation are orientated to each other in a head to tail or head to head fashion, addition of complementary target caused the change of the colour of the solution from red to purple within 10 (for head to tail orientation) or 8 (for head to head orientation) hours (Figure D1, Appendix D). This colour change can be attributed to formation of nanoparticle aggregates, which leads to a red shift in the surface plasmon resonance from 525 to 539 nm in the case of probes orientated to each other in a head to tail fashion and from 527 to 537 nm for the probes orientated in a head to head fashion. The red shift of the gold surface plasmon band is accompanied by its broadening and significant decrease. The small value observed for the red shift could indicate that small nanoparticle aggregates are formed during the hybridisation process, which might be explained by the fact that very few DNA strands were attached to the nanoparticle probes (0.2 on average) used in the experiment. Formation of large, three dimensional aggregates is not possible in this case. In the presence of non-complementary target only a small red shift (2-3 nm), slight broadening and decreasing of gold plasmon band was observed for both probe orientations. The lack of aggregation observed in the presence of non-complementary target could indicate that the aggregation process observed in the presence of perfect target is driven by hybridisation of the probes in a sequence specific manner.

For the sample containing probes, which, after hybridisation, are orientated to each other in a tail to tail fashion, no colour change was observed within 48 hrs after addition of complementary or non-complementary target. Only a small red shift (2 nm), slight broadening and decrease of gold plasmon band is observed in both cases in extinction spectra (Figure D1, Appendix D). The hybridisation of the probes to complementary target did not occur.

Melting analysis of the solutions with resuspended aggregates were performed by monitoring the absorbance at 260 and 520 nm as a function of temperature (Figure D2, Appendix D). Unfortunately, the melting behaviour typical for the nanoparticle aggregates formed by hybridisation of oligonucleotide functionalised probes to fully complementary target was not observed. This indicated that aggregate formation observed for head to tail and head to head orientated samples was not likely to be driven by hybridisation of the probes to the complementary DNA sequence. Detection

of the specific DNA sequence by the use of 18 nm Au-F-DNA probes was not successful.

A similar experiment was performed for 18 nm Au-fluorescein linker-DNA conjugated to sequences 3 and 4 (Figure D3, Appendix D). Unfortunately significant changes in the extinction spectra taken from the samples containing both probes (at different orientations) and complementary target or red to purple colour change, were not observed. It can be concluded that addition of fully complementary target to the solution containing two types of nanoparticle probes did not cause formation of the aggregates through hybridisation of the probes to the complementary target. The use of 18 nm Au-F-DNA conjugates as probes for detection of a specific DNA sequence was not successful. Due to the lack of aggregate formation the melting analysis of the samples containing both probes and complementary target was not performed.

4.2.4 The BHQ linker probes

The changes observed in the extinction and SERRS spectra, after addition of complementary or non-complementary target to the solution containing the BHQ linker probes, are shown on Figures E1-E8 and summarized in Table E1, Appendix E.

For both types of gold nanoparticles used for Au-BHQ-DNA (sequences 1, 2, 3 and 4) preparation and for all probe orientations investigated, no changes in the extinction spectra taken from the samples containing complementary or non-complementary target were observed (Figures E1, E2, E5 and E6, Appendix E). In all cases the expected colour change indicating formation of aggregates by hybridisation of the probes to fully complementary sequence was not observed.

No changes in the SERRS spectra allowing discrimination between samples containing fully complementary target or imperfect sequence were noted (Figures E3, E4, E7 and E8, Appendix E). It can be concluded that for both types of probes used and for all orientations investigated addition of target did not cause hybridisation of the probes to the complementary strand and nanoparticle aggregates were not formed in a sequence specific manner.

Melting analysis of the samples containing Au-BHQ-DNA probes and complementary target were not performed as it was noted that nanoparticle aggregates were not formed during hybridisation experiments.

4.2.5 Other performed hybridisation experiments

The experiments described within this chapter are only a small part of all hybridisation assays performed. The following alternative strategies were also used (for the following linker-nanoparticle conjugates: 18 nm Au-Af; 50 nm Au-Af; 18 nm Au-F; 18 nm Au-T, 18 nm Au-BHQ; 50 nm Au-BHQ):

- **Probe preparation**-conjugates prepared by coupling of linker functionalized nanoparticles to amino modified oligonucleotides in the presence of DMT MM in 0.1 M PBS buffer (pH=7 and pH=7.2) or EDC·HCl, sulfo NHS in 0.1 M PBS (pH=6.0 in first step, pH=7.2 in second step) were also used as a probes in DNA detection assay investigated within this work. Experimental details are described in Sections 6.3.1, 6.3.3 and 6.3.5. In order to increase the yield of the conjugation reaction the amide bond forming reaction was performed twice for the same probes: after conjugation of linker functionalized nanoparticles to ssDNA, prepared probes were centrifuged, washed with water, then centrifuged again. Resuspension of the probes in water or buffer (dependent upon type of coupling agent used) was followed by second addition of DNA and coupling agent to the samples. Unfortunately no significant change in the number of DNA strands attached to the linker-nanoparticle conjugate was observed.
- **Preparation of mixed layer of linker and thiolated DNA on the nanoparticles surface**-the synthesized linkers were used as Raman tags in the approach similar to the one described previously in the literature [50, 60, 68]. Gold nanoparticles were functionalized with thiolated oligonucleotides first (with and without salt ageing), then the linker was added. Experimental details are described in Section 6.3.2. It was observed that after addition of the linker the nanoparticles started to slowly aggregate. The aggregation was faster in solution with higher salt concentration. It was concluded that the linker displaces the oligonucleotides from the nanoparticles which results in aggregation of the colloid.
- **Target concentration-t**he concentration of complementary and non-complementary targets used in the experiments were as indicated, for each type of linker-nanoparticle conjugates, within this chapter, however

concentrations the same as probes concentration, and 10, 50, 100, 500 and 1000 times higher than probes concentrations were also used. Experimental details are described in Tables 10 and 11 in Section 6.5.

- **Hybridisation buffer-** different hybridisation buffers, such as 0.1 M PBS (pH=7.0; pH=7.2); 0.3 M PBS (pH=7.0; pH=7.2) [5, 7, 21, 22, 36, 37, 60, 76, 81]; 50 mM NaCl in 1xTris EDTA pH=7.5 [52] were also used in DNA detection experiments performed with the use of all types of probes prepared. Experimental details are given in Section 6.5.
- **Hybridisation conditions-a**fter addition of complementary or non-complementary target to the solution containing two types of nanoparticle probes functionalized with different DNA strands the samples were either heated to 75°C for 5-10 mins [21, 22, 82] or to 95°C for 5-10 mins [44, 52], or frozen on dry ice [5, 20], as it was proven that it will remove secondary structures and improve hybridisation efficiency. The samples were also allow to hybridize to the targets at 37°C or at room temperature. Experimental details are given in Section 6.5.
- **Preparation of mixed monolayers of linkers on the nanoparticles surface-** in order to increase the number of DNA strands which attach to the nanoparticle surface (Au and Ag) and increase the stability of silver nanoparticles probes in hybridisation buffers mixed monolayers containing 25, 50 or 75% of one of the synthesized linker and 75, 50 or 25% of Peg 41 TA linker (the same as the one used for pH sensing probes preparation-Chapter 5) or Peg 11 TA linker (prepared in similar way to Peg 41 TA linker but with the use of shorter Peg unit) or short, thiolated oligonucleotide (SH AAAAA) or thiolated Peg [SH-$(CH_2)_9$-CH_2O-$(C_2H_4O)_2$-CH_2-CH_2-OH) was formed on all types of metallic nanoparticles used. Formation of such mixed monolayers on metal surface should reduce the number of linker molecules, which attached to metal surface, thus improve linker packing geometry and availability of linker COOH groups for conjugation with amino-modified DNA. Experimental details are described in section 6.3.2. Conjugates prepared in such a way were then reacted with amino modified oligonucleotides in the presence of DMT MM or EDC·HCl (experimental details are given in section 6.3.5), then used as probes in hybridisation assay. Formation of a mixed monolayer on the

nanoparticles surface did not increase the stability of the silver nanoparticle probes and did not improve significantly the number of DNA strands conjugated to linkers attached to nanoparticle surface.

- **Spacer bases -s**ingle stranded, amino modified DNA without a spacer or containing 3 or 10 A spacer between the amino modifier and recognition sequence were used for probe preparation.
- **Probe concentration-t**he probe concentrations were kept constant in all extinction experiments performed, however concentrations 2 and 3 times higher were used in SERRS experiments. Experimental details are given in Section 6.5.
- **Different DNA sequences-**all sequences used are listed in Appendix A

Unfortunately similar results were obtained in all experiments. Addition of complementary target to the solution containing two probes mixed in a 1:1 molar ratio did not cause red-to-purple colour change; broadening, decreasing and red shifting of gold plasmon band or increase of the intensity of SERRS signal obtained from the system, which would indicate that the nanoparticle aggregates were formed. This is probably caused by the fact that very few DNA strands attached to each type of conjugate. Low numbers of oligonucleotides attached to nanoparticles functionalized with trifunctional, Raman active linkers allowing attachment of biomolecules to nanoparticles surface by reacting free linker COOH groups with amine group of molecule of interest have been reported in the literature. McKenzie *et al.* [65, 124] found that the number of oligonucleotides attached to the linker functionalized 15 nm Au nanoparticles vary between 0.3-24.5 strands per one nanoparticle dependent upon the type of linker used. Those results are in close agreement with data obtained within this work-it was found that number of DNA strands attached to 18 nm Au nanoparticles functionalized with BHQ, aminofluorescein and fluorescein linkers varies between 0.2-0.7 strands per one nanoparticle. About 25 oligonucleotides attached to one 18 nm Au-T nanoparticle, when the coupling reaction is performed in the presence of DMT MM in water. The use of the probes prepared by conjugation of oligonucleotides to multifunctional linker molecules attached to metallic nanoparticles surface was not reported in the literature.

4.3 Conclusions

The following nanoparticle probes were used in a DNA detection assay based upon formation of nanoparticle aggregates by hybridisation of the probes to a complementary target: 18 nm Au-F-DNA, 18 nm Au-Af-DNA, 50 nm Au-Af-DNA, 18 nm Au-T-DNA, 18 nm Au-BHQ-DNA, 50 nm Au-BHQ-DNA. Conjugation of the linker functionalized Ag EDTA nanoparticles to amino-modified oligonucleotides was also possible, however the conjugates were not stable in buffers usually used for DNA hybridizations [zeta potential values measured for oligonucleotide functionalized Ag EDTA conjugates were very low (Table 7, Chapter 3) indicating the low stability of the colloidal suspension] thus they were not used as probes in the DNA detection assay. All probes used in the experiments were prepared by attachment of the linker to the nanoparticle first, then linker terminal COOH groups were conjugated to amino modified, single stranded DNA in the presence of DMT MM in water. Conjugates prepared in such a way were assessed for their ability to detect specific DNA sequences. In a typical experiment two probes containing different DNA strands were mixed in a 1:1 molar ratio, then target complementary to both probes (or non-complementary for control samples) was added. The samples were heated for 5 mins at 75°C, then allow to hybridize at room temperature. Hybridisation experiments described in this Chapter were performed in 0.1 M PBS, pH=7.2; probes concentration was kept constant (1.62 nM for 18 nm Au probes, 3.78×10^{-11} M for 50 nm Au probes), target concentration was dependent upon number of DNA strands attached to each type of the probes. The changes occurring in the samples after addition of fully complementary or imperfect sequence were monitored by UV-Vis spectroscopy and by SERRS (Experimental details are described in Section 6.5).

For all types of probes investigated addition of complementary target to the solution containing two nanoparticle probes functionalized with different DNA strands did not cause the expected increase in the intensity of SERRS signal obtained from the sample. Additionally, only very weak or no signals at all were obtained. The red shift, broadening and decreasing of the gold plasmon band in extinction spectra indicating nanoparticle aggregate formation were also not observed in most of the cases. Changes in extinction spectra were noted for samples containing 18 nm Au-F-DNA and 18 nm Au-Af-DNA, however sharp melting transitions characteristic of

nanoparticle aggregates formed by hybridisation of oligonucleotide functionalized nanoparticles to complementary targets were not obtained indicating that the aggregates were formed rather due to the low stability of the probes in DNA hybridisation buffer rather than by hybridisation of the probes to the target in a sequence specific manner.

The lack of the changes as indicated by extinction and SERRS spectra and no red-to-purple colour change observed for the samples containing complementary target make it impossible to discriminate between the samples containing fully complementary and imperfect DNA sequence. The use of the nanoparticle conjugates as probes for the detection of specific DNA sequences was not successful.

Metallic nanoparticles functionalized with thiolated or multithiol modified oligonucleotide are most commonly used as probes in a sandwich assay format allowing detection of specific DNA sequences [5, 7, 15, 23, 28, 110, 124]. It was found that the DNA surface coverage obtained for such probes is much higher than the one observed for the probes investigated within this work. For gold nanoparticles functionalized with thiolated oligonucleotides the surface coverage varies between 12-20 [15], 13-50 [23], 15-35 [110] pmol/cm^2 dependent on the type of sequence used. When thioctic acid modified oligonucleotides were used to functionalize gold nanoparticles the surface coverage was found to be 7-60 pmol/cm^2 dependent on the type of sequence. When the trithiol is used in the place of cyclic disulphide 80-130 DNA strands attached to one Au nanoparticle [28]. The DNA surface coverage for silver nanoparticles functionalized with Raman tag and thiolated oligonucleotides was found to be 35 pmol/cm^2 [60, 68]. These values are much higher than the surface coverage values obtained in this work (0.02-2 for all types of Au nanoparticle conjugates used in investigated DNA detection assay).

Low numbers of DNA strands attached to the nanoparticle surface might be caused by non-specific adsorption of DNA on the nanoparticle surface, however it shouldn't be a problem when the metal surface is protected by a layer of linker molecules. Large numbers of linker molecules attached to the nanoparticle surface (Table 1, Chapter 2) could indicate that more than a monolayer of linker molecules is formed on the metal surface. The linker molecules can be orientated in the layer in such a way that most of the linker COOH groups are not available for conjugation with the amino-modified oligonucleotides. When a smaller amount of linker was added to nanoparticles prior to

oligonucleotide attachment the nanoparticles were unstable and irreversibly aggregated after addition of DNA and the coupling agent.

Low yield of conjugation of terminal linker COOH groups to amino-modified DNA might also be caused by a folded structure of the oligonucleotides used, which would change the charge density on DNA molecules and could impair conjugation process. The possibility of formation of folded secondary structures was checked for all ssDNA strands used in hybridisation experiments using Professor M. Zuker's mfold software. It was found that formation of folded structures is possible for strands 1, 2, 4, 8 and 14 at 0.1 M NaCl concentration (Appendices A and F). For the rest of the sequences folding is not possible under the same conditions. Adamcik *et al.* [148] reported that in solution at very low salt concentration DNA does not form secondary structures, thus it can be concluded that no folded DNA structures are formed when linker functionalized nanoparticles are conjugated to oligonucleotides in water, in the presence of DMT MM. Due to the fact that low DNA surface coverage values were obtained for all types of linker functionalized nanoparticles conjugated to sequences able and not able to form folded structures it was concluded that the possibility of formation of secondary structures is not the main reason causing low yield of investigated conjugation process.

Very low yield of reaction of all linkers synthesized with amino-modified oligonucleotides were also observed when the coupling reaction was performed before attachment of the linker to nanoparticle surface. This may be caused by the formation of hydrogen bonds within the linker structure, thus the terminal COOH groups may be hidden and not available for conjugation reaction.

It can be concluded that due to the very low number of DNA strands attached to the linker-nanoparticle conjugates, they can not be used for detection of specific DNA sequences either by extinction spectroscopy or by SERRS. Addition of complementary target to the solution containing two probes functionalized with different DNA sequences did not cause formation of larger nanoparticle aggregates by hybridisation of the probes to complementary target.

The linkers can act as SERRS nanoparticle labels on their own right. Additionally, due to the presence of the terminal COOH group which allows attachment of the biomolecules, they can be useful for tagging antibodies and proteins. The low number of biomolecules attached to the nanoparticles may be beneficial for some applications.

Chapter 5

SERS as a pH sensor

One of the aims of this thesis is to develop SERS active, pH sensitive probes, which could be used for the detection of intracellular pH. This chapter describes preparation of such probes and their use for the detection of pH inside HeLa and macrophages cells.

5.1 Introduction

Acidification of endosomes is thought to play a central role in a number of pathologies, including cystic fibrosis, kidney diseases and certain types of cancer [87, 88, 94, 95]. Thus the development of novel optical probes capable of providing information regarding changes to the chemical environment inside living cells may allow understanding of the biochemistry of diseases [87-89, 94, 136, 137]. Detection of such intracellular changes is a vital area of biochemistry and cell biology research.

SERRS is a very sensitive, spectroscopic technique capable of providing chemically specific information based on the unique vibrational modes of molecule adsorbed on enhancing surface. It can be applied to the study of biological systems as the low laser powers and short collection times make the technique suitable for studying biological processes. Furthermore the high multiplexing capability due to the large number of available probes and labels is another advantage of this spectroscopic tool. SERRS also enables spatial high-resolution analysis, facilitating chemical probing of intracellular structures [87, 97, 137, 140, 142]. Many different metals can be used to provide surface enhancement, however gold and silver nanoparticles are most commonly used for that purpose [51, 142].

Sharing a similar size range to many common biomolecules, metallic nanoparticles can be used to prepare probes for biosensing and bioimaging in cell and molecular biology research [138, 140, 141, 142, 143, 144]. It was reported that gold and silver nanoparticles can be used to deliver enhanced SERS signal from biological molecules present inside living cells. Additionally metallic nanoparticles functionalised with a reporter molecule, after incubation with the cells, were found to be capable of highlighting the intracellular structures by obtaining the SERS signature of Raman active label used for probes preparation [55, 87-93, 95, 99, 138, 139]. When nanoparticles are functionalised with a reporter molecule which exhibits pH dependent SER(R)S responses, such probes can be used as intracellular pH sensors. A number of Raman active molecules, including: 4-mercaptobenzoic acid [55, 87,93,

95, 98, 99], 4-mercaptopyridine [85, 88, 90] and 2-aminothiophenol [89], have been reported in the literature as potential pH probes. pH sensitive nanoparticles can be introduced into living cells, allowing the detection of intracellular pH. It has been reported that upon incubation nanoparticle probes are taken up by the cells by an endocytotic mechanism and analysis has suggested they remain trapped in endosomes and lysosomes. As such nanoparticle pH probes may be used to monitor the acidification of endosomal pH, an important marker for the early detection of some pathogenic diseases [87, 93, 95, 137, 140].

Diagnosis of disease phenotypes, identification of drug candidates and treatment of diseases could all be significantly improved if efficient transport of materials, such as nanoparticle based probes to the cell nucleus was possible [138, 139, 140]. Many strategies allowing delivery of metallic nanoparticles into the cell nucleus exist, such as: conjugation of cell penetrating peptides, such as TAT to the nanoparticle surface, which forms biocompatible probes able to cross cell and nuclear membranes and accumulate inside cell nucleus [138, 140, 141]; formation of a mixed monolayer of nuclear localization sequences (NLS) and PEG or cell penetrating peptide on the nanoparticle surface [139-141]; interaction between transferrin and its receptor [140]; the use of transfection reagents, such as polyethyleneimine; incorporation of nanoparticles inside or on the surface of liposomes [140] and physical methods (sonoporation, genegun, microinjection) [140]. In order to detect the pH values inside other cell organelles, such as the nucleus, a mixed monolayer of a pH sensitive Raman reporter and a molecule, which can be conjugated to cell penetrating peptides or other molecules allowing the conjugate to cross cell and nuclear membranes, need to be prepared.

5.2 2-aminothiophenol and 4-mercaptopyridine as pH sensing molecules

Two molecules exhibiting a pH dependent SERS signal were used within this work to functionalise gold (18 nm) and silver (Ag citrate and Ag EDTA) nanoparticles: 4-mercaptopyridine and 2-aminothiophenol. Probes were prepared by addition of a $1x10^{-3}$ M solution of pH sensitive Raman reporter to gold or silver colloid. After 16 hours of incubation the probes were centrifuged. The supernatants were discarded, the pellets washed with water, centrifuged (20 mins, 6500 rpm), then resuspended with phosphate buffers with a pH range from 3 to 8 and incubated for a further 16 hours

(experimental details are described in Section 6.6.1). Then SERS spectra of all probes were taken using a laser excitation frequency of 633 nm. 5 samples of each kind were incubated in each of the buffers; SERS spectra were recorded in triplicates.

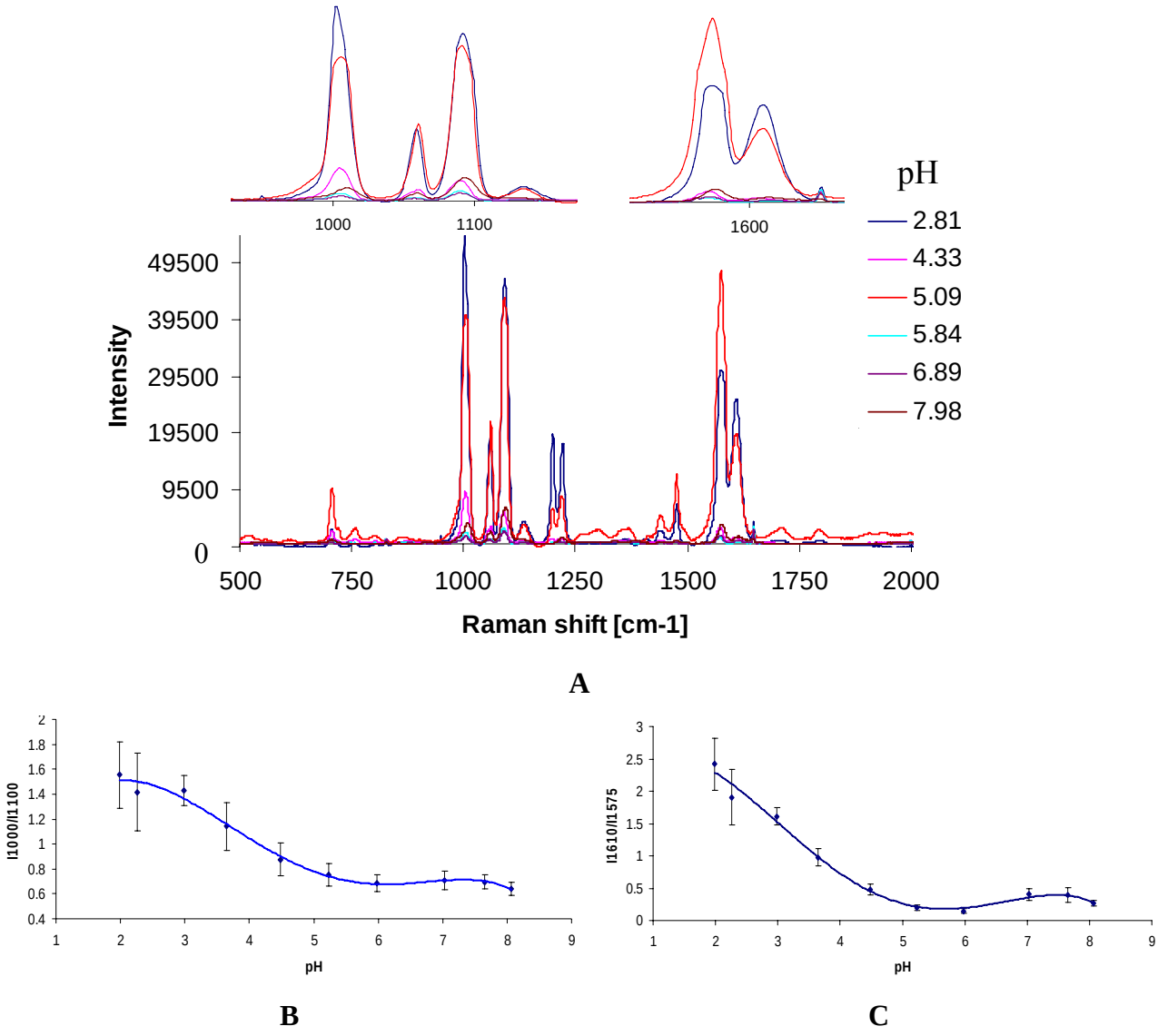

Figure 65: **SERS spectra of Ag EDTA nanoparticles functionalised with 4-mercaptopyridine at different pH values (A) (inset shows peaks which intensities were used to prepare titration curves); titration curves obtained (B, C).**

In the case of the 4-mercaptopyridine functionalised nanoparticles, the largest changes in the SERS spectra were observed for the following peaks: 1000 cm^{-1} (when pH increases the intensity decreases due to greater aromaticity of the 4-mercaptopyridine protonated form), 1100 cm^{-1} (the intensity increases when pH

increases due to increasing double bond character of the C-S bond), 1610 cm $^{-1}$ (due to the protonation of 4-mercaptopyridine the intensity decreases, when pH increases) and 1575 cm $^{-1}$ (the intensity increases when pH increases, this peak corresponds to non-aromatic C=C vibrational modes in non-protonated molecule) [85, 88, 90].

The titration curves for 4-mercaptopyridine based pH sensing probes were prepared by plotting the ratio of the intensities of the peaks at 1000 and 1100 cm^{-1} or 1610 and 1575 cm^{-1} versus pH of the buffer in which the probes were incubated (Figure 65, B and C; Figure 68, B and C; Figure 70, B and C).

If the pKa values of all protons present in the analyte are known then the shape of pH titration curves can, in principle, be predicted using the Henderson-Hasselbach equation which is defined as:

$$\mathbf{pH = pKa + \log [A^-]/[HA]}$$

$$\mathbf{pOH = pKb + \log [BH^+]/[B]}$$

where: A-acid, B-base, pKa=-logKa, pKb=-logKb, Ka-the acid dissociation constant, Kb-the base dissociation constant [2]. However, attempts to apply this equation to fit the data obtained here were unsuccessful. One possible reason for this is due to the fact that both pH sensing molecules used (4-mercaptopyridine and 2-aminothiophenol) after adsorption on to the metal surface are not titrated. They are equilibrated at different pH buffers and then the structural changes of the molecules adsorbed on the metal nanoparticle surface are detected by SERS. The Henderson-Hasselbach equation is usually used to calculate the concentration of [H^+]/[OH^-] ions, which has to be added to the analyte solution in order toachieve the pH of the solution equal to the pKa value of the proton present within the analyte.

Both types of silver nanoparticles used, after adsorption of 4-mercaptopyridine on their surface, allow detection of pH values from 2-5 (Figure 65, B and C; Figure 67, B and C), however the intensity of SERS signal obtained is much higher for Ag EDTA probes. Interestingly gold nanoparticles functionalized with the same pH sensing molecule allowed detection of pH values from 6 to 8.

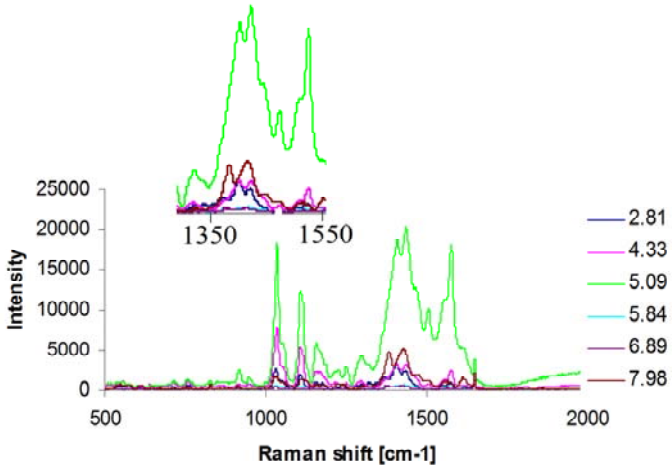

A

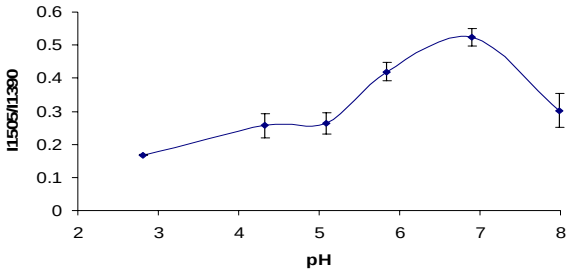

B

Figure 66: SERS spectra of Ag EDTA nanoparticles functionalised with 2-aminothiophenol at different pH values (A) (inset shows peaks which intensity was used to prepare titration curve); titration curve obtained (B).

The intensity of SERS signals obtained from Au probes is much lower than the one observed for silver nanoparticles functionalised with 4-mercaptopyridine. Results indicate that the type of nanoparticles used for the probe preparation have a big influence on the sensor detection range. It can be concluded that due to the very strong SERS signal obtained from Ag EDTA nanoparticles functionalised with 4-mercaptopyridine, and the ability of detection for more acidic conditions, this type of nanoparticle was chosen as most suitable to use along with this pH sensitive Raman reporter in order to prepare probes for pH sensing.

For nanoparticles functionalised with 2-aminothiophenol the biggest changes in the SERS spectrum were observed for the peaks at 1505 cm^{-1} (benzene ring vibrations) and 1390 cm^{-1} (NH_2 rocking mode, the intensity of the band increases when pH increases). The titration curve for 2-aminothiophenol based probes was prepared by plotting the ratio of the intensities of peaks at 1505 and 1390 cm^{-1} against pH of the buffer in which the probes were incubated (Figure 66 B, 68 B and 70 B).

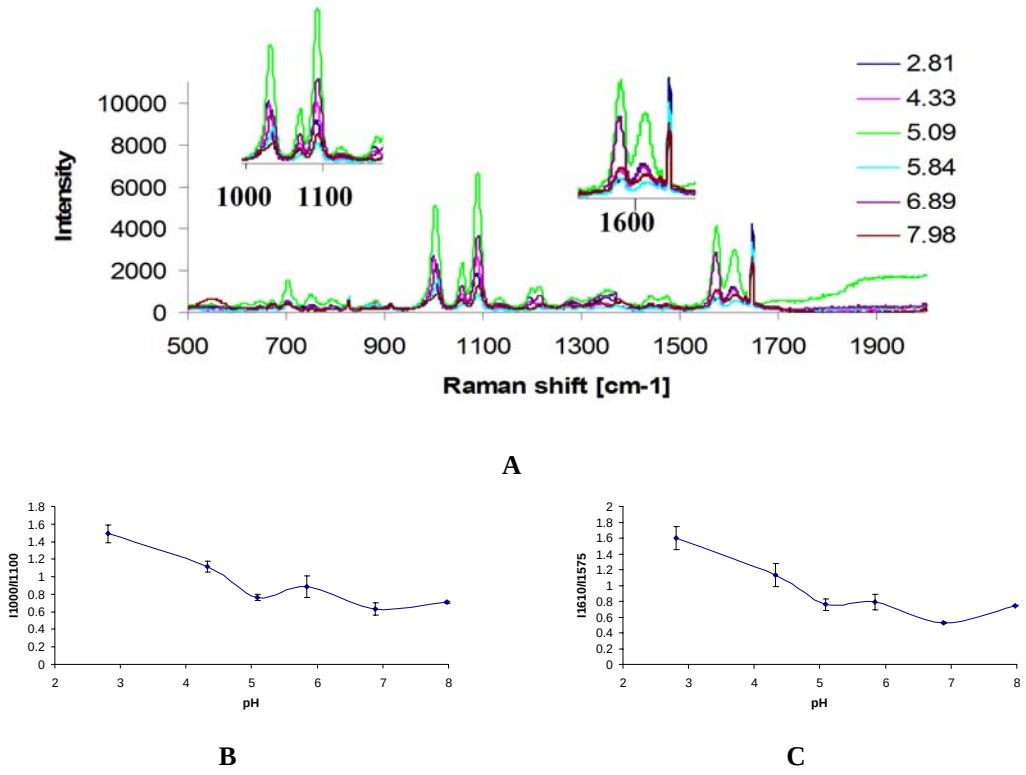

Figure 67: **SERS spectra of Ag citrate nanoparticles functionalised with 4-mercaptopyridine at different pH values (A) (inset shows peaks which intensities were used to prepare titration curves); titration curves obtained (B, C).**

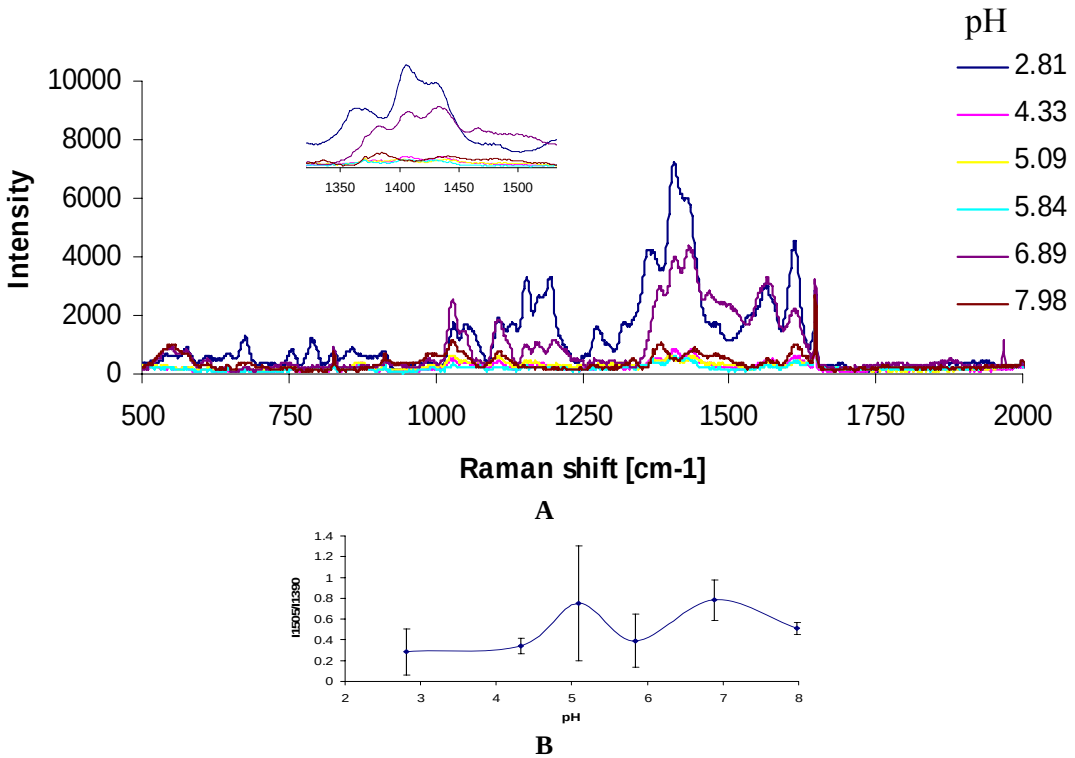

Figure 68: **SERS spectra of Ag citrate nanoparticles functionalised with 2-aminothiophenol at different pH values (A) (inset shows peaks which intensities were used to prepare titration curve); titration curve obtained (B).**

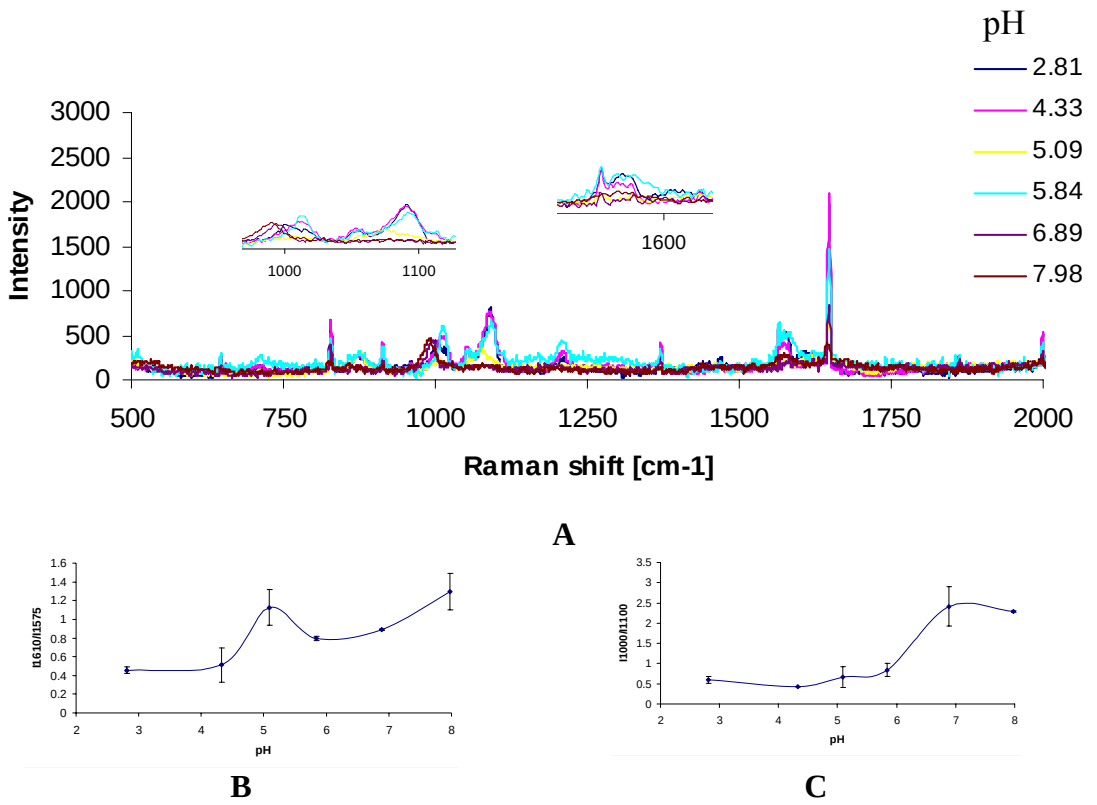

Figure 69: **SERS spectra of 18 nm Au nanoparticles functionalised with 4-mercaptopyridine at different pH values (A) (inset shows peaks which intensities were used to prepare titration curves); titration curves obtained (B,C).**

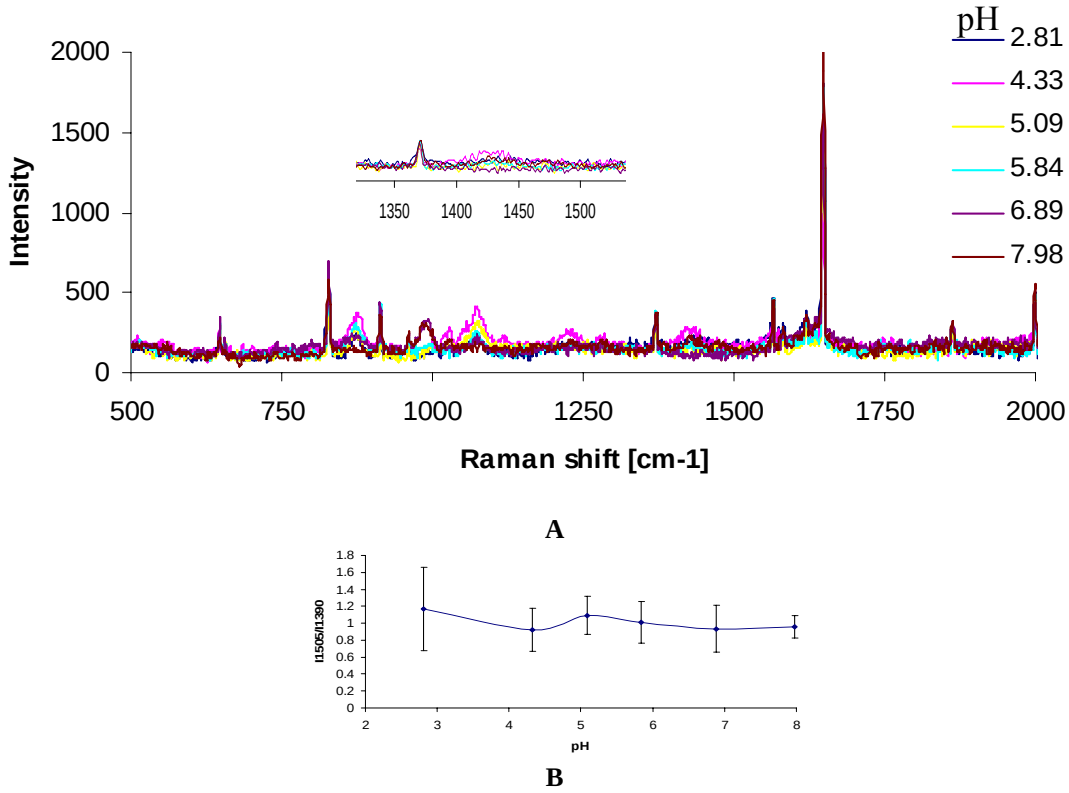

Figure 70: **SERS spectra of 18 nm Au nanoparticles functionalised with 2-aminothiophenol at different pH values (A) (inset shows peaks which intensities were used to prepare titration curve); titration curve obtained (B).**

Ag EDTA nanoparticles functionalised with 2-aminothiophenol allows the detection of pH values between 5-7. The Ag citrate and 18 nm Au nanoparticles functionalised with the same pH sensitive Raman reporter were unable to allow detection of pH values of the surrounding medium (Figures 68 and 70).

Due to higher intensity of SERS signals obtained from probes containing 4-mercaptopyridine and its broader pH detection range only 4-mercaptopyridine was carried forward to further work.

5.3 Nanoparticles with mixed monolayer of Peg 41-TA linker and 4-mercaptopyridine.

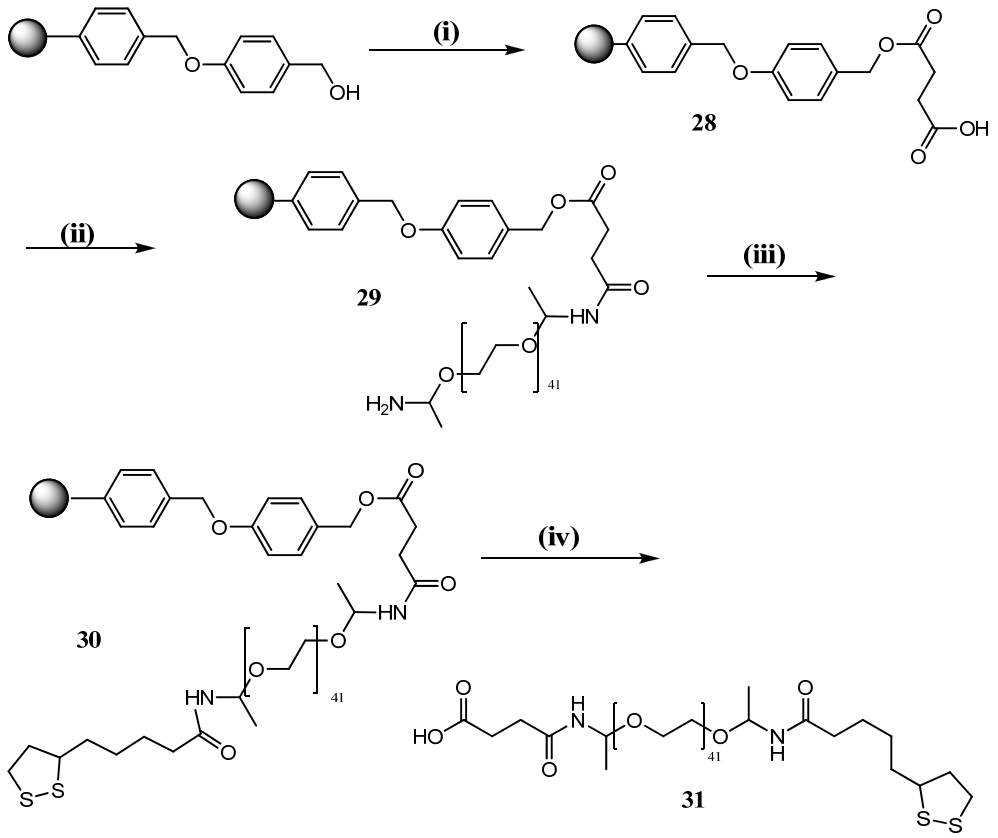

Figure 71: **Synthesis of the PEG 41-TA linker (31); (i) succinic anhydride, DMAP, DCM; (ii) O, O'-bis-(2-aminopropyl)-polypropylene glycol-block-polyethylene glycol-block-polypropylene glycol 1900, DIC, DCM; (iii) thioctic acid, DIC, DCM; (iv) 10% TFA/DCM.**

When nanoparticles are incubated with cells they are believed to be taken up by the cell through an endocytotic mechanism. Further analysis suggests, that the

nanoparticles, after passing the cell membrane, remain trapped in endosomes. The exposure of nanoparticles into cell medium during their incubation with the cells can also have a big influence on nanoparticle uptake due to numerous non-specific interactions between nanoparticles and cell medium components. One of the ways to overcome those non-specific interactions is to functionalise the nanoparticles surface with PEG. Many authors have reported that covering the nanoparticle surface with PEG can impair nanoparticles uptake [140, 145, 146], however conflicting reports indicate that the uptake of PEG modified nanoparticles into cells is possible [140]. Additionally it was reported that formation of a mixed monolayer of cell penetrating peptide or NLS and PEG on the nanoparticle surface can significantly improve the nanoparticle uptake [140, 147] and make it possible to deliver nanoparticles into the cell nucleus [138-141].

In order to prepare pH sensing nanoparticles, which could be delivered to the cell nucleus a mixed monolayer of PEG 41-thioctic acid linker (Peg 41-TA) and pH sensitive Raman reporter-4-mercaptopyridine was formed on Ag EDTA nanoparticles surface. Experimental details are described in Section 6.6.2. The use of PEG 41-TA prevents non-specific interactions of nanoparticles with proteins present in cell medium, and also, due to the presence of a free COOH group within the linker structure, allows conjugation of prepared pH sensitive probes to biomolecules, such as peptides or DNA.

Wang resin, which is commonly used for solid phase synthesis, was chosen as a solid support during PEG 41-TA linker synthesis. It was used in a similar way during the BHQ linker synthesis. In the first step of the synthesis the resin was reacted with succinic anhydride in the presence of DMAP to form modified resin (**28**). Terminal COOH groups of (**28**) were then reacted with *O, O'-bis*-(2-aminopropyl) polypropylene glycol-block-polyethylene glycol-block polypropylene glycol 1900 (PEG 41) to form (**29**). In the next stage of the synthesis primary NH_2 groups present on the solid support (**29**) were reacted with thioctic acid in the presence of DIC to form the modified support (**30**). Newly formed PEG 41-TA linker (**31**) was cleaved from the resin by the use of 10% TFA in DCM (Figure 71). All experimental details are described in Section 6.1.5.

In order to prepare a mixed monolayer of 4-mercaptopyridine and PEG 41-TA on a Ag EDTA surface a solution containing 75 or 50% of $1x10^{-3}$ M 4-mercaptopyridine (in MeOH) and 25 or 50% of PEG 41-TA ($1x10^{-3}$ M in MeOH) was added to Ag

EDTA nanoparticles. The samples were allowed to react for 16 hrs, then they were centrifuged. The pellets were washed with water, before incubation in one of the phosphate buffers (pH between 2-8) for 16 hrs. Experimental details are given in Section 6.6.2. SERS spectra of all prepared samples (5 of each kind were incubated in each of the buffers) were taken in triplicate using a laser excitation frequency of 633 nm.

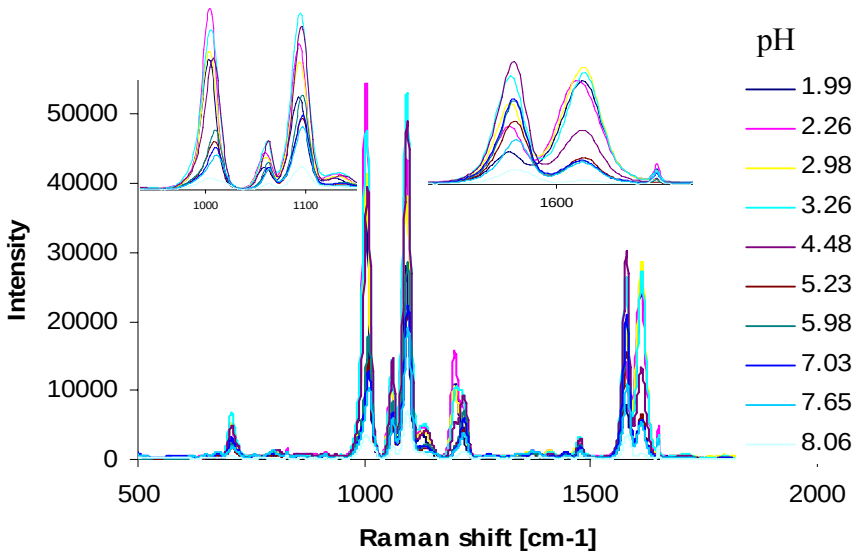

Figure 72: SERS spectra of Ag EDTA nanoparticles functionalised with 25% of PEG 41-TA and 75% of 4-mercaptopyridine using excitation at 633nm. The inset shows peaks taken into account during preparation of titration curves.

The intensity of SERS signals obtained from the probes prepared by formation of the mixed monolayer containing 25 or 50% of PEG 41-TA linker and 4-mercaptopyridine on Ag EDTA nanoparticles is similar to the intensity of SERS signals obtained from Ag EDTA-4-mercaptopyridine probes (Figures 65, 72 and 74). Titration curves for those probes were prepared in the same way as for Ag EDTA nanoparticles functionalised with 4-mercaptopyridine. The ratios of the intensities of the peaks at 1000 and 1100 cm^{-1} or 1610 and 1575 cm^{-1} versus pH value of the buffer in which the samples were incubated were plotted (Figures 73 and 75).

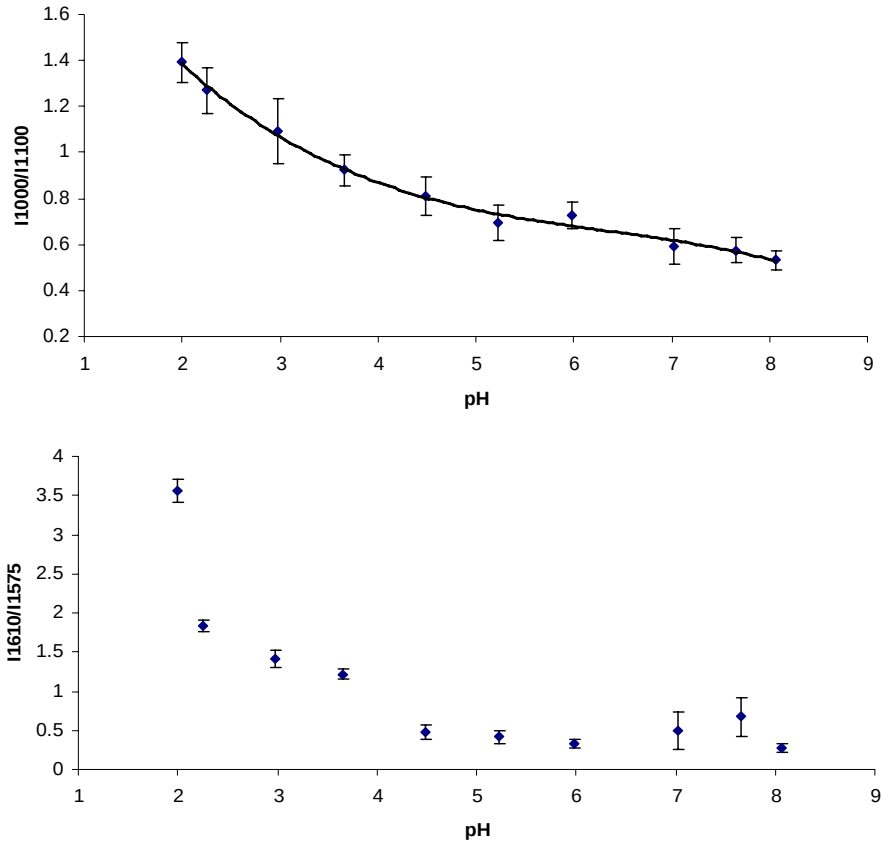

Figure 73: **Titration curves obtained from the probes prepared by formation of mixed monolayer of 4-mercaptopyridine (75%) and PEG 41-TA (25%) on Ag EDTA surface.**

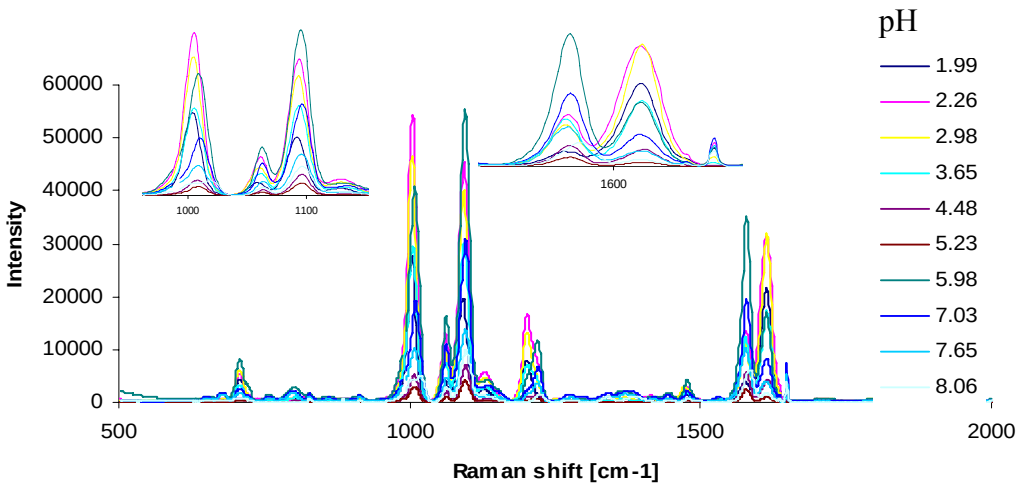

Figure 74: **SERS spectra of Ag EDTA nanoparticles functionalised with 50% of PEG 41-TA and 50% of 4-mercaptopyridine using excitation at 633nm. The inset shows peaks taken into account during preparation of titration curves.**

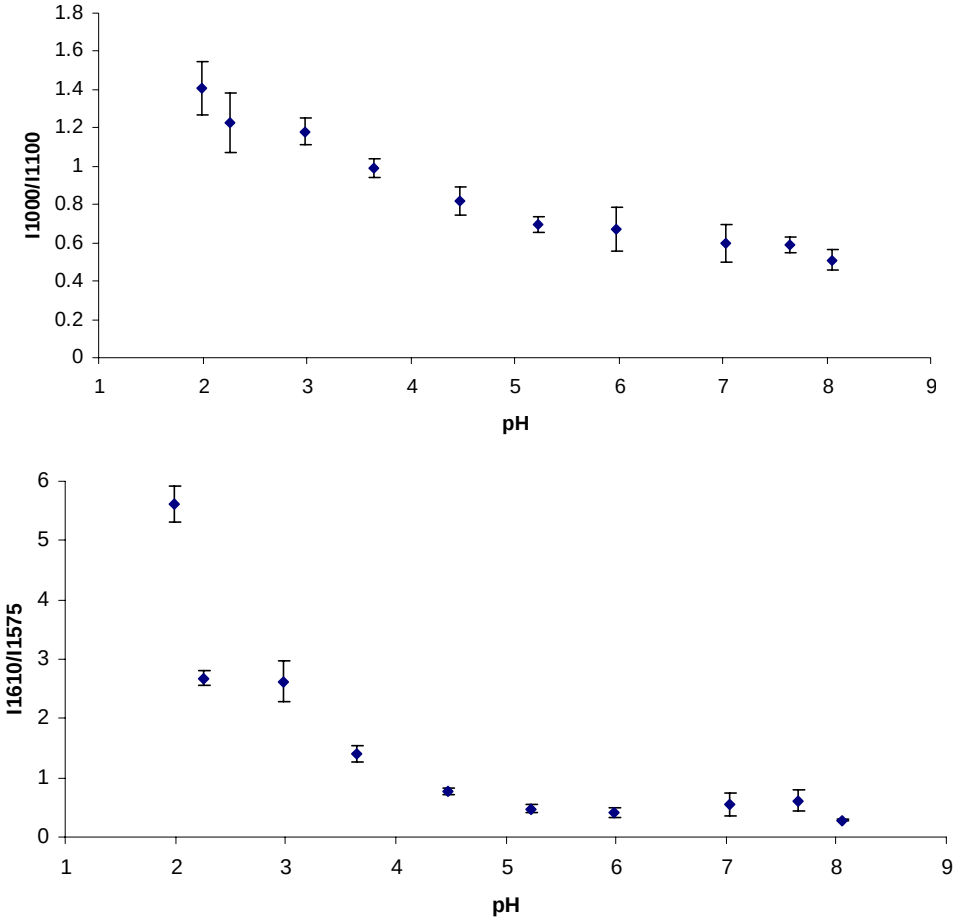

Figure 75: Titration curves obtained from the probes prepared by formation of mixed monolayer of 4-mercaptopyridine (50%) and PEG 41-TA (50%) on Ag EDTA surface.

It can be concluded that the formation of mixed monolayer of 4-mercaptopyridine and PEG 41-TA linker on Ag EDTA surface does not cause any changes to the sensitivity of the prepared pH sensor. The pH sensing range of the probes containing PEG 41-TA and 4-mercaptopyridine is the same as the one observed for Ag EDTA nanoparticles functionalised with 4-mercaptopyridine only. All prepared pH sensing probes allow detection of pH values between 2 and 5. Similar results were obtained for pH sensitive probes with monolayers containing 25 and 50% PEG 41-TA linker on their surface. When monolayer contains 50% PEG 41-TA linker there is a possibility of conjugation of the probe to a larger number of biomolecules of interest, thus pH sensitive probes with monolayer containing 50% of PEG 41-TA linker and 50% of 4-mercaptopyridine were carried forward to further work.

5.4 Oligonucleotide functionalised nanoparticles as a probes for pH sensing

It has been reported that conjugation of nanoparticles to cell penetrating peptides or NLS's make it possible to deliver the nanoparticles into cell nucleus [138-141]. In order to check if addition of biomolecules (in this case ssDNA) did not cause any changes in the pH sensing range of the prepared sensor a mixed monolayer of 4-mercaptopyridine (50%) and PEG 41-TA (50%) was formed on Ag EDTA nanoparticles.

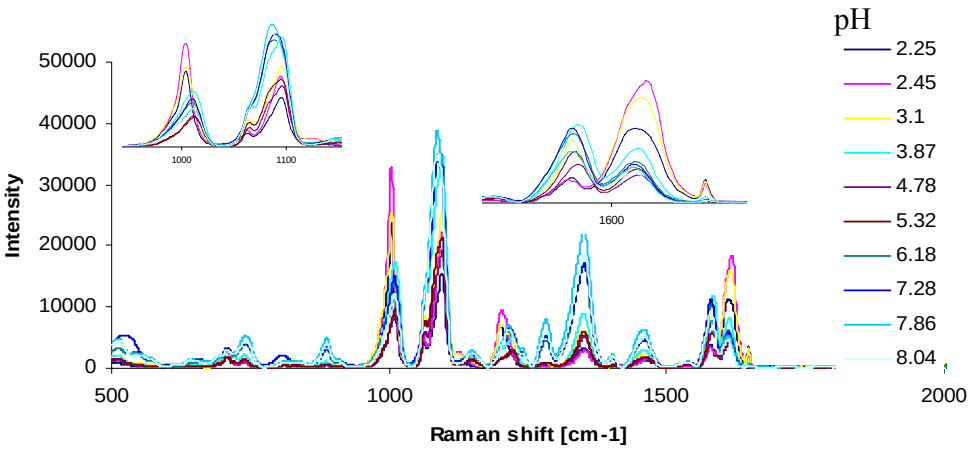

Figure 76: **SERS spectra of Ag EDTA nanoparticles functionalised with 50% of PEG 41-TA and 50% of 4-mercaptopyridine after oligonucleotides attachment using excitation at 633nm. Inset shows peaks taken into account during preparation of titration curves.**

The terminal COOH groups of the PEG 41-TA linker were conjugated to amino modified ssDNA (5' AAA TTC TTC TAC G 3') in the presence of DMT MM in water. The prepared oligonucleotide functionalised nanoparticles were washed with water in order to remove non-conjugated oligonucleotides. Experimental details regarding preparation of pH sensitive probe conjugated to oligonucleotides are described in Section 6.6.3. The nanoparticles were then incubated in phosphate buffers with a pH range from 2 to 8. SERS spectra of all samples (in triplicate) were taken using excitation at 633 nm. The titration curves were prepared in the same way as previously described for Ag EDTA-4-mercaptopyridine and Ag EDTA-4-mercaptopyridine/PEG 41-TA probes.

The intensity of SERS signal obtained from oligonucleotide functionalised Ag EDTA-4-mercaptopyridine/PEG 41-TA (50/50) probes is slightly lower than the

intensity of SERS signals obtained from the same probes prior to oligonucleotide attachment (Figures 72 and 74).

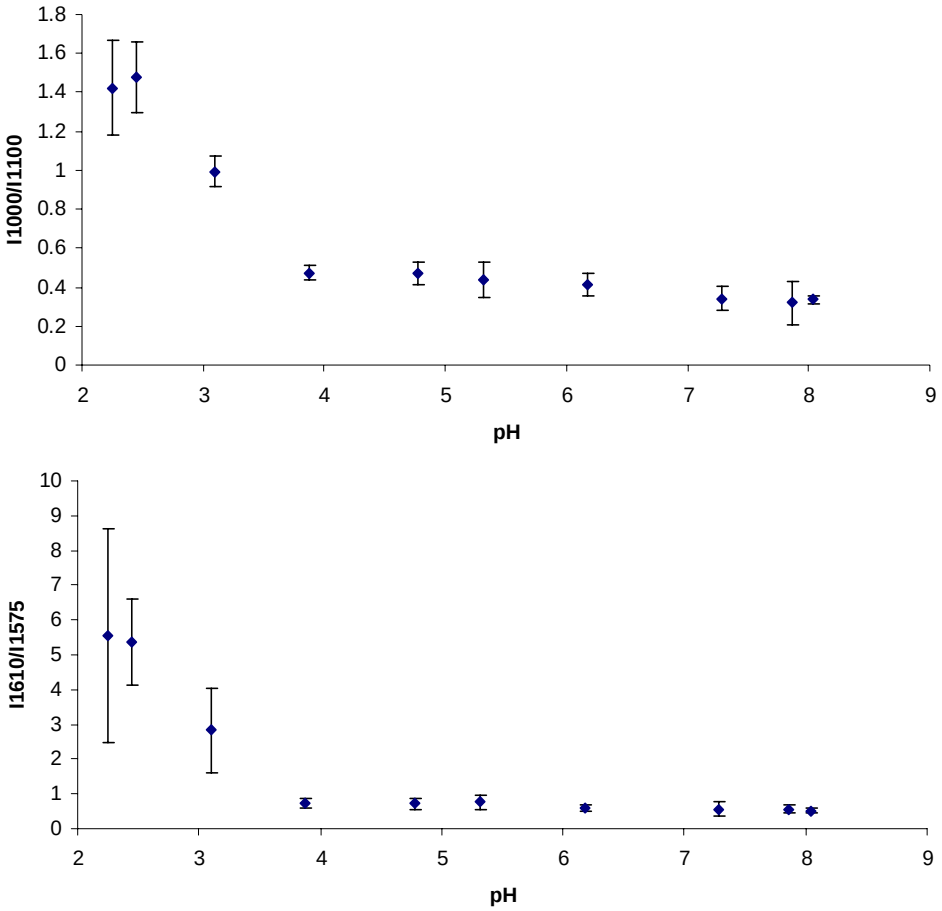

Figure 77: Titration curves obtained from oligonucleotide functionalised Ag EDTA-4-mercaptopyridine/PEG 41-TA (50/50) pH sensing probes.

Similarly as for Ag EDTA-4-mercaptopyridine and Ag EDTA-4-mercaptopyridine/PEG 41-TA probes titration curves obtained for oligonucleotide functionalised Ag EDTA pH sensing probes allows to detect pH values between 2 and 5 (Figure 77), however error bands calculated for those probes are bigger than the one calculated for the probes in the absence of oligonucleotides. It might be caused by the fact that oligonucleotides contain a lot of Lewis base sites within their structure, thus the competitive protonation of those sites with the 4-mercaptopyridine may occur.

A similar experiment was performed using 18 nm Au nanoparticles as a SERS template. Mixed monolayers of 50% 4-mercaptopyridine and 50% PEG 41-TA was prepared on the nanoparticle surface, before the terminal COOH group of the linker was conjugated to the same DNA sequence as the one used for preparation of

oligonucleotide functionalised Ag EDTA probes. Again DMT MM in water was used as an amide linkage forming reagent. The intensity of SERS signals obtained from oligonucleotide functionalised Au nanoparticles was much higher than the intensity of the SERS signals obtained from the probes which lack oligonucleotides (Figure 69 and 78). Such a big increase of the intensity is probably caused by formation of small aggregates (dimers, trimers) during oligonucleotides conjugation. Change of the orientation of Raman active molecule on nanoparticles surface causes only small changes of the intensity of SERS signals observed from the system. This assumption was confirmed by DLS and zeta potential measurements (Table 9). A large increase of the hydrodynamic diameter of the functionalised nanoparticles was observed after conjugation of 18 nm Au-4-mercaptopyridine-PEG 41 (50/50) to amino modified DNA. The increase of the size is accompanied by the decrease of zeta potential value, indicating that the nanoparticle suspension is not stable.

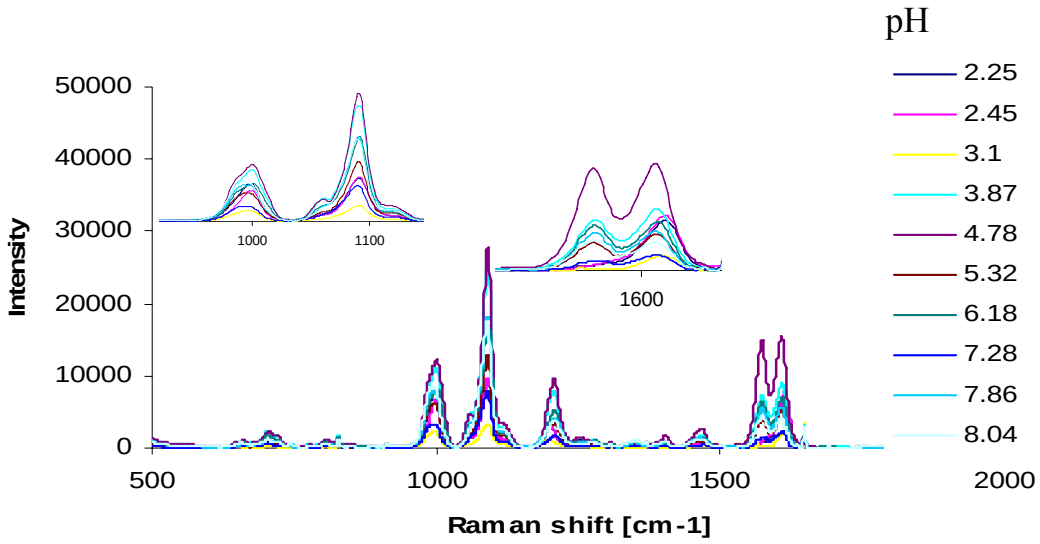

Figure 78: **SERS spectra of 18 nm nanoparticles functionalised with 50% of PEG 41-TA and 50% of 4-mercaptopyridine after oligonucleotides attachment using excitation at 633nm. Inset shows peaks taken into account during preparation of titration curves.**

Interestingly, the pH sensing range of 18 nm Au-4-mercaptopyridine/ PEG 41-TA-DNA [2-5 (Figure 79)] differs significantly from the pH sensing range of 18 nm Au functionalised with 4-mercaptopyridine only [6-8 (Figure 69 C)]. However the error bands calculated for 18 nm Au pH sensing probes are much bigger than the one calculated for oligonucleotide functionalised Ag EDTA pH sensitive probes, thus it

can be concluded that Ag EDTA-4-mercaptopyridine based probes offer better sensitivity and will be used as probes in a further work in this area.

Table 9: Zeta particle size (diameter) and zeta potential of formed 18 nm Au based pH sensing probes.

Type of probes	Zeta particle size [nm]	Zeta potential [mV]
18 nm Au	36.50±1.54	-34.5±9.0
18 nm Au-4-Mercaptopyridine	41.97±2.31	-31.8±5.3
18 nm Au-4-Mercaptopyridine/PEG 41-TA (50/50)	51.20±2.43	-41.6±6.6
Oligonucleotide functionalised 18 nm Au-4-Mercaptopyridine/PEG 41-TA (50/50)	92.15±26.6	-21.5±3.3

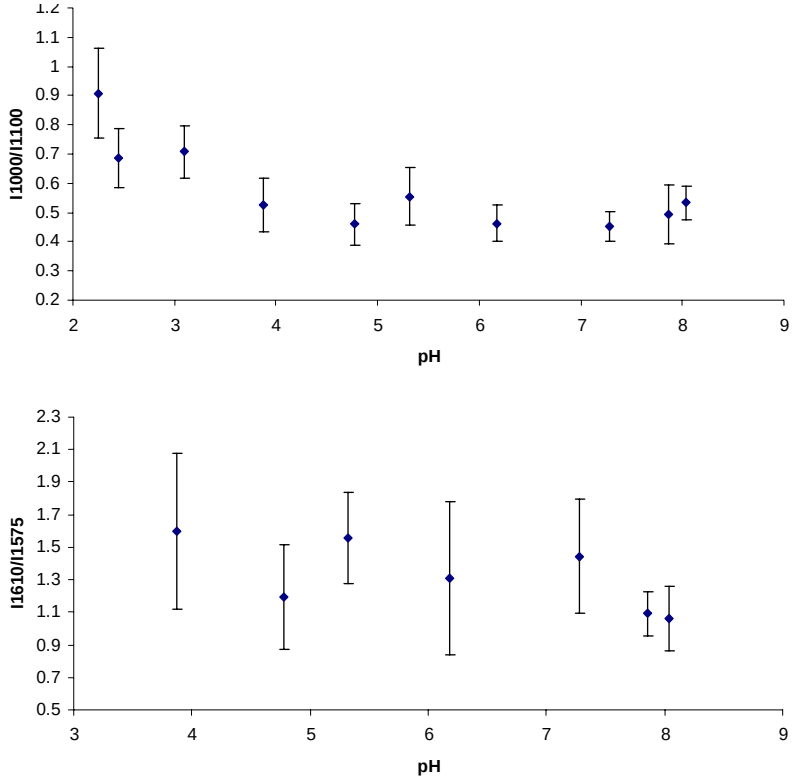

Figure 79: Titration curves obtained from oligonucleotide functionalised 18 nm Au-4-mercaptopyridine/PEG 41-TA (50/50) pH sensing probes.

5.5 pH sensing inside cells

In order to use pH probes to detect a pH value inside cells, Ag EDTA nanoparticles functionalised with 4-mercaptopyridine were incubated with macrophages (white blood cells responsible for the immune response through

phagocytosis) for 24 hrs, at 37°C, 5% CO_2. The cells were fixed by the use of 5% of paraformaldehyde. Experimental details are described in Section 6.6.4. The bright-field image and corresponding SERS map of the cells after incubation with pH sensing probes are shown in Figure 81. The presence of intense SERS signals (represented by bright colours) were obtained from some parts of the cell indicating that during incubation the silver nanoparticle sensing probes were uptaken by the cells.

(A)

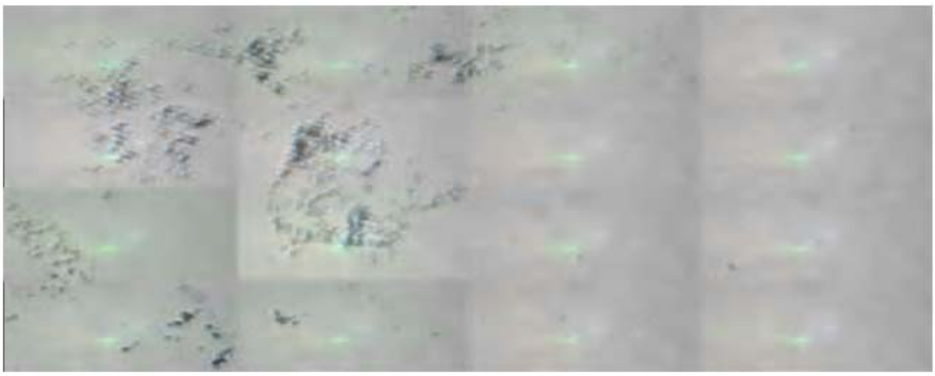

(B)

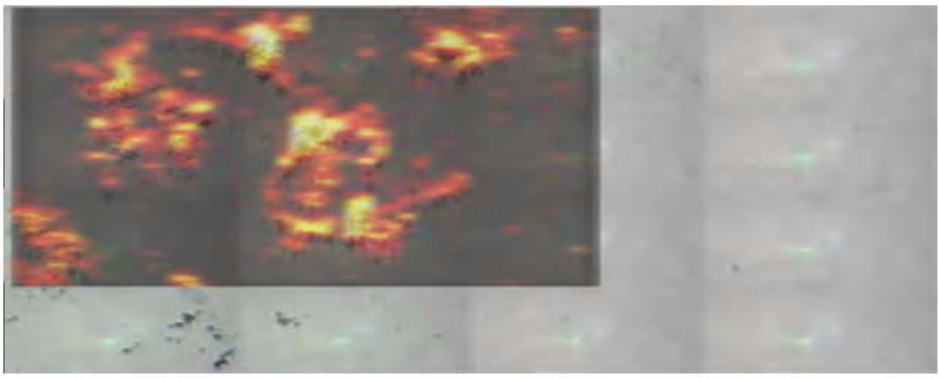

Figure 80: **Bright-field image of macrophages after incubation with silver sensing probes and fixing (A). (B) SERS map of the same macrophages as in (A). Courtesy of Dr Ross Stevenson and Maartje Geboers.**

The SERS map presented in Figure 80 B was created by taking the SERS spectra, using an excitation frequency of 633 nm, for each pixel of the map. The brighter areas visible on the map can be assigned to the places within the cell where more intense SERS signals are obtained (Figure 81 B, C and D). Shown by the absence of colour in Figure 81 A no SERRS signal were obtained when laser beam was focused outside the cells.

(A)

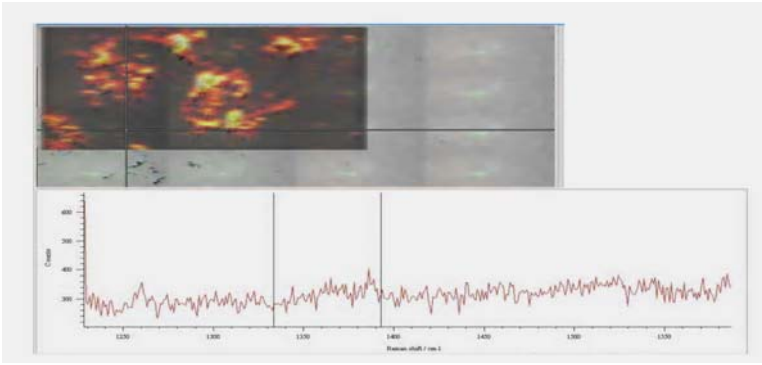

(B)

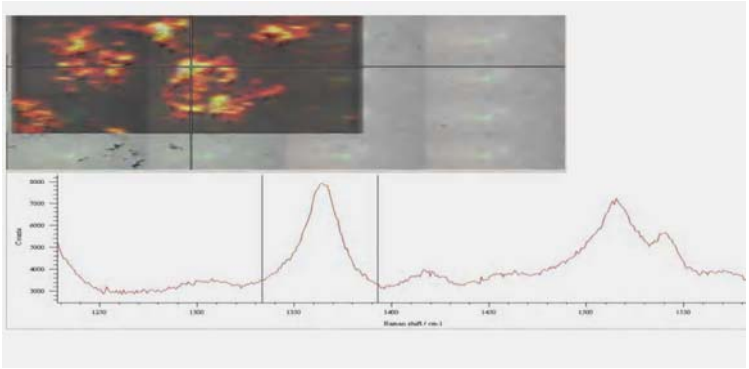

(C)

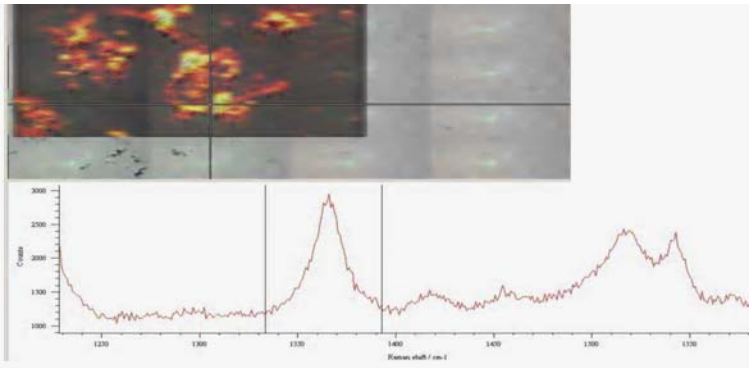

(D)

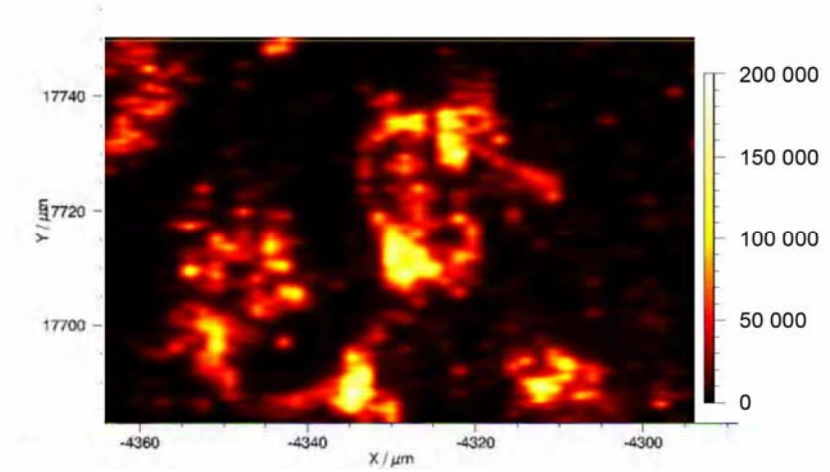

Figure 81: **SERS spectra of the area outside the cell (A), different areas of the same cell (B and C). Crosshairs indicate where the laser beam was focused. D- scale of the intensity of observed SERRS signal (plotted for signal at 1000 cm^{-1}). Courtesy of Dr Ross Stevenson and Maartje Geboers.**

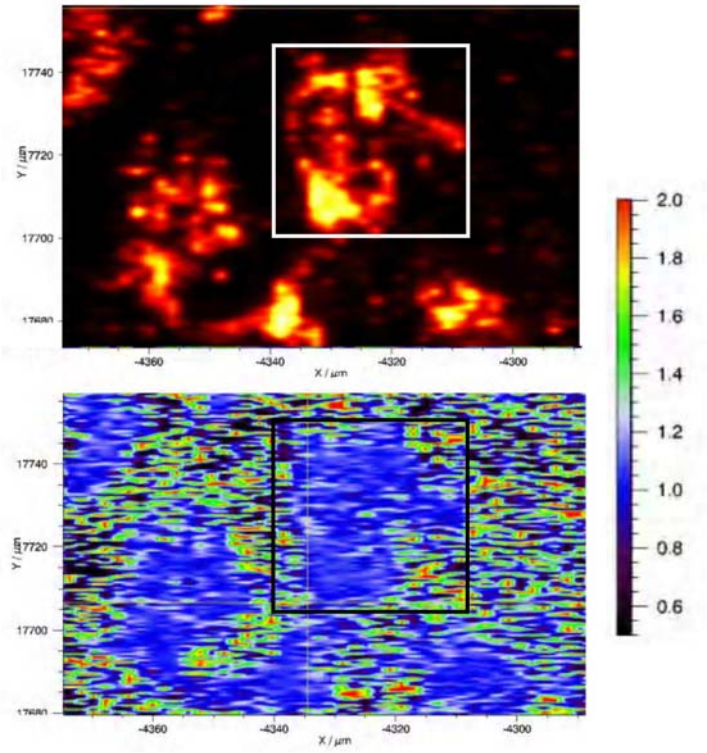

Figure 82: pH map of the macrophages cells (bottom) with the scale indicating the value of the ratio of the intensities of the SERS peaks at 1000 and 1100 cm^{-1}. The top graph helps to visualise the macrophage cell on the pH map. Courtesy of Dr Ross Stevenson and Maartje Geboers.

In order to create the pH map of the macrophage cells used in this study the ratio of the intensities of the peaks at 1000 and 1100 cm^{-1} was calculated for each pixel of the created SERS map (Figure 82). Unfortunately the software used does not allow calculation of the ratios of the intensities of the peaks of interest only from the areas where the SERS signal is produced, thus the ratio was calculated also for the areas of the sample where the SERS active probes were not present. The work on the creation of new software allowing calculation of the ratio of the intensities of the Raman peaks only from the parts of the map where the nanoparticles are present is ongoing within the group and with Renishaw.

Figure 82 indicates that the ratio of the intensities of the peaks at 1000 and 1100 cm^{-1} calculated for the SERS signals obtained from the pH sensing probes present inside macrophages cells is 0.95 to 1.30. The pH value can be calculated from the titration curve obtained for the Ag EDTA nanoparticles functionalised with 4-mercaptopyridine (Figure 65). It was found that the pH value inside macrophage cells is equal to 3.13 (for the ratio of the peaks intensities equal 1.3-white colour on the

SERS map) to 4.39 (for the ratio of the peak intensities equal to 0.95-dark blue colour on the SERS map). It was reported in the literature that pH inside macrophages endosomes varies between 6 (early endosomes) and 4.7-4.8 (lysosomes) [149-151]. After 24 hours of incubation of the pH probe with the macrophages most of the nanoparticles were probably present in lysosomes-the dark blue areas on the SERS map probably correspond to them. Lower pH value was probably detected in the areas of the cell where nanoparticle probes were not present and SERS signal not detected.

A similar experiment was performed with the use of the same type of pH sensing probes and human HeLa cells.

(A)

(B)

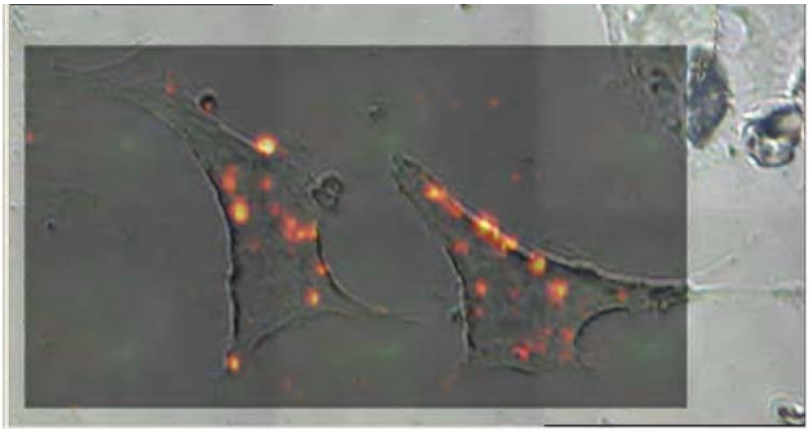

Figure 83: **Bright-field image (A) and SERS map (B) of the same HeLa cells after 24 hrs of incubation with Ag EDTA-4-mercaptopyridine pH sensing probes. Courtesy of Dr Ross Stevenson and Maartje Geboers.**

(A)

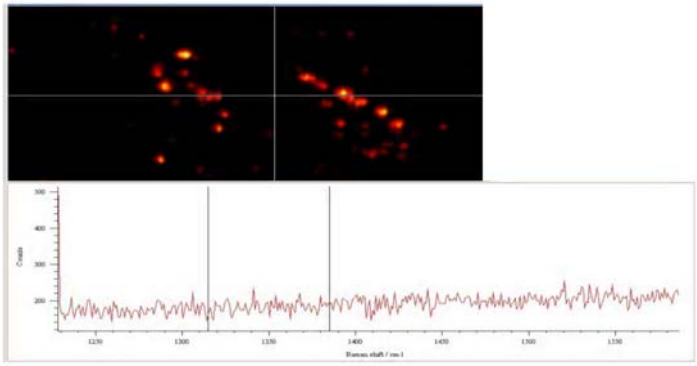

(B)

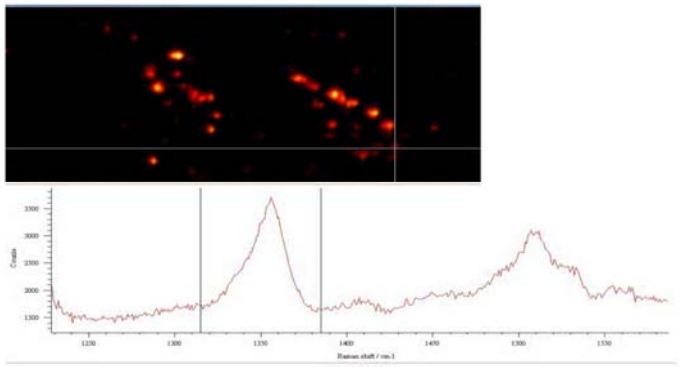

(C)

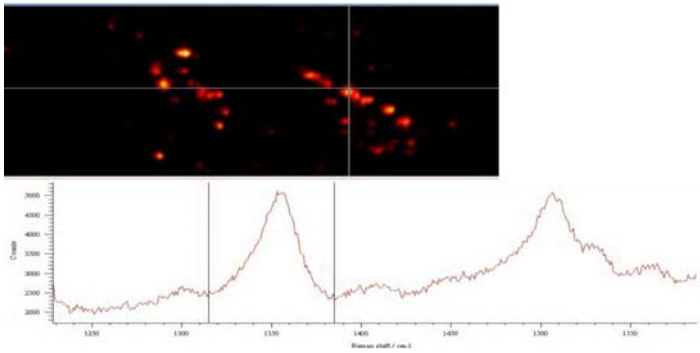

(D)

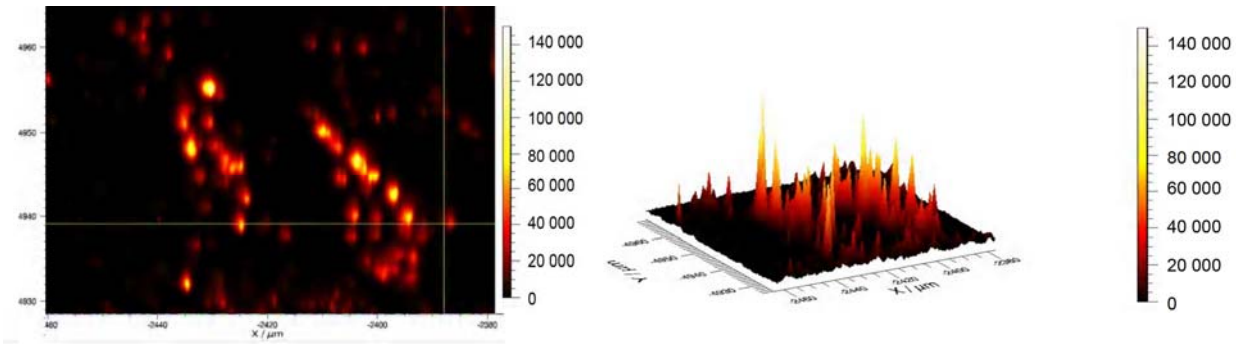

Figure 84: **SERS spectra of: the area outside the cell (A), different areas of the same cell (B and C). D- scale of the intensity of SERS signal (plotted for signal at 1000 cm^{-1}) observed from different areas of the same HeLa cell. Courtesy of Dr Ross Stevenson and Maartje Geboers.**

The cells were incubated with Ag EDTA-4-mercaptopyridine nanoparticles for 24 hrs at 37°C, 5% CO_2. Then they were fixed for 5 mins by the use of 5% of paraformaldehyde. The bright-field image and the SERRS map of HeLa cells are presented in Figure 83.

It can be concluded that fewer nanoparticles were taken up by the HeLa cells than by the macrophage cells (Figure 80). It can be explained by the fact that macrophages are specialized phagocytotic cells which protect leaving organisms by ingestion of the harmful, foreign nanoparticles. Similarly as in the previous experiment when the laser beam was focused outside the cell area no SERS signals were obtained (Figure 84 A). Intensities of SERS signals obtained from different parts of the cells differs as well (Figures 84 B, C and D).

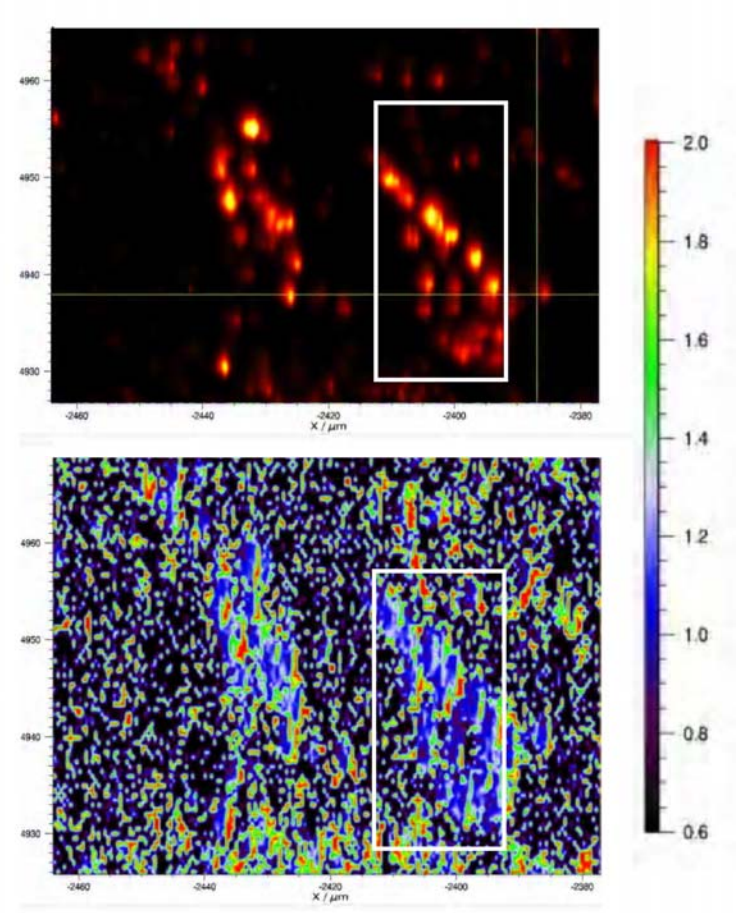

Figure 85: pH map of the HeLa cells (bottom graph) with the scale indicating the value of the ratio of the intensities of the SERS peaks at 1000 and 1100 cm^{-1}. The top graph helps to visualize the HeLa cell on the pH map. Courtesy of Dr Ross Stevenson and Maartje Geboers.

The pH map of the HeLa cells created by calculating the ratios of the intensities of SERS peaks at 1000 and 1100 cm^{-1} is shown in Figure 85. The value of the ratio of

the intensities of the peaks taken into account is from 1.05 to 2 for the SERS spectra obtained from the cell area. The pH value inside HeLa cells, calculated from the titration curve obtained for the Ag EDTA-4-mercaptopyridine sensing probe (Figure 88) was found to be between 1.39 (red colour on the map) and 3.99 (blue colour on the map). Similarly as in previous experiment used software calculated the ratios of the intensities of the peaks of interest for each pixel of the map, not only for the areas of the cell where nanoparticle probes were present and SERS signal obtained. It was reported in the literature that the pH value inside HeLa endosomes varies between 6.5-6.2 (early endosomes), 5.6-5.5 (late endosomes), <4.5 (lysosomes) [152, 153]. After 24 hours of incubation of the cells with nanoparticle probes most of the nanoparticles were probably present in lysosomes, thus the blue areas on the SERS map (pH~4) probably correspond to them. Low pH value (1.39) was probably detected in the areas of the cell where nanoparticle probes were not present and SERS signal not obtained.

5.6 Conclusions

Two different pH sensitive SERS active molecules: 4-mercaptopyridine and 2-aminothiophenol were used to functionalise the following types of metallic nanoparticles: 18 nm Au, Ag EDTA and Ag citrate. Both pH sensing molecules investigated contain a thiol group within the structure, thus can be easily attached to the nanoparticles surface via formation of a metal-sulphur bond. SERS active, pH sensitive probes were incubated in phosphate buffers with pH values differing from 2 to 10, and then SERS spectra of the probes were recorded using a laser excitation frequency of 633 nm. It was found that the best sensitivity and highest SERS signal intensity were obtained for Ag EDTA nanoparticles functionalised with 4-mercaptopyridine, thus this assembly was used in further experiments.

It was reported that conjugation of metallic nanoparticles to cell penetrating peptides or NLS make it possible to deliver nanoparticles into the cell nucleus [138-141]. Thus a mixed layer of 4-mercaptopyridine and PEG41-TA linker was formed on Ag EDTA nanoparticles. Probes prepared in such a way allow the measurement of pH in the surrounding media and also, due to the presence of free COOH group within the PEG 41-TA linker structure, allow conjugation of the probes to biomolecules such as DNA or proteins. Additionally the presence of PEG in the layer formed on

nanoparticles surface helps to prevent non-specific interactions of the probes with the components of the cell media. Ag EDTA-4-mercaptopyridine/PEG 41-TA conjugates were then reacted with amino-modified DNA in the presence of DMT MM in water. It was found that additional modifications of the surface of Ag EDTA nanoparticles, such as formation of a mixed monolayer of pH sensing molecule and PEG 41-TA linker or conjugation of the probes to DNA has no influence on the sensitivity of the pH sensor. The pH sensing range of Ag EDTA-4-mercaptopyridine, Ag EDTA-4-mercaptopyridine/PEG 41-TA, Ag EDTA-4-mercaptopyridine/PEG 41-TA-DNA is the same, with detection possible from pH 2 to 5.

In order to check if the prepared pH sensor allows the detection of intracellular pH, Ag EDTA-4-mercaptopyridine probes were incubated with macrophages and HeLa cells. It was found that in both cases the nanoparticles were taken up by the cells. The SERS maps of the cells were than created by taking the SERS spectrum of each pixel of the map. Calculating the ratio of the intensities of the peaks of interest (in case of 4-mercaptopyridine peaks at 1000 and 1100 cm^{-1}) for each pixel of the SERS map made it possible to create a pH map of the cell. Experiments indicate that after 24 hrs of incubation of the probes with the cells the nanoparticles were trapped inside lysosomes. The pH value inside lysosomes of HeLa cell was detected to be 3.99; inside lysosomes of macrophages cell 4.39. Obtained data are with close agreement with reported in the literature pH values which were detected inside lysosomes of the same cell types.

Further work described within this chapter, involving preparation of Ag EDTA-4-mercaptopyridine/PEG 41-TA probes conjugated to a nuclear localization sequence peptide and use of such probes to detect the pH value inside the cell nucleus are currently ongoing within the Centre for Molecular Nanometrology at the University of Strathclyde.

All experiments described in section 5.5 were conducted by Dr Ross Stevenson and Maartje Geboers.

Chapter 6

Experimental

6.1 Chemistry

General methods

Reagents were purchased from Aldrich, Acros Organics, Alfa Aesar, Ana Spec, New England BioLabs or Cambridge Bioscience Ltd and used without further purification. ^{1}H NMR and ^{13}C NMR experiments were recorded on a Bruker DPX 400 MHz spectrometer with the appropriate solvent peak as a reference. J values are quoted in Hertz. Mass spectrometry was carried out as a service by the EPSRC National Mass Spectrometry Service Centre, Swansea.

6.1.1 Synthesis of the 6-aminofluorescein linker

Ethyl 4-amino-2-(6-hydroxy-3-oxo-3*H*-xanthen-9-yl) benzoate (1) (Ethyl 2-(6-hydroxy-3-oxo-3*H*-xanthen-9-yl) benzoate (7)). H_2SO_4 (Af: 0.77 ml, 14.4 mmol; F: 0.80 ml, 15.00 mmol) was added dropwise to the suspension of 6-aminofluorescein (Af) (1.00 g, 2.88 mmol) or fluorescein (F) (1.000g, 3.0 mmol) in EtOH. After stirring at reflux for 24 hrs the EtOH was removed under reduced pressure. The residue was diluted in $CHCl_3$ with a few drops of MeOH. Solid $NaHCO_3$ was added until gas evolution ceased. The resulting mixture was filtered, then the organic phase was dried over anhydrous Na_2SO_4, filtered and concentrated under reduced pressure. The residue was subjected to silica gel chromatography eluting with EtOAc, then MeOH/DCM (1:9) to afford the title compound as a dark orange solid (**1**) (1.082 g, 99%) or brown solid (**7**) (0.814 g, 75%).

1: ^{1}H NMR (400 MHz, DMSO) δ 0.86 (3H, t, 7.1, CH_3), 3.71 (2H, q, 7.1, CH_2), 6.43 (1H, s, CH), 6.66 (4H, d, 7.4, 4xCH), 6.78 (1H, d, 8.7, CH), 7.01 (2H, d, 9.7, 2xCH), 7.89 (1H, d, 8.7, CH). ^{13}C NMR (100.62 MHz, DMSO) δ 13.50, 15.09, 59.62, 61.07, 102.92, 113.57, 113.97, 114.60, 115.15, 130.50, 132.81, 135.81, 152.83, 164.58. HRMS 376.20 $[(M+H)^+]$ ($C_{22}H_{18}O_5N$ requires 376.62).

7: ^{1}H NMR (400 MHz, DMSO) δ 0.83 (3H, t, 8.0, CH_3), 3.91 (2H, q, 8.0, CH_2), 5.75 (1H, s, OH), 7.07 (2H, d, 10.0, 2xCH), 7.22 (2H, s, 2xCH), 7.29 (2H, d, 12.0, 2xCH)), 7.54 (1H, d, 6.0, CH), 7.86 (1H, t, 8.0, CH), 7.93 (1H, t, 8.0, CH), 8.28 (1H, d, 8.0, CH). ^{13}C NMR (100.62 MHz, DMSO) δ 13.29, 15.10, 61.11, 61.24, 102.35, 116.13, 120.56, 129.43, 130.15, 130.88, 130.97, 132.62, 133.18, 158.32, 164.50, 171.35. HRMS 361.11 $[(M+H)^+]$ ($C_{22}H_{17}O_5$ requires 361.17).

Ethyl 4-amino-2-[(6-tert-butoxy-2-oxoethoxy)-3-oxo-3*H*-xanthen-9-yl] benzoate (2) (Ethyl 2-[6-(2-tert-butoxy-2-oxoethoxy)-3-oxo-3H-xanthen-9-yl] benzoate (8)). *tert*-butyl bromoacetate (Af: 0.47 ml, 3.17 mmol; F: 0.37 ml, 2.48 mmol) was added to the mixture of compounds (**1**) (1.082 g, 2.88 mmol) or (**7**) (0.814 g, 2.26 mmol) and K_2CO_3 (Af:0.44 g, 3.17 mmol; F: 0.34 g, 2.48 mmol) in the minimum amount of DMF. After stirring for 3 hrs at room temperature the reaction mixture was diluted with H_2O and extracted with EtOAc (3x20 ml). The organic phase was washed with 1M $NaHCO_3$ and sat. NaCl, then dried over anhydrous Na_2SO_4, filtered and concentrated under reduce pressure. The residue was subjected to silica gel chromatography eluting with EtOAc, then MeOH/DCM (1:9) giving 0.79 g (**2**) or 0.66 g (**8**) of title compounds as an orange solids (2: 56%; 8: 62%) .

2: ^{1}H NMR (400 MHz, DMSO) δ 0.84 (3H, t, 7.1, CH_3), 1.43 (9H, s, $C(CH_3)_3$), 3.81-3.89 (2H, m, CH_2), 4.86 (2H, s, CH_2), 6.21 (1H, s, CH), 6.39-6.45 (2H, m, 2xCH), 6.77 (1H, d, 7.6, CH), 6.90 (3H, m, 3xCH), 7.16 (1H, s, CH), 7.89 (1H, d, 8.7, CH). ^{13}C NMR (100.62 MHz, DMSO) δ 13.54, 27.68, 59.62, 81.80, 104.44, 113.42, 129.01. HRMS 490.76 [$(M+H)^+$] ($C_{28}H_{28}O_7N$ requires 490.20).

8: ^{1}H NMR (400 MHz, DMSO) δ 0.85 (3H, t, 8.0, CH_3), 1.42 (9H, s, $C(CH_3)_3$), 3.92-4.05 (2H, m, CH_2), 4.87 (2H, s, CH_2), 6.44 (1H, s, CH), 6.38 (1H, d, 8.0, CH), 6.80-6.92 (3H, m, 3xCH), 7.20 (1H, s, CH), 7.50 (1H, d, 8.0, CH), 7.76 (1H, t, 4.0, CH), 7.79 (1H, t, 8.0, CH), 8.18 (1H, d, 8.0, CH). ^{13}C NMR (100.62 MHz, $CDCl_3$) δ 13.86, 13.92, 28.40, 53.73, 61.74, 104.14, 114.01, 115.33, 122.43, 129.60, 130.08, 130.60, 130.79, 130.91, 131.02, 131.52, 131.61, 132.76, 132.91, 134.38, 135.52, 155.47, 158.01, 165.70, 175.75. HRMS 475.1751 [$(M+H)^+$] ($C_{28}H_{27}O_7$ requires 475.1751).

2-{9-[5-amino-2-(ethoxycarbonyl)phenyl]-3-oxo-3*H*-xanthen-6-yloxy} acetic acid (3) (2-{9-[2-(ethoxycarbonyl)phenyl]-3-oxo-3*H*-xanthen-6-yloxy}acetic acid (9)). TFA (3 ml) was added to the solution of 2 (0.79 g, 1.61 mmol) or 8 (0.66 g, 1.40 mmol) in DCM (3 ml). After stirring for 3 hrs at room temperature DCM and TFA were evaporated. The residue was solidified by addition of diethyl ether, then it was filtered and washed with the same solvent giving after drying 0.36 g of the title compound as an orange solid (52%) (**3**) or 0.33 g of a title compound as a dark yellow solid (57%) (**9**).

3: ^{1}H NMR (400 MHz, DMSO) δ 0.85 (3H, t, 5.7, CH_3), 3.82-3.89 (2H, m, CH_2), 4.96 (2H, s, CH_2), 6.46 (1H, s, CH), 6.55 (1H, s, CH), 6.64 (1H, d, 7.7, CH), 6.81 (1H, d, 7.0, CH), 7.05 (1H, d, 7.2, CH), 7.13-7.16 (2H, m, 2xCH), 7.33 (1H, s, CH), 7.91 (1H, d, 8.7, CH). ^{13}C NMR (100.62 MHz, DMSO) δ 13.54, 59.74, 65.23, 101.16, 103.78, 113.77, 113.97, 115.07, 115.34, 116.42, 131.44, 132.84, 135.55, 152.89, 154.51, 158.69, 164.54, 169.21. HRMS 434.20 [$(M+H)^+$] ($C_{24}H_{20}O_7N$ requires 434.70).

9: ^{1}H NMR (400 MHz, DMSO) δ 0.86 (3H, t, 7.1, CH_3), 3.93-4.01 (2H, m, CH_2), 4.95 (2H, s, CH_2), 6.49 (1H, s, CH), 6.57 (1H, d, 9.6, CH), 6.95-7.04 (3H, m, 3xCH), 7.32 (1H, s, CH), 7.52 (1H, d, 7.6, CH), 7.79 (1H, t, 7.7, CH), 7.87 (1H, t, 7.5, CH), 8.21 (1H, d, 8.2, CH). ^{13}C NMR (100.62 MHz, DMSO) δ 13.32, 60.96, 65.16, 101.28, 104.22, 114.62, 129.42, 129.83, 130.19, 130.49, 130.71 130.87, 169.26. HRMS 419.40 [$(M+H)^+$] ($C_{24}H_{19}O_7$ requires 419.20).

***tert*-butyl 1-{[9-(5-amino-2-ethoxycarbonyl) phenyl]-3-oxo-3*H*-xanthen-6-yloxy}-2-oxo-6, 9, 12-trioxa-3-azapentadecan-15-oate (4).** (**3**) (0.36 g, 0.83 mmol) was dissolved in small amount of DMF. HATU (0.378 g, 0.995 mmol) and DIPEA (0.32 g, 2.500 mmol) were added. After stirring for 15 minutes at room temperature *tert*-butyl-12-amino-4,7,10-trioxadodecanoate (0.23 g, 0.83 mmol) was added. After stirring for 3 hrs at room temperature another portions of HATU (0.378 g, 0.995 mmol) and DIPEA (0.32 g, 2.500 mmol) were added. After stirring for another 20 hrs at room temperature the reaction mixture was diluted with water, then extracted with Et_2O (3x20 ml). The organic phase was dried over anhydrous Na_2SO_4, filtered and concentrated under reduced pressure. The residue was subjected to silica gel chromatography eluting with MeOH/DCM 1-20% giving 0.142 g of a title compound (25%) as an orange solid. ^{1}H NMR (400 MHz, DMSO) δ 0.86 (3H, t, 7.1, CH_3), 1.42 (9H, s, $C(CH_3)_3$), 2.40 (2H, t, 6.2, CH_2), 2.85 (2H, t, 5.4, CH_2), 3.48-3.52 (10H, m, 5xCH_2), 3.56 (2H, t, 6.2, CH_2), 3.81-3.91 (2H, m, CH_2), 4.32 (2H, s, CH_2), 6.20 (1H, s, CH), 6.30 (2H, s, NH_2), 6.36 (1H, d, 9.7, CH), 6.42 (1H, s, CH), 6.76-6.82 (2H, m, 2xCH),6.89-6.93 (3H, m, 3xCH), 7.88 (1H, d, 8.7, CH). ^{13}C NMR (100.62 MHz, DMSO) δ 13.63, 27.76, 35.81, 66.22, 69.65. HRMS 693.3018 [$(M+H)^+$], ($C_{37}H_{44}O_{11}N_2$ requires 693.3020).

***tert*-butyl 1-{9-[5-(1,2-dithiolan-3-yl) pentanamido]-2-[(ethoxycarbonyl) phenyl]-3-oxo-3*H*-xanthen-6-yloxy}-2-oxo-6, 9, 12-trioxa-3-azapentadecan-15-oate (5).** Thioctic acid (0.107 g, 0.210 mmol) and DIC (0.132 g, 0.520 mmol) were added to the solution of (**4**) (0.142 g, 0.210 mmol) in DCM. After stirring for 48 hrs at room temperature the reaction mixture was concentrated under reduced pressure. The residue was subjected to silica gel chromatography eluting with MeOH/DCM (0.1:9.9), then (0.5:9.5) giving 0.18 g of title compound as a yellow solid (97%) ^{1}H NMR (400 MHz, Acetone) δ 0.95 (3H, t, 7.2 CH_3), 1.49 (9H, s, $C(CH_3)_3$), 1.69-1.75 (6H, m, 3xCH_2), 1.90-1.95 (2H, m, CH_2), 2.35 (2H, t, 6.5, CH_2), 2.45 (2H, t, 6.5, CH_2), 3.11-3.20 (2H, m, CH_2), 3.50-3.64 (12H, m, 6xCH_2), 3.55 (2H, t, 5.2, CH_2), 3.95-4.01 (2H, m, CH_2), 4.60 (2H, s, CH_2), 6.44 (1H, s, CH), 6.48 (1H, s, CH), 6.55 (1H, d, 9.7, CH), 6.79 (1H, d, 8.9, CH), 6.83 (1H, d, 8.6 CH), 6.97-7.07 (3H, m, 3xCH), 8.08 (1H, d, 8.6, CH). ^{13}C NMR (100.62 MHz, DMSO) δ 25.64, 26.28, 26.74, 28.34, 29.41, 29.44, 30.40, 30.43, 70.26. HRMS 881.3327 $[(M+H)^{+}]$ ($C_{45}H_{57}O_{12}N_2S_2$ requires 881.3347).

1-(9-{5-[5-(1,2-dithiolan-3-yl) pentanamido]-2-(ethoxycarbonyl) phenyl}-3-oxo-3*H*-xanthen-6-yloxy)-2-oxo-6, 9, 12-trioxa-3-azapentadecan-15-oic acid (<u>6-aminofluorescein linker</u>) (6) TFA (3 ml, 99.5%) was added to the solution of (**5**) (0.18 g) in DCM (3 ml). After stirring for 3 hrs at room temperature DCM and TFA were removed under reduced pressure. The residue was solidified by addition of diethyl ether, then it was filtered and washed with the same solvent and dried to afford the title compound as a yellow solid (0.165 g, 98 %). ^{1}H NMR (400 MHz, Acetone) δ 0.92 (3H, t, 7.1, CH_3), 1.57-1.65 (6H, m, 3xCH_2), 2.18-2.20 (2H, m, CH_2), 2.49-2.55 (5H, m, 2xCH_2, CH), 3.53-3.92 (16H, m, 8xCH_2), 3.90-3.93 (2H, m, CH_2), 4.72 (2H, s, CH_2), 6.27 (1H, s, CH), 6.42 (1H, d, 9.7, CH), 6.62 (1H, s, CH), 6.92-6.98 (2H, m, 2xCH), 7.03-7.14 (3H, m, 3xCH), 8.00 (1H, d, 8.7, CH). ^{13}C NMR (100.62 MHz, $CDCl_3$) δ 23.04, 24.62, 39.70, 43.66. HRMS 639.20 + 188.00 (TA) $[(M+H)^{+}]$ ($C_{41}H_{50}O_{12}S_2N_2$ requires 826.20).

6.1.2 Synthesis of the fluorescein linker

***tert*-butyl 10-{[(9*H*-fluoren-9-yl) methoxy] carbonylamino}-2, 2-dimethyl-4, 11-dioxo-3, 5, 18, 21-tetraoxa-5, 12-diaza-tetracosan-24-oate (10).** *tert*-butyl-12-amino-4, 7, 10-trioxadodecanoate (0.148 g, 0.53 mmol) and DIC (0.074 g, 0.58 mmol) were added to the solution of 2-(*N*-Fmoc), 6-(*N*-Boc)-diamino caproic acid (0.250 g, 0.53 mmol) in DCM. After stirring for 24 hrs at room temperature the reaction mixture was filtered and concentrated under reduced pressure. The residue was subjected to silica gel chromatography eluting with Pet Ether/EtOAc (2.5:7.5) to afford a title compound as a white solid (0.358 g, 92%). ^{1}H NMR (400 MHz, $CDCl_3$) δ 1.25-1.28 (2H, m, CH_2), 1.30-1.41 (2H, m, CH_2), 1.44 (18H, s, 2x$C(CH_3)_3$), 1.48-1.53 (2H, m, CH_2), 2.47 (2H, t, 6.5, CH_2), 3.11 (2H, s, CH_2), 3.47 (2H, s, CH_2), 3.55-3.60 (10H, m, 5xCH_2), 3.68 (2H, t, 8.8, CH_2), 4.10-4.17 (1H, m, CH), 4.20-4.24 (1H, m, CH), 4.40-4.42 (2H, m, CH_2), 7.30 (2H, t, 7.4, 2xCH), 7.39 (2H, t, 7.4, 2xCH), 7.60 (2H, d, 7.4, 2xCH), 7.76 (2H, d, 7.4, 2xCH). ^{13}C NMR (100.62 MHz, $CDCl_3$) δ 22.73, 28.34, 28.69, 29.89, 36.43, 39.58, 47.43, 67.10, 69.86, 70.56, 70.66, 70.77, 120.22, 125.33, 127.33, 127.96, 141.55. HRMS 506.30 + 223.00 (Fmoc) [$(M+H)^+$] ($C_{39}H_{58}O_{10}N_3$ requires 728.88).

***tert*-butyl 5-(4-aminobutyl)-1-(9*H*-fluoren-9-yl)-3, 6-dioxo-2, 10, 13, 16-tetraoxa-4, 7-diazanonadecan-19-oate (11).** $BiCl_3$ (0.030 g, 0.096 mmol) was added to a solution of (**10**) (0.350 g, 0.48 mmol) in acetonitrile/water (5 ml/100 µl). The reaction mixture was stirred at 55°C for 5 hours. Additional portions of $BiCl_3$ (0.030 g, 0.096 mmol) were added after 1 and 3 hours from reaction beginning. Then solid $NaHCO_3$ was added and the reaction mixture was filtered and concentrated under reduced pressure. The residue was subjected to silica gel chromatography eluting with MeOH/DCM (1:9), then (2:8) giving 0.094 g of a title compound (31%) as a colourless solid. ^{1}H NMR (400 MHz, $CDCl_3$) δ 1.40 (9H, s, $C(CH_3)_3$), 1.51-1.58 (2H, m, CH_2), 1.81-1.91 (4H, m, 2xCH_2), 2.46 (2H, t, 6.3, CH_2), 3.03-3.05 (2h, m, CH_2), 3.57-3.69 (14H, m, 7xCH_2), 4.17 (1H, t, 7.0, CH), 7.27 (2H, t, 8.6, 2xCH), 7.35 (2H, t, 7.3, 2xCH), 7.59 (2H, d, 7.3, 2xCH), 7.72 (2H, d, 7.5, 2xCH). ^{13}C NMR (100.62 MHz, $CDCl_3$) δ 28.34, 39.33, 47.32, 67.14, 120.13, 125.50, 127.36, 127.91, 141.46. HRMS 628.3596 [$(M+H)^+$] ($C_{34}H_{49}O_8N_3$ requires 628. 3592).

***tert*-butyl 5—{4-[5-(1, 2-dithiolan-3-yl) pentanamido] butyl}-1-(9*H*-fluoren-9-yl)-3, 6-dioxo-2, 10, 13, 16-tetraoxa-4, 7-diazanonadecan-19-oate (12).** Thioctic acid (0.036 g, 0.176 mmol) and DIC (0.022g, 0.176 mmol) were added to the solution of (**11**) (0.092 g, 0.146 mmol) in DCM with a few drops of Et_3N. After stirring for 24 hrs at room temperature the reaction mixture was concentrated under reduced pressure. The residue was subjected to silica gel chromatography eluting with EtOAc, then MeOH/DCM (1:9) giving 0.035 g of a title compound (29%) as a slightly yellow solid. ^{1}H NMR (400 MHz, $CDCl_3$) δ 1.41 (9H, s, $C(CH_3)_3$), 1.48-1.56 (2H, m, CH_2), 1.62-1.74 (10H, m, 5xCH_2), 1.87-1.95 (2H, m, CH_2), 2.15 (2H, t, 4.4, CH_2), 2.42-2.44 (1H, m, CH), 2.45 (2H, t, 6.4, CH_2), 3.08-3.21 (4H, m, 2xCH_2), 3.46-3.60 (12H, m, 6xCH_2), 3.67 (2H, t, 6.5, CH_2), 4.20-4.22 (1H, m, CH), 7.30 (2H, t, 7.7, 2xCH), 7.39 (2H, t, 7.7, 2xCH), 7.61 (2H, d, 4.5, 2xCH), 7.76 (2H, d, 7.5, 2xCH). ^{13}C NMR (100.62 MHz, $CDCl_3$) δ 22.69, 22.81, 23.57, 24.68, 24.72, 25.63, 28.30, 28.64, 28.90, 28.94, 29.11, 33.87, 33.91, 34.80, 34.84, 36.41, 36.62, 38.65, 38.69, 39.11, 39.59, 40.42, 42.61, 47.39, 56.51, 56.62, 67.06, 67.21, 69.76, 70.43, 70.51, 70.61, 70.72, 120.20, 125.32, 127.30, 127.95, 141.50, 144.00, 172.20, 173.32, 178.23. HRMS 833.4197 [$(M+NH_4)^+$], ($C_{42}H_{61}O_9N_3S_2$ requires 833.4187).

***tert*-butyl 15-amino-25-(1, 2-dithiolan-3-yl)-14, 21-dioxo-4, 7, 10-trioxa-13, 20-diazapentacosan-1-oate (13).** (**12**) (0.033 g, 0.040 mmol) was stirred for 2 hrs at room temperature with 20% piperidine in CH_3CN. Then the reaction mixture was concentrated under reduced pressure. The residue was dissolved in EtOH and concentrated again giving 0.022 g of the title compound (92%) as a slightly yellow solid. HRMS 594.3244 [$(M+H)^+$], ($C_{27}H_{51}O_7N_3S_2$ requires 594.3241).

***tert*-butyl 25-(1, 2-dithiolan-3-yl)-15-({2-[9-(2-ethoxycarbonyl) phenyl]-3-oxo-3*H*-xanthen-6-yloxy} acetamido)-14, 21-dioxo-4, 7, 10-trioxa-13, 20-diazapentacosan-1-oate (14).** (**9**) (0.015 g, 0.036 mmol) was dissolved in small amount of DMF. HATU (0.017 g, 0.044 mmol) and DIPEA (0.014 g, 0.11 mmol) were added. After stirring for 15 minutes at room temperature (**13**) (0.022 g, 0.036 mmol) was added. The reaction mixture was stirred for 3 hrs at room temperature, then another portions of HATU (0.017 g, 0.044 mmol) and DIPEA (0.014 g, 0.11

mmol) were added. After stirring for 20 hrs at room temperature the reaction mixture was diluted with water (50 ml), extracted with Et_2O (3x20 ml). The organic phase was washed wit sat NaCl, then dried over anhydrous Na_2SO_4, filtered and concentrated under reduced pressure. The residue was subjected to silica gel chromatography eluting with MeOH/DCM (0.5:9.5) giving 0.022 g of the title compound (60%) as a yellow solid. ^{1}H NMR (400 MHz, $CDCl_3$) δ 0.84 (3H, t, 10.6, CH_3), 1.44 (9H, s, $C(CH_3)_3$, 1.51-1.59 (2H, m, CH_2), 1.62-1.73 (10H, m, 5xCH_2), 1.90-1.95 (2H, m, CH_2), 2.10-2.20 (2H, m, CH_2), 2.35-2.40 (2H, m, CH_2), 2.45-2.54 (1H, m, CH), 3.09-3.20 (4H, m, 2xCH_2), 3.38-3.41 (2H, m, CH_2), 3.47-3.59 (10H, m, 5xCH_2), 3.60-3.64 (2H, m, CH_2), 4.03-4.05 (2H, m, CH_2), 4.20-4.22 (1H, m, CH), 4.81 (2H, s, CH_2), 6.47 (1H, s, CH), 6.55 (1H, d, 10.4, CH), 6.82-7.01 (4H, m, 4xCH), 7.66-7.77 (3H, m, 3xCH), 8.27 (1H, d, 10.6, CH). ^{13}C NMR (100.62 MHz, $CDCl_3$) δ 14.24, 23.65, 23.96, 24.77, 25.35, 25.79, 26.77, 29.13, 29.36, 30.57, 33.32, 34.99, 3 8.70, 38.95, 40.45, 42.51, 42.88, 46.90, 56.53, 56.69, 68.37, 107.94, 113.63, 119.93, 1 21.20, 127.25, 128.93, 131.07. HRMS 994.4192 [$(M+H)^+$], ($C_{51}H_{67}O_{13}N_3S_2$ requires 994.4188).

25-(1, 2-dithiolan-3-yl)-15-(2-{9-[2-(ethoxycarbonyl) phenyl]-3-oxo-3*H*-xanthen-6-yloxy} acetamido)-14, 21-dioxo-4, 7, 10-trioxa-13, 20-diazapentacosan-1-oic acid (<u>fluorescein linker</u>) (15). (**14**) (0.022 g, 0.022 mmol) was stirred with TFA (2ml) and DCM (2ml) at room temperature for 3 hours. Then the reaction mixture was concentrated under reduced pressure, and dried on high vac line for 48 hrs. 0.012 g of the title compound was formed (57%) as a yellow solid. ^{1}H NMR (400 MHz, $CDCl_3$) δ 0.88-0.972 (3H, m, CH_3), 1.514-1.701 (14H, m, 7xCH_2), 2.33-2.38 (2H, m, CH_2), 2.42-2.53 (1H, m, CH), 3.11-3.18 (4H, m, 2xCH_2), 3.40-3.50 (2H, m, CH_2), 3.59-3.66 (12H, m, 6xCH_2), 4.03-4.06 (2H, m, CH_2), 4.21-4.24 (1H, m, CH), 4.81 (2H, s, CH_2), 6.46 (1H, s, CH), 6.55 (1H, d, 9.6, CH), 6.82-7.00 (4H, m, 4xCH), 7.67-7.73 (3H, m, 3xCH), 8.25 (2H, d, 8.0, CH). ^{13}C NMR (100.62 MHz, $CDCl_3$) δ 11.16, 14.24, 23.18, 23.67, 23.97, 24.74, 25.78, 29.14, 30.58, 32.94, 38.96, 42.50, 68.38, 129.01, 131.08. HRMS 936.3420 [$(M-H)^-$], ($C_{47}H_{59}O_{13}N_3S_2$ requires 936.3417), 938.3560 [$(M+H)^+$], ($C_{47}H_{59}O_{13}N_3S_2$ requires 938.3562).

6.1.3 Synthesis of the TAMRA linker

***tert*-butyl-10-amino-2, 2-dimethyl-4, 11-dioxo-3, 15, 18, 21-tetraoxa-5, 12-diazatetracosan-24-oate (16). (10**) (0.055 g, 0.068 mmol) was stirred with 20% piperidine in CH_3CN for 2 hrs at room temperature. Then the reaction mixture was concentrated under reduced pressure. The residue was dissolved in EtOH and concentrated again giving 0.035 g of the title compound (92%) as a white solid. HRMS 506.3430 [$(M+H^+)$] ($C_{24}H_{47}O_8N_3$ requires 506. 3436).

***t*ert-butyl-10-[5-(1, 2-dithiolan-3-yl) pentanamido]-2, 2-dimethyl-4, 11-dioxo-3, 5, 18, 21-tetraoxa-5, 12-diazatetracosan-24-oate (17).** Thioctic acid (0.021 g, 0.103 mmol) and DIC (0.013 g, 0.103 mmol) were added to the solution of (**16**) (0.035 g, 0.069 mmol) in DCM. After stirring for 24 hrs at room temperature the reaction mixture was filtered and concentrated under reduced pressure. The residue was subjected to silica chromatography eluting with EtOAc, then MeOH/DCM (1:9) giving 0.040 g of the title compound (85%) as a slightly yellow oil. ^{1}H NMR (400 MHz, $CDCl_3$) δ 1.33-1.45 (2H, m), 1.47 (18 H, s, 2x$C(CH_3)_3$), 1.64-1.95 (10 H, m), 2.21 (2H, t, 7.5, CH_2), 2.36 (2H, t, 7.4, CH_2), 2.44-2.48 (1H, m, CH), 2.50 (2H, t, 6.5, CH_2), 3.45-3.65 (12H, m), 3.71 (2H, t, 6.5, CH_2), 4.40 (1H, q, 7.1, CH). ^{13}CNMR (100.62 MHz, $CDCl_3$) δ 14.51, 22.84, 25.61. 28.43, 28.77, 29.17, 34.94, 36.59, 38.78, 39.65, 40.54, 53.12, 67.23, 69.92, 70.62, 70.69, 70.81, 70.91. HRMS 711.4030 [$(M+NH_4)^+$] ($C_{32}H_{59}O_9N_3S_2$ requires 711.4031).

15-(4-aminobutyl)-21-(1, 2-dithiolan-3-yl)-14, 17-dioxo-4, 7, 10-trioxa-13, 16-diazahenicosan-1-oic acid (18). TFA (3 ml) was added to the solution of (**17**) (0.040 g, 0.057 mmol) in DCM (3 ml). After stirring for 3 hrs at room temperature DCM and TFA were removed under reduced pressure. The residue was washed with the same solvent and dried to afford the title compound as a yellow oil (0.027 g, 89%). ^{1}H NMR (400 MHz, $CDCl_3$) δ 1.33-1.45 (2H, m), 1.64-1.95 (10 H, m), 2.21 (2H, t, 7.5, CH_2), 2.36 (2H, t, 7.4, CH_2), 2.44-2.47 (1H, m, CH), 2.48 (2H, t, 6.5, CH_2), 3.55-3.80 (14 H, m, 7xCH_2), 4.47 (1H, q, 7.1, CH). ^{13}CNMR (100.62 MHz, $CDCl_3$) δ 23.30, 43.20, 70.44, 120.71. HRMS 538.50 [$(M+H)^+$] ($C_{23}H_{44}O_7N_3S_2$ requires 538.62).

5-{14-[5-(1, 2-dithiolan-3-yl) pentanamido]-1-carboxy-13-oxo-3, 6, 9-trioxa-12-azaoctadecan-18-ylcarbamoyl}-2-[6-(dimethylamino)-3*H*-xanthen-9-yl] benzoate (TAMRA linker) (19). 5-carboxytetramethylrhodamine –*N*-succinimidyl ester (TAMRA SE) (0.005 g, 0.0095 mmol) was dissolved in CH_3CN. (**18**) (0.0066 g, 0.0123 mmol) and resin - morpholinomethyl polystyrene (0.012 g, $1 \cdot 10^{-3}$ mol/g) were added. After stirring for 24 hours at room temperature the reaction mixture was filtered and concentrated under reduced pressure. The residue was subjected to silica gel chromatography eluting with MeOH/DCM (1:9), then (2:9) giving 0.0033 g of the title compound (37%) as a pink solid. HRMS 950.4041 $[(M+H)^+]$ ($C_{48}H_{64}O_{11}N_5S_2$ requires 950.4038).

6.1.4 Synthesis of the BHQ linker

6-amino-2-(*tert*-butoxycarbonylamino) hexanoic acid (20). 2-(*N*-Boc), 6-(*N*-Fmoc)-diamino caproic acid (0.107 g, 0.23 mmol) was stirred for 2 hrs at room temperature with 20% piperidine in CH_3CN. Then the reaction mixture was concentrated under reduced pressure. The residue was dissolved in EtOH and concentrated again giving 0.056 g of the title compound (99%) as a white solid. HRMS 247.1654 $[(M+H)^+]$, ($C_{11}H_{23}O_4N_2$ requires 247.1652).

6-[5-(1, 2-dithiolan-3-yl)pentanamido]-2-(*tert*-butoxycarbonylamino)hexanoic acid (21). 6-amino-2-(*tert*-butoxycarbonylamino) hexanoic acid (**20**) (0.056 g, 0.23 mmol) was dissolved in DCM with few drops of MeOH. 1-{[(5-dithiolane-3-yl)pantanoyl]oxy}-2, 5-pyrrolidinedione (0.069 g, 0.23 mmol, prepared as described on next page) was added. The reaction mixture was stirred over night at room temperature, then it was concentrated under reduced pressure. The residue was subjected to silica gel chromatography eluting with MeOH/DCM (0.1:9.9; 0.2:9.8; 0.3:9.7; 0.4:9.6 then 0.5:9.5, finally 1:9) giving 0.045 g of the title compound (46%) as a slightly yellow solid. ^{1}H NMR (400 MHz, DMSO) δ 1.23-1.34 (6H, m, 3xCH_2), 1.37 (9H, s, $C(CH_3)_3$), 1.46-1.58(4H, m, 2xCH_2), 1.62-1.70 (2H, m, CH_2), 1.81-1.90 (1H, m, CH), 2.02-2.05 (2H, t, 7.3, CH_2), 2.37-2.44 (1H, m, CH), 2.97-3.00 (2H, q, 6.2, CH_2), 3.03-3.21 (2H, m, CH_2), 3.57-3.63 (1H, m, CH), 3.76-3.79 (1H, m, CH). ^{13}C NMR (100.62 MHz, DMSO) δ 23.02, 25.06, 25.21, 28.22, 28.32, 28.83,

34.12, 38.09, 38.16, 54.90, 56.10, 171.71, 172.76. HRMS 435.1983 [$(M+H)^+$], ($C_{19}H_{35}O_5N_2S_2$ requires 435.1982).

6-[5-(1, 2-dithiolan-3-yl)pentanamido]-2-aminohexanoic acid (22). 6-[5-(1, 2-dithiolan-3-yl)pentanamido]-2-(*tert*-butoxycarbonylamino)hexanoic acid (**21**) (0.035 g, 0.08 mmol) was stirred with TFA (2ml) and DCM (2ml) at room temperature for 3 hours. Then the reaction mixture was concentrated under reduced pressure, and dried on high vacc line for 48 hrs. 0.027 g of the title compound was formed (99%) as a yellow solid. HRMS 335.1463 [$(M+H)^+$], ($C_{14}H_{27}O_3N_2S_2$ requires 335.1385).

6-[5-(1, 2-dithiolan-3-yl)pentanamido]-2-(4-{[4-(1E)-(2, 5-dimethoxy-4-{[4-nitrophenyl]diazenyl}phenyl)methyl]amino}butanamido)hexanoic acid (23). BHQ succinimidyl ester (BHQ SE) (0.01 g, 0.017 mmol) was dissolved in DCM. 6-[5-(1, 2-dithiolan-3-yl)pentanamido]-2-aminohexanoic acid (**22**) (0.0087 g, 0.026 mmol) was dissolved in DCM with few drops of MeOH and Et_3N (12µl, 0.086 mmol) then added to BHQ NHS solution. After stirring for 24 hours at room temperature the reaction mixture was concentrated under reduced pressure. The residue was subjected to silica gel chromatography eluting with MeOH/DCM (0.5:9.5, then 1:9) affording 0.011 g of the title compound (76%) as a purple solid. HRMS 823.3262 [$(M+H)^+$], ($C_{39}H_{51}O_8N_8S_2$ requires 823.3193).

1-{[(5-dithiolane-3-yl)pantanoyl]oxy}-2, 5-pyrrolidinedione. *N*-(3-dimethylaminopropyl)-*N'*-ethyl carbodiimide hydrochloride (EDC·HCl, 0.67 g, 3.5 mmol) was dissolved in anhydrous DCM. After stirring for 10 mins *N*-hydroxysulfosuccinimide (sulfo NHS, 0.47 g, 4.07 mmol) was added. The reaction mixture was stirred on ice bath. Then thioctic acid (0.60 g, 2.9 mmol) dissolved in DCM was added slowly to reaction mixture. After stirring for 18 hrs at room temperature the reaction mixture was washed with 5% HCl (2x), and water (2x). Then the organic phase was dried over anh. Na_2SO_4, filtered and concentrated under reduced pressure. The residue was subjected to silica gel chromatography eluting with MeOH/DCM (0.5:9.5) giving 0.61 g of the title compound (69%) as a yellow solid. ^{1}H NMR (400 MHz, $CDCl_3$) δ 1.48-1.71 (2H, m, CH_2), 1.71-1.84 (4H, m, 2xCH_2, 1.90-1.98 (1H, m, CH), 2.44-2.52 (1H, m, CH), 2.62 (2H, t, 7.3, CH_2), 2.84 (4H, s,

2xCH_2), 3.10-3.23 (2H, m, CH_2), 3.56-3.63 (1H, m, CH). ^{13}C NMR (100.62 MHz, DMSO) δ 24.58, 25.80, 28.52, 31.00, 34.63, 38.72, 40.36, 56.29, 168.61, 169.29. HRMS 304.0671 [$(M+H)^+$]; 321.0936 [$(M+NH_4)^+$], ($C_{12}H_{17}NO_4S_2$ requires 304.0672 [$(M+H)^+$]; 321.0937 [$(M+NH_4)^+$]).

BHQ linker (27). Wang resin (~1 mmol/g, 200-400 mesh) (0.15 g, 0.15 mmol) was resuspended in DCM. Succinic anhydride (0.045 g, 0.45 mmol) and 4-dimethylaminopyridine (DMAP) (0.055 g, 0.45 mmol) were added. The reaction mixture was kept at 70°C without stirring for 7 hrs. Then it was allowed to cool down to room temperature. The resin was filtered off, washed with DCM and MeOH, then dried to afford functionalized resin (**24**). Formed resin (**24**) was resuspended in DCM. O, O'-Bis-(2-aminopropyl) polypropylene glycol-block-polyethylene glycol-block polypropylene glycol 1900 (PEG 41) (0.86 g, 0.45 mmol) and *N, N*-diisopropylcarbodiimide (DIC) (70 µl, 0.045 mmol) were added. The reaction mixture was shaken over night at room temperature. Then PEG functionalized resin (**25**) was filtered off, washed with DCM and MeOH, then dried. Resin (**25**) was resuspended in DCM, then reacted with 6-[5-(1, 2-dithiolan-3-yl)pentanamido]-2-(4-{[4-(1E)-(2, 5-dimethoxy-4-{[4-nitrophenyl]diazenyl}phenyl)methyl]amino}butanamido)hexanoic acid (**23**) (0.011 g, 0.013 mmol) in the presence of DIC (70 µl, 0.45 mmol). The reaction mixture was shaken over night at room temperature, then the resin was filtered off, washed with DCM and MeOH, then dried to form modified resin (**26**). BHQ linker (**27**) was cleaved from the resin (**26**) by the use of 10% of trifluoroacetic acid (TFA) (0.815 µl) in DCM (8.5 ml). After two hours of stirring at room temperature the reaction mixture was filtered then concentrated under reduced pressure. Then formed product was dissolved in DCM. Anion exchange resin-morpholinomethyl polystyrene was added. The reaction mixture was stirred for 30 mins, then it was filtered and dried under reduced pressure to afford 0.07 g of the title compound as a dark purple solid.

6.1.5 Synthesis of the PEG 41-thioctic acid linker (PEG 41-TA) (31) and the PEG 11-thioctic acid linker (PEG 11-TA)

Wang resin (~1 mmol/g, 200-400 mesh) (2.0 g, 2.0 mmol) was resuspended in DCM. Succinic anhydride (0.60 g, 6.0 mmol) and 4-dimethylaminopyridine (DMAP) (0.76 g, 6.0 mmol) were added. The reaction mixture was kept at 70°C without stirring for 7 hrs. Then it was allowed to cool down to room temperature. The resin was filtered off, washed with DCM and MeOH, then dried to afford functionalized resin (**28**). Formed resin (**28**) was resuspended in DCM. O, O'-Bis-(2-aminopropyl) polypropylene glycol-block-polyethylene glycol-block polypropylene glycol 1900 (PEG 41) (11.4 g, 6.0 mmol) [or O, O'-Bis-(2-aminopropyl) polypropylene glycol-block-polyethylene glycol-block-polypropylene glycol 500 (PEG11) (0.3 g, 6.0 mmol)] and *N, N*-diisopropylcarbodiimide (DIC) (930 µl, 6.0 mmol) were added. The reaction mixture was shaken over night at room temperature. Then PEG functionalized resin (**29**) was filtered off, washed with DCM and MeOH, then dried. Resin (**29**) was then resuspended in DCM, thioctic acid (1.24 g, 6.0 mmol) and DIC (930 µl, 6.0 mmol) were added and reaction mixture was shaken over night at room temperature. Formed resin (**30**) was filtered off, then washed with MeOH and DCM, then dried. PEG 41-TA linker was cleaved from the resin by the use of 10% TFA (3.26 ml) in DCM (34 ml). After two hours of stirring at room temperature the reaction mixture was filtered, then concentrated under reduced pressure. Then formed product was dissolved in DCM. Anion exchange resin-morpholinomethyl polystyrene was added. The reaction mixture was stirred for 30 mins at room temperature, then it was filtered and dried under reduced pressure to afford 1.61 g (PEG 41-TA); 0.71 g (PEG 11-TA) of the title compounds as a colorless solid.

6.1.6 Synthesis of 4-(4,6-dimethoxy-1,3,5-triazin-2-yl)-4-methylmorpholinium chloride -DMT MM

DMT MM was synthesized as previously described by Kunishima *et al*. [122, 123]. 2-chloro-4, 6-dimethoxy-1, 3, 5-triazine (CDMT) (0.386 g, 2.2 mmol) was dissolved in THF. Then *N*-methylmorpholine (NMM) (0.202g, 2.0 mmol) dissolved in THF was added. The reaction mixture was stirred for 30 mins at room temperature. Formed white solid was filtered off, washed with THF, dried to give DMT MM (0.46 g, 75%). ^{1}H NMR (400 MHz, D_2O) δ 3.61 (3H, s, CH_3), 3.88-4.01 (4H, m, 2xCH_2),

4.14-4.20 (2H, m, CH_2), 4.23 (6H, s, 2xCH_3), 4.68-4.74 (2H, m, CH_2). ^{13}CNMR (100.62 MHz, D_2O) δ 55.25, 56.59, 59.55, 61.55, 173.38. HRMS 241.1295 [$(M+H)^+$] ($C_{10}H_{17}O_3N_4$ requires 241.1295).

6.2 Colloids preparation

6.2.1 18 (1) and 50 (2) nm gold colloid.

Sodium tetrachloroaurate (1) (0.05g, 0.14 mmol); (2) (0.0575 g, 0.161 mmol) was dissolved in 10 ml of water, then added to 500 ml of warm water and brought to boil. Sodium tricitrate (1) (0.075 g, 0.25 mmol) (2) (0.0605 g, 0.20 mmol) was dissolved in 10 ml of water, then added to the reaction mixture. The reaction mixture was left at boiling temperature for 15 minutes then it was allowed to cool down to room temperature. To calculate the colloid concentration the Beer-Lambert equation was used with gold extinction coefficient value $2.4x10^8$ [114] for 18 nm Au and $1.469x10^{10}$ for 46 nm Au nanoparticles [115].

6.2.2 40 nm silver citrate stabilised colloid.

500 ml of water was heated to 45°C, then silver nitrate (0.09 g, 0.53 mmol) dissolved in 10 ml of water was added. The reaction mixture was heated to 98°C, then sodium citrate (0.11 g, 0.37 mmol) dissolved in 10 ml of water was added. The reaction mixture was kept for 90 mins at 98°C, then cooled down to room temperature. The concentration of colloid was calculated from the Beer-Lambert equation using a silver extinction coefficient value of $2x10^{10}$ [116].

6.2.3 40 nm silver EDTA stabilised colloid.

Ethylenediaminetetraacetic acid (EDTA) (0.095 g, 0.32 mmol) was dissolved in 2000 ml of water. Sodium hydroxide (0.35 g, 8.75 mmol) was dissolved in 20 ml of water, then added to the reaction mixture. The reaction mixture was bring to boil then silver nitrate (0.088 g, 0.52 mmol) dissolved in 20 ml of water was added. The reaction mixture was kept at boiling temperature for 15 mins, then it was cooled down to room temperature. The concentration of colloid was calculated from the Beer-Lambert equation using a silver extinction coefficient value of $2x10^{10}$ [116].

6.3 Conjugates preparation

6.3.1 Preparation of linker-nanoparticles conjugates

$1x10^{-3}$ M solutions of all linkers in MeOH were prepared. In order to form linker-nanoparticles conjugates 2eq of linker solution (based on calculated number of linker molecules which attach to one nanoparticle-Table 1) were added to 1 ml of nanoparticle suspension with known concentration (found using the Beer-Lambert equation). In the case of BHQ and 6-aminofluorescein (with 50 nm Au) linkers usually 10-20µl of linker solution was added to gold or silver colloid. After addition of the linkers, samples were left to incubate for 16 hrs, then centrifuged (20 mins, 6500 rpm). The supernatants were discarded and the pellets were resuspended to 500 µl with water. This washing step is to ensure that the excess linker which did not bind to the nanoparticle is removed from the sample. Fluorescent spectroscopy study performed for fluorescein and aminofluorescein linkers indicated that one wash step was sufficient to remove all excess linker from the sample. In the case of the TAMRA linker two washing steps were necessary to achieve that. A fluorescence study was performed by taking the fluorescence spectra of each supernatant discarded from the sample after each washing step. In the next stage of conjugate preparation the samples were centrifuged again (20 mins, 6500 rpm). Then the supernatants were discarded and the pellets resuspended with the desired volume of water or buffer.

6.3.2 Formation of mixed layer of linkers on nanoparticles surface

10 µl of $1x10^{-3}$ M solution containing 25, 50 or 75 % of one of the synthesized linkers and 75, 50 or 25 % of PEG 41-TA or PEG 11-TA or thiolated PEG [SH-$(CH_2)_9$-CH_2O-$(C_2H_4O)_2$-CH_2-CH_2-OH] in MeOH was added to 1 ml of nanoparticle suspension. Samples were then left to incubate for 24 hours, then they were centrifuged for 20 mins at 6500 rpm. Supernatants were discarded, pellets washed with water, then centrifuged again for 20 mins at 6500 rpm. Supernatants were discarded, the pellets resuspended with desired volume of water or buffer.

In the case of a mixed layer containing one of the synthesized linkers and short oligonucleotide (SH AAAAA) 10 µl of $1x10^{-3}$ M solution containing 25, 50 or 75 % of one of the synthesized linkers and 75, 50 or 25 % of SH AAAAA in water was added to 1 ml of nanoparticle suspension. The samples were incubated for 24 hours, then 100 mM phosphate buffer pH=7 was added to obtain final buffer concentration

in sample of 10 mM. The samples were left for another 24 hours, then small portions of 2M NaCl were added over 48 hours in order to obtain final salt concentration of 0.1M. The samples were then centrifuged for 20 mins at 6500 rpm, washed with water, then centrifuged again (20 mins, 6500 rpm). The supernatants were discarded, pellets resuspended in the desired volume of water or buffer.

6.3.3 Preparation of oligonucleotide functionalized nanoparticles (EDC·HCl)

Linker functionalized nanoparticles were prepared as described in section 6.3.1, then centrifuged (20 mins, 6500 rpm). Supernatants were discarded and the pellets resuspended with 500 µl of 0.1 M PBS, pH=7.6. EDC·HCl (10 µl, 2mg/1ml) and sulfo NHS (10 µl, 2mg/1ml) were then added. The reaction mixture was allowed to react for 30 mins, then amino-modified DNA was added (5 or 10 µl, 100pmol/µl). The reaction mixture was shaken for 16 hrs. The samples were then centrifuged for 20 mins at 6500 rpm, washed with water then centrifuged again (20 mins, 6500 rpm). The supernatants were discarded and the pellets resuspended with 500 µl of 0.1 or 0.3 M PBS.

6.3.4 Preparation of oligonucleotide functionalized nanoparticles (DMT MM).

Linker functionalized nanoparticles were prepared using the same protocol as described in section 6.3.1, then centrifuged for 20 mins at 6500 rpm. The supernatants were discarded, the pellets resuspended with 500 µl of water, 10% MeOH in water, 0.1 M PBS pH=7.0 or 0.1 M PBS pH=7.6. Amino-modified DNA (5 or 10 µl, 100 pmol/µl) and DMT MM (10 µl, 2mg/1ml of water or MeOH-for conjugation performed in 10% MeOH in water) were then added. Samples were shaken for 16 hrs, then they were centrifuged for 20 mins at 6500 rpm, washed with water, then centrifuged again (20 mins, 6500 rpm). Supernatants were discarded and the pellets resuspended with 0.1 or 0.3 M PBS.

6.3.5 Preparation of oligonucleotide functionalized nanoparticles with formed mixed layer of the linkers on the surface.

A mixed layer of linkers was prepared on the nanoparticles surface following the protocol described in section6.3.2. The conjugation of functionalized nanoparticles to amino-modified DNA was performed following protocols described in sections 6.3.3 and 6.3.4.

6.3.6 Conjugation of linkers to amino-modified oligonucleotides

EDC·HCl (10 µl, 2 mg/1ml, 2 eq) and sulfo NHS (10 µl, 2 mg/1 ml, 2 eq) were added to 500 µl of linker solution ($1 \cdot 10^{-3}$ M in phosphate buffer pH=7.6). After shaking for 30 mins, DNA (50 µl, 100 pmol/ µl, 0.01 eq) was added. The volume of reaction mixture was taken up to 1 ml by the addition of the phosphate buffer, then the sample was allowed to react for 16 hrs at room temperature, then it was purified by HPLC (Phenomenex column).

When DMT MM was used as an amide bond forming reagent, DNA (50 µl, 100 pmol/ µl, 0.01 eq) was added to 500 µl of linker solution ($1x10^{-3}$ M in phosphate buffer pH=7.6 or in water). Then DMT MM (15 µl, 2 mg/1 ml, 1.1 eq) was added. The volume of reaction mixture was taken up to 1 ml by the addition of the phosphate buffer or water. The sample was allowed to react for 16 hrs at room temperature, then it was purified by HPLC (Phenomenex column).

6.4 Analysis of properties of formed conjugates

6.4.1 Calculation of number of linker molecules which attach to one nanoparticle

Linker-nanoparticles conjugates were prepared as described in section 6.3.1, the only difference is that the washing step was repeated three times to ensure that excess linker molecules which did not attach to nanoparticles surface were removed from the samples. After the third washing step samples were centrifuged (20 mins, 6500 rpm), the supernatants were discarded and the pellets resuspended with 500 µl of water. Then the extinction spectra of the samples were taken in order to calculate concentration of the nanoparticles in each sample. In the next stage of the protocol, samples were centrifuged again (20 mins, 6500 rpm), the supernatants discarded and the pellets resuspended in 900 µl of 10 mM phosphate buffer pH=8. Then 100 µl of 1 M DTT was added to each sample to obtain final DTT concentration of 0.1 M. The red-to-purple color change indicated that DTT displaced linker molecules from the nanoparticles surface. Samples were left over night, then they were centrifuged (20 mins, 7000 rpm). Fluorescence spectra of all supernatants were then taken. The concentration of the linker in each supernatant was calculated from the calibration curve prepared by taking the fluorescence spectra of samples with known linker concentrations using the same buffer and DTT concentrations (linkers were dissolved in 900 µl of 10 mM phosphate buffer pH=8.0 and 100 µl of 1 M DTT). The number

of linker molecules which attached to one nanoparticle was found by dividing the concentration of the linker in the supernatant by the concentration of nanoparticles in the same samples. The surface coverage was calculated by dividing the amount of linker (pmol) attached to one nanoparticle by the estimated particle surface area (assuming spherical nanoparticles). 10 samples of each type were analyzed in triplicates. Presented results are the average values obtained from 10 samples of the same type.

6.4.2 Quantification of number of DNA strands attached to one nanoparticle (DNAse I method).

Oligonucleotide functionalized nanoparticles were prepared by following protocols described in sections 6.3.3 and 6.3.4 using FAM or TAMRA labelled DNA strands. The samples were then centrifuged for 20 mins at 6500 rpm. The supernatants were discarded and the pellets resuspended with 500 μl of water. This washing procedure was repeated three times in order to remove any unbound DNA from the samples. Then the extinction spectra of all samples were taken and the concentrations of nanoparticles in each sample calculated using the Beer-Lambert equation. The samples were then centrifuged (20 mins, 6500 rpm), the pellets resuspended with DNAse I reaction buffer (New England BioLabs). DNAse I (final concentration of 125 units/ml, New England BioLabs) was then added to DNA-nanoparticle conjugates, and the samples were incubated for 16 hrs at 37°C. The samples were then centrifuged, the supernatants were analyzed by fluorescence spectroscopy. The concentration of dye labeled oligonucleotides in supernatant was determined using a calibration curve of dye labeled DNA solutions in DNAse I reaction buffer with known concentrations. The number of DNA strands attached to one nanoparticle was calculated by evaluation of dye labeled oligonucleotides concentration in supernatant against concentration of the nanoparticles in the sample.

6.4.3 Zeta particle size and zeta potential measurements

Malvern High Performance Particle Sizer was used to measure the zeta size of formed conjugates. Linker functionalised nanoparticles were prepared as described in section 6.3.1. Nanoparticle-linker-DNA conjugates were prepared in water, in the presence of DMT MM, using the protocol described in section 6.3.4. All prepared conjugates were washed with water (500 μl), then centrifuged for 20 mins at 6500

rpm. The supernatants were discarded, pellets resuspended in water (500 µl). UV-Vis spectra of all samples were taken in order to calculate probes concentrations. The samples were prepared by dilution of prepared solutions with water to the following concentrations: for 18 nm Au conjugates $7.95x10^{-10}$ M; for 50 nm Au conjugates $2.52x10^{-11}$ M, for both types of silver nanoparticles $3x10^{-11}$ M. 1ml of each sample was used.

Samples for zeta potential measurements were prepared in the same way as samples for DLS, but they were diluted to the following concentrations: $2.65x10^{-10}$ M for 18 nm Au conjugates, $8.4x10^{-12}$ M for 50 nm Au conjugates, $1x10^{-11}$ M for silver nanoparticles conjugates. 3 ml of each sample was used. Malvern Zetasizer 2000 was used to measure the zeta potential of all probes.

6.4.4 Gel electrophoresis

1.5% agarose gels were prepared by heating 1.5 g of agarose in 100 ml of 0.5xTBE buffer. Linker-nanoparticle and DNA-linker-nanoparticle conjugates were prepared as described in sections 6.3.3 and 6.3.4, the concentration of prepared samples was calculated using the Beer-Lambert equation. The concentration of the samples loaded on the gel was kept constant: for 18 nm Au nanoparticles conjugates: $3.63x10^{-8}$ M, for 50 nm Au nanoparticles conjugates: $1.14x10^{-9}$ M, for Ag citrate nanoparticles conjugates: $1.16x10^{-9}$ M, for Ag EDTA nanoparticles conjugates: $6.86x10^{-10}$ M. The calculated volumes of each sample was diluted to 10 µl, then 10 µl of 10% glycerol was added before loading of the samples in the gel wells. The gels were run for 60 mins at 120 mV.

6.4.5 SERRS Analysis

All SERRS spectra were recorded using a Leica DM/LM microscope equipped with an Olympus 20x/0.4 long working distance objective, which was used to collect 180^0 backscattered light from a microtiter plate (in case of linker-nanoparticle conjugates – Chapter 2 and pH sensing experiments- Chapter 5) or macrosampler (in case of linker-nanoparticle conjugates and nanoparticle-linker-DNA conjugates- Chapter 3; hybridisation experiments – Chapter 4). The spectrometer system was Renishaw inVia with 632.8 nm line of helium-neon laser or 514 nm Ar ion laser or 785 nm Diode laser coupled to Renishaw Ramascope System 2000.

All probes were prepared as described in sections 6.3.1, 6.3.3 and 6.3.4. Nanoparticle-linker-DNA conjugates were prepared in water, in the presence of DMT MM. The concentration of the analysed samples was kept constant in all experiments: 3.25×10^{-9} M for 18 nm Au conjugates, 7.56×10^{-11} M for 50 nm Au conjugates and both types of silver nanoparticles conjugates.

6.5 Hybridisation assay

In order to prepare probes for DNA detection assay linker functionalized gold nanoparticles were conjugated to amino-modified oligonucleotides in water, in the presence of DMT MM (protocol described in section 6.3.4). UV-Vis spectra of the probes were then taken in order to calculate probes concentrations from the Beer-Lambert equation. The concentration of the probes was kept constant in all experiments: 1.62 nM for 18 nm Au probes and 3.78×10^{-11} M for 50 nm Au probes. The hybridisation samples were prepared in such a way, that their final volume was 500 μl in all experiments. The concentration of complementary or non-complementary targets used was the same as the concentration of oligonucleotides attached to nanoparticle surface, e. g. for 18 nm Au-TAMRA-DNA conjugates it was calculated that about 25 DNA strands attach to one nanoparticle so used target concentration was 25 times higher than the probes concentration. The experiments were also performed for target concentrations the same as probes concentration, and also 10, 50, 100, 500 and 1000 times higher than probes concentration. All target concentrations used are given in Table 10 and 11.

The hybridisation samples were prepared by mixing calculated volumes of both probes (1:1 molar ratio). Then 0.1 or 0.3M PBS (the buffer volumes were calculated in such a way to ensure that after target addition the volume of the sample will be equal to 500 μl) and target were added. The samples were heated to 75°C for 5 mins, then they were allow to cool down to room temperature. The hybridisation process was monitored by UV-Vis spectroscopy and by SERRS.

During the UV-Vis experiments extinction spectra of the samples were taken every 30 mins for 18 hrs (after heating the samples) using Scanning Kinetics software.

Melting analysis were performed by monitoring the absorbance at 260 nm, 520 nm (18 nm Au) or 530 nm (50 nm Au) as a function of temperature using Thermal software. The temperature range was 20-80°C; the temperature increases 0.5°C/min.

The samples were kept for 2 mins at 80°C and for 60 mins at 20°C. 6 cycles of heating (3) and cooling (3) were performed in each sample.
During SERRS experiments SERRS spectra (at 633 nm) of the samples were taken every 60 mins for 5 hrs (after heating the samples).

Table 10: Volumes of targets used in DNA hybridisation experiments.

Type of nanoparticles	Linker	Target concentration [M]	Volume of target added to hybridisation sample [µl]
18 nm Au	Af	$8.10 \cdot 10^{-10}$ (x0.5)	40.5 ($1 \cdot 10^{-8}$M)
	F	$3.24 \cdot 10^{-10}$ (x0.2)	16.2 ($1 \cdot 10^{-8}$ M)
	T	$4.05 \cdot 10^{-8}$ (x25)	20.3 ($1 \cdot 10^{-6}$ M)
	BHQ	$1.13 \cdot 10^{-9}$ (x0.7)	0.57 ($1 \cdot 10^{-6}$ M)
50 nm Au	Af	$7.56 \cdot 10^{-10}$ (x20)	37.8 ($1 \cdot 10^{-8}$ M)
	BHQ	$5.67 \cdot 10^{-9}$ (x140)	2.64 ($1 \cdot 10^{-6}$ M)

Table 11: Volumes of targets used in DNA hybridisation experiments.

Type of nanoparticles	Target concentration	Volume of target added to hybridisation sample [µl]
18 nm Au	$1.62 \cdot 10^{-9}$ (x1)	0.812 ($1 \cdot 10^{-6}$ M)
	$1.62 \cdot 10^{-8}$ (x10)	8.12 ($1 \cdot 10^{-6}$ M)
	$8.10 \cdot 10^{-8}$ (x50)	40.6 ($1 \cdot 10^{-6}$ M)
	$1.62 \cdot 10^{-7}$ (x100)	81.2 ($1 \cdot 10^{-6}$ M)
	$8.1 \cdot 10^{-7}$ (x500)	0.406 ($1 \cdot 10^{-4}$ M)
	$1.62 \cdot 10^{-6}$ (x1000)	0.812 ($1 \cdot 10^{-4}$ M)
50 nm Au	$3.78 \cdot 10^{-11}$ (x1)	1.89 ($1 \cdot 10^{-8}$ M)
	$3.78 \cdot 10^{-10}$ (x10)	18.9 ($1 \cdot 10^{-8}$ M)
	$1.89 \cdot 10^{-9}$ (x50)	94.5 ($1 \cdot 10^{-8}$ M)
	$3.78 \cdot 10^{-9}$ (x100)	1.89 ($1 \cdot 10^{-6}$ M)
	$1.89 \cdot 10^{-8}$ (x500)	9.45 ($1 \cdot 10^{-6}$ M)
	$3.78 \cdot 10^{-8}$ (x1000)	18.9 ($1 \cdot 10^{-6}$ M)

6.6 pH sensing experiments

6.6.1 4-mercaptopyridine and 2-aminotiophenol probes

5 µl of $1x10^{-3}$ M 4-mercaptopyridine or 2-aminotiophenol in MeOH was added to 1 ml of colloid (Ag EDTA or Ag citrate or 18 nm Au). The samples were left for 16 hours, then centrifuged for 20 mins at 6500 rpm, the supernatants were discarded, the pellets washed with 500 µl of water, then centrifuged again (20 mins, 6500 rpm). After discarding the supernatants the pellets were resuspended in one of the phosphate buffers with pH between 2 and 8. The samples were incubated for 16 hrs, then SERS spectra of all samples were taken using laser excitation frequency of 633 nm.

6.6.2 Ag EDTA-4-mercaptopyridine/PEG 41-TA probes

5 µl of the solution containing 75 or 50% of $1x10^{-3}$ M 4-mercaptopyridine in MeOH and 25 or 50% of $1x10^{-3}$ M PEG 41-TA in MeOH was added to 1 ml of Ag EDTA colloid. Samples were left for 16 hours, then centrifuged for 20 mins at 6500 rpm, the supernatants were discarded, the pellets washed with 500 µl of water, then centrifuged again (20 mins, 6500 rpm). After discarding the supernatants the pellets were resuspended in one of the phosphate buffers with pH between 2 and 8. The samples were incubated for 16 hrs, then SERS spectra of all samples were taken using laser excitation frequency of 633 nm.

6.6.3 Oligonucleotide functionalized Ag EDTA and 18 nm Au 4-mercaptopyridine/PEG 41-TA (50/50) probes

5 µl of the solution containing 50% of $1x10^{-3}$ M 4-mercaptopyridine in MeOH and 50% of $1x10^{-3}$ M PEG 41-TA in MeOH was added to 1 ml of Ag EDTA or 18 nm Au colloid. The samples were left for 16 hrs, then centrifuged for 20 mins at 6500 rpm. The supernatants were discarded, the pellets washed with 500 µl of water. Then the samples were centrifuged again (20 mins, 6500 rpm), the supernatants were discarded, the pellets resuspended with 500 µl of water. ssDNA (5' AAA TTC TTC TAC G 3', 100 pmol/µl; 8 µl) and DMT MM (2 mg/ml; 10 µl) were added. The samples were shaken for 16 hours at room temperature, then they were centrifuged for 20 mins at 6500 rpm. The supernatants were discarded, the pellets washed with 500 µl of water, then centrifuged again (20 mins, 6500 rpm). After discarding the supernatants the pellets were resuspended in one of the phosphate buffers with pH between 2 and 8. The samples were incubated for 16 hrs, then SERS spectra of all samples were taken using laser excitation frequency of 633 nm.

6.6.4 SERS mapping experiments

SERS mapping was performed using Renishaw *InVia* Raman inverted and upright microscope (Renishaw, Wotton-under-Edge, UK), equipped with 100x/0.75 and 50x/0.5 long working distance objectives. The x100 LWD objective was used in all experiments. 632.8 (HeNe, ca. 30 mV) was used as an excitation source.Line mapping was performed using a Streamline Raman mapping system (Renishaw, UK). The detector used was a deep depletion Renishaw CCD Camera (400x576). 1800 line/mm

gratings were used in all experiments. 10 s exposure time for macrophages and 20 s for HeLa cells were used.

6.7 Instrumentation

Raman spectroscopy - All SERRS spectra were recorded using a Leica DM/LM microscope equipped with an Olympus 20x/0.4 long working distance objective, which was used to collect 180^0 backscattered light from a microtiter plate or macrosampler. The spectrometer system was Renishaw inVia with 632.8 nm line of helium-neon laser or 514 nm Ar ion laser or 785 nm Diode laser coupled to Renishaw Ramascope System 2000.

UV-visible spectroscopy – All UV-Vis spectra were recorded using CARY 300 Bio UV-Visible spectrophotometer.

Fluorescence spectroscopy – All fluorescence spectra were recorded using Varian CARY Eclipse Fluorescence Spectrophotometer.

Malvern High Performance Particle Sizer and **Malvern Zetasizer 2000** were used to measure zeta size and zeta potential of prepared conjugates.

HPLC – was carried out on a Dionex UVD170U detector fitted with a P680 pump through a Phenomenex Clarity column.

Chapter 7

Conclusions

The aim of this work was to prepare SERRS active, oligonucleotide functionalised nanoparticles which can be used as probes in a hybridisation based DNA detection assay. In order to achieve this, four different linkers containing a surface complexing group (thioctic acid) allowing attachment to the metal surface; a PEG unit, which prevents non-specific interactions and increases the stability of the formed conjugates, a fluorescent (aminofluorescein, fluorescein, TAMRA) or non-fluorescent Raman reporter (BHQ) and free COOH group, which allows the conjugation of the linker to biomolecules, were designed. Fluorescein (F), aminofluorescein (Af), TAMRA (T) and BHQ linkers were successfully synthesised with good yields. All the linkers were then used to functionalise gold (citrate stabilised 18 and 50 nm) and silver (citrate and EDTA stabilised) nanoparticles.

It was found that the best SERRS response was obtained using laser excitation of 633 nm from all types of prepared conjugates. The signal intensity was the highest for BHQ and T conjugates and much weaker for F and Af conjugates. As expected the SERRS signals obtained from linker functionalised silver nanoparticles were much stronger than the one obtained from Au-linker conjugates. Good SERRS signals were also obtained from both types of silver nanoparticles functionalised with the BHQ linker using excitations at 514 and 785 nm.

Measurements of the hydrodynamic diameter (by DLS) of the linker-nanoparticle conjugates and its zeta potential confirmed surface modification and indicated that the prepared conjugates exhibited high stability.

Two different methods to conjugate biomolecules to linker functionalised nanoparticles were used within this work. The first of them, used EDC·HCl, sulfo NHS in phosphate buffer. Due to the low stability of all of the silver nanoparticle conjugates and also 50 nm Au-T and 50 nm Au-F this method can not be used for conjugation of those probes to oligonucleotides. The second, novel method, in which DMT MM in water, phosphate buffer or alcohol was used as an amide bond forming reagent had not been used for bioconjugations before. This method allows attachment of oligonucleotides to all of the linker-nanoparticle conjugates. It was found that for smaller gold nanoparticles functionalised with all types of linkers, both coupling chemistries investigated exhibit similar effectiveness (under the same conditions, in phosphate buffer). For the larger Au nanoparticles used in this study DMT MM was found to be more effective than EDC·HCl.

The DMT MM activated amide bond formation reaction can be performed in different solvents, such as water, buffers or MeOH. In order to find the most suitable conditions for amide linkage formation the effectiveness of DMT MM in water, phosphate buffer (pH=7.0, pH=7.6) and 10% of MeOH in water were compared. It was found that the biggest DNA surface coverage was obtained when the coupling reaction was performed in water. For all types of conjugates the less costly DMT MM was found to be more efficient as an amide bond forming reagent allowing conjugation of the free COOH groups of the linkers attached to the nanoparticles to amino-modified oligonucleotides when the coupling reaction was performed in water. The use of this new, less time consuming, simple one-step bioconjugation method allows attachment of oligonucleotides to nanoparticles which are not stable in buffers, such as 10 mM phosphate buffer.

The attachment of oligonucleotides to linker-nanoparticle conjugates was confirmed by gel electrophoresis and DLS measurements of the hydrodynamic diameter of formed probes. All types of oligonucleotide functionalised nanoparticles, except Ag-EDTA conjugates, exhibited high, negative zeta potential indicating their high stability.

For most of the prepared nanoparticle-linker-DNA conjugates a small increase in the intensity of the SERRS signal obtained from the system was observed after oligonucleotides attachment. This is probably caused by the change of orientation of a Raman reporter, present within the linker structure, on the metal surface after addition of ssDNA in such a way that the label is experiencing stronger surface enhancement. DLS measurements indicated that the large increase of the intensity of SERRS signal observed for Ag EDTA-Af and Ag citrate-BHQ after addition of oligonucleotides is caused by the formation of small aggregates during conjugation process.

In the case of all types of fluorescein linker conjugates and 18 nm Au-BHQ-DNA probes no SERRS signals were observed using excitation at 633 nm.

The following types of prepared probes were used to detect specific DNA sequences in a hybridisation based DNA detection assay: 18 nm Au-F-DNA; 18 nm Au-Af-DNA, 50 nm Au-Af-DNA, 18 nm Au-T-DNA, 18 nm Au-BHQ-DNA, 50 nm Au-BHQ-DNA. All types of silver nanoparticle probes were not stable in buffers usually used for DNA hybridisation, thus they were not used as a probes for that purpose. In a typical hybridisation experiment two nanoparticle probes functionalised with different DNA sequences were mixed together in a 1:1 molar ratio. Then target,

complementary (or not complementary for control samples) to both probes, was added. The hybridisation experiments were performed for the probes prepared in the presence of DMT MM and EDC·HCl. The concentration of the probes was kept constant during all experiments, however 6 different target concentrations were used in hybridisation experiments performed with the use of each type of the probes. Different hybridisation buffers were also used: 0.1 M PBS (pH=7.0, pH-7.2), 0.3 M PBS (pH=7.0, pH=7.6), 1xTris EDTA buffer. After addition of the targets, the samples were heated to 75 or 95°C for 5-10 mins, frozen on dry ice or allowed to hybridise at room temperature or at 37°C. Unfortunately the expected changes in the intensity of SERRS signal or changes in gold plasmon band were not observed after addition of the complementary target. The number of DNA strands attached to probes prepared within this work is much lower than the number of DNA strands attached to probes which were reported to be successfully used to detect DNA sequences in a sandwich assay format, such as gold nanoparticles functionalised with thiolated oligonucleotides or silver nanoparticles with a mixed layer of Raman reporter and thiolated oligonucleotides. It was concluded that the lack of nanoparticle aggregate formation after addition of complementary target to the sample containing two types of nanoparticle probes is due to the low number of DNA strands attached to the probes. This low DNA surface coverage might be caused by an unsuitable orientation of linker COOH groups on nanoparticle surface for bioconjugation.

In order to increase DNA loading on the nanoparticle surface a mixed layer containing one of the synthesised linkers and PEG 41-TA or PEG11-TA linker, or thiolated PEG or short oligonucleotide was formed. This should reduce the number of linkers attached to the metal surface and change the orientation of the linker COOH groups in such a way that more conjugation reaction will take place. Unfortunately the increase in the number of oligonucleotides attached was not observed. It was concluded that due to the very low number of oligonucleotides attached the use of such a probe in a DNA detection assay was not successful. However, the synthesised linkers can act as SERRS nanoparticle labels in their own right. Additionally the presence of terminal carboxyl groups within the linker structure, which allows conjugation to the biomolecules, give the opportunity to use the linkers for tagging antibodies and proteins.

The other aim of the current work was to prepare SERS active, pH sensitive probes allowing the detection of the changes in intracellular pH. Two different pH sensitive

molecules, 4-mercaptopyridine and 2-aminothiophenol, were used to functionalize Ag EDTA, Ag citrate and 18 nm Au nanoparticles via metal-thiol interaction. It was found that the greatest sensitivity and highest signal intensity was obtained from Ag EDTA nanoparticles functionalised with 4-mercaptopyridine.

As it was proven that functionalisation of metallic nanoparticles with nuclear localization sequences or cell penetrating peptides make it possible to deliver nanoparticles components of a cell, a SERS active, pH sensitive probe allowing the attachment of biomolecules to the nanoparticle surface was designed. In order to prepare such a probe a mixed layer of pH sensitive Raman reporter and PEG 41-TA linker was formed on the nanoparticle. It was noted that the created pH sensor does not lose sensitivity, when compared with nanoparticles functionalised with pH sensitive Raman reporter only. Use of the PEG 41-TA linker containing free COOH groups allowed conjugation of biomolecules such as DNA or peptides.

The prepared pH sensitive probes were successfully used to detect pH values inside HeLa and macrophages cells. Further work involving the preparation of Ag EDTA-4-mercaptopyridine-PEG 41/TA probes conjugated to nuclear localization sequence and detection of pH values inside a cell nucleus is ongoing in the Centre for Molecular Nanometrology at the University of Strathclyde.

References:

1. Solomon, E.P., Berg, L. R., Martin, D. W., Vilee, C. A., **1996**, *Biology*, Multico, Warszawa

2. McMurry, J., **2000**, *Chemia Organiczna*, Wydawnictwo Naukowe PWN, Warszawa

3. Berg, J., Tymoczko, J., Stryer, L., **2002**, *Biochemistry*, W. H. Frejman and Company

4. Blackburn, M. G., Gait, M. J., **1996**, *Nucleic acids in chemistry and biology*, Oxford University Press, New York.

5. Cao, Y. C., Jin, R., Thaxton, S., Mirkin, C. A., **2005,** *Talanta*, 67, 449-455

6. Elghanian, R., Storhoff, J. J., Mucic, R. C., Letsinger, R. L., Mirkin, C. A., **1997,** *Science*, 277, 5329, 1078-1081

7. Storhoff, J. J., Elghanian, R., Mucic, R. C., Mirkin, C. A., **1998,** *J. Am. Chem. Soc.*, 120, 1959-1964.

8. Li, H., Rothberg, L., **2004,** *PNAS*,101, 39, 14036-14039.

9. Schubert, F., Knaf, A., Möller, V., Cech, D., **1995,** *Nucl. Acids Res.*, 23, 22, 4657-4663.

10. Wang, Z., Hu, J., Jin, Y., Yao, X., Li, J., **2006,** *Clin. Chem.*, 52, 10, 1958-1961.

11. Tizard, R., Cate, R. C., Ramachandran, K. L., Wysk, M., Voyta, J. C., Murphy, O. J., Bronstein, I., **1990,** *PNAS USA*,87, 4514-4518.

12. Liu, C. H., Li, Z. P., Du, B. A., Duan, X. R., Wang, Y. C., **2006,** *Anal. Chem.*, 78, 3738-3744.

13. Thaxton, S. D.; Georganopoulou, G. D.; Mirkin, C. A.; (**2006)**, *Clin. Chim. Acta*, 363, 120-126

14. Thompson, D. G., Stokes, R. J., Martin, R. W., Lundahl, P. J., Faulds, K., Graham, D., **2006,** *small*, 4, 1054-1057.

15. Dougan, J. A.; Karlsson, C.; Smith, W. E.; Graham, D; (**2007)**, *Nucl. Acids Res.*, 35, 3668-3675.

16. Wang, Z., Ma, L., **2009,** *Coordination Chemistry Reviews*, 253, 1607-1618.

17. Wilson, R., **2008,** *Chem. Soc. Rev.*,37, 2028-2045.

18. Sperling, R. A., Gil, P. R., Zhang, F., Zanella, M., Parak, W. J., **2008,** *Chem. Soc. Rev.*, 37, 1896-1908.

19. Thomas, K. G., Ipe, B. I., Sudeep, P. K., **2002,** *Pure Appl. Chem*., 74, 9, 1731-1738.

20. Sato, K., Hosokawa, K., Maeda, M., **2007,** *Anal. Sci.,* 23, 17-20.

21. Jin, R., Wu, G., Li, Z., Mirkin, C. A., Schatz, G. C., **2003,** *J. Am. Chem. Soc.,* 125, 1643-1654.

22. Storhoff, J. J., Lazarides, A. A., Mucic, R. C., Mirkin, C. A., Letsinger, R. L., Schatz, G. C., **2000,** *J. Am. Chem. Soc.,* 122, 4640-4650.

23. Zu, Y., Gao, Z., **2009,** *Anal. Chem.,* 81, 8523-8528.

24. Zhao, W., Hsing, I. M., **2010,** *Chem. Commun.,* 46, 1314-1316.

25. Hurst, S. J., Fill, H. D., Mirkin, C. A., **2008,** *J. Am. Chem. Soc.,* 130, 12192-122200.

26. Sato, K., Hosokawa, K., Maeda, M., **2003,** *J. Am. Chem. Soc.,* 125, 8102-8103.

27. Rho, S., Kim, S. J., Lee, S. C., Chang, J. H., Kang, H. G., Choi, J., **2009,** *Curr. Appl. Phys.,* 9, 534-537.

28. Li, Z., Jin, R., Mirkin, C. A., Letsinger, R. L., **2002,** *Nucl. Acids Res.,* 30, 7, 1558-1562.

29. Stakenborg, T., Peeters, S., Reekmans, G., Laureyn, W., Jans, H., Borghs, G., Imberechts, H., **2008,** *J. Nanopart. Res.,* 10, 143-152.

30. Letsinger, R. L., Elghanian, R., Viswanadham, G., Mirkin, C. A., **2000,** *Bioconjug. Chem.,* 11, 289-291.

31. Zhao, L., Lee T. M. H., Leung S. S. Y., Hsing, I. M., **2007,** *Langmuir,* 27, 7143-7147.

32. Claridge S. A., Goh, S. L., Frechet J. M. J., Williams, S. C., Micheel, C. M., Alivisatos, A. P., **2005,** *Chem. Mater.,* 17, 1628-1635.

33. Storhoff, J. J., Elghanian, R., Mirkin, C. A., Letsinger, R. L., **2002,** *Langmuir,* 18, 6666-6670.

34. Brown, K. A., Park, S., Hamad-Schifferli, K., **2008,** *J. Phys. Chem. C.,* 112, 20, 7517-7521.

35. Park, S., Brown, K. A., Hamad-Schifferli, K., **2004,** *Nano Lett.,* 4, 10, 1925-1925.

36. Thompson, D. G., Enright, A., Faulds, K., Smith, W. E., Graham, D., **2008,** *Anal. Chem.,*80, 8, 2805-2810.

37. Vidal, B. C., Deivaraj, T. C., Yang, J., Too, H. P., Chow, G. M., Gan, L. M., Lee, J. Y., **2005,** *New J. Chem.,* 29, 812-816.

38. Lee, J. S., Lytton-Jean, A. K. R., Hurst, S. J., Mirkin, C. A., **2007,** *Nano Lett.,* 7, 7, 2112-2115.

39. Cao, Y. W., Jin, R., Mirin, C. A., **2001,** *J. Am. Chem. Soc.,* 123, 7961-7962.

40. Lim, D. K., Kim, I. J., Nam, J. M., **2008,** *Chem. Commun.,* 5312-5314.

41. Doria, G., Larguinho, M., Dias, J. T., Pereira, E., Franco, R., Baptista, P. V., **2010,** *Nanotechnology,* 21, 255101 (5pp).

42. Link, S., Wang Z. L., El-Sayed, M. A., **1999,** *J. Phys. Chem. B,* 103, 3529-3533.

43. Baptista, P. V., Koziol-Montewka, M., Paluch-Oles, J., Doria, G., Franco, R., **2006,** *Clin. Chem.,* 52, 7, 1433-1434.

44. Baptista, P., Doria, G., Henriques, D., Pereira, E., Franco, R., **2005,** *J. Biotechnology,* 119, 111-117.

45. Conde, J., de la Fuente, J. M., Baptista, P. V., **2010,** *J. Nanobiotechnology,* 8:5.

46. Smith, E., Dent, G., **2008,** *Modern Raman Spectroscopy. A Practical Approach,* John Wiley & Sons, Ltd.

47. Szczepański W., **2002,** *Analiza Instrumentalna,* Wydawnictwo Naukowe PWN, Warszawa.

48. Lee, S. J., Guan, Z., Xu, H., Moskovits, M., **2007,** *J. Phys. Chem. C,* 111, 49, 17985-17989.

49. Faulds, K., Smith, W. E., Graham, D., **2005,** *Analyst,* 130, 1125-1131.

50. Graham, D., Faulds, K., Thompson, D., McKenzie, F., Stokes, R., Dalton, C., Stevenson, R., Alexander, J., Garside, P., McFarlane, E., **2009,** *Biochem. Soc. Trans.,* 37, 697-701.

51. Graham, D., Faulds, K., **2009,** *Expert Rev. Mol. Diagn.,* 9, 6, 537-539.

52. Barhoumi, A., Zhang, D., Tam, F., Halas, N. J., **2008,** *J. Am. Chem. Soc.,* 130, 5523-5529.

53. Graham, D., Faulds K. Smith, W. E., **2006,** *Chem. Commun.,* 4363-4371.

54. Harpster, M. H., Zhang, H., Sankara-Warrier, A. K., Ray, B. H., Ward, T. R., Kollmar, J. P., Carron, K. T., Mecham, J. O., Corcoran, R. C., ilson, W. C., Johnson, P. A., **2009,** *Biosen. Bioelectron.,* 25, 674-681.

55. Kneipp, J., Wittig, B., Bohr, H., Kneipp, K., **2009,** *Theor. Chem. Acc.*,125, 319-327.

56. Faulds, K., Barbagallo, R. P., Keer, J. T., Smith, W. E., Graham, D., **2004,** *The Analyst,* 129, 7, 567-568.

57. Macaskill, A., Chernonosov, A. A., Koval, V. V., Lukyanets, E. A., Fedorova, O. S., Smith, W. E., Faulds, K., Graham, D., **2007,** *Nucl. Acids Res.,* 1-6.

58. Faulds, K., Littleford, R. E., Graham, D., Dent, G., Smith, W. E., **2004,** *Anal. Chem.,* 76, 592-598.

59. Faulds, K., McKenzie, F., Graham, D., **2007,** *Analyst,* 132, 1100-1102.

60. Graham, D., Thompson, D. G., Smith, W. E., Faulds, K., **2008,** *Nature Nanotechnology,* 3, 548-551.

61. Cormack, P. A. G., Hernandez-Santana, A., Prasath, R. A., McKenzie, F., Graham, D., Smith, W. E., **2008,** *Chem. Commun.,* 2517-2519.

62. Wang, G., Park, H. Y., Lipert, R. J., **2009,** *Anal. Chem.,* 81, 23, 9643-9650.

63. Graham, D., Faulds, K., **2008,** *Chem. Soc. Rev.*, 37, 1042-1051.

64. Cao, Y. W. C., Jin, R., Mirkin, C. A., **2002,** *Science,* 297, 1536-1540.

65. McKenzie, F., Ingram, A., Stokes, R., Graham, D., **2009,** *Analyst,* 134, 549-556.

66. Graham. D., Mallinder, B. J., Smith, W. E., **2000,** *Biopolymers,* 57, 85-91.

67. Stokes, R. J., Macaskill A., Lundahl, P. J., Smith, W. E., Faulds, K., Graham, D., **2007,** *small,* 3, 9, 1593-1601.

68. McKenzie, F., Graham, D., **2009,** *Chem. Commun.,* 5757-5759.

69. Aslan, K., Luhrs, C. C., Perez-Luna, V. H., **2004,** *J. Phys. Chem. B,* 108, 15631-15639.

70. Graham, D., Smith, W. E., Linacre, A. M. T., Munro, C. H., Watson, N. D., White, P. C., **1997,** *Anal. Chem.,* 69, 4703-4707.

71. Gill, R., Lucassen, G. W., **2010,** *Anal. Methods,* 2, 445-447.

72. Doering, W. E., Nie, S., **2003,** *Anal. Chem.,* 75, 6171-6176.

73. Isola, N. R., Stokes, D. L., Vo-Dinh, T., **1998,** *Anal. Chem.,* 70, 1352-1356.

74. Allain, L. R., Vo-Dinh, T., **2002,** *Anal. Chim. Acta,* 469, 149-154.

75. Su, X., Zhang, J., Sun, L., Koo, T. W., Chan, S., Sundararajan, N., Yamakawa, M., Berlin, A. A., **2005,** *Nano Lett.,* 5, 1, 49-54.

76. Su, L., Yu, C., Irudayaraj, J., **2007,** *Anal. Chem.,* 79, 11, 3981-3988.

77. Vo-Dinh, T., Allain, L. R., Stokes, D. L., **2002,** *J. Raman Spectrosc.,* 33, 511-516.

78. Faulds, K., Smith, W. E., Graham, D., **2004,** *Anal. Chem.,* 76, 412-417.

79. Graham, D., Mallinder, B. J., Smith, W. E., **2000,** *Angew. Chem. Int. Ed.,* 39, 6, 1061-1063.

80. Faulds, K., Stewart, L., Smith, W. E., Graham, D., **2005,** *Talanta,* 67, 667-671.

81. MacAskill, A., Crawford, D., Graham, D., Faulds, K., **2009,** *Anal. Chem.,* 81, 8134-8140.

82. Thuy, N. T. B., Yokogawa, R., Yoshimura, Y., Fujimoto, K., Koyano, M., Maenosono, S., **2010,** *Analyst,* 135, 595-602.

83. Mahajan, S., Richardson, J., Brown, T., Bartlett, P. N., **2008 ,** *J. Am. Chem. Soc.,* 130, 46, 15589-15601.

84. McKenzie, F., Faulds, K., Graham, D., **2010,** *Nanoscale,* 2, 78-80.

85. Jung, H. S., Kim, K., Kim, M. S., **1997,** *J. Mol. Struct.,* 407, 139-147.

86. Lim, J. K., Joo, S. W., **2006,** *Applied Spectroscopy,* 60, 8, 847-852.

87. Kneipp, J., Kneipp, H., Wittig, B., Kneipp, K., **2007,** *Nano Lett.,* 7, 9, 2819-2823.

88. Jensen, R. A., Sherin, J., Emory, S. R., **2007,** *Appl. Spectrosc.,* 61, 8, 832-838.

89. Wang, Z., Bonoiu, A., Samoc, M., Cui, Y., Prasad, P. N., **2008,** *Biosen. Bioelectron.,* 23, 886-891.

90. Nowak-Lovato, K. L., Rector, K. D., **2009,** *Appl. Spectrosc.,* 63, 4, 387-395.

91. Lee, S. Y., Joo, S. W., Lee, s., Lim, M., **2009**, *BMB Rep.*, 42, 4, 223-226.

92. Kneipp, K., Haka, A. S., Kneipp, H., Badizadegan, K., Yoshizawa, N., Boone, C., Shafer-Peltier, K. E., Motz, J. T., Dasari, R. R., Feld, M. S., **2002,** *Appl. Spectrosc.,* 56, 2, 150-154.

93. Shamsaie, A., Jonczyk, M., Sturgis, J., Robinson, J. P., Irudayaraj, J., **2007,** *J. Biomed. Opt.,* 12, 2.

94. Llopis, J., McCaffery, J. M., Miyawaki, A., GFarquhar, M. G., Tsien, R. Y., **1998,** *PNAS,* 95, 6803-6808.

95. Kneipp, J., Kneipp, H., Wittig, B., Kneipp, K., **2010,** *J. Phys. Chem.,* 114, 7421-7426.

96. Polwart, E., Keir, R. L., Davidson, C. M., Smith, W. E., Sadler, D. A., **2000,** *Appl. Spectrosc.,* 54, 4, 522-526.

97. Stokes, R. J., McKenzie, F., McFarlane, E., Ricketts, A., Tetley, L., Faulds, K., Alexander, J., Graham, D., **2009,** *Analyst,* 134, 170-175.

98. Bishnoi, S. W., Rozell, C. J., Levin, C. S., Gheith, M. K., Johnson, B. R., Johnson, D. H., Halas, N. J., **2006,** *Nano Lett.,* 6, 8, 1687-1692.

99. Talley, C. E., Jusinski, L., Hollars, C. W., Lane, S. M., Huser, T., **2004,** *Anal. Chem.,* 76, 7064-7068.

100. Adamczyk, M., Grote J., **2000**, *Bioorg. Medicinal Chem. Lett.*, 10, 1539-1541.

101. Sameiro, M., Goncalves, T., **2009,** *Chem. Rev.,* 109, 190-212.

102. Gao, J.; Wang, P.; Giese, R. W., **2002**, *Anal. Chem*., 74, 6397-6401.

103. Klonis, N., Sawyer, W. H., **2000**, *Photochem. Photobiol.*, 72, 179-185.

104. Orndorff, W. R.; Hemmer, A. J., **1927**, Fluorescein and some of its derivatives, Contribution from the Baker Laboratory of Chemistry, Cornell University

105. Hurd, C. D.; Schmerlin, L., **1937**, Alkenyl Derivatives of Fluorescein, Contribution from the Chemical Laboratory of Northwestern University

106. Falck, J. R.; Krieger, M.; Goldstein, J. L.; Brown, M. S., **1981**, *J. Am. Chem. Soc.,* 103, 7396-7398.

107. Burchak, O. N.; Mugherli, L., Chatelain, F.; Balakirev, M. Y., **2006**, *Bioorg. Medicinal Chem*., 14, 2559-2568.

108. Lohse, J.; Nielsen, P. E.; Harhit, N.; Dahl, O., **1997**, *Bioconjug. Chem.,* 8, 503-509.

109.

http://www.sigma.aldrich.com/life-science/custom-oligos/dna-probes/product-lines/lna-probes/black-hole-quencher; 11.05.2010.

110. Demers, L. M., Mirkin, C. A., Mucic, R. C., Reynolds, R. A., Letsinger, R. L., Elghanian, R., Viswanadham.G., **2000**, *Anal. Chem*.,72, 22, 5535-5541.

111. Nguyen, T., Francis M. B., **2003**, *Org. Lett.*, 5, 3245-3248.

112. Kazzouli, S. E., Koubachi, J., Berteina-Raboin, S., Mouaddib, A., Guillaumet, G., **2006,** *Tetrahedron Lett.*, 47, 8575-8577.

113. Navath, R. S., Pabbisetty, K. B., Hu, L., **2006**, *Tetrahedron Lett.*, 47, 389-393.

114. Lohse, J.; Nielsen, P. E.; Harhit, N.; Dahl, O., **1997**, *Bioconjug. Chem.,* 8, 503-509.

115. Courtesy of BBInternational Life Sciences.

116. Yugerabide, J., Yguerabide E. E., **1998**, *Anal. Biochem.*, 262, 157-176.

117. http://www.malvern.com/LabEng/technology/dynamic_light_scattering/dynamic_light_scattering.htm, 22.11.2010

118. HPPS Operators Guide, MANO314, Issue 1.0 Dec. 2001, Malvern Instruments Ltd. 2001.

119. Finsy, R., **1994,** *Adv. Colloid Interface Sci.*, 52, 79-143.

120. http://www.malvern.com/LabEng/technology/zeta_potential/zeta_potential_LDE.htm, 22.11.2010

121. Hermanson, G. T., **2008,** *Bioconjugates techniques, 2nd edition,* Academic Press.

122. Kunishima, M., Kawachi, C., Morita, J., Terao, K., Iwasaki, F., Tani, S., **1999,** *Tetrahedron,* 55, 13159-13170.

123. Kunishima, M., Kawachi, C., Hioki, K., Terao, K., Tani, S., **2001,** *Tetrahedron,* 57, 1551-1558.

124. McKenzie, F., Stevens, V., Ingram, A., Graham, D., **2009,** *Chem. Commun.,*2872-2874.

125. Hanauer, M., Pierrat, S., Zins, I., Lotz, A., Sonnishen, C., **2007,** *Nano Lett.,* 7, 9, 2881-2885.

126. Parak, W. J., Pellegrino, T., Micheel, C. M., Gerion, D., Williams, S. C., Alivisatos, A. P., **2003,** *Nano Lett.,* 3, 1, 33-36.

127. Zanchet, D., Micheel, C. M., Parak, J., Gerion, D., Alivisatos, A. P., **2001,** *Nano Lett.,* 1, 1, 32-35.

128. Pellegrino, T., Sperling, R. A., Alivisatos, A. P., Parak, W. J., **2007**, *J. Biomed. Biotechnol.,* doi:10.1155/2007/26796.

129. Claridge, S. A., Liang, H. W., Basu, S. R., Frechet, J. M. J., Alivisatos, A. P., **2008,** *Nano Lett.,* 8, 4, 2202-2206.

130. Zanchet, D., Micheel, C. M., Parak, W. J., Gerion, D., Williams S. C., Alivisatos, A. P., **2002,** *J. Phys. Chem. B,* 106, 11758-11763.

131. http://www.azonano.com/Details.asp?ArticleID=2601, 10.12.2010.

132. Ackerson, C. J., Sykes, M. T., Kornberg, R. D., **2005,** *PNAS,* 102, 38, 13383-13385.

133. Ding, B., Cabrini, S., Zuckermann, R. N., Bokor, J., **2009,** *J. Vac. Sci. Technol. B,* 27, 1, 184-187.

134. Moskovits, M., **1982,** *J. Chem. Phys.,* 77, 9, 4408-4416.

135. Lin-Vien, D., Colthup, N. B., Fateley, W. G., Grasseli, J. G., The Handbook of Infrared and Raman Characteristic Frequencies of Organic Molecules, Academic Press Inc, 1991

136. Hong, S. H., Hong, S. W., Jo, W. H., **2010,** *Macromol. Chem. Phys.,* 211, 1054-1060.

137. Schwartzberg, A. M., Oshiro, T. Y., Hang, J. Z., Huser, T., Talley, C. E., **2006,** *Anal. Chem.,* 78, 4732-4736.

138. de la Fuente, J. M., Berry, C. C., **2005,** *Bioconjug. Chem.,* 16, 1176-1180.

139. Kang, B., Mackey, M. A., El-Sayed, M. A., **2010,** *J. Am. Chem. Soc.,* 132, 1517-1519.

140. Levy, R., Shaheen, U., Cesbron, Y., See, V., **2010,** *Nano Rev.,* 1, 4888-DOI: 10.3402/nano.v1i0.4889.

141. Mandal, D., Maran, A., Yaszemski, M. J., Bolander, M. E., Sarkar, G., **2009,** *J. Mater Sci: Mater Med,* 20, 347-350.

142. Lin, J., Chen, R., Feng, S., Li, Y., Huang, Z., Xie, S., Yu, Y., Cheng, M., Zeng, H., **2009,** *Biosen. Bioelectron.,* 25, 2, 388-394.

143. AshaRani, P. V., Mun, G. L. K., Hande, M. P., Valiyaveettil, S., **2009,** *ACS Nano,* 3, 2, 279-90.

144. Greulich, C., Diendorf, J., Simon, T., Eggeler, G., Epple, M., Koller, M., **2011,** *Acta Biomater.,* 7, 1, 347-354.

145. Eghtedari, M., Liopo, A. V., Copland, J. A., Oraevslty, A. A., Motamedi, M., **2009,** *Nano Lett.,* 9, 287-291.

146. Nativo, P., Prior, I. A., Brust, M., **2008,** *ACS Nano,* 2, 1639-1644.

147. Liu, C. J., Wang, C. H., Chien, C. C., Yang, T. Y., Chen, S. T., Leng, W. H., **2008,** *Nanotechnology,* 19, 295104.

148. Adamcik, J., Valle, F., Witz, G., Rechendorf, K., Dietler G., **2008,** *Nanotechnology,* 19, 384016.

149. Ohkuma, S., Pool B., **1978,** *PNAS USA,* 75, 3327-3331.

150. Geisow, J. M., Hart, P. D., Young, M. R., **1981,** *J. Cell Biol.,* 89, 3, 645-652.

151. Liu, X., Lu, L., Yang, Z., Palaniyandi, S., Zeng, R., Gao, L. Y., Mosser, D. M., Roopenian, D. C., Zhu, X., **2011,** doi:10.4049/jimmunol.1003584.

152. Bayer, N., Schober, D., Prchla, E., Murphy, R. F., Blaas, D., Fuchs, R., **1998,** *J. Virol.,* 72, 12, 9645-9655.

153. You, J. O., Auguste,D. T., **2010,** *Biomaterials,* 31, 6859-6866.

Appendix A: Other DNA sequences used in hybridisation assay

Strand 1: 5’ AAA AGC TAA GTC T 3’

Strand 2: 5’ AAA ATG GGA AGC T 3’

Target 1,2: 5’ AGA CTT AGC TAG CTT CCC AT 3’

Strand 3: 5’ AAA TCT CAA CTC GTA 3’

Strand 4: 5’ AAA CGC ATT CAG GAT 3’

Target 3,4: 5’ TAC GAG TTG AGA ATC CTG AAT GCG 3’

Strand 5: 5’ TTC TTC TAC G 3’

Strand 6: 5’ ACA GTC AGC C 3’

Target 5,6: 5’ CGT AGA AGA AGG CTG ACT GT 3’

Strand 7: 5’ TCC CCT CTA A 3’

Strand 8: 5’ CAC CAC ACT G 3’

Target 7,8: 5’ TTA GAG GGG ACA GTG TGG TG 3’

Strand 9: 5’ GCT TGT CCT C 3’

Strand 10: 5’ CTC TCT GCT C 3’

Target 9,10: 5’ GAG GAC AAG CGA GCA GAG AG 3’

Strand 11: 5’ CGA CTC TAG C 3’

Strand 12: 5’ CAA CCT GTC C 3’

Target 11,12: 5’ GCT AGA GTC GGG ACA GGT TG 3’

Strand 13: 5’ ATG TAA AGA A 3’

Strand 14: 5’ CCG CTC CCA G 3’

Target 13,14: 5’ TTC TTT ACA TCT GGG AGC GG 3’

Appendix B: Hybridisation assay-the TAMRA linker probes

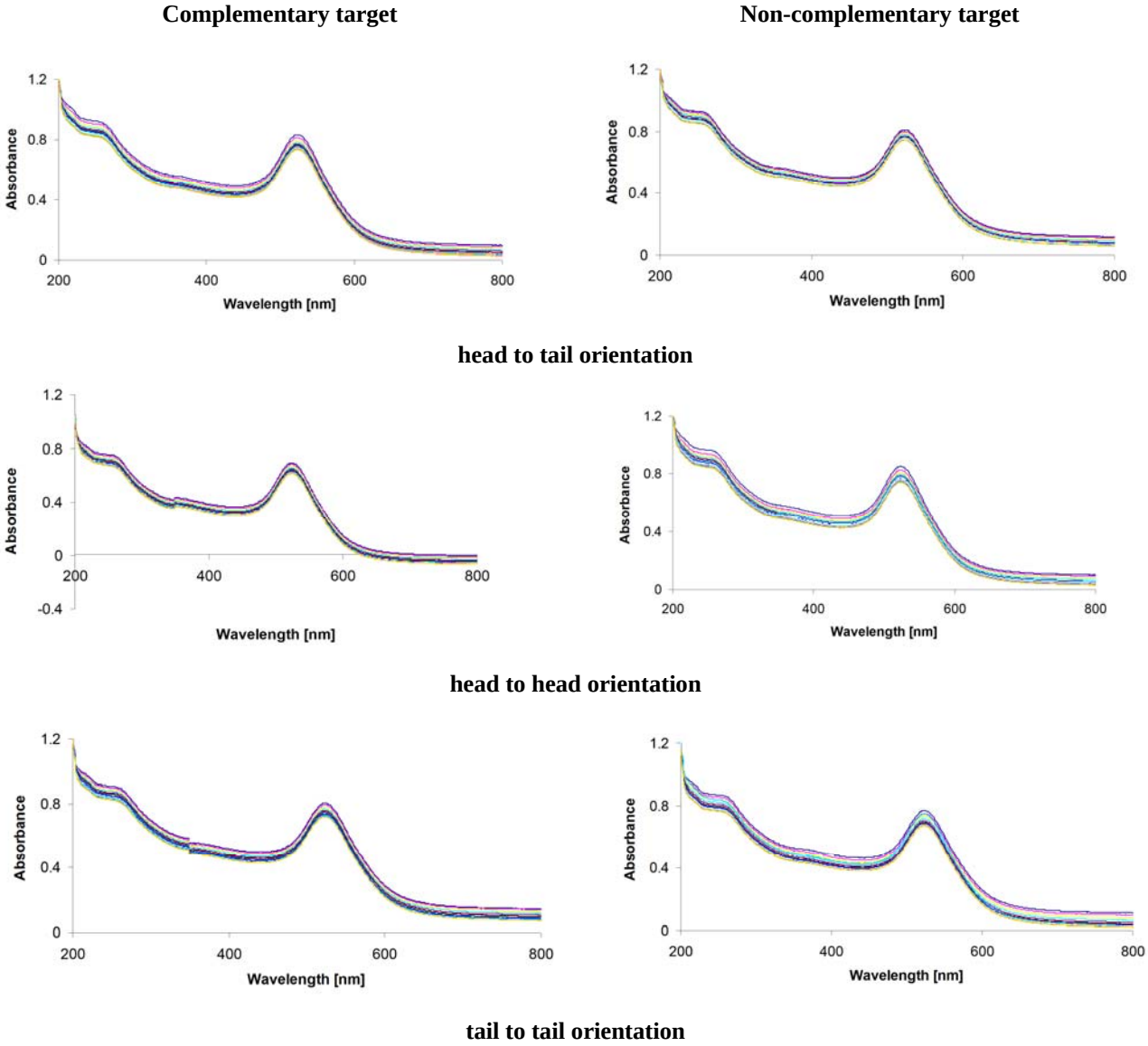

Figure B1: **Changes in the extinction spectra observed with time for the samples containing two 18 nm Au-T-DNA (sequences 3 and 4) probes (1.62 nM) and complementary or non-complementary target ($4.05 \cdot 10^{-8}$ M) for different probes orientations.**

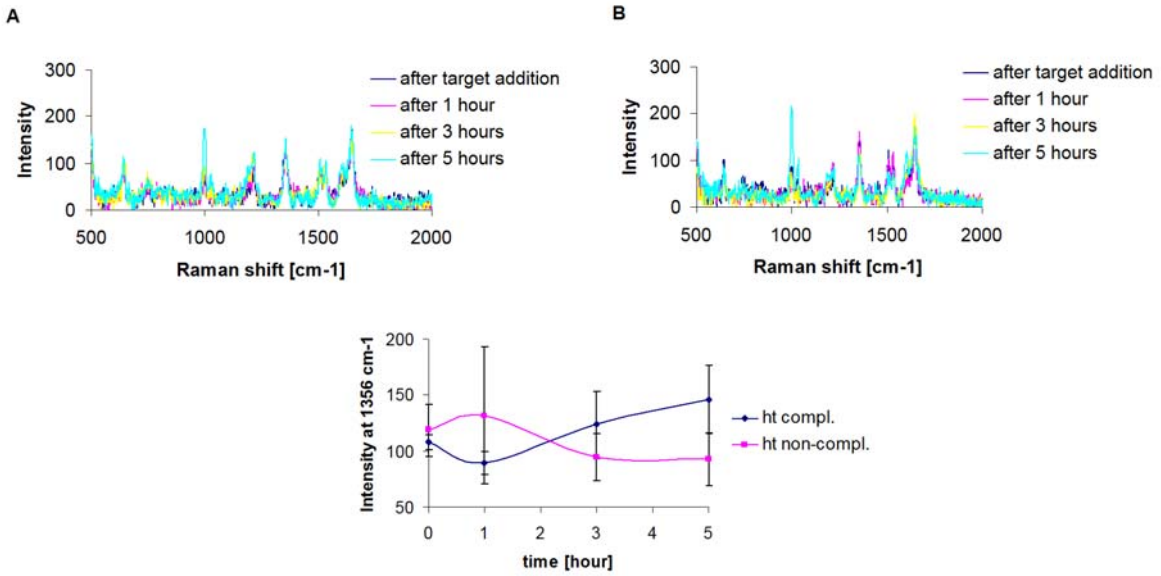

Figure B2: **Changes in the intensity of SERRS signals observed after addition of target (complementary (A) or non-complementary (B)) to the solution containing two 18 nm Au-T-DNA (sequences 3 and 4) probes (1.62 nM) hybridizing to the target ($4.05 \cdot 10^{-8}$ M) in a head to tail (ht) fashion. The bottom graph shows changes of the intensity of the peak at 1356 cm^{-1} with time, after addition of complementary and non-complementary target.**

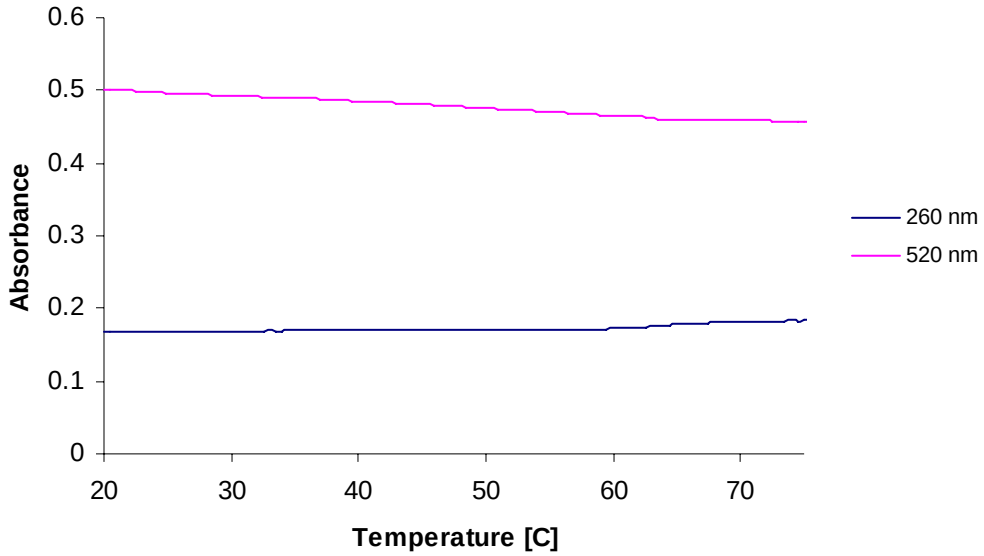

Figure B3: **Melting profiles of aggregates formed from 18 nm Au-T-DNA (sequences 3 and 4) probes in a head to tail orientation at 260 nm and 520 nm.**

Appendix C: Hybridisation assay-the aminofluorescein linker probes

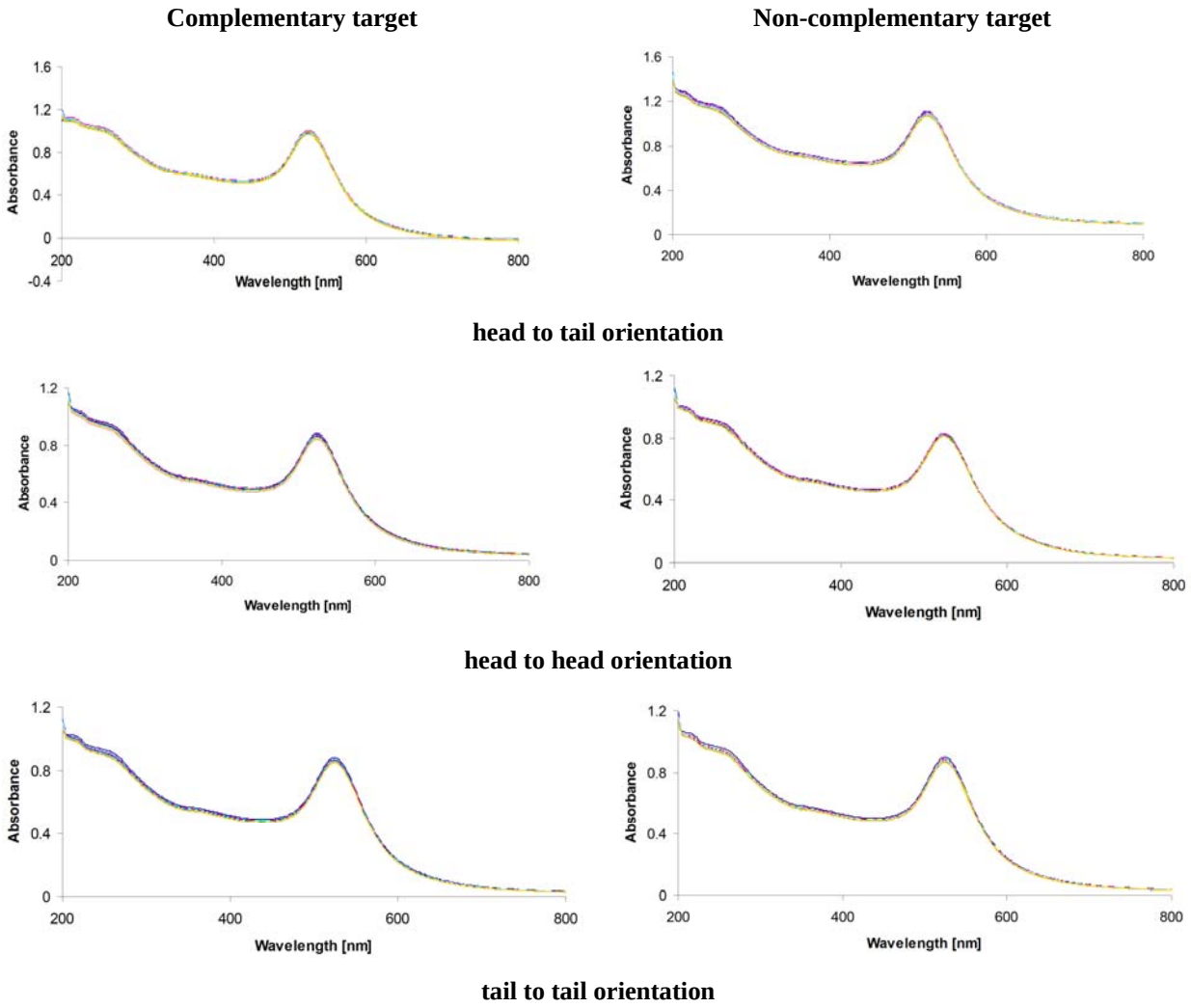

Figure C1: **Changes in the extinction spectra observed with time for the samples containing two 18 nm Au-Af-DNA (sequences 1 and 2) probes (1.62 nM) and complementary or non-complementary target ($8.1 \cdot 10^{-10}$M) for different probes orientations.**

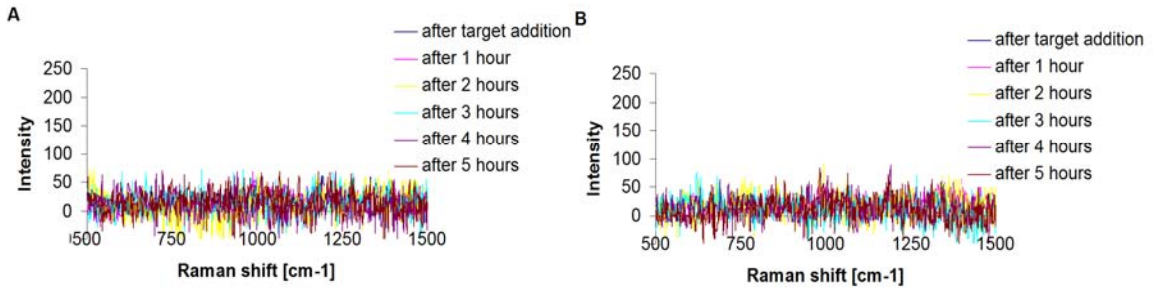

Figure C2: **Changes in the intensity of SERRS signals observed after addition of target (complementary (A) or non-complementary (B)) to the solution containing two 18 nm Au-Af-DNA (sequences 1 and 2) probes (1.62 nM) hybridizing to the target ($8.1 \cdot 10^{-10}$M) in a head to tail fashion.**

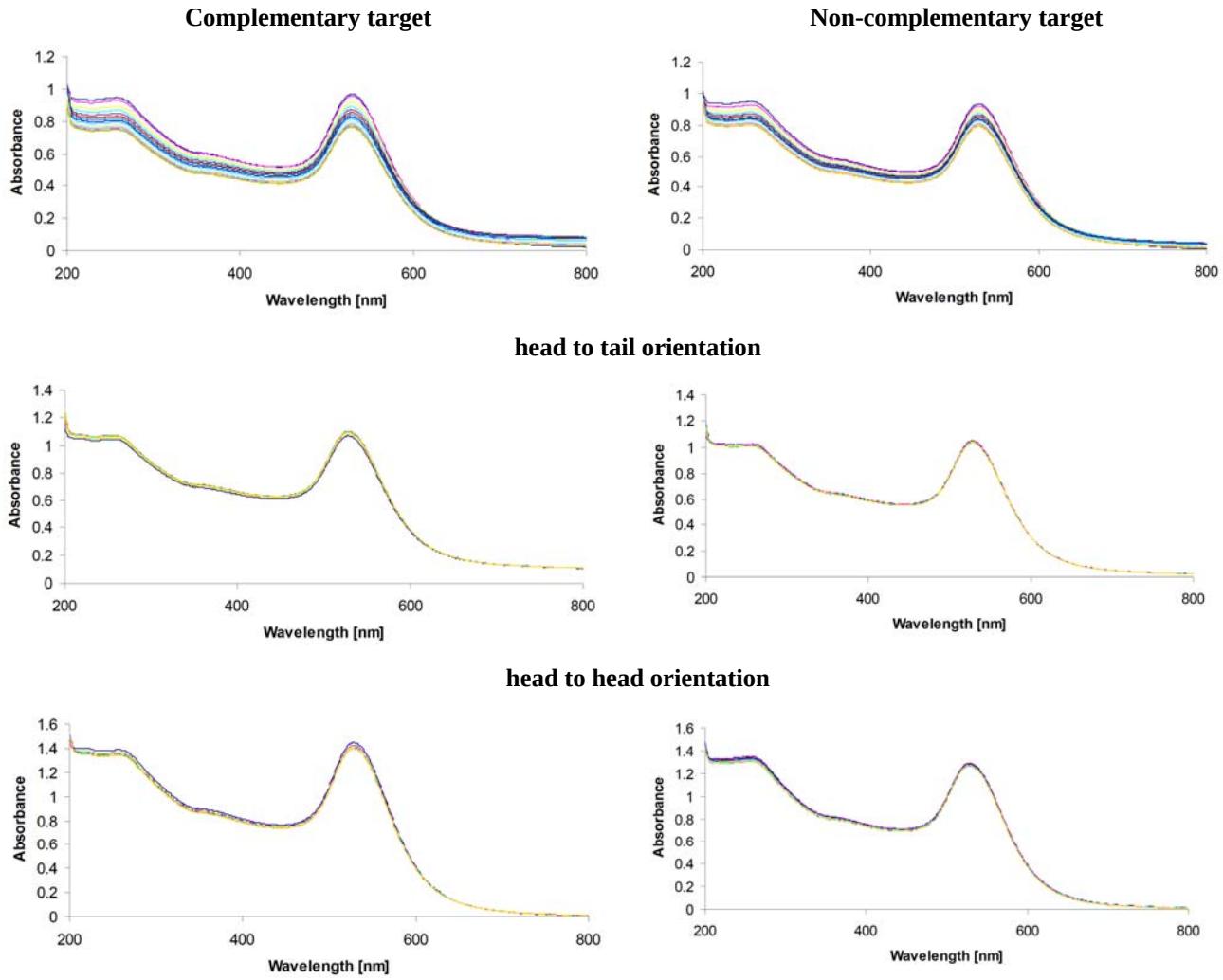

Figure C3: **Changes in the extinction spectra observed with time for the samples containing two 50 nm Au-Af-DNA (sequences 1 and 2) probes ($3.78 \cdot 10^{-11}$ M) and complementary or non-complementary target ($7.56 \cdot 10^{-10}$ M) for different probes orientations.**

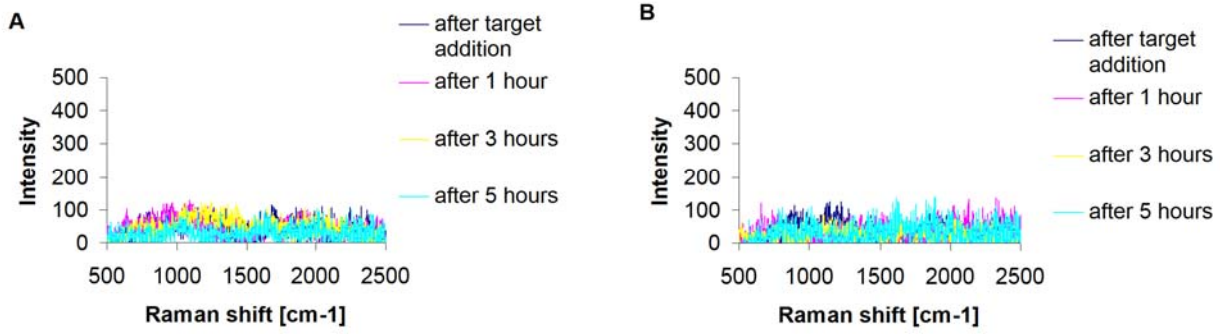

Figure C4: **Changes in the SERRS signal observed after addition of target (complementary (A) or non-complementary (B)) to the solution containing two 50 nm Au-Af-DNA (sequences 1 and 2) probes ($3.78 \cdot 10^{-11}$ M) hybridizing to the target ($7.56 \cdot 10^{-10}$ M)in a head to tail fashion.**

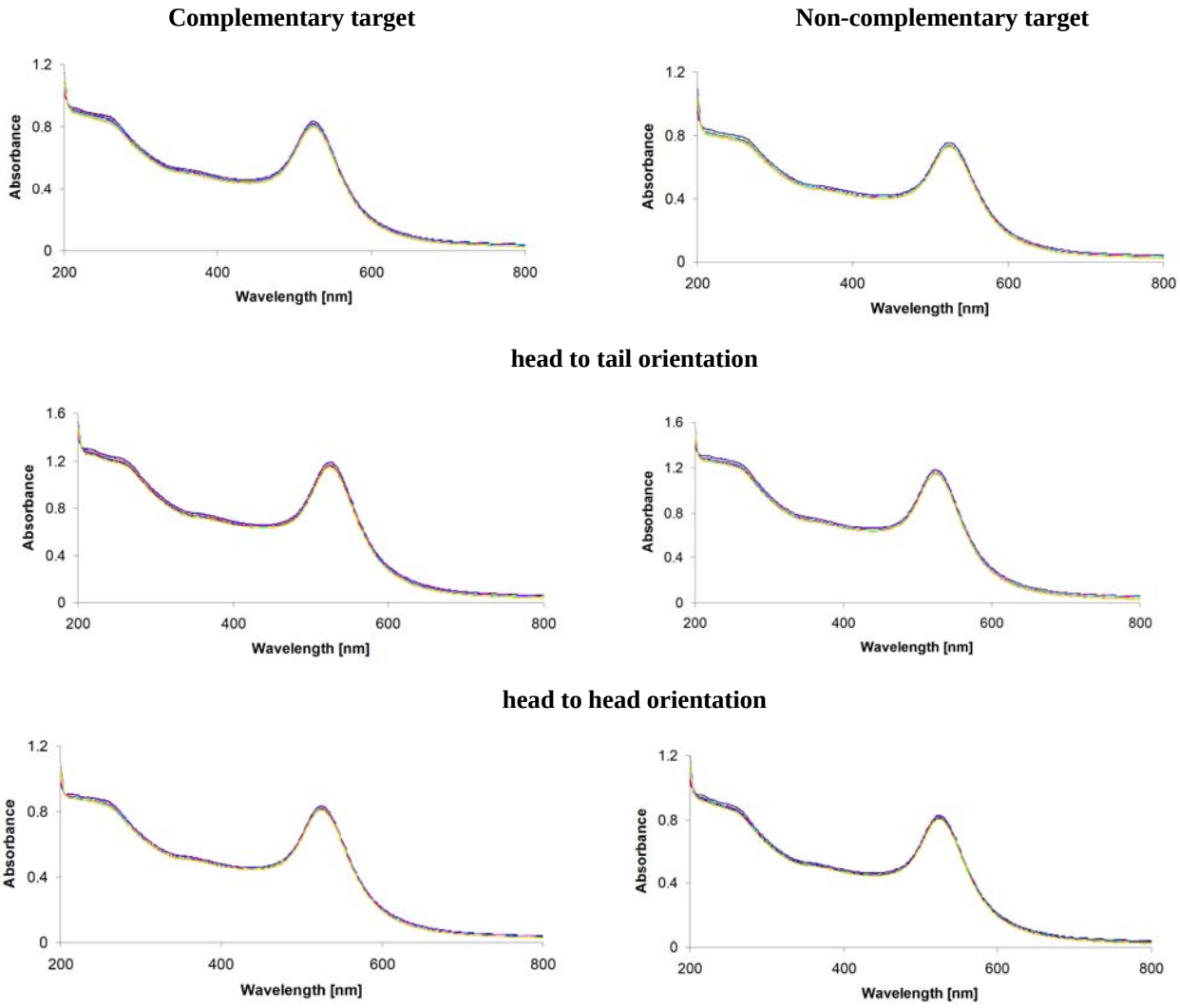

Figure C5: **Changes in the extinction spectra observed with time for the samples containing two 18 nm Au-Af-DNA (sequences 3 and 4) probes (1.62 nM) and complementary or non-complementary target ($8.1 \cdot 10^{-10}$M) for different probes orientations.**

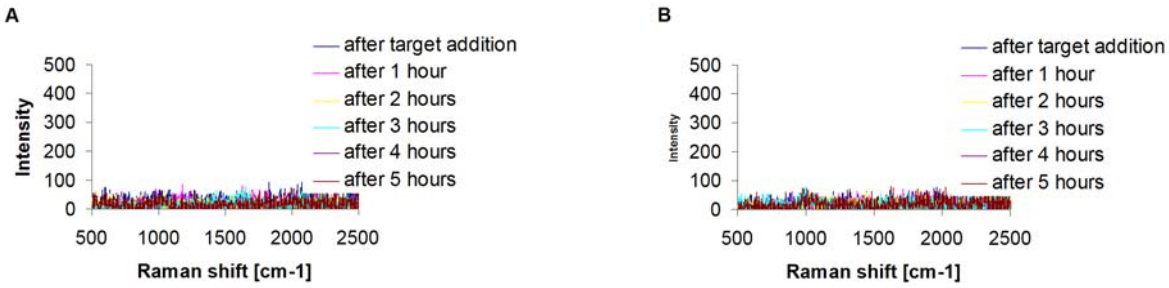

Figure C6: **Changes in the SERRS signal observed after addition of target (complementary (A) or non-complementary(B)) to the solution containing two 18 nm Au-Af-DNA (sequences 3 and 4) probes (1.62 nM) hybridizing to the target ($8.1 \cdot 10^{-10}$M) in a head to tail fashion.**

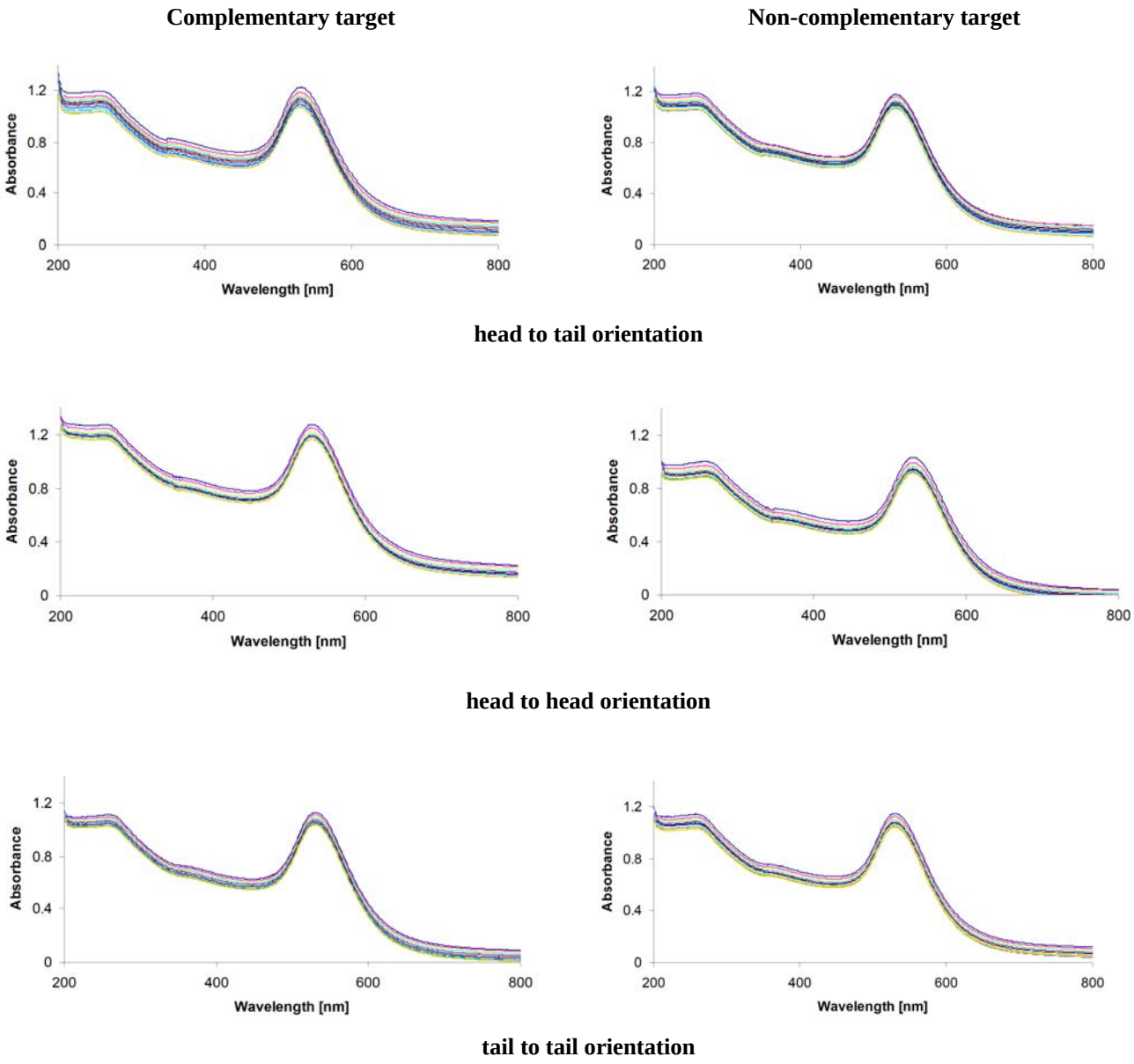

Figure C7: **Changes in the extinction spectra observed with time for the samples containing two 50 nm Au-Af-DNA (sequences 3 and 4) probes ($3.78 \cdot 10^{-11}$ M) and complementary or non-complementary target ($7.56 \cdot 10^{-10}$ M) for different probes orientations.**

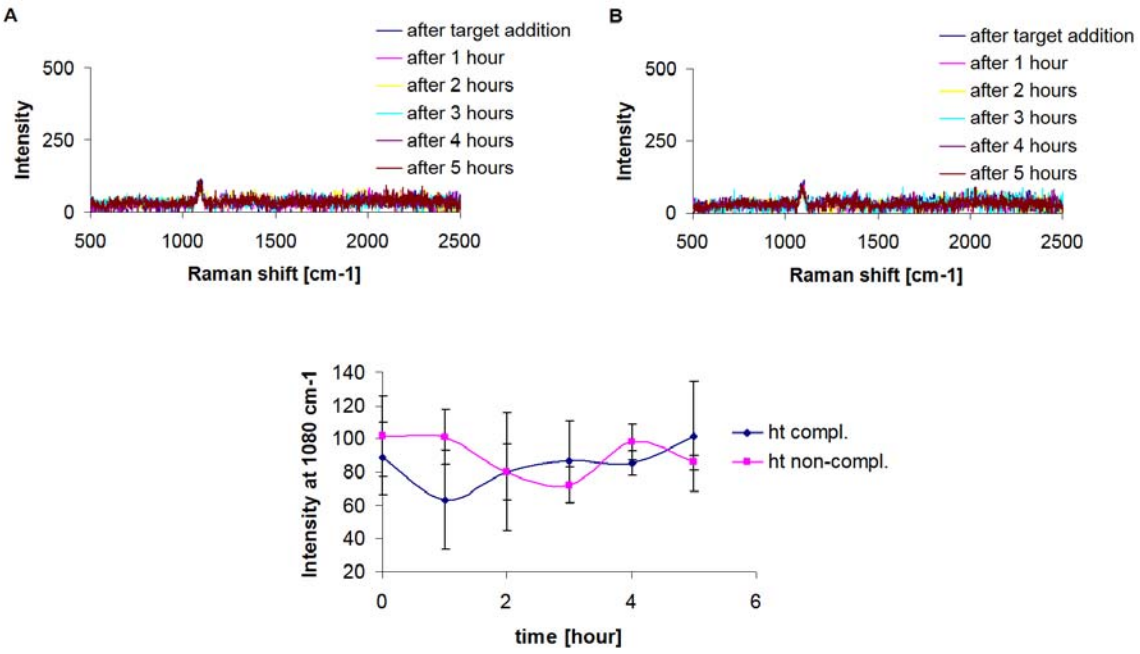

Figure C8: **Changes in the intensity of the SERRS signal observed after addition of target (complementary (A) or non-complementary (B)) to the solution containing two 50 nm Au-Af-DNA (sequences 3 and 4) probes ($7.56 \cdot 10^{-11}$ M) hybridizing to the target ($1.512 \cdot 10^{-9}$ M) in a head to tail (ht) fashion.**

Table C1: Summary of the changes observed in the extinction and SERRS spectra after addition of complementary or imperfect target to the solution containing the aminofluorescein linker probes.

Type of colloid	Probes orientation	DNA sequences	Target	Changes observed in the UV-Vis spectrum	Changes observed in the SERRS spectrum
18 nm Au	head to head	1 and 2	compl.	No changes observed.	No changes observed.
18 nm Au	head to head	1 and 2	non-compl.	No changes observed.	No changes observed.
18 nm Au	head to tail	1 and 2	compl.	No changes observed.	No changes observed.
18 nm Au	head to tail	1 and 2	non-compl.	No changes observed.	No changes observed.
18 nm Au	tail to tail	1 and 2	compl.	No changes observed.	No changes observed.
18 nm Au	tail to tail	1 and 2	non-compl.	No changes observed.	No changes observed.
50 nm Au	head to head	1 and 2	compl.	No changes observed.	No changes observed.
50 nm Au	head to head	1 and 2	non-compl.	No changes observed.	No changes observed.
50 nm Au	head to tail	1 and 2	compl.	Small decrease in gold plasmon band observed.	No changes observed.
50 nm Au	head to tail	1 and 2	non-compl.	Small decrease in gold plasmon band observed.	No changes observed.
50 nm Au	tail to tail	1 and 2	compl.	No changes observed.	No changes observed.
50 nm Au	tail to tail	1 and 2	non-compl.	No changes observed.	No changes observed.
18 nm Au	head to head	3 and 4	compl.	No changes observed.	No changes observed.
18 nm Au	head to head	3 and 4	non-compl.	No changes observed.	No changes observed.
18 nm Au	head to tail	3 and 4	compl.	No changes observed.	No changes observed.
18 nm Au	head to tail	3 and 4	non-compl.	No changes observed.	No changes observed.
18 nm Au	tail to tail	3 and 4	compl.	No changes observed.	No changes observed.
18 nm Au	tail to tail	3 and 4	non-compl.	No changes observed.	No changes observed.
50 nm Au	head to head	3 and 4	compl.	Small decrease in gold plasmon band observed.	No changes observed.
50 nm Au	head to head	3 and 4	non-compl.	Small decrease in gold plasmon band observed.	No changes observed.
50 nm Au	head to tail	3 and 4	compl.	Small decrease in gold plasmon band observed.	No changes observed.
50 nm Au	head to tail	3 and 4	non-compl.	Small decrease in gold plasmon band observed.	No changes observed.
50 nm Au	tail to tail	3 and 4	compl.	Small decrease in gold plasmon band observed.	No changes observed.
50 nm Au	tail to tail	3 and 4	non-compl.	Small decrease in gold plasmon band observed.	No changes observed.

Probes concentration: 1.62 nM (18 nm Au), 3.78×10^{-11}M (50 nm Au); target concentration: 8.1×10^{-10}M (18 nm Au), 7.56×10^{-10}M (50 nm Au); SERRS experiments were performed using excitation at 633 nm.

Appendix D: Hybridisation assay-the fluorescein linker probes

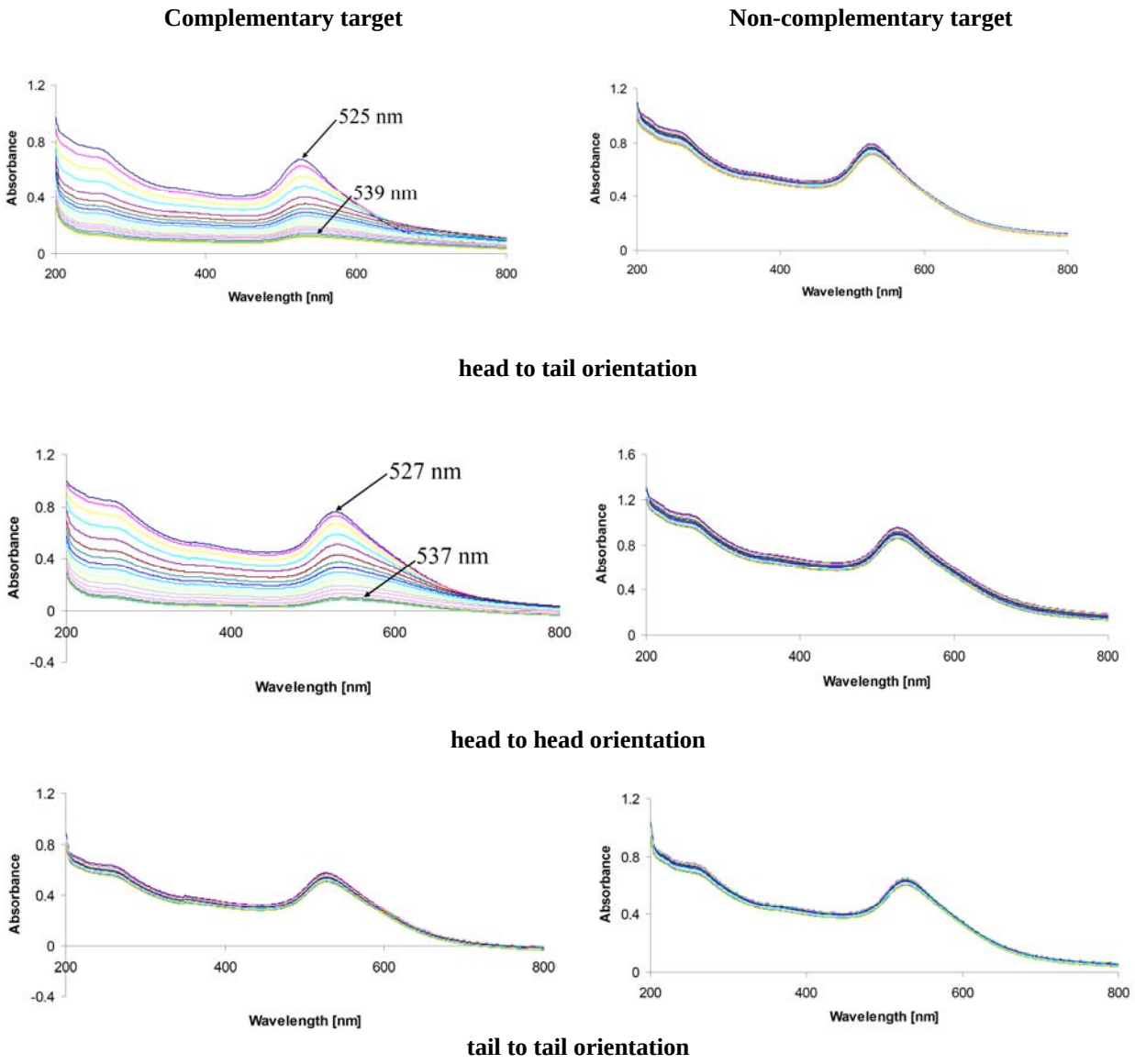

Figure D1: **Changes in the extinction spectra observed with time for the samples containing two 18 nm Au-F-DNA (sequences 1 and 2) probes (1.62 nM) and complementary or non-complementary target ($3.24 \cdot 10^{-10}$M) for different probes orientations.**

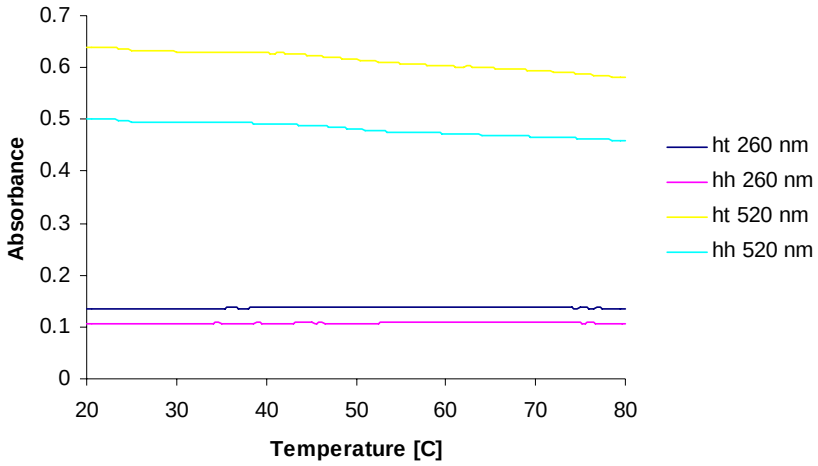

Figure D2: **Melting profile of aggregates formed from 18 nm Au-F-DNA in a head to tail (ht) and head to head (hh) orientations at 260 nm and 520 nm.**

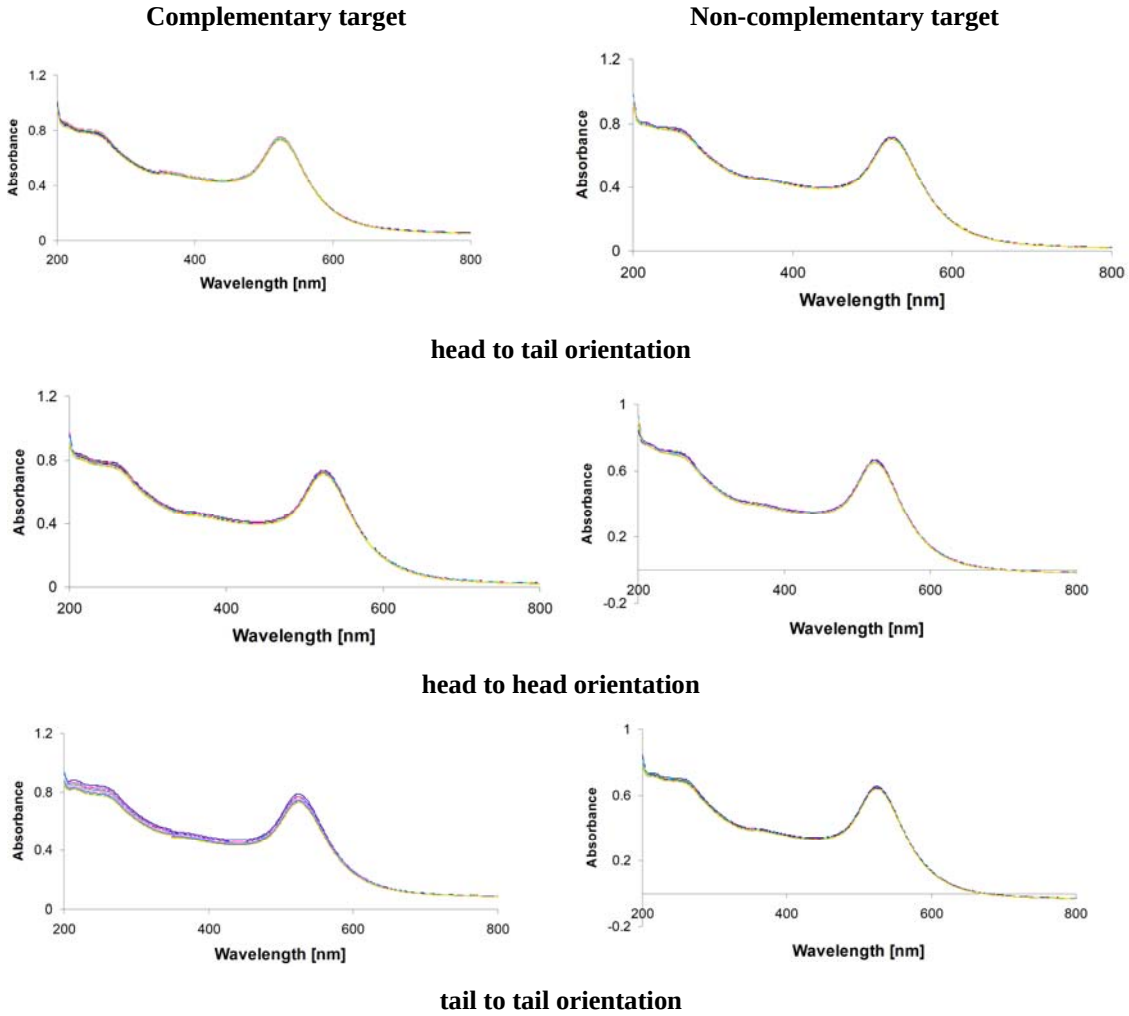

Figure D3: **Changes in the extinction spectra observed with time for the samples containing two 18 nm Au-F-DNA (sequences 3 and 4) probes (1.62 nM) and complementary or non-complementary target ($3.24 \cdot 10^{-10}$M) for different probes orientations.**

Table D1: Summary of the changes observed in the extinction spectra after addition of complementary or imperfect target to the solution containing the fluorescein linker probes.

Type of colloid	Probes orientation	DNA sequence	Target	Changes observed in the UV-Vis spectrum	Melting analysis	
					260 nm	520 nm
18 nm Au	head to head	1 and 2	compl.	Decrease and red shift (10 nm) of the gold plasmon band observed.	Sharp melting curves not observed.	Sharp melting curves not observed.
18 nm Au	head to head	1 and 2	non-compl.	Small decrease and a small red shift (2 nm) of the gold plasmon band observed	N/A	N/A
18 nm Au	head to tail	1 and 2	compl.	Decrease and red shift (12 nm) of the gold plasmon band observed.	Sharp melting curves not observed.	Sharp melting curves not observed.
18 nm Au	head to tail	1 and 2	non-compl.	Small decrease and a small red shift (3 nm) of the gold plasmon band observed.	N/A	N/A
18 nm Au	tail to tail	1 and 2	compl.	Small decrease and a small red shift (2 nm) of the gold plasmon band observed.	N/A	N/A
18 nm Au	tail to tail	1 and 2	non-compl.	Small decrease and a small red shift (2 nm) of the gold plasmon band observed	N/A	N/A
18 nm Au	head to head	3 and 4	compl.	No changes observed.	N/A	N/A
18 nm Au	head to head	3 and 4	non-compl.	No changes observed.	N/A	N/A
18 nm Au	head to tail	3 and 4	compl.	No changes observed.	N/A	N/A
18 nm Au	head to tail	3 and 4	non-compl.	No changes observed.	N/A	N/A
18 nm Au	tail to tail	3 and 4	compl.	No changes observed.	N/A	N/A
18 nm Au	tail to tail	3 and 4	non-compl.	No changes observed.	N/A	N/A

Probes concentration: 1.62 nM; target concentration: 3.24×10^{-10}M. N/A – melting analysis was not performed.

Appendix E: Hybridisation assay- the BHQ linker probes

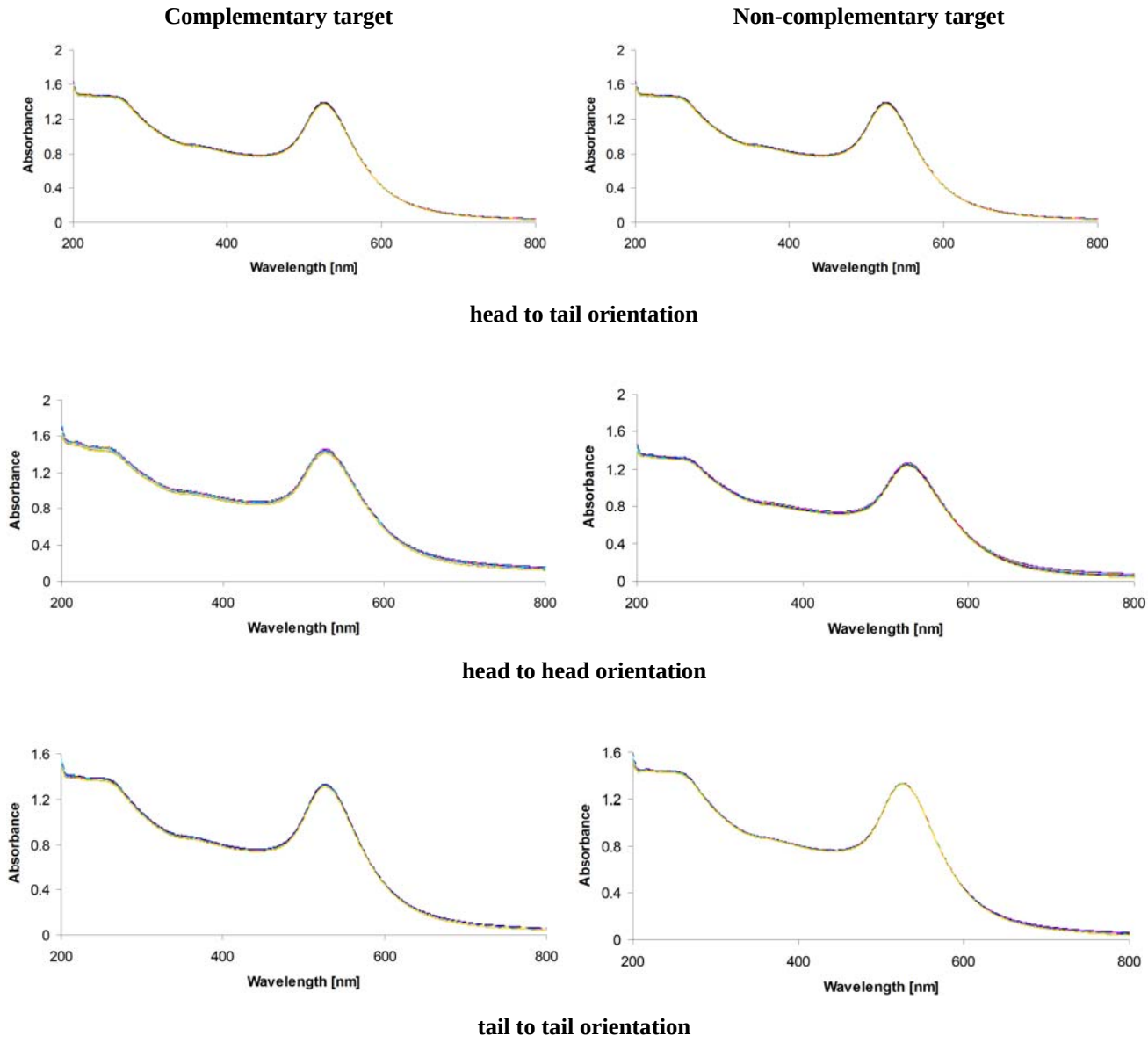

Figure E1: **Changes in the extinction spectra observed with time for the samples containing two 18 nm Au-BHQ-DNA (sequences 1 and 2) probes (1.62 nM) and complementary or non-complementary target ($1.13 \cdot 10^{-9}$ M) for different probes orientations.**

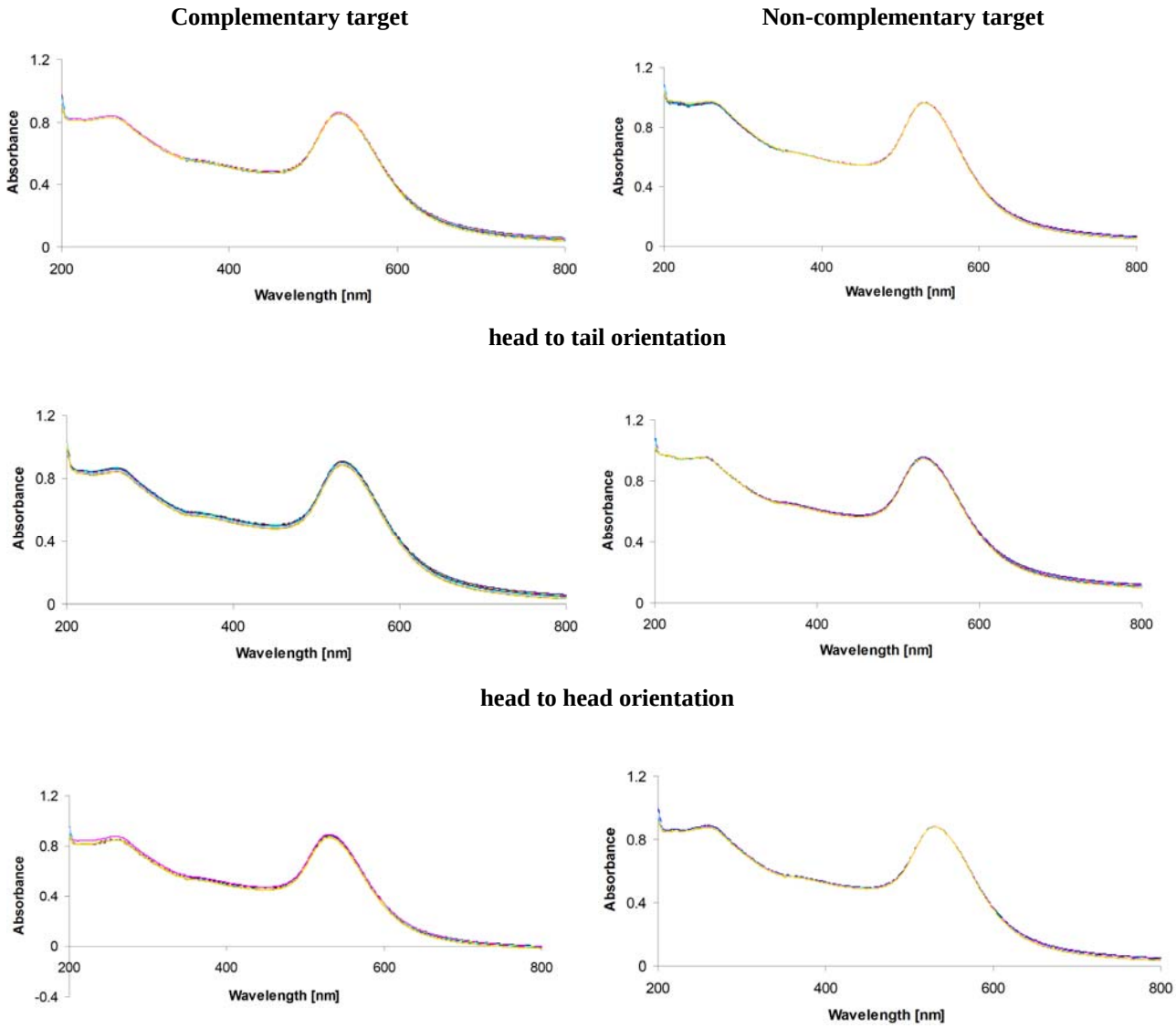

Figure E2: **Changes in the extinction spectra observed with time for the samples containing two 50 nm Au-BHQ-DNA (sequences 1 and 2) probes ($3.78 \cdot 10^{-11}$ M) and complementary or non-complementary target ($5.67 \cdot 10^{-9}$ M) for different probes orientations.**

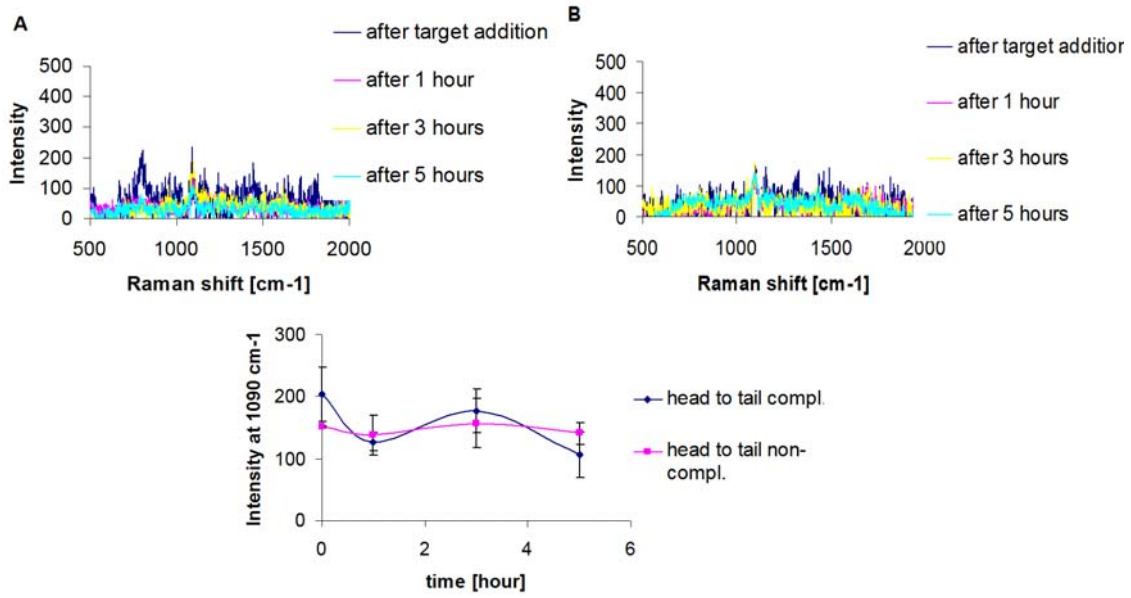

Figure E3: **Changes in the intensity of the SERRS signal observed after addition of target (complementary (A) or non-complementary(B)) to the solution containing two 18 nm Au-BHQ-DNA (sequences 1 and 2) probes (1.62 nM)hybridizing to the targets ($1.13 \cdot 10^{-9}$ M) in a head to tail fashion. The bottom graph shows changes of the intensity of the peak at 1090 cm^{-1} with time, after addition of complementary and non-complementary target.**

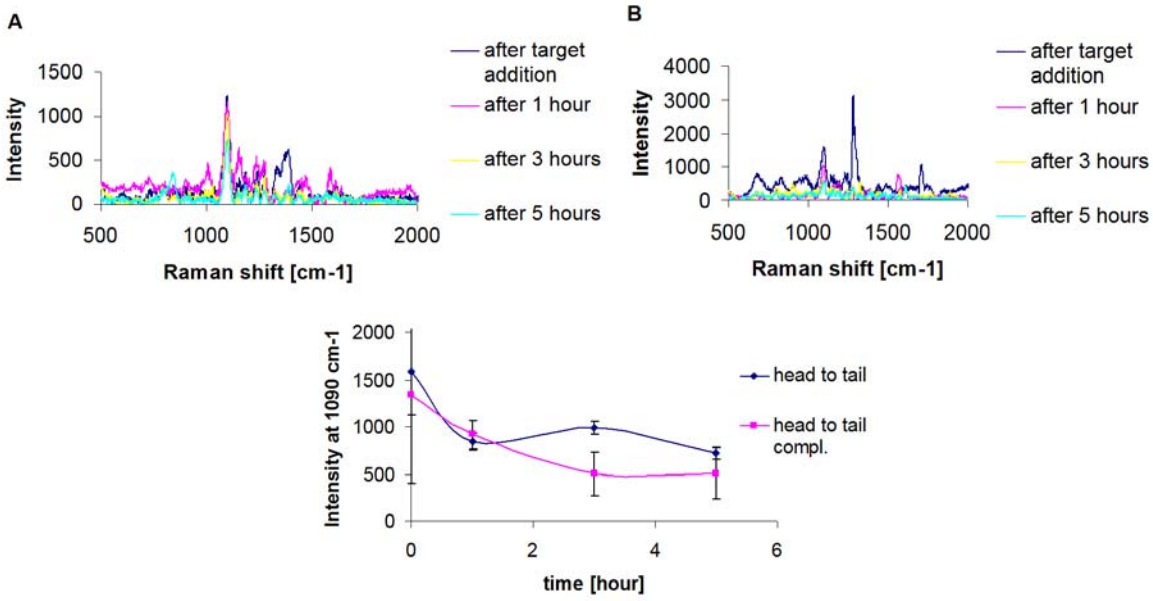

Figure E4: **Changes in the intensity of the SERRS signal observed after addition of target (complementary or non-complementary) to the solution containing two 50 nm Au-BHQ-DNA (sequences 1 and 2) probes ($3.78 \cdot 10^{-11}$ M) hybridizing to the targets ($5.67 \cdot 10^{-9}$ M) in a head to tail fashion. The bottom graph shows changes of the intensity of the peak at 1090 cm^{-1} with time, after addition of complementary and non-complementary target.**

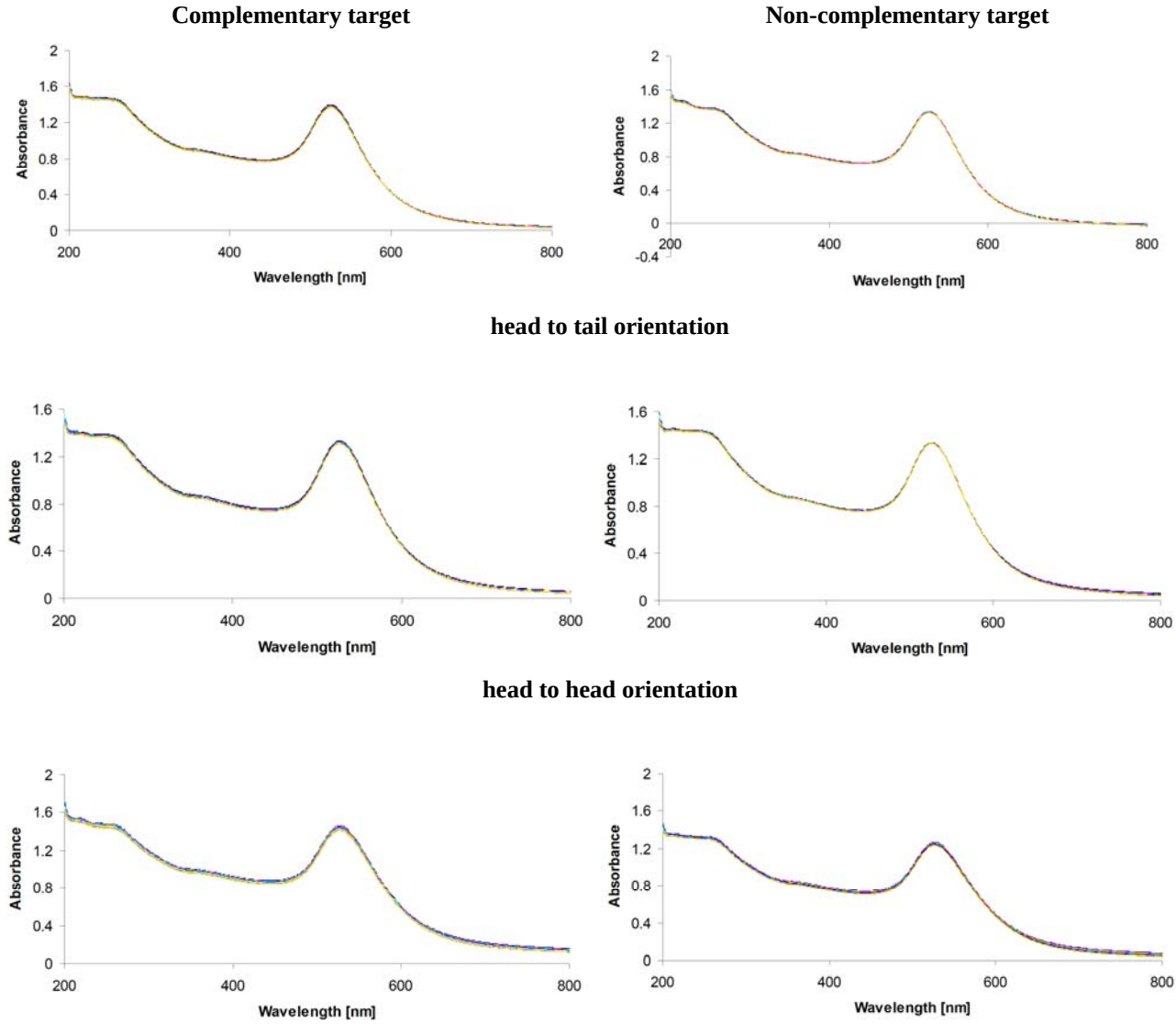

Figure E5: **Changes in the extinction spectra observed with time for the samples containing two 18 nm Au-BHQ-DNA (sequences 3 and 4) probes (1.62 nM) and complementary or non-complementary target ($1.13 \cdot 10^{-9}$ M) for different probes orientations.**

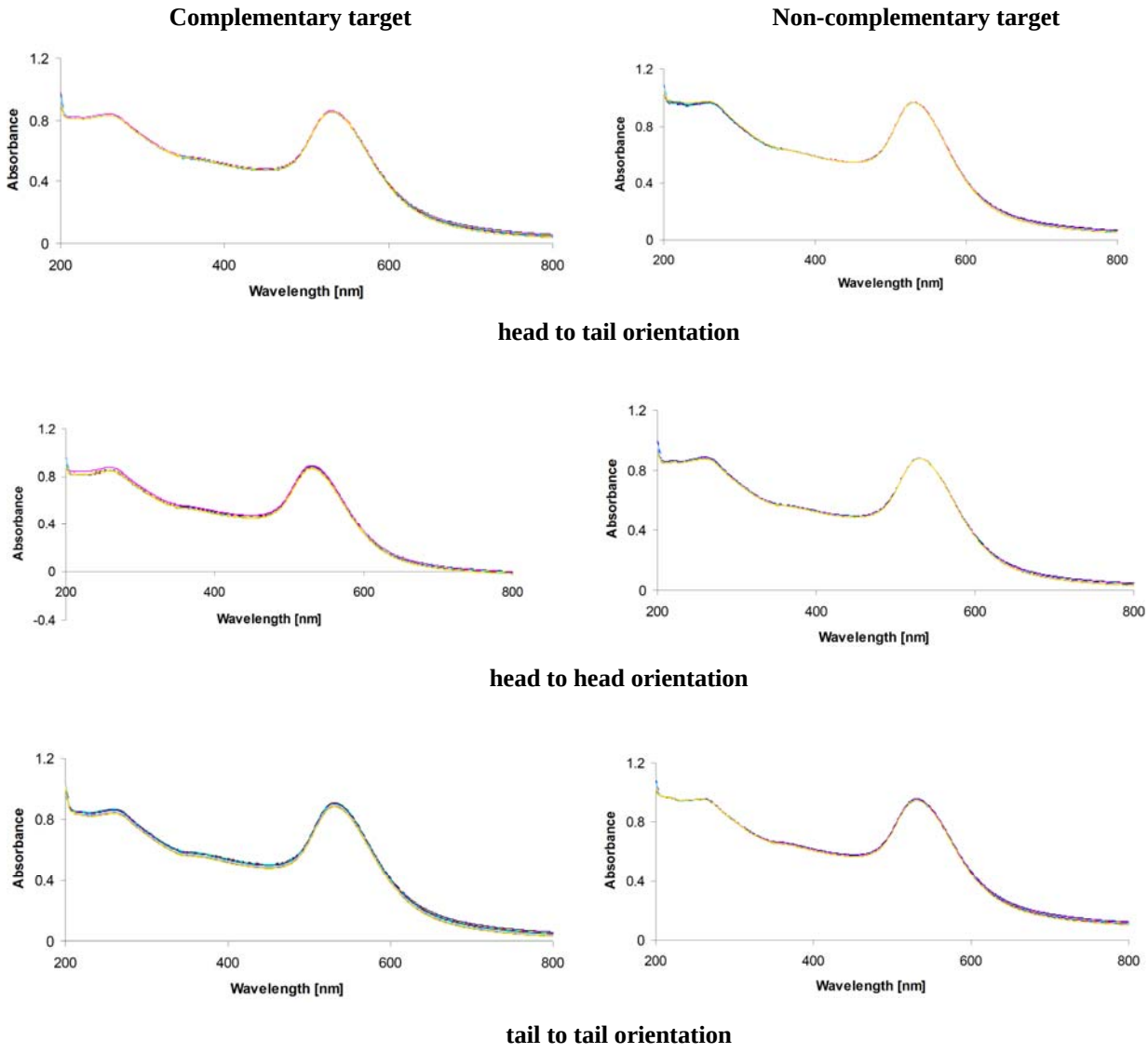

Figure E6: **Changes in the extinction spectra observed with time for the samples containing two 50 nm Au-BHQ-DNA (sequences 3 and 4) probes ($3.78 \cdot 10^{-11}$ M) and complementary or non-complementary target ($5.67 \cdot 10^{-9}$ M) for different probes orientations.**

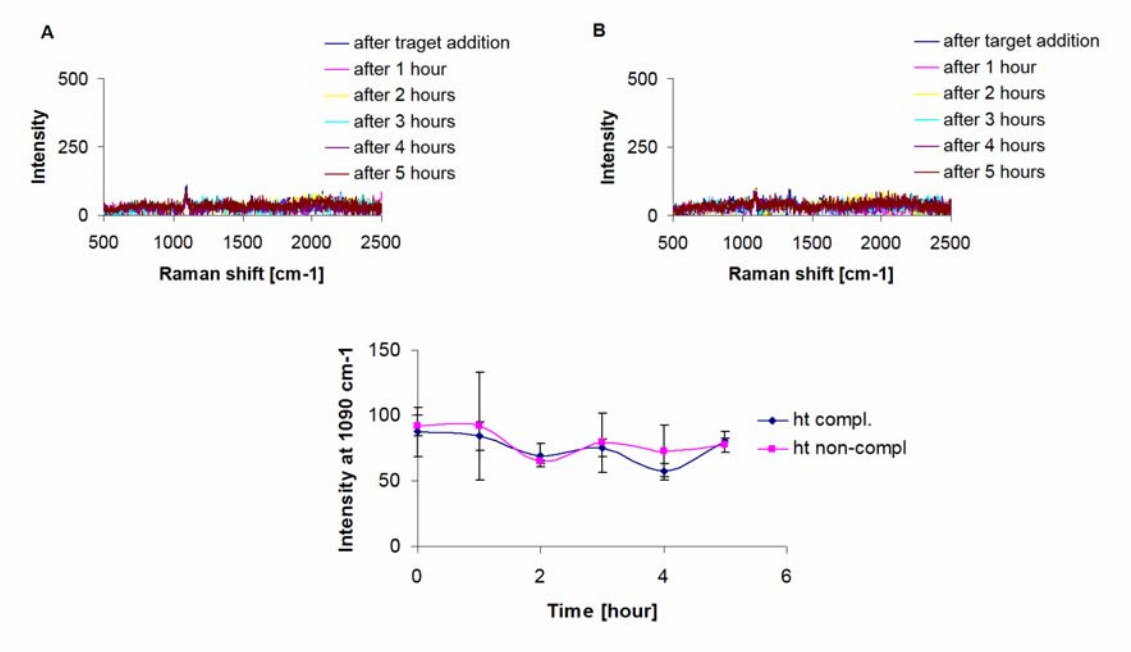

Figure E7: **Changes in the intensity of the SERRS signal observed after addition of target (complementary (A) or non-complementary (B)) to the solution containing two 18 nm Au-BHQ-DNA (sequences 3 and 4) probes (1.62 nM) hybridizing to the target ($1.13 \cdot 10^{-9}$ M) in a head to tail (ht) fashion. The bottom graph shows changes in the intensity of the peak at 1090 cm^{-1} with time, after addition of complementary and non-complementary target.**

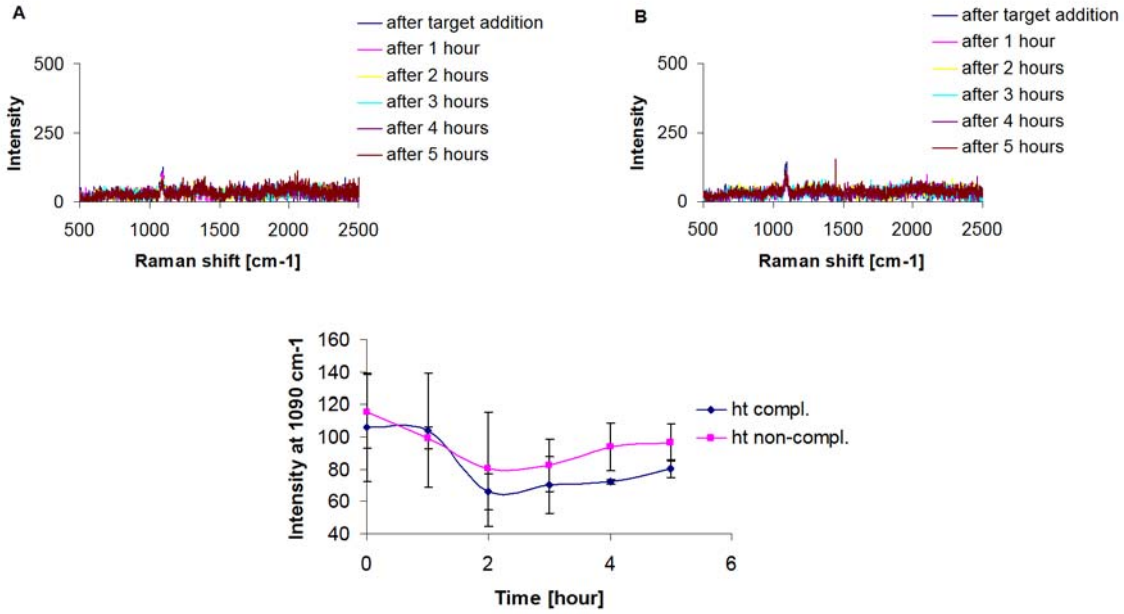

Figure E8: **Changes in the intensity of the SERRS signal observed after addition of target (complementary(A) or non-complementary(B)) to the solution containing two 50 nm Au-BHQ-DNA (sequences 3 and 4) probes ($3.78 \cdot 10^{-11}$ M)hybridizing to the target ($5.67 \cdot 10^{-9}$ M) in head to tail (ht) fashion. The bottom graph shows changes of the intensity of the peak at 1090 cm^{-1} with time, after addition of complementary and non-complementary target.**

Table E1: Summary of the changes observed in the extinction and SERRS spectra after addition of complementary or imperfect target to the solution containing the BHQ linker probes.

Type of colloid	Probes orientation	DNA sequences	Target	Changes observed in the UV-Vis spectrum	Changes observed in the SERRS spectrum
18 nm Au	head to head	1 and 2	compl.	No changes observed.	No changes observed.
18 nm Au	head to head	1 and 2	non-compl.	No changes observed.	No changes observed.
18 nm Au	head to tail	1 and 2	compl.	No changes observed.	No changes observed.
18 nm Au	head to tail	1 and 2	non-compl.	No changes observed.	No changes observed.
18 nm Au	tail to tail	1 and 2	compl.	No changes observed.	No changes observed.
18 nm Au	tail to tail	1 and 2	non-compl.	No changes observed.	No changes observed.
50 nm Au	head to head	1 and 2	compl.	No changes observed.	No changes observed.
50 nm Au	head to head	1 and 2	non-compl.	No changes observed.	No changes observed.
50 nm Au	head to tail	1 and 2	compl.	No changes observed.	No changes observed.
50 nm Au	head to tail	1 and 2	non-compl.	No changes observed.	No changes observed.
50 nm Au	tail to tail	1 and 2	compl.	No changes observed.	No changes observed.
50 nm Au	tail to tail	1 and 2	non-compl.	No changes observed.	No changes observed.
18 nm Au	head to head	3 and 4	compl.	No changes observed.	No changes observed.
18 nm Au	head to head	3 and 4	non-compl.	No changes observed.	No changes observed.
18 nm Au	head to tail	3 and 4	compl.	No changes observed.	No changes observed.
18 nm Au	head to tail	3 and 4	non-compl.	No changes observed.	No changes observed.
18 nm Au	tail to tail	3 and 4	compl.	No changes observed.	No changes observed.
18 nm Au	tail to tail	3 and 4	non-compl.	No changes observed.	No changes observed.
50 nm Au	head to head	3 and 4	compl.	No changes observed.	No changes observed.
50 nm Au	head to head	3 and 4	non-compl.	No changes observed.	No changes observed.
50 nm Au	head to tail	3 and 4	compl.	No changes observed.	No changes observed.
50 nm Au	head to tail	3 and 4	non-compl.	No changes observed.	No changes observed.
50 nm Au	tail to tail	3 and 4	compl.	No changes observed.	No changes observed.
50 nm Au	tail to tail	3 and 4	non-compl.	No changes observed.	No changes observed.

Probes concentration: 1.62 nM (18 nm Au), 3.78×10^{-11}M (50 nm Au); target concentration: 1.13×10^{-9}M (18 nm Au), 5.67×10^{-9}M (50 nm Au); SERRS experiments were performed using excitation at 633 nm.

Appendix F: Possible fold structures of sequences 1, 2 and 4.

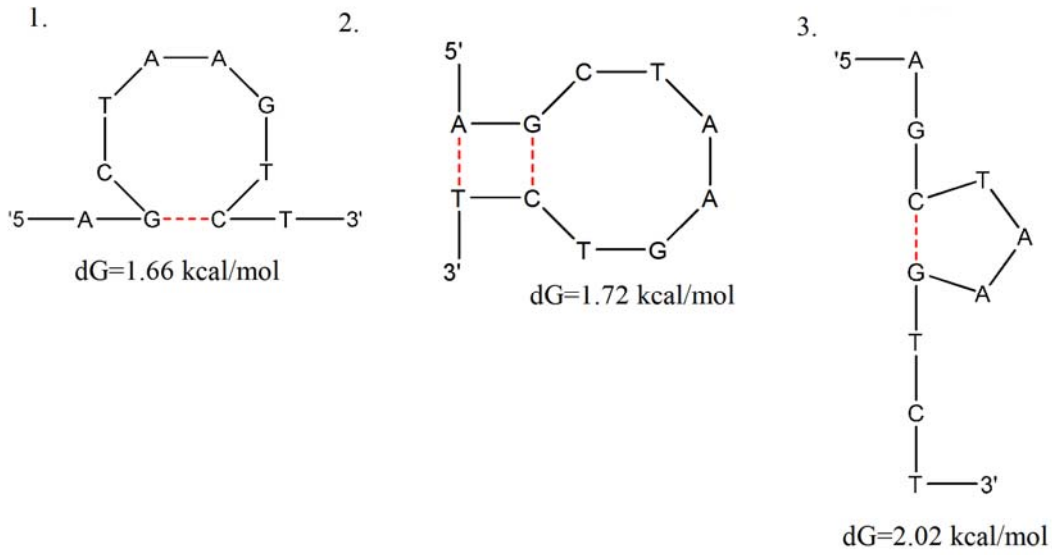

Figure A: **Possible folded structures of strand 1: 5' AGC TAA GTC T 3'.**

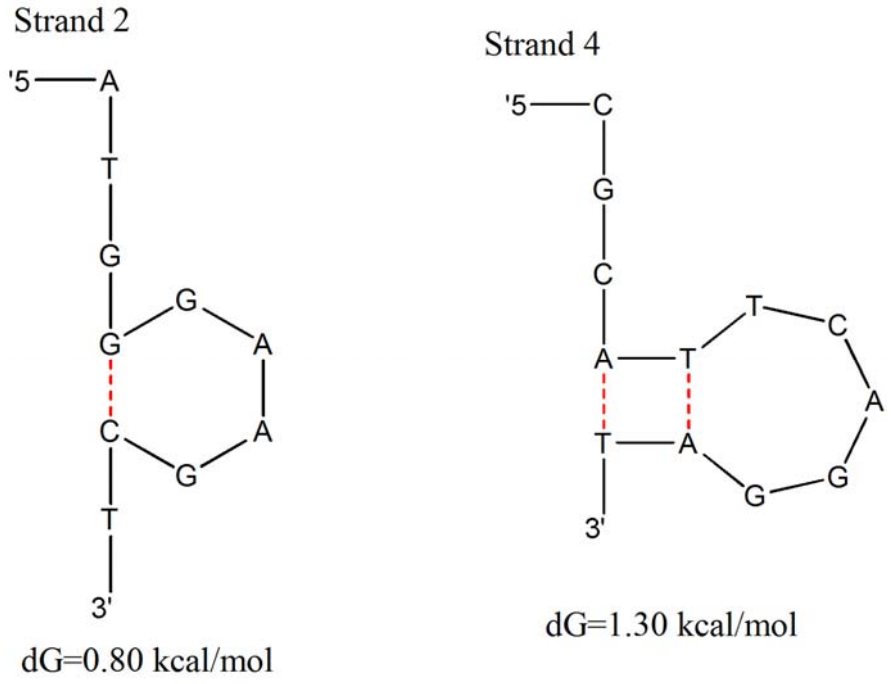

Figure B: **Possible folded structures of strands: 2 (5' ATG GGA AGC T 3') and 4 (5' CGC ATT CAG GAT 3').**